Novel Methods for Active Reservoir Monitoring and Flow Rate Allocation of Intelligent Wells

Reza Malakooti

A thesis submitted for the Degree of Doctor of Philosophy
School of Energy, Geoscience, Infrastructure and Society
Heriot-Watt University
Edinburgh, Scotland, UK

September 2015

Abstract

The value added by intelligent wells (I-wells) derives from real-time, reservoir and production performance monitoring together with zonal, downhole flow control. Unfortunately, downhole sensors that can directly measure the zonal flow rates and phase cuts required for optimal control of the well's producing zones are not normally installed. Instead, the zonal, Multi-phase Flow Rates (MPFRs) are calculated from indirect measurements (e.g. from zonal pressures, temperatures and the total well flow rate), an approach known as soft-sensing.

To-date all published techniques for zonal flow rate allocation in multi-zone I-wells are "passive" in that they calculate the required parameters to estimate MPFRs for a fixed given configuration of the completion. These techniques are subject to model error, but also to errors stemming from measurement noise when there is insufficient data duplication for accurate parameter estimation.

This thesis describes an "active" soft-sensing technique consisting of two sequential optimisation steps. First step calculates MPFRs while the second one uses a direct search method based on Deformed Configurations to optimise the sequence of Interval Control Valve positions during a routine multi-rate test in an I-well. This novel approach maximises the accuracy of the calculated reservoir properties and MPFRs.

Four "active monitoring" levels are discussed. Each one uses a particular combination of available indirect measurements from well performance monitoring systems. Level one is the simplest, requiring a minimal amount of well data. The higher levels require more data; but provide, in return, a greater understanding of produced fluids volumes and the reservoir's properties at both a well and a zonal level.

Such estimation of the reservoir parameters and MPFRs in I-wells is essential for effective well control strategies to optimise the production volumes. An integrated, control and monitoring (ICM) workflow is proposed which employs the active soft-sensing algorithm modified to maximise I-well oil production via real-time zonal production control based on estimates of zonal reservoir properties and their updates. Analysis of convergence rate of ICM workflow to optimise different objective functions shows that very accurate zonal properties are not required to optimise the oil production. The proposed reservoir monitoring and MPFR allocation workflow may also be used for designing in-well monitoring systems i.e. to predict which combination of sensors along with their measurement quality is required for effective well and reservoir monitoring.

Dedication

This Thesis is gratefully dedicated to my amazing wife

Mehrnoush Malakouti

whose sacrificial care for me made it possible for me to complete this work.

Acknowledgements

It is a pleasure to thank those who made this thesis possible.

I owe my deepest gratitude to my supervisors Prof. David Davies and Dr. Khafiz Muradov who provided a great support and invaluable help during this long period of my PhD study.

I wish to thank the examiners Prof. Bjarne Foss and Prof. Mahmoud Jamiolahmady for spending their time in reading this thesis and valuable comments given during the thesis examination.

In addition I gratefully acknowledge Dr. Alexander Kuznetsov from Weatherford for his great support and advice in optimisation methods.

My sincere gratitude to my colleagues in IWFsT and VAWE JIP projects: Dr. Yousef Rafiei, Dr. Ivan Grebenkin, Faraj Zarei, Morteza Haghighat, Mojtaba Moradi, Eltazi Khalid, Bona Prakasa, Akindolu Dada and Ehsan Nikjoo for their moral support and invaluable discussions.

I would like to thank all sponsors of IWFsT and VAWE JIP projects for the financial support, data provided for my study and valuable discussions and suggestions during JIP meetings as well as Weatherford and Schlumberger Information Systems for access to their software.

I greatly acknowledge the Heriot-Watt University staff for continuous support throughout this study.

I would like to thank my parents and my sisters who were far, but remained close and backed me up along the way.

My final and deepest gratitude to my wife Mehrnoush for her patience and major role in my success. She was of big importance and created a great environment for me along these years. Without her I would not have the strength to peacefully follow my path in order to make this achievement.

ACADEMIC REGISTRY
Research Thesis Submission

Name*:*	Reza Malakooti		
School/PGI:	School of Energy, Geoscience, Infrastructure and Society		
Version: *(i.e. First, Resubmission, Final)*	Final	Degree Sought (Award **and** Subject area)	PhD in Petroleum Engineering

Declaration

In accordance with the appropriate regulations I hereby submit my thesis and I declare that:

1) the thesis embodies the results of my own work and has been composed by myself
2) where appropriate, I have made acknowledgement of the work of others and have made reference to work carried out in collaboration with other persons
3) the thesis is the correct version of the thesis for submission and is the same version as any electronic versions submitted*.
4) my thesis for the award referred to, deposited in the Heriot-Watt University Library, should be made available for loan or photocopying and be available via the Institutional Repository, subject to such conditions as the Librarian may require
5) I understand that as a student of the University I am required to abide by the Regulations of the University and to conform to its discipline.

* *Please note that it is the responsibility of the candidate to ensure that the correct version of the thesis is submitted.*

Signature of Candidate*:*		Date:	

Submission

Submitted By *(name in capitals):*	REZA MALAKOOTI
Signature of Individual Submitting:	
Date Submitted:	

For Completion in the Student Service Centre (SSC)

Received in the SSC by *(name in capitals):*			
Method of Submission *(Handed in to SSC; posted through internal/external mail):*			
*E-thesis Submitted (**mandatory for final theses**)*			
Signature:		Date:	

Table of Contents

List of Figures

List of Tables

Nomenclature

A	cross sectional area before ICV
A	Weight factor defined by equation 3-7
A_o	ICV cross sectional area
a_P	sensitivity coefficient defined by equation 4-1
B	basis matrix
B	Weight factor defined by equation 3-8
B_g	gas formation volume factor
B_o	oil formation volume factor
b_P	sensitivity coefficient defined by equation 4-2
B_w	water formation volume factor
C_d	discharge coefficient based on valve position
c_d	speed of the sound down the well
C_p	Mass heat capacity at constant pressure
c_t	total compressibility
C_u	conversion factor, $(1.049 \times 10^{-3}\ in\ Field\ unit\ system)$
c_u	speed of the sound up the well
d	tubing diameter
$\bar{d}$	direction search
f	friction factor
g	gravity acceleration standard
g_c	conversion factor, (32.2 lbm-ft/(lbf-sec^2))
GOR	gas-oil ratio
h	reservoir thickness
$h_{lat,jj'}$	latent enthalpy of phase j', dissolved in phase j per unit mass
H_l	liquid hold-up
H_0	null hypothesis
H_1	alternative hypothesis
K	number of flow tests

k	displaced vertices of the simplex
K_{JT}	Joule-Thompson coefficient
k_h	horizontal permeability
k_x	horizontal permeability
k_v	vertical permeability
k_z	vertical permeability
$\left(\frac{k}{\mu}\right)_t$	total mobility
l	lower bound
L_w	horizontal wellbore length
M	total mass flow through ICV
m	reflected vertices
M_g	gas mass flow through ICV
M_P	mass flow rate
n	number of zones
neq	number of equality constraints
p_{an}	zonal annulus pressure
p_{ave}	average reservoir pressure
p_{bp}	Bubble point pressure
p_{bhp}	bottomhole pressure
p_i	initial reservoir pressure
P_P	wellbore pressure
p_r	reservoir pressure
p_{tub}	zonal tubing pressure
p_{wf}	flowing bottom-hole pressure
PI_o	oil productivity index
PI_l	liquid productivity index
r	number of constraints
R_{ci}	casing inner radius
R_s	Solubility (in-situ)
R_{ti}	tubing inner radius

r_w	wellbore radius
S	Sample standard deviation
S_p	Combined (pooled) estimator of population standard deviation
s	skin
s_c	convergence skin
s_d	damage skin
SOS	speed of sound
T	temperature
T_{an}	annulus temperature
$T_{d,ICV}$	downstream temperature of ICV
T_f	formation temperature
T_I	inflow temperature
T_{mix}	tubing and annular fluids mixing temperature
T_{tub}	tubing temperature
t	time
t_0	test statistic
$t_{\alpha/2,n-1}$	upper $\alpha/2$ percentage point of standard normal distribution of t with $n-1$ degrees of freedom
$t_{\alpha/2,n_1+n_2-2}$	upper $\alpha/2$ percentage point of standard normal distribution of t with n_1+n_2-2 degrees of freedom
t_0^*	test statistic
Q_g	well gas flow rate
q_g	zonal gas flow rate
Q_l	well liquid flow rate
Q_o	well oil flow rate
q_o	zonal oil flow rate
q_V	volumetric flow rate through icv
Q_w	well water flow rate
q_w	zonal water flow rate
u	upper bound
U_{af}	overall heat transfer coefficient between annulus and formation
U_{at}	overall heat transfer coefficient between annulus and tubing

v	fluid velocity (flow speed)
w	mass flow rate
w'	mass inflow rate per unit well length
wc	water-cut
$\bar{X}$	sample mean
X_E	estimated value of the parameter
X_T	true value of the parameter
x	Gas mass fraction
y	used to evaluate effect of interaction with adjacent layers
Z	tubing length
$Z_{\alpha/2}$	upper $\alpha/2$ percentage point of standard normal distribution of Z
Z_0	test statistic
α	simplex size coefficient defined in Equation **Error! Reference source not found.**
α	significance level
γ	parameter of the search direction
δ	uncertainty
θ	tubing angle to the horizontal
μ	Population mean
μ_g	gas viscosity
μ_o	oil viscosity
μ_w	water viscosity
ρ_f	fluid density
ρ_g	gas density
ρ_l	liquid density
ρ_m	momentum fluid density
$\emptyset$	porosity
Δp	pressure drop
ΔT	temperature drop
σ	Population standard deviation
ϑ	degrees of freedom

Abbreviations

AFI	Annular Flow Isolation
AICD	Autonomous Inflow Control Device
AICV	Autonomous Interval Control Valve
AOF	Absolute Open Flow
APF	Auxiliary Particle Filter
D	Day
DAS	Distributed Acoustic Sensing
DCS	Distributed Chemical Sensing
DPS	Distributed Pressure Sensing
DSS	Distributed Strain Sensing
DTS	Distributed Temperature Sensing
DVS	Distributed Vibration Sensor
DC	Deformed Configuration
EnKF	Ensemble Kalman Filter
EKF	Extended Kalman Filter
ESP	Electrical Submersible Pump
FBG	Fiber Bragg Grating
FD	Fluidic Diode
GNA	Gauss-Newton Algorithm
GOR	Gas-oil Ratio
GRG	Generalised Reduced Gradient
GUI	Graphical User Interface
ICD	Inflow Control Device
ICV	Interval Control Valve
ICM	Integrated Control and Monitoring
IPR	Inflow Performance Relationship
IWC	Intelligent Well Completion
I-well	Intelligent Well
KF	Kalman Filter

LMA	Levenberg-Marquardt
LP	Linear Programming
MMSCF	Million Standard Cubic Feet
MPFM	Multi-phase Flow Meter
MPFR	Multi-phase Flow Rate
OTDR	Optical Time Domain Reflectometry
P	Pressure
PBU	Pressure Build-up
PDG	Permanent Downhole Gauge
PLT	Production Logging Tool
PTTA	Pressure and Temperature Transient Analysis
PVT	Pressure Volume Temperature
RTCM	Real-Time Compaction Monitoring
RCP	Rate Controlled Production
SAGD	Steam Assisted Gravity Drainage
SAS	Standalone Screen
SCADA	Supervisory Control and Data Acquisition
SLP	Successive Linear Programming
SONAR	Sound Navigation and Ranging
SQP	Successive Quadratic Programming
STB	Stock Tank Barrel
T	Temperature
UKF	Unscented Kalman Filter
VLP	Vertical Lift Performance
VSP	Vertical Seismic Profiling
WGR	Water-gas Ratio

Chapter 1 Introduction

1.1 Motivation

Production and cost optimisation is the ultimate goal of all efforts on developing oil and gas fields. Real-time production operation systems are used to achieve these objectives through monitoring and controlling the production. These systems provide a better understanding of current state of the field and enable asset managers to make real-time decisions and efficient solutions to operational issues. Section 1.1.1 explains the production controlling to optimise the field objectives while section 1.1.2 discusses the role of reservoir and production monitoring in the real-time production operation system.

Simple nodal analysis can be adequate to optimise the production operation of single-zone single wells while commingled production systems (multi-zone intelligent well (I-well) or several wells in a single production network) require more sophisticated approach (Wang et al., 2002b). This thesis specifically focuses on the problem of flow rate allocation and production monitoring in a simpler case of multi-zone I-well, although many findings can be directly translated to a more common case of several conventional wells within a single production network.

1.1.1 Petroleum Production Optimisation

Time horizons for making optimal decisions on different aspects of petroleum production are planned in the scale of long-term, medium term and short-term. Long term decisions include drainage strategies, technologies and infrastructure development to optimise a life cycle of an asset while medium term decisions involve well location, well design and production and injection rates to manage a reservoir performance during months or a few years. Short-term operational decisions focus on rate allocation problem where the system layout together with the reservoir properties is considered fixed at this stage (Foss and Jensen, 2011). Multi-phase flow rate allocation problem is referred to allocating production rate, injection gas/water rate and lift gas rate into either single wells in a production network or individual zones in an (I-well) to achieve certain operational goals (Bieker et al., 2007). Maximisation of daily oil rate or

minimisation of production costs is the typical operational goal. However, these goals may vary from field to field with time.

The production/injection allocation problem is addressed as optimisation problems in which the control variables are optimised to meet the objective of maximising profits while simultaneously honouring all the constraints. Control variables are usually production/injection rates, lift gas rates and the well connection to the flow lines while constraints are referred to multiple capacity, safety and economic constraints. Several optimisation techniques including linear programming (Bohannon, 1970, Lang and Horne, 1983, Brown et al., 1988, Lo et al., 1995), mixed-integer linear programming (Wang et al., 2002a, Guyaguler and Byer, 2008) and sequential quadratic programming (Wang et al., 2002b, Davidson and Beckner, 2003) are proposed to solve the flow rate allocation problem. When the flow interaction among wells/zones plays an important role in the rate allocation problem nonlinear optimisation methods are preferred since they are capable of incorporating pipe and facility devices in the formulation and capturing gathering system impact of individual well/zone performance.

1.1.2 Petroleum Production Monitoring

Reservoir and production monitoring is understood as using integrated real-time measurements to identify downhole events (e.g. multi-phase flow rates) in order to aid long-term, medium term and short-term operational decisions making. Well monitoring and data acquisition is one of the main parts of the real-time production optimisation loop (Figure 1-1). This is really important especially when productions from different sources are commingled at single point. Commingled production in this study is achieved by production from a multi-zone I-well.

To date, a wide range of sensors have been introduced to the industry which are capable of either direct or indirect measurement of multi-phase flow rates. Multi-phase flow meters (MPFMs) installed downhole can measure zonal multi-phase flow rates.

MPFMs can be of different types and working principles, but in general they are quite sensitive to the fluid properties and flow regimes (Falcone et al., 2001) which make them accurate only within a limited operating range. Alternatively or additionally, algorithms are developed to calculate zonal multi-phase flow rates (MPFRs) using indirect measurements such as pressure, temperature and total well rates. These algorithms, often called soft-sensors, aim to estimate unknown zonal properties required to estimate MPFRs.

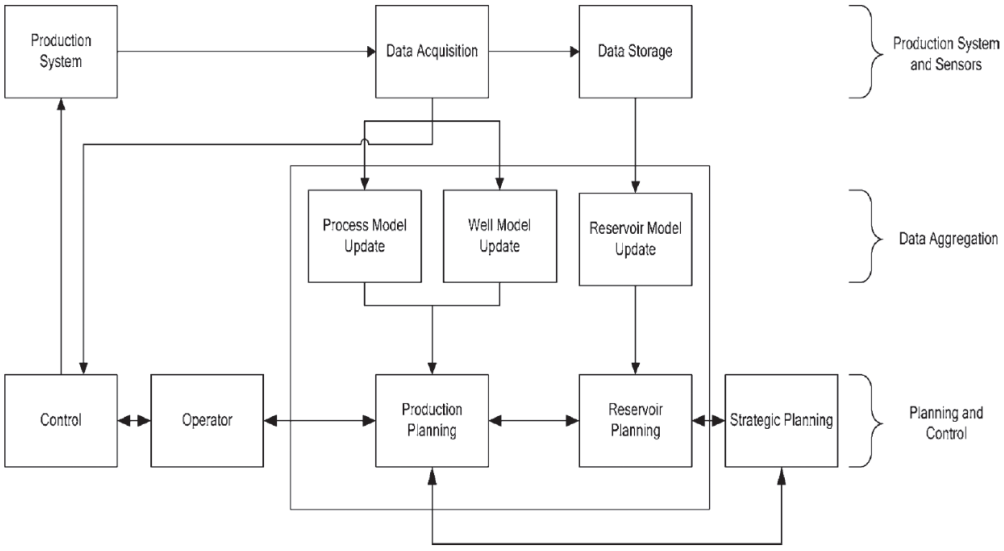

Figure 1-1 Real-time production optimisation loop (Bieker et al., 2007)

Soft-sensor techniques include side measurements together with multi-phase flow model to describe the relations between the measured information and zonal properties required for MPFRs estimation (Gryzlov et al., 2009, Leskens et al., 2008, Lorentzen et al., 2010b, Muradov and Davies, 2009b). The inverse modelling is usually implemented to estimate MPFRs until the calculated pressure, temperature and well rate match the original data. A review of techniques being used in the soft-sensing methods is given in Chapter 2. It should be noted that the principle of MPFMs technology is also based on the soft-sensing concept in which parameters of flow rate are measured in order to calculate phase flow rates. There are two approaches to measure the flow rates of a three-phase flow. The first approach measures the parameters of the flow such as a pressure drop across a Venturi, the attenuation of a gamma beam and the impedance of the mixture and then relationships are established between these measurements and flow rates of the respective phases. While the second approach involves measuring the basic parameters of phase velocities and phase cross sectional fractions (holdups) or quantities that can be explicitly related to these phase flow rates (Falcone et al., 2001).

To my knowledge, all published techniques to estimate MPFRs in multi-zone I-wells use pressure, temperature and well rate measurements for a fixed configuration of a completion. However, the active flow control valves (e.g. Interval Control Valves (ICVs)) installed downhole in I-wells can be used to perform multi-zone flow tests where their fraction of opening area (here called "position") is regulated. Additional measurements provided by these flow tests add the value to the soft-sensing technique by improving the accuracy of the estimated downhole flow rates especially when the

erroneous measurements are encountered in the algorithm. This forms the concept of active soft-sensing technique in which the estimation of zonal properties and flow rates are updated after ICVs configuration is changed to design a new flow test. A recent paper has been published by the author of this thesis to prove the applicability of active soft-sensing algorithm to estimate the multi-phase flow rates in multi-zone I-wells (Malakooti et al., 2015).

The main question of active soft-sensing technique is how to design the flow tests since engineers prefer to minimise the number of ICV operations in order to reduce the risk of operational failure. Mathematically, it is a problem of finding a relationship between the ICV's position and the objective functions defined in the soft-sensing algorithms. The latter are mainly the difference between the measured parameters and the predicted values. A derivative-free optimisation method is introduced to overcome these issues by designing the minimum number of flow tests to achieve the acceptably accurate estimation of zonal properties and, as a result, MPFRs. The optimisation method has the potential to be applied for multi-phase flow rate allocation between conventional wells where the flow tests are designed by choking the wellhead valves of the individual wells.

Multi-rate flow tests are not only used to monitor reservoir properties and inflow rates, but are also designed to maximise the production or to speed-up well start-up. The Integrated Control and Monitoring (ICM) workflow is proposed to estimate zonal properties while well production rate is maximised using the active soft-sensing algorithm simultaneously. This integrated workflow is compared against the sequential version in which the zonal properties are first estimated and then the optimum ICV configuration is determined to maximise the instantaneous oil production rate.

1.2 Thesis Scope

This thesis is devoted to develop active soft-sensing methodologies to estimate reservoir properties and monitor the MPFRs in multi-zone I-wells using integrated measurements. A multi-phase flow model is used in the active soft-sensing algorithm, which accounts for transient pressure together with a stabilised annulus and tubing pressure, temperature and well rate measurements. The algorithm is tested under two different objective function optimisations 1) maximise reliability of estimated zonal MPFRs and 2) maximise oil production rate. Then a workflow is proposed to compare the reliability of the estimated zonal MPFRs achieved by these two optimisation strategies. Finally,

guidelines are suggested to design a monitoring I-well system using multiple noisy sensors including MPFMs, pressure and temperature gauges.

1.3 Thesis Outline

The organization of this thesis can be summarized as follows:

Chapter 2 reviews the control and monitoring components installed in I-wells. These components include various types of downhole flow control valves and downhole sensors to provide production control and monitoring along individual production intervals respectively. The applications of multi-zone I-wells completed with ICVs are classified into different categories to understand the importance of multi-phase flow rate estimation in multi-zone I-wells. Then published techniques for multi-zone multi-phase flow metering are listed. These techniques may be in form of either multi-layer pressure transient testing or multi-phase flow rate soft-sensing to calculate necessary zonal parameters. The limitations of these techniques are addressed to emphasise the motivations to develop a new algorithm called active MPFR soft-sensing.

Chapter 3 presents the active MPFR soft-sensing algorithm where different optimisation parts within the algorithm are explained. Solutions to optimise the accuracy of estimated zonal properties and multi-rate flow tests are discussed. These solutions include generalised reduced gradient method to minimise the mismatch between measured information and predicted ones and deformed configuration method to design minimum number of flow tests required to estimate the most accurate zonal flow rates.

The active soft-sensing is implemented in four levels based on availability and richness of measured data set and understanding of reservoir rock and fluid properties. Level zero requires minimum set of measurements including well rates and one stabilised measured bottomhole pressure at upper completion part. Annular zonal pressures, tubing zonal pressures together with annular zonal temperature and tubing zonal temperature are added in levels one to three respectively. These levels result in determination of zonal reservoir pressures, zonal productivity indices and zonal annular gas mass fractions except level one that cannot be used to calculate zonal annular gas mass fractions. These properties are sufficient to estimate multi-phase inflow rates from different production intervals. Level four is dependent on availability of any zonal build-up tests during multi-rate test which leads to calculate zonal permeabilities and

skin factors. Additional required information regarding reservoir fluid and rock properties to implement soft-sensing levels will be summarised as well in this chapter.

The multi-phase flow model is described to formulate pressure and temperature changes across reservoir, wellbore and ICVs during multi-rate flow tests. The analytical equations are relevant to the measurements used in each soft-sensing Level.

Chapter 4 validates the active soft-sensing technique through several synthetic multi-zone I-wells modelled in a commercial, coupled, transient reservoir/wellbore simulator and a real I-well case. Commercial OLGA/ROCX^{TM} simulator is used since it captures transient hydraulic and thermal effects between reservoir, wellbore and intelligent well completions. The synthetic examples illustrate the potential of active soft-sensing to 1) estimate zonal oil, water and gas rates in oil and gas reservoirs, 2) detect the cross-flow in the wellbore between zones, 3) account for non-operational ICVs and 4) evaluate gauge drift errors. Results will be discussed in terms of optimum number of flow tests required for zonal properties to converge to their input values in the simulator.

The applicability of active soft-sensing algorithm to estimate zonal flow rates is tested for a real 2-zone I-well. Zonal multi-rate test and well build-up test are analysed to propose different steps to reduce the relative error between measured well rates and estimated ones. It is shown that production and well test history data add values to the performance of soft-sensing algorithm by estimating more accurate zonal properties.

Additionally, a normal (Gaussian) confidence interval is used to prove the algorithm robustness with respect to erroneous measurements. The errors are randomly modelled in simulated well rate and annular/tubing zonal pressures which are considered as input measurements of the active soft-sensing algorithm. It shows that satisfactory interval estimations of zonal properties are obtained using the active soft-sensing algorithm within which it is expected to find the true value of those properties.

Chapter 5 presents a workflow to design required flow tests to initiate the active soft-sensing algorithm especially when the MPFR estimation problem is applied for higher number of zones in the I-well. A reactive control strategy based on nodal analysis concept is used to obtain optimum ICVs configuration to maximise oil production. This strategy is repeated to design initial flow tests while zonal properties are updated after each flow test.

This chapter describes two approaches for controlling the production rate of a multi-zone I-well when the zonal properties are not known. A synthetic 5-zone I-well is built to compare the performance of these approaches 1) separated control and monitoring

approach 2) ICM workflow (simultaneous control and monitoring). The separated control and monitoring approach uses the active soft-sensing to estimate the zonal properties and then is followed by a reactive control strategy to design one extra flow test to maximise oil production. While the ICM workflow finds the optimum ICVs configuration to estimate the unknown zonal properties and maximise oil production at the same time.

Different optimisation objective functions are included in the ICM workflow to explore their convergence rate to either maximise oil production rate or maximise the reliability of estimated zonal properties. The comparison is conducted for ten noisy measurement samples where random errors are added into the measurements. Results are discussed to evaluate the performance of the ICM workflow using two optimisation objective functions. The ICM workflow is fast to find optimum ICVs configuration in order to maximise oil production but less accurate to predict the zonal flow rates as the flow tests are designed close to the optimum one. However, the ICM workflow provides more accurate estimation of zonal flow rates since it searches for optimum ICVs configuration in a larger search space when the objective function is maximising the reliability of zonal properties. Hypothesis testing workflow is proposed to find out whether the observations from these two optimisation strategies are true or not.

Chapter 6 extends the concept of active soft-sensing to design a well monitoring system. Sources of uncertainties are divided into errors in prediction model and measurements. The zonal properties are estimated using active soft-sensing under model uncertainty, random and drift errors in pressure, temperature and well rate measurements. The effects of measurement uncertainty on estimation of zonal properties are explained through the analytical multi-phase flow model used to estimate pressure, temperature and well rate. The sensitivity of zonal properties to erroneous measurements is also studied to investigate which zonal properties are difficult to be estimated accurately using the active soft-sensing algorithm under model and measurement uncertainties. Then guidelines recommend which physical quantities, together with their accuracy, should be measured for effective multi-phase flow monitoring.

Chapter 7 concludes the thesis with a summary of the findings and recommendations for future study.

Chapter 2 Intelligent Well Background

2.1 Introduction

There are multiple classes and designs of wells. The details depend on the well's location, the reservoir's depth and properties as well as the well's function. They may be classified into different types including exploration and appraisal, observation, production and injection based on the well objective. Today, horizontal and multi-lateral wells are often preferred to conventional wells with deviations of 60^0 or less in many reservoir situations due to their increased reservoir/well contact. This well architecture results in a number of potential advantages in terms of well productivity, drainage area, sweep efficiency and delayed water or gas breakthrough.

Moreover, long, horizontal production sections present an additional set of challenges during drilling and completion, clean-up, well stimulation and reservoir drainage control that are not encountered in conventional wells. The greater well productivity reduces the drawdown required in a horizontal well to achieve a given production rate, but this well design also leads to a significant frictional pressure drop along the horizontal wellbore. This results in a greater reservoir drawdown pressure at the well's heel than at its toe. This differential pressure, known as heel-toe effect, creates an uneven inflow distribution along the wellbore and often leads to early gas or water breakthrough at the heel (Figure 2-1). Additionally, gas and water normally have a lower viscosity than oil, resulting in the unwanted phases dominating the inflow when combined with the greater drawdown. This causes an early end to the well's economically productive life with substantial volume of unrecovered hydrocarbons being left in the reservoir. Such early breakthrough of unwanted fluids may also occur as a result of permeability variations or heterogeneity (Al-Khelaiwi and Davies, 2007).

I-well completion technology with its downhole flow control and monitoring sensors is one approach that has become widely available to the petroleum industry to solve the above challenges. A wide range of tools can be installed in an I-well to control reservoir in-flow. These include passive devices (Inflow Control Devices), active valves (Interval Control Valves) and self-adjusting devices {(Autonomous Inflow Control Devices and Autonomous Interval Control Valves)}. Information, including reservoir and well performance, must be monitored at regular intervals to provide the information

necessary to optimally adjust the active downhole flow control tools to support flow control decisions efficiently. This chapter discusses the main components of an intelligent completion including the downhole flow control valves and measurement tools which support the control and monitoring abilities of an I-well. The chapter then reviews the field applications of I-wells and essential downhole measurements required to monitor downhole events. The review highlights the importance of quantification of multi-phase flow rates along the production intervals. Finally, the publications discuss the use of indirect measurements, especially pressures and temperatures, to calculate multi-phase flow rates.

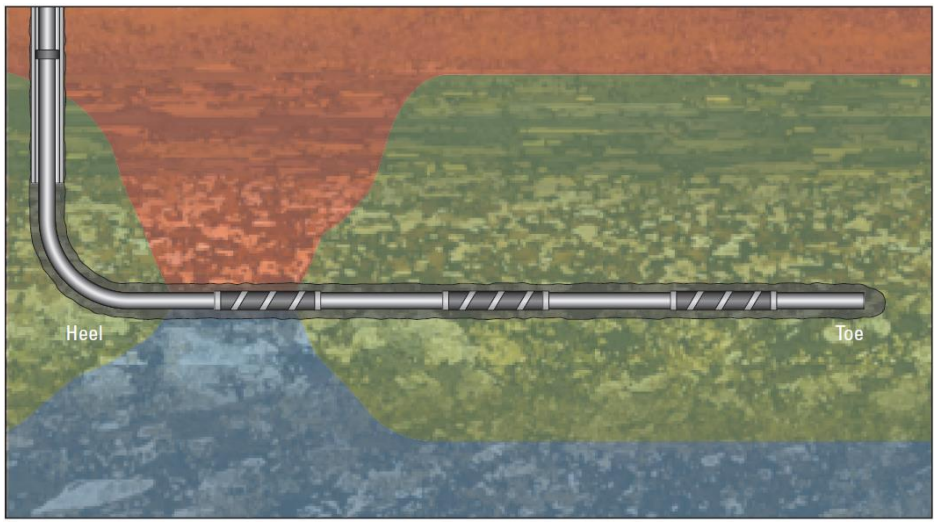

Figure 2-1 Heel-toe effect – Oil (green) from sections near toe arrives at the wellbore while gas (red) and water (blue) are inflowing at the heel (Ellis et al., 2010)

2.2 Intelligent Well Control System

2.2.1 Inflow Control Device (ICD)

An ICD is a passive downhole flow restriction installed in the well completion hardware to control the fluid flow from reservoir sandface into the tubing. The ICD improves the uneven inflow profile rate along the wellbore caused by the heel-toe effect and/or a heterogeneous permeability distribution along the wellbore (Figure 2-2). This is achieved by the ICD creating an additional pressure drop to provide a higher flow rate along the borehole sections that are more resistant to flow. This technology is regarded as passive inflow control since the size of the ICD restriction is fixed prior to the installation. ICDs delay the water or gas breakthrough into the well. However, an ICD will not reduce or stop the breakthrough of unwanted fluid once it has occurred. There

are multiple designs of ICD restrictions including nozzles, orifices, tubes, helical and labyrinthine provided by different suppliers which react differently to the flowing fluid's properties (Al-Khelaiwi et al., 2010).

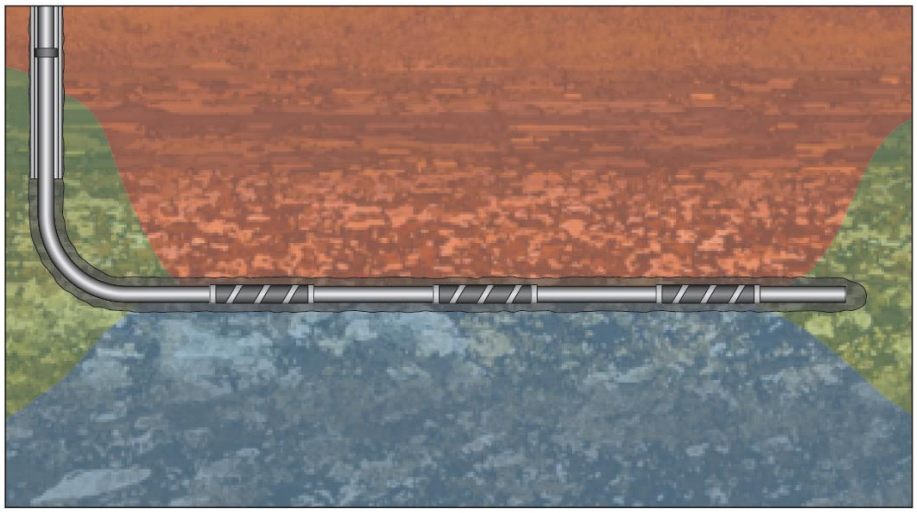

Figure 2-2 ICDs equalise the pressure drop along the entire horizontal wellbore (Ellis et al., 2010)

2.2.2 Autonomous Inflow Control Device (AICD)

An AICD not only provides the passive control of fluid influx along the wellbore, but also reactive control of the unwanted fluids (gas and water). Once the water or excess gas production occurs at the sandface formation, the device restricts the flow of unwanted fluids after breakthrough without any connection to the surface. The AICD may change the geometry of the fluid's flow path or alter the flow path. It can thus react autonomously to changes in fluid properties (Least et al., 2013). (Eltaher et al., 2014) listed the initial AICD concept designs, which have never been reported as commercial engineering developments. Commercial AICDs include the rate controlled production (RCP) valve and the fluidic diode (FD). The RCP design uses a floating disc to alter the geometry of the flow path when the fluid flowing properties change (Halvorsen et al., 2012); while the flow path of the two phases is changed in the FD AICD type based on the inertia difference between oil and water (Fripp et al., 2013).

2.2.3 Interval Control Valve (ICV)

An ICV is an active downhole valve to selectively control the inflow from (or injection to) multiple zones in one or multiple reservoirs. It is controlled remotely from the

surface through a hydraulic, electric or electrohydraulic actuation system (Al-Khelaiwi et al., 2010) and can only be operated over a limited number of the zones (e.g. 5 per well (Knabe et al. (2014), Skilbrei et al., 2003)). The ICVs are classified into three types determined by their functionality designs:

1. On/Off valves. Only two positions are present - fully open and fully closed.
2. Discrete vales. They have a fixed number, normally 10 or fewer positions.
3. Infinitely variable valves. These may occupy any position between fully open and fully closed.

ICVs are relatively expensive equipment in terms of their installational and operational cost and complexity. This is partly due to the presence of additional components, such as multi-phase flow meters and pressure/temperature sensors to monitor downhole flow conditions and rates. This valuable information is essential for efficient regulation of the ICVs using a reactive or proactive I-well control strategy (Grebenkin and Davies, 2012, Haghighat Sefat et al., 2013) to optimise the instantaneous or future production volumes respectively.

2.2.4 Autonomous Interval Control Valve (AICV)

ICDs have proved their potential to increase the production performance and oil recovery by controlling the inflow along the wellbore (Al-Khelaiwi and Davies, 2007). However, neither ICDs nor AICDs are able to shut off the zones producing unwanted fluid production completely. An AICV combines the best of the AICD and ICV (Mathiesen et al., 2011, Halvorsen et al., 2012). It is a self-regulating valve without any requirements which is installed in the completion system in the same way as ICD. Unlike AICDs, AICVs have the potential to autonomously stop unwanted fluid production after water or gas breakthrough; an action which encourages the other completion zones to increase their oil production. AICDs and AICVs are both autonomously reversible, since they react to the local fluid properties (Mathiesen et al., 2014).

Aakre et al. (2013) presented the physics behind the AICV technology which consists of two different flow restrictors (laminar and turbulent flow) placed in series. The engineering development of this technology is still in the testing stage. Their simulation results showed an increase in oil recovery when the horizontal well was completed with AICVs rather than ICDs. Later, Aakre et al. (2014) performed experimental tests with

gas, oil and water together with reservoir simulations to confirm the significant increased recovery by deploying AICV technology in the field suffering from excessive gas or water production. (Eltaher et al., 2014) published the first AICV modelling workflow for integrated well/reservoir simulators that allow engineers to evaluate the viability of an AICV completion and its potential added value. They used simulation results from a box-shaped reservoir model to compare AICV performance with standalone screen (SAS) and ICD completions.

2.2.5 Annular Flow Isolation (AFI)

The fluid flow in the annular space between the completion tubular and the sandface or the cemented and perforated casing is known as annular flow which occurs due to several reasons such as 1) relatively large annulus flow area compared to the area of the tubing, 2) permeability contrast along the wellbore, 3) commingled production from zones with different pressures 4) poor gravel packing of the annulus area and 5) uneven collapse of the formation around the tubing (Al-Khelaiwi, 2013). The AFI tools range from conventional isolation packers to gravel packs. The former is the most common type used in the well completion while the latter is usually applied to minimise the sand production and causes high well impairment. The AFI strategy mitigates the effect of water coning or gas cresting through fractured zones, halts annular flow between compartments and allows for isolation of potential wet zones. MoradiDowlatabad et al. (2014) developed a new AFI design workflow that accounts for well's lifetime performance while the previous designs were based on either a single well parameter or static well/reservoir model that do not consider the lifetime benefits of the technology. The annulus pressure was used as a key parameter in the workflow to improve the design of AFI number, location and types.

2.3 Intelligent Well Monitoring System

Intelligent completions consist of reliable downhole sensors for in-well monitoring, adding the value by optimising production and forewarning operators of problems so that preventive or corrective actions can be taken (Eck et al., 2000). Downhole sensors measure different physical quantities including pressure, temperature, flow, acceleration (seismic and acoustic) and strain for downhole, near wellbore monitoring. Deeper reservoir monitoring requires the measurement of new physical quantities such as

permanent, in-well seismic, electromagnetic method and streaming potential, which are still in the early stages of development. These measurements are transferred to the acquisition unit at surface through cable and then stored in a data historian for easy access.

Downhole sensors are usually classified into electronic or optical (based on permanent mechanism) and single point, quasi-distributed and distributed (based on the number of monitored points). Quasi-distributed sensors measure the physical quantities at a distinct number of positions across the reservoir or interval of the interest while distributed sensors monitor the same physical quantity at a spatial resolution as small as 0.5 m. Surveillance of the completion's inflow efficiency using multiple tracers is also possible. Their ability to provide quantitative information on the inflow along the completion design have been proved in the field (Williams and Vilela, 2012, Williams and Brough, 2012, Montes et al., 2013, Nutricato et al., 2013).

2.3.1 Electronic sensors

Since the 1930s operators deployed mechanical gauges in the wells to capture downhole pressure data (Ennaifer et al., 2014). Electronic gauges were introduced in the oil industry in the 1970s as the electronic design and reliability were improved by Hewlett-Packard Company. Both strain and vibrating quartz electronic gauges were widely used within the industry. Quartz gauges eventually became the standard permanent downhole gauge (PDG) for measuring downhole pressure and temperature due to their superior metrological. Strain gauges operated on the principle of a resistance circuit placed on a pressure sensitive diaphragm and were capable of 0.1 psi resolution. In contrast, quartz gauges used the piezo-electric effect to measure the strain caused by pressure imposed upon the sensing mechanism. A typical resolution of a quartz pressure gauge is 0.01 psi (Ennaifer et al., 2014). Permanent downhole gauges prevent hazardous well interventions as well as provide continuous data measurements without the costs associated with wireline-conveyed downhole surveys (production logs). Da Silva et al. (2012) reviewed the intelligent well monitoring systems, their availability, applicability and limitations. They listed the available electronics sensors for both near wellbore and deep reservoir monitoring as:

- Single-point pressure and temperature
- Quasi-distributed temperature
- Single phase and two-phase flowmeter

- Streaming potential
- Permanent 3D resistivity
- Permanent downhole seismic

Recognition of the value of permanent downhole monitoring resulted in an increasing number of electrical gauges being installed in wells during the late 1980's and into the 90's. However, the application of permanent electrical-based sensing system is more limited than the opportunities offered by fiber optic based sensing systems.

2.3.2 Fiber Optic Sensors

Downhole fiber optic sensors were introduced to the oil and gas industry more than 20 years ago. The first in-well fiber optic pressure /temperature sensor was installed successfully in a land well in Netherlands in 1993 (Drakeley et al., 2006). Fiber Bragg Grating (FBG) technology provides the fiber optical alternative to the electronic single point and quasi-distributed sensors. Multi-drop technology allows an electronic quasi-distributed sensor to incorporate a large number of sensors on the same cable (>45) (Da Silva et al., 2012). FBGs are essentially reflectors built inside the core of an optical fiber. They are created by exposing the core of single-mode fiber to the high power ultraviolet laser beams (Figure 2-3). The exposure produces a permanent increase in the refractive index of the fiber's core, creating a fixed index modulation called a Bragg grating. A portion of the beam continues to travel (transmitted) whereas a portion is reflected back when light passes through this grating with the reflection being limited to grating's wavelength. External factors such as vibration or heating cause shift in the wavelength of the reflected light. These variations can be translated into physical engineering units such as temperature, amplitude and strain. These FBG measurements are not technically distributed since the monitoring measurements are only made at a large number of distinct points along the length of the fiber (Figure 2-4).

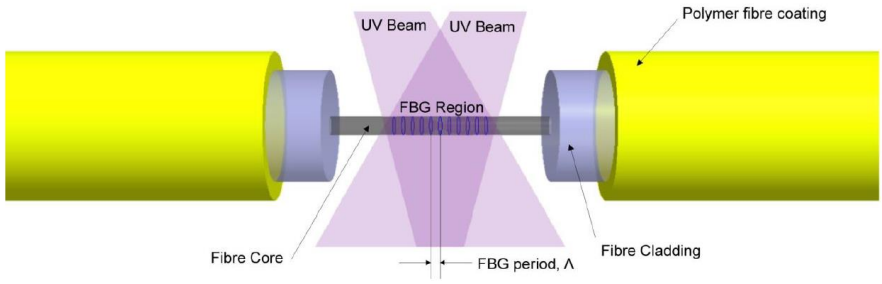

Figure 2-3 Principle of a FBG (Hunter, 2014)

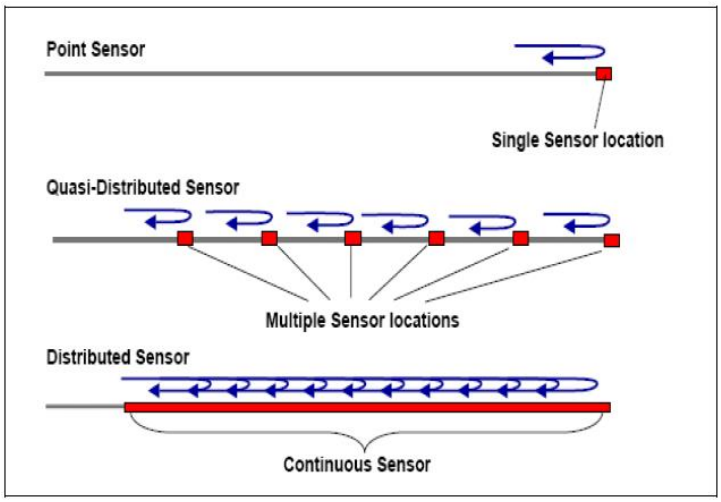

Figure 2-4 Different fiber optic sensing configurations (Molenaar et al., 2012a)

Figure 2-5 compares the basics of electronic and fiber optic systems. Fiber optic technology is being developed as a replacement of traditional electronic sensors due to their intrinsic capacities (Stalford et al., 2014):

- Distributive sensing
- High-bandwidth, low-loss transmission, high information transmission rates (1×10^{12} bites/second)
- No downhole electronics that degrade at elevated temperatures,
- Immunity to electromagnetic radiation
- Flexible configurations, greater sensitivity
- Very thin and relatively cheap with multiple fibers being installed to create system redundancy

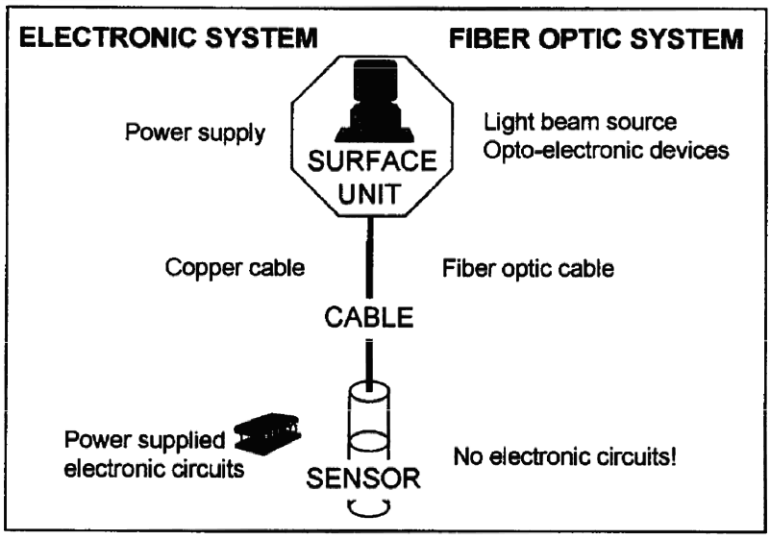

Figure 2-5 Basics of electronic and fiber optic systems (Botto et al., 1994)

Distributed temperature sensors were the first application in which fiber optic cable was used as a distributed measurement medium. The principle of distributed fiber-optic systems is based on emission of a light pulse by a laser at the surface. A small amount of the light is naturally scattered in the fiber and returns to the surface when a light pulse travels down an optical fiber. The backscattered light is made up of different spectral components; Rayleigh, Brillouin and Raman bands (Figure 2-6). Raman scattered light is much weaker and harder to detect compared to the other spectral components. Both Raman and Brillouin bands have a frequency shifted with them called the Stokes and anti-Stokes components towards shorter wavelength (higher frequency) while Rayleigh scattering has no frequency shift associated with it. Raman based detection systems are limited to about 8 km whereas Brillouin and Rayleigh based systems can be extended to around 50 km (Eisler and Lanan, 2012). Currently, the surface sensor units can measure a wide range of subsurface distributed parameters: (1) temperature sensing (DTS), (2) pressure sensing (DPS), (3) strain sensing (DSS), (4) acoustic sensing (DAS) and (5) chemical sensing (DCS) (Koelman et al., 2012). The metrological specifications and basic principles of the technology of available fiber optic sensors to monitor the near wellbore and deep reservoir events have been summarised by Da Silva et al. (2012).

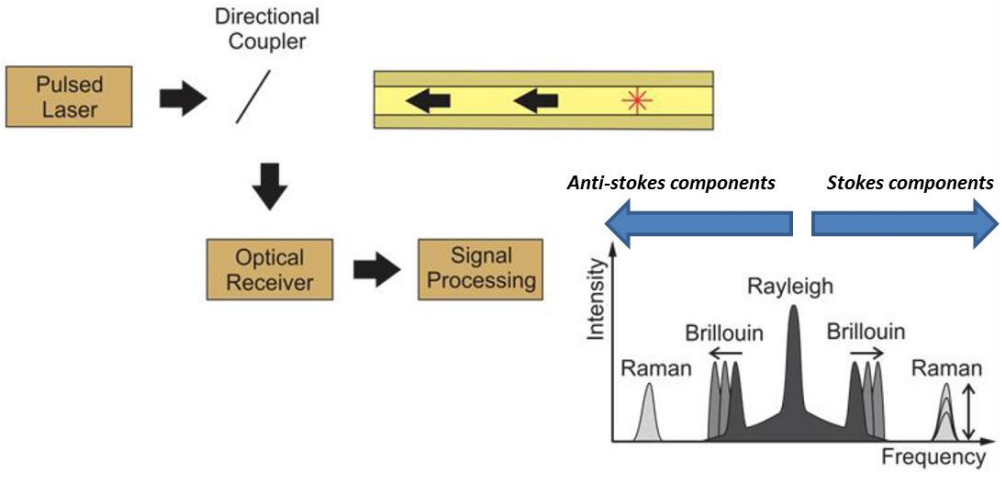

Figure 2-6 Backscattered light spectrum (Da Silva et al., 2012)

The fiber optic technology forms the backbone of a well and reservoir surveillance capability that provides a more complete picture of relevant downhole processes and events in contrast to electronic sensors only. However, application of the technology has created challenges in well data management due to the volume of data, but has also

highlighted the lack of quantitative processing and interpretation workflows (Koelman et al., 2012). Figure 2-7 indicates how the downhole data management challenges has increased with the progression from PDGs to fiber optic DTS followed by fiber optic systems integrating multiple distributed sensing measurements. Measurement combinations such as DAS, DTS and DPS have the potential to enhance downhole flow monitoring; though their use is currently limited to qualitative data interpretation only. Further advances in the modelling of the underlying physics together with the development of robust interpretive methodologies are required before quantitative analysis of all types of data measurements becomes possible. Moreover, the cost of fiber optic deployment needs to be reduced below the typical current costs along with improving the effectiveness and robustness of the installation for integrating it into the oilfield standard set (Koelman et al., 2012)

.

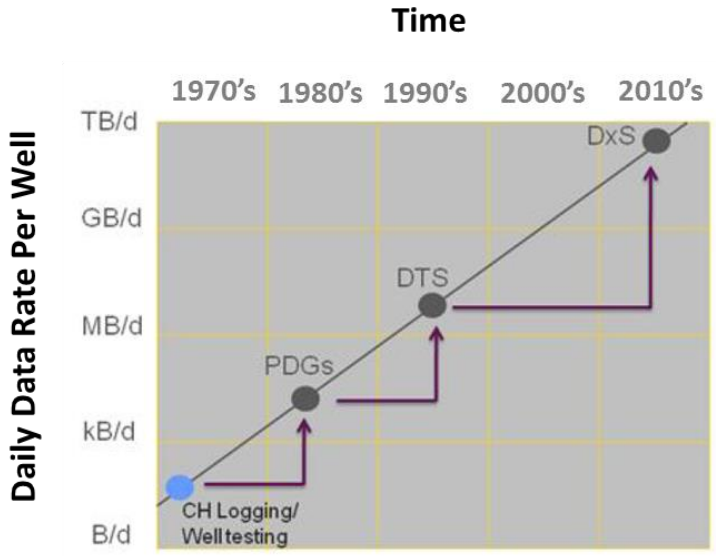

Figure 2-7 Trend line showing the downhole sensing history with daily data rates per well (Koelman et al., 2012)

2.3.3 Distributed Temperature Sensors

Steam flood enhanced oil recovery operations were the first large scale onshore oil field applications of DTS fiber optic technology. Such application is challenging as the fiber is exposed to high temperature (around 400 ^{o}F) downhole environment (Karaman et al., 1996, Carnahan et al., 1999). This required improvements to be made in optical fiber manufacturing technology before permanent installation at such high temperatures could be envisaged. Other successful applications of DTS have been reported in

offshore North Sea oil field environments with conventional oil production and water injector wells (Woodrow and Drummond, 2001, Brown et al., 2000). Later, this technology became an integral part of intelligent wells to provide downhole monitoring and control of multiple producing zones (Tolan et al., 2001). DTS can be installed in cables or inside the control lines to take the measurements along the entire length of the wellbore. However, operators have traditionally decided not to deploy the DTS over the reservoir interval of the lower completion due to complexity of the completion especially for many offshore wells where connecting cables and hydraulic lines between the upper and lower completions is extremely problematic (Algeroy et al., 2010).

DTS, the most popular sensing option with at least a thousand logging and permanent installations to-date (Johannessen et al., 2012), uses the interaction of the source light with thermal variations (Raman scattering) to determine the temperature at multiple points (typically 1 m apart) along the fiber. As the fiber is sensitive to the temperature, the intensity of frequency shifts in the anti-stokes band (measuring difference between Stokes and anti-Stokes components) is used to quantify the temperature value.

A large number of publications have addressed the potential of DTS in different downhole applications such as steam injection/production profiling (Foo et al., 2014, Rahman et al., 2011, Wang and Bussear, 2011), multi-phase flow rate allocation (Muradov and Davies, 2009b), cross-flow between zones identification (Oftedal et al., 2013), detection of scale and wax deposition (Al-mutairi and Davies, 2008, Guzman, 2012), hydraulic fracture diagnostics (Tabatabaei and Zhu, 2012), acid treatment optimisation (Sharma et al., 2010), gas lift systems optimisation (Brown et al., 2005)and well integrity diagnostics (Gonzalez et al., 2012).

2.3.4 Distributed Acoustic Sensors

The first field trial of DAS technology was conducted by Shell Canada during the completion of a tight gas well in February 2009 (Molenaar et al., 2012b). DAS is more promising due to its potential to monitor the well and reservoir properties and use these information for production optimisation to a level that is not possible with DTS alone. The technology is based on optical time domain reflectometry (OTDR) where the mean intensity of the Rayleigh backscattered light is used to determine the optical loss along the fiber (Figure 2-8).

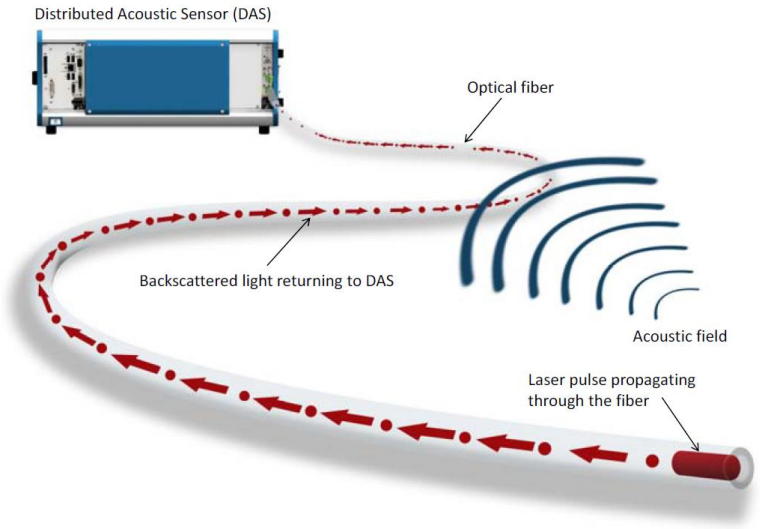

Figure 2-8 Principle operation of DAS (Johannessen et al., 2012)

Fiber optic cables may be manufactured as either single-mode or multi-mode. Single-mode fibers require only one axis in which the light is allowed to travel down the fiber. On the other hand, multi-mode fibers allow the light to travel down the fiber in transverse mode such as helically (spiral) and zig-zag modes as illustrated in Figure 2-9.

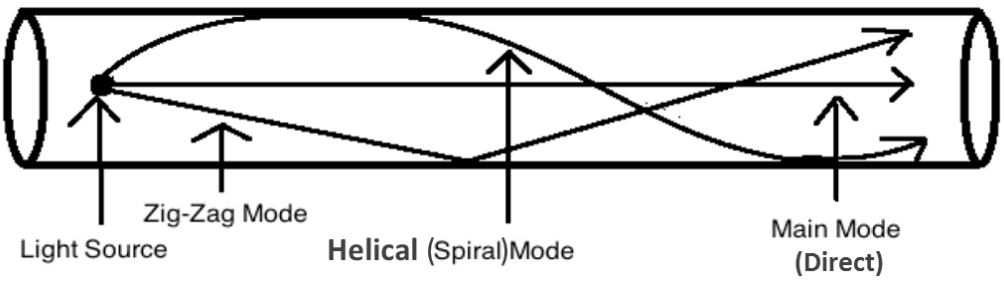

Figure 2-9 Modes of light travelling down a fiber (Cannon and Aminzadeh, 2013)

The added value achieved by DAS technology has been proved in a wide variety of downhole applications:

a) Hydraulic fracture monitoring: Some vendors install DAS for near wellbore monitoring during hydraulic fracturing jobs to detect the setting of the packers, dropping of the balls, movement of the sliding sleeve valves, effectiveness of frac ball diverters and fluid flow detection either behind the packer or through the perforations. The location and intensity of noise due to fluid flow is also used to quantify the amount of fluids accepted by formation during individual fracturing stages. Several case histories have shown how DAS was able to

monitor these events (Molenaar et al., 2012a, Molenaar et al., 2012b, MacPhail et al., 2012).

b) Flow profiling: DAS has great advantages over production logs that it does not require an intervention and are prone to errors. It provides information on the location of the production inflow or injection (In 't Panhuis et al., 2014). Gas production is also recognised due to generation of higher frequency noise than observed with oil production. Oil produces an even lower frequency signal than water. A library of noise profiles corresponding to different flow regimes have been developed to predict the rate and phase of flow contributions from perforations (Cannon and Aminzadeh, 2013).

c) Well integrity monitoring: Leaks through or behind the casing due to poor cementing or formation geomechanical changes can be localized using installed permanently DAS or a light well intervention by temporarily installing a fiber in the well. Advances in both DAS and processing algorithms provide monitoring system for a wide variety of leak scenarios, including low rate leak detection, multiple source leaks, pipe integrity failures, zonal isolation issues, long term well monitoring, CO_2 storage and monitoring and evaluating intervention effectiveness (Hull et al., 2010).

d) Vertical seismic profiling (VSP): VSP is a geophysical technique to generate velocity maps of the surrounding formations. DAS down-hole acquisition is inherently simpler, safer and faster than traditional acquisition with geophones, hydrophones and accelerometers downhole in that the entire well is covered with a single shot. Such VSP measurements have a reduced cost; can be easily made and show a better repeatability. For example, DAS has been used to record the VSP data which is in turn utilised to monitor CO_2 saturation profile changes over time and the effectiveness of the containment of CO_2 in carbon capture storage projects. It can also provide accurate VSP images in very deep formations or in slim-hole environments (Mateeva et al., 2012, Mestayer et al., 2011).

e) Gas-lift optimisation: Real-time monitoring of the gas-lift performance as reservoir and fluid properties change over time can be used to increase the well's production. DAS is capable of tracking the velocity of the slug flow along the tubing and recognising the opening and closing of individual gas-lift valves (Johannessen et al., 2012, Koelman et al., 2012).

f) Sand detection: The acoustic energy emitted by produced colliding with the fiber can be detected directly by DAS. It enables operators to modify choke settings immediately, thereby reducing wear on the pre-installed screens and maximising the production (Cannon and Aminzadeh, 2013).
g) Electrical submersible pump (ESP) monitoring: DAS is able to predict the ESP failures by monitoring the changes in the acoustic output of the ESP from the baseline signal at time when it was operating properly. In addition, pump rates can be optimised if the ESP and fluid movements in the well are monitored with DAS. An increased efficiency of a Steam Assisted Gravity Drainage (SAGD) project in heavy oil reservoir can be achieved (Cannon and Aminzadeh, 2013).

Gas breakthrough detection is one of the possible applications with current capabilities of DAS while multi-phase flow measurements and micro-seismic monitoring are the unproven applications of DAS that have potential in the years to come (Cannon and Aminzadeh, 2013).

Distributed vibration sensors (DVS) (Shatalin et al., 1998) also provide local vibrational disturbances along the fiber. They have been introduced into the oil and gas industry in a number of applications such as detection of sand production (Mullens et al., 2010). DVS technology is based on interference effects that are associated with the OTDR signal. However, these sensors are not able to determine the full vector acoustic field – the amplitude, frequency and phase – of the signal. There is no accepted generic architecture for a DAS system. This means that there is a large variation in the fundamental design and performance of systems marketed as distributed acoustic sensors. For example, the distributed vibration sensors described above are often described as DAS systems (Parker et al., 2014).

The combination of DAS used in conjunction with DTS can provide more reliable flow information about downhole applications such as hydraulic fracturing and SAGD ESP monitoring. Several DTS and DAS deployments were carried out in Shell Canada's tight sand and shale gas fields in 2009 and 2010 to monitor hydraulic fracturing operations in real-time (Molenaar et al., 2011). These measurements are recorded during hydraulic fracturing and flow back operations to provide post-job diagnostics and analyses of the stimulation. For example, DTS measurements displayed the cooling effect of a zone taking fluid during a hydraulic fracturing job. However the DAS data showed that this observation was erroneous due to the absence of acoustic energy related to injection (compare real-time DAS and DTS data recorded for perforated zone

#9 in Figure 2-10 and Figure 2-11 respectively). Figure 2-11 shows cooling at zones #10, #9 and #8 after the hydraulic fracture initiation, indicating these zones are open for injection while real-time DAS data confirms that zone #9 was most probably not being properly stimulated. The evenly distributed temperature along zones #10, #9 and #8 appears due to good thermal contact with the fibre optic cable and the casing.

DTS readings also identify which zones are hottest and contributing to production in SAGD operation while DAS data confirm this assumption as fluid movement can be seen around these same regions (Figure 2-12).

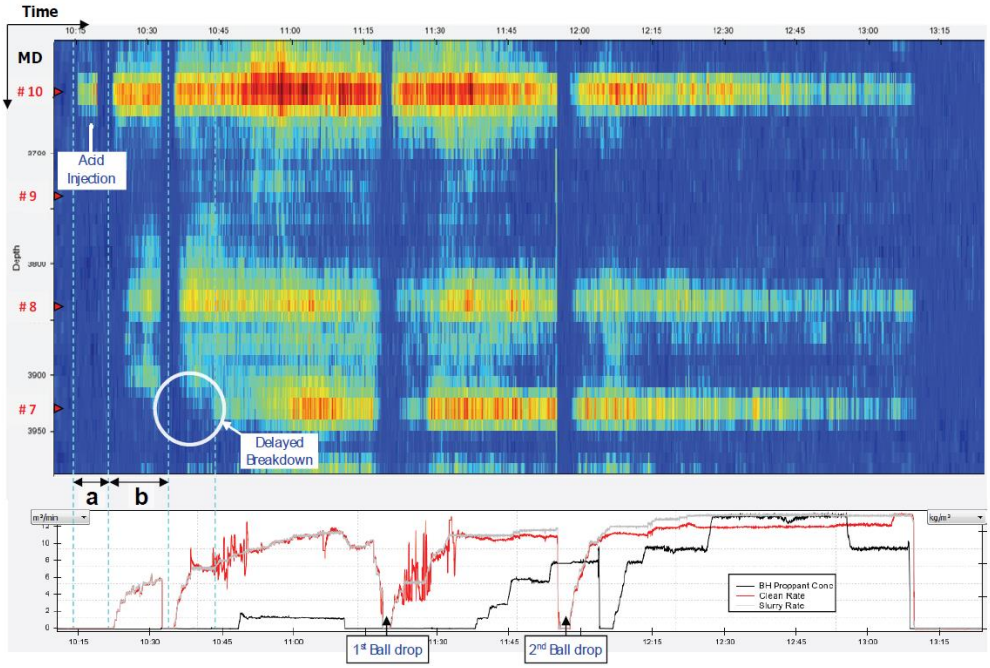

Figure 2-10 DAS measurements from a horizon wellbore during a hydraulic fracturing treatment. The colour shows the acoustic energy level (red is high and blue is low) (Molenaar et al., 2011)

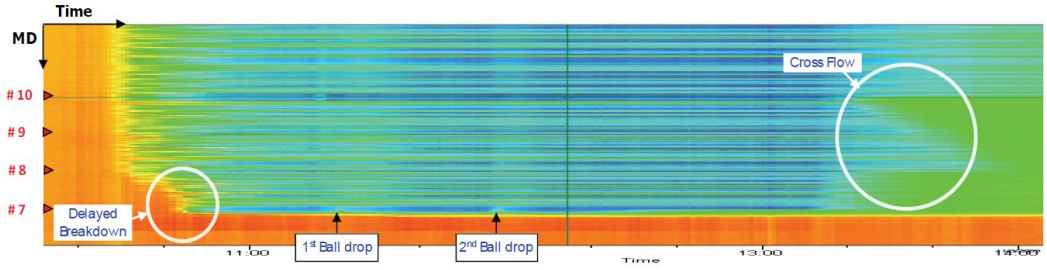

Figure 2-11 DTS measurements shows cooling at all perforations after the hydraulic fracturing initiated (red is hot and blue is cool). (Molenaar et al., 2011)

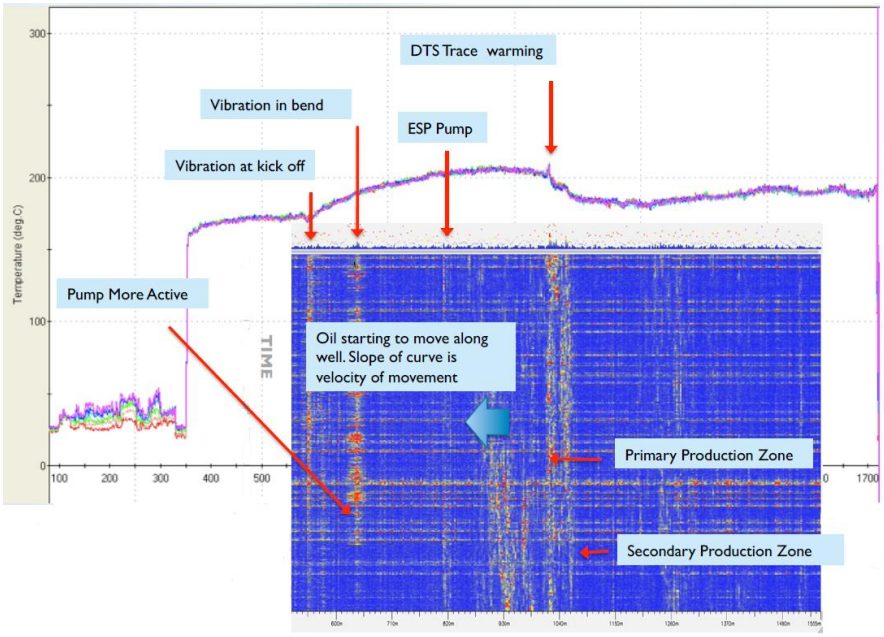

Figure 2-12 DTS and DAS readings on SAGD well (Cannon and Aminzadeh, 2013)

2.3.4.1 DAS Data Analysis

DAS measurements record the propagated acoustic energy along the optical fiber deployed along the wellbore. The measurement system uses a digital optoelectronics detection technique to capture the amplitude and phase of the acoustic waves over a wide frequency (1 mHz – 100 kHz) and high dynamic (>120 dB) ranges (Xiao et al., 2014). A frequency-wavenumber (f-k) plot can then be generated by use of a powerful array processing techniques. The Doppler shift induced by moving fluid between the up-going and the down-going speeds of sound can be used to estimate the fluid velocity along the wellbore (Johannessen et al., 2012, Xiao et al., 2014, Xiao et al., 2013b). Figure 2-13 shows an example of frequency vs. wavenumber (f-k) plot in which the 'V' shape corresponds to detection of sound travelling at a single speed.

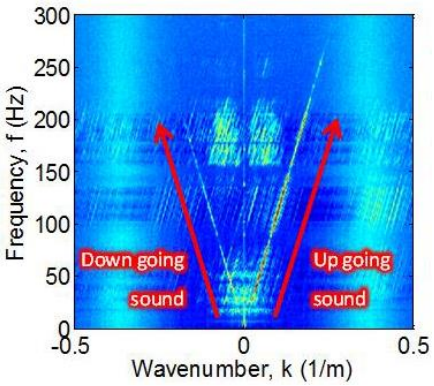

Figure 2-13 frequency-wavenumber plot (Xiao et al., 2013a)

The speed of sound and flow are calculated by measuring the speed of sound in both up and down directions within the well (Da Silva et al., 2012).

$$v = \frac{c_u - c_d}{2} \quad 2\text{-}1$$

$$SOS = \frac{c_u + c_d}{2} \quad 2\text{-}2$$

In above equations, v and SOS represent the flow speed and speed of sound and C_u and C_d are speed of the sound up and down the well respectively. The speed of sound is affected by fluid compositions as well as the completion materials and structure. Different phases (oil, gas and water) and materials e.g. steel will have the different speeds of the sound associated with them. Variations in cross section dimensions result in changes of the speed of the sound which can be used to monitor the fluid flow through the inflow devices and confirm the valve's open position.

2.3.5 Distributed Strain Sensors

DSS allows operators to detect casing deformation trends and to prevent future well failure, but can also yield valuable information on the reservoir's geomechanical response to production or injection (Earles et al., 2010, Pearce et al., 2010). DSS is also expected to be practical for long-term well and cement integrity and fluid containment monitoring in CO_2 sequestration wells. Three-dimensional images of well deformation at a fine spatial resolution can be obtained by helically wrapping the optical fiber around casing, sandscreen or well tubular. If DSS data is acquired in combination with DTS data, the measured strains can be decomposed into mechanically and thermally induced strains. DTS system is sensitive to thermal effects only while the DSS respond to both mechanical and thermal strains and generate data at a higher spatial resolution. Combined DSS and DTS technology is based on Brillouin scattering occurred due to interaction between the propagating optical signal and an acoustic wave giving rise to frequency shifted component. The diffracted light intensity caused by the acoustic wave propagates at the acoustic velocity in the fiber. The acoustic velocity is directly related to the medium density which is temperature and strain dependent. Therefore, the Brillouin frequency shift carries the information about the local temperature and local strain of the fiber (Ravet et al., 2013).

Pearce et al. (2010) developed the real-time compaction monitoring (RTCM) system for continuously monitoring of well deformation and integrity. The RTCM technology was verified by deploying successfully in both experimental tests and real land wells.

Figure 2-14 indicates combined DSS/DTS data obtained in a surface test of horizontal gravel pack installation in which thermal and mechanical perturbations on the sand control system are shown in the right and left hand sides respectively.

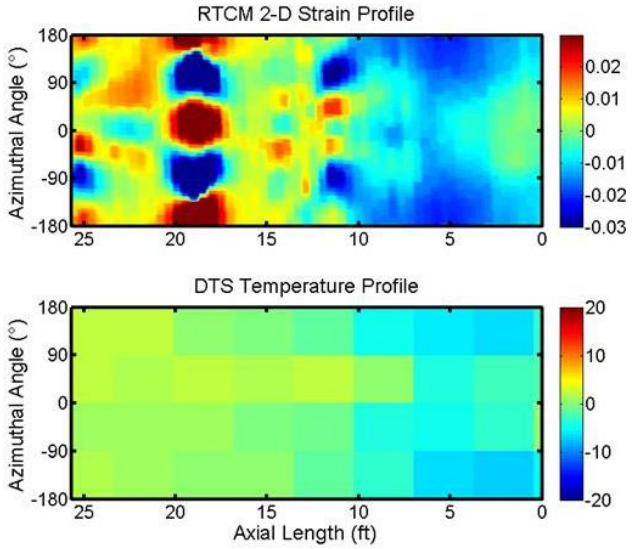

Figure 2-14 DSS/DTS data obtained in a horizontal gravel pack installation test (Pearce et al., 2010)

The principle of passive sound navigation and ranging (SONAR) technology used in the optical fiber single phase and two-phase flowmeter is based on dynamic strain changes in the well completion caused by pressure fluctuation due to the turbulent flow are measured (Gysling and Loose, 2003). The strain is measured by an array of optical, spatially distributed strain sensors located on the outer surface of the pipe. Downhole, multi-phase flowmeters have been installed in a maximum reservoir contact well in Saudi Arabia (Unalmis et al., 2010). The three laterals of the smart well were equipped with ICVs and the permanent monitoring system included three 2-phase optical flow meters integrated with pressure and temperature gauges. This permanent downhole flowmeter operates satisfactorily over a wide range of pressures, temperatures, mixtures of fluids and flow regimes, but is only suited to relatively high rate wells.

2.3.6 Distributed Pressure Sensors

The technology to develop DPS has long existed, but the investment to develop and deploy a fully qualified sensing system has not materialised due to the lack of clear value statement. There are several techniques can be used to develop this sensing technology (Da Silva et al., 2012, Drakeley et al., 2006):

a) Brillouin scattering: Frequency shift of the backscattered light is dependent on the local strain and consequently on the local pressure. However, high accuracy pressure measurements (<1 bar) is difficult to attain. Combination of Brillouin and Raman backscatter may also be exploited to measure both distributed strain/pressure and temperature.
b) Optical fiber polarimetry: Pressure affects the local polarisation properties of the fiber (birefringence). Backscattering measurement techniques can be used to determine the spatial distribution of these properties and hence pressure distribution along the fiber.
c) FBG sensors are the alternatives to the true DPS. Changes in the local strain, which is related to the local pressure, cause a shift in the reflected wavelength. A number of FBGs can be positioned along the same fiber with spatial separation down to a few centimetres to form a quasi-distributed sensing network (Hunter, 2014).

Farshbaf Zinati et al. (2010) examined theoretically the possibility of estimating the near-wellbore permeability from distributed pressure measurements in the well. They presented an inversion algorithm using a semi-analytical model and/or adjoint formulation to compute the necessary gradient information.

2.3.7 Distributed Chemical Sensors

DCS is the latest version of a distributed fiber optic sensor. It is being developed by TNO, a Netherlands-based R&D organisation, together with Shell. A polymeric coating on the outside of the fiber deforms in the presence of a specific chemical compound and stretches the FBG (Figure 2-15). The observed shift in the wavelength provides quantitative information on the concentration of the chemical component. This technology is not mature, but is expected to become available in the next few years. Potential applications range from production and IOR/EOR monitoring (e.g. water breakthrough and injected EOR fluids tracking) to HSE and containment monitoring (e.g. CO_2 and H_2S) (Koelman et al., 2012, Koelman et al., 2011).

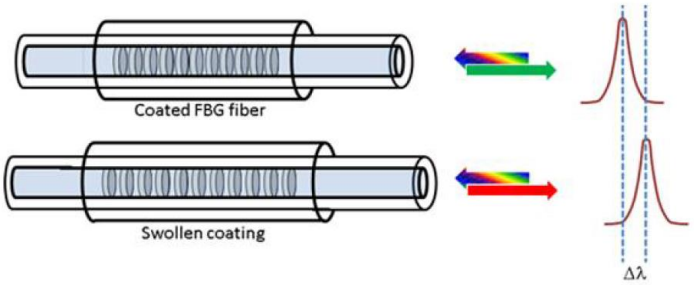

Figure 2-15 Working principle of a DPS (Koelman et al., 2012)

2.4 Intelligent Well Applications

One purpose of installing intelligent wells is reservoir management optimization; either through acceleration or maximization of oil production. Intelligent well completion provides a conventional well with the ability to install, operate, monitor and control the completion without a well intervention. Purpose of intelligent well completion depends on monitoring and controlling areas in which an intelligent well is designed to be useful. This thesis divides the application of intelligent well or field into four categories, all of which allow an added value to be created by a simple ICV completion in a vertical/horizontal/slanted well or a multi-branch completion with ICVs:

1. Commingled Production
2. Fluid Transfer for Sweep, Pressurisation or Lifting
3. Well Stimulation
4. Data Acquisition

Relevant information must be available to the advanced completion in order to achieve the potential added value in each category. The valuable information acquired through downhole sensor helps field operators to optimise the performance of the production and injection wells. The following sections explain each category with examples of their successful application in the industry together with the downhole sensors required to obtain key information.

2.4.1 Comingled Production

Commingling production manages the flow in wells that intercept more than one hydrocarbon-bearing zone (either reservoir or layer) (Figure 2-16). It can deliver the maximum well potential, but reservoir management remains a concern. ICVs are capable of controlling the uneven, invading fluid fronts that may have developed along

the wellbore length due to permeability differences, reservoir compartmentalisation or different strength aquifer/gas cap support (Ebadi, 2006).

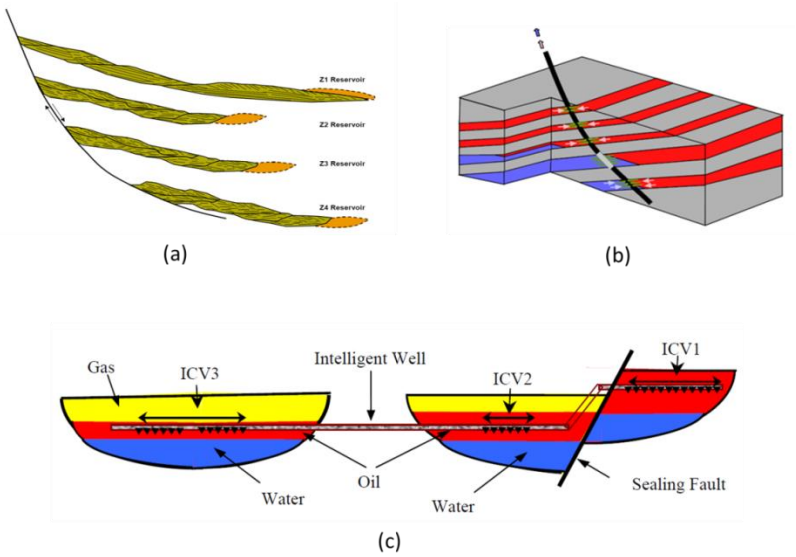

Figure 2-16 Commingled production from different sands using an IW, (a) (Rester et al., 1999), (b) (Ebadi, 2006) and (c) (Ebadi et al., 2005)

Ebadi et al. (2005) investigated the applicability of the intelligent well system technology in a wide range of reservoir types (layered, fractured, channelised, etc.) where the oil production is improved and water production is reduced with the correct choice of the number of ICVs and their location along the length of the wellbore. Reservoir simulation studies revealed that the appropriate intelligent completion scenario has the potential to improve the project economics and accelerate the production in deepwater Gulf of Mexico field that consists of several stacked sandstone reservoirs separated by shales (Rester et al., 1999). The first intelligent well in this field was completed with stacked gravel packs to produce two independent zones. The intelligent completion allows monitoring the pressure and temperature from either zone and producing from the lower zone, the upper zone, either zones, or neither (Jackson and Tips, 2001). Yu et al. (2000) used a simplified simulation model of a typical North Sea field case to quantify the benefits of installing ICVs in slanted wells and multi-lateral wells. The intelligent multilateral wells allow the completion to the uncertainty of the reservoir (presence of a continuous permeability barrier and size of the aquifer) being compensated for by the well's intelligence.

Control production approaches using intelligent well completions to improve reservoir management are not applicable without knowledge of downhole flow information. Oil,

water and gas flow rate profiles along the wellbore length together with sand production are the main information required to optimise the commingled production from multiple zones. A number of approaches including periodic production logging tool (PLT), geochemical fingerprinting, downhole pressure/temperature combined with multi-rate tests, acoustic passive listening, employing valves and downhole gauges as flow meters, venture or fiber-optic flow meters or testing zones by regulating ICVs have been suggested to obtain either qualitative or quantitative estimations of downhole multi-phase flow rates (Glandt, 2005). DAS/DVS measurements have enabled operators to identify the sand entry depth and the corresponding sand production intervals, eliminating the need for further high risk well interventions. Table 2-1 lists the measured information together with required sensors to control inflow rates in a commingled production system.

Table 2-1 The information and downhole sensors required to control the commingled production

Information Measured	**Sensor Type**	**Number of Monitored points**	**Technology Employed**	**Level of Maturity of Data Processing**
Water/gas/oil flow rate profile	Single phase & Two phase Flow Meter	Single	Fiber optic/ electronic	Mature
	Single, Two or Three Phase Flow Meter	Quasi-distributed	Fiber optic	Mature
	Temperature & pressure	Single/Quasi-distributed/ Distributed	Fiber optic/ electronic	Mature
	Acoustic	Quasi-distributed/ Distributed	Fiber optic	Qualitative rather than Quantitative
Sand Production	Acoustic	Single/quasi-distributed/distributed	Fiber optic	Mature
	Vibration	Distributed	Fiber optic	Mature

2.4.2 Fluid Transfer for Sweep, Pressurisation or Lifting

This category includes all the applications in which water or gas transfer results in oil production increase through different operations such as:

1. Internal gas lift operation to reduce the hydrostatic head of the oil column in the well (see Figure 2-17)
2. Gas injection into the gas cap overlying the oil reservoir for pressurisation (see Figure 2-18)
3. Water or gas flooding into the oil reservoir for sweep efficiency improvement (see Figure 2-19)

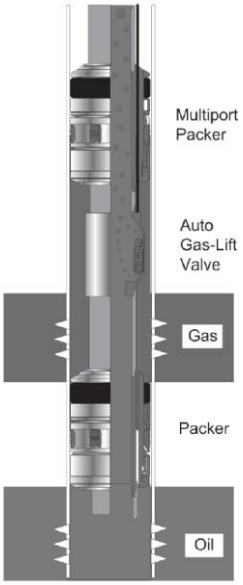

Figure 2-17 schematic of an auto gas lift well (Vasper, 2008)

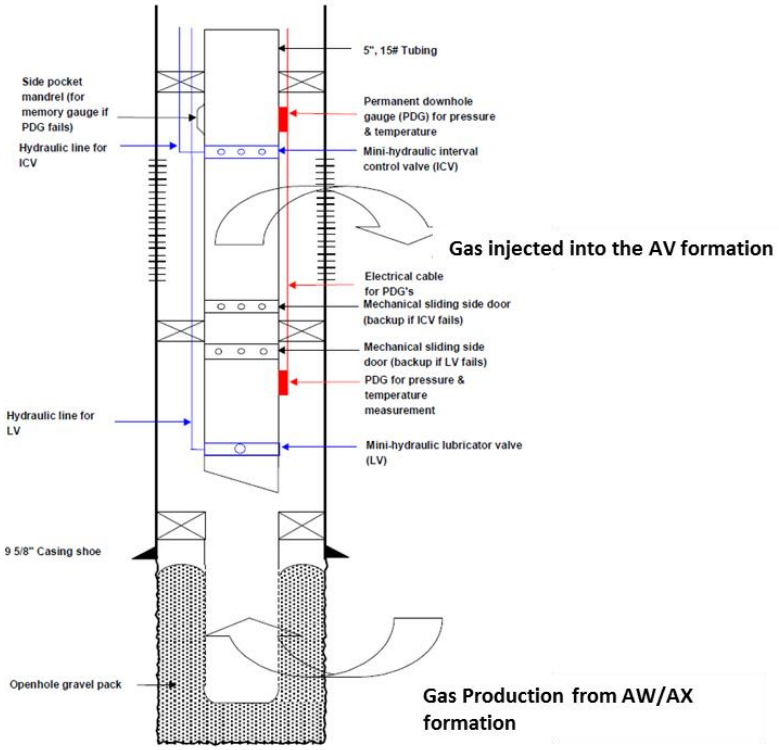

Figure 2-18 Schematic of internal gas injector (Lau et al., 2001)

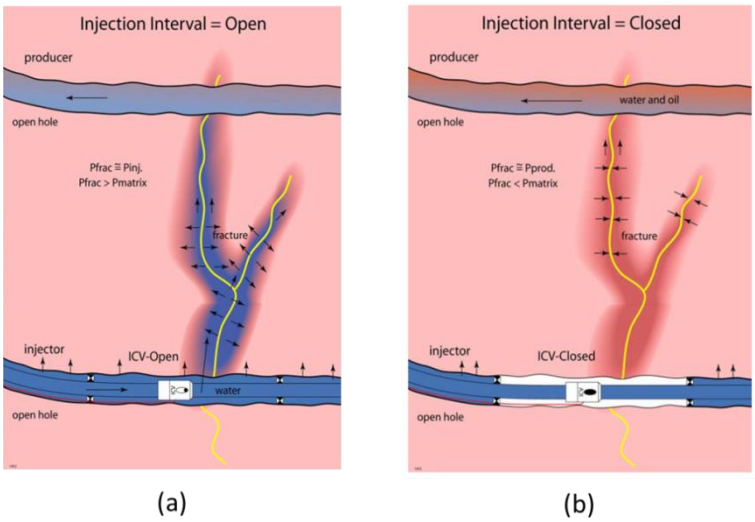

Figure 2-19 (a) ICV is open and water is injected into both the fractured zone and the matrix, (b) ICV is closed and water injection occurs only via the matrix which is in contact with the well (Arenas and Dolle, 2003)

The majority of the auto (natural or in-situ) gas lifts have been installed in the Scandinavian sector of the North Sea (Al-Kasim et al., 2002, Betancourt et al., 2002, Clarke et al., 2006, Vasper, 2008). Unlike the conventional gas lift, an auto gas lifted well has a downhole gas zone completion from which gas is bled into the tubing via an auto gas lift valve designed for gas operations. Brunei Shell Petroleum Company completed its first internal gas injector in the SW Ampa Block 11 field in February 2000 where the controlled gas crossflow from the deep gas reservoirs into the gas cap overlying the oil reservoir resulted in a pressure maintenance scheme that does not require any surface facilities (Lau et al., 2001). Smart injector wells completed with ICVs have a great impact on the performance of waterflooding in the tight fractured reservoirs. ICVs are either opened or closed based on the measured water cuts in the conventional producer to maximize oil production, minimize water production, and maintain reservoir pressure (Arenas and Dolle, 2003, van Nispen et al., 2006, Harris et al., 2008). Meshioye et al. (2010) presented an optimisation methodology based on zonal rate allocation in a smart injector well to help optimise the net present value of the field during waterflooding recovery mechanism.

Downhole gauges are normally used in these operations to set up a surveillance plan in order to evaluate the performance of the gas lift well and water or gas injector wells. The annulus and tubing pressure gauges near the auto gas lift valve greatly improve the ability to model and subsequently optimize auto gas-lift wells. These pressures enable gas-lift rates to be calculated. Additionally the valve performance curves are calibrated

using sufficiently accurate measured gas rates at surface (Vasper, 2008). Reservoir pressure, phase volume injection and production rate profile are similarly measured using sensors in Table 2-1. These are the key parameters must be monitored to assure the success of water or gas flooding projects.

2.4.3 Well Stimulation

Acid stimulation and hydraulic fracturing techniques are routinely used to improve the recovery by removing or bypassing the formation damage in the near-wellbore area and increasing the formation's natural inflow capacity. Unlike the use of the traditional ball diverters, intelligent completions with ICVs allow effective treatment of the whole production interval in long horizontal wellbores without rig, coiled tubing or wireline interventions (Bellarby et al., 2003, El-Sayed et al., 2014, Kent et al., 2014). Implementation of the stimulation with multi-zone downhole pressure and temperature data provides real-time evaluation of downhole fluid distribution which is essential for the acid treatment success. Pressure and temperature data are interpreted for acid impact on the formation, annular fluid contraction and adjacent zone response (Bellarby et al., 2003). Recently DTS was used to obtain both qualitative and quantitative flow distributions in matrix treatments resulting in better understanding of the acid placement and diversion and more efficient use of stimulation fluids (Glasbergen et al., 2009, Tabatabaei et al., 2011).

Acceptance of the technology, deployment costs and added values are the reasons that DTS applications have extended to understand and optimise the hydraulic fracture treatments (Nath et al., 2006, Huckabee, 2009). Sierra et al. (2008) discussed different methods of visualisation and analysis of DTS data to obtain information about fluid placement, flow behind casing and other fracture parameters. In addition to DTS, DAS systems have the potential to monitor downhole audible sounds for fracture diagnosis. However, their use is currently limited to qualitative interpretation and future applications of DAS such as distributed flow prediction require quantitative interpretation to determine the multi-phase flow rates from acoustic data. Microseismic monitoring is also being employed during fracturing treatments to understand fracture geometry and reservoir drainage. The technology resembles a passive listening from another wellbore with an array of geophones to the seismic response of rock shear events during a stimulation treatment (Sierra et al., 2008). Table 2-2 summarises

necessary measurements to monitor successfully acidizing and hydraulic fracturing treatments.

Table 2-2 The information and downhole sensors required to control well stimulation operations

Information Measured	Sensor Type	Number of Monitored points	Technology Employed	Level of Maturity of Data Processing
Fractured intervals	Temperature	Distributed	Fiber Optic	Mature
	Acoustic	Distributed	Fiber Optic	Mature
Acidized intervals	Temperature & Pressure	Single/ quasi-distributed/ distributed	Electronic/ Fiber Optic	Mature

2.4.4 Data Acquisition

Installation of downhole sensors provides well test information for field development planning. This information results in reduced cost and accelerated and increased production, and also delivers more realistic reservoir estimate, reservoir boundaries and optimum position of the future injection well (Ebadi, 2006). Well tests can be carried out each time the I-well is shut-in during e.g. a surface facility trip (shutdown). The data acquisition process can be automated with software routines that automatically increase the frequency of the data recording when the measured values change rapidly. Smart wells equipped with downhole flow meters and pressure gauges may be used for downhole production testing performed between wells employing shut-in or active wells recompleted in the new interval (Glandt, 2005). The same concept can be applied in an environmentally friendly manner at exploration time where the cross flow can occur between the zones due to the pressure difference. The techniques of in-well seismic, electromagnetic survey and streaming potential tools provide deep reservoir monitoring however they are at the development stage for intelligent well applications.

2.5 Multi-zone Multi-phase Flow Metering

Review of the applications of I-wells completed with ICV illustrates that downhole oil, water and gas flow rates are key parameters that must be monitored to ensure the success of different operations discussed before. This highlights the interest of the industry to develop most accurate tools and algorithms to estimate the multi-phase flow rates which supports decisions on production enhancement, operations optimisations

and field development plan. Additionally, it provides the critical information to perform a history match of the reservoir models and evaluates the remaining producible oil or gas in a reservoir.

2.5.1 Multi-layer Pressure Transient Testing

Lefkovits et al. (1961) study was the earliest work aimed at computing the reservoir properties of multi-layer reservoirs. The average formation properties (permeability-thickness, skin factor and reservoir pressure) were derived via a mathematical model of a multi-layer reservoir.

Kuchuk et al. (1986a) introduced the first true "multi-layer test" technique consisting of a number of sequential flow tests for analysing more than two layers. Layer permeability and skin factor were derived by simultaneously recording wellbore pressure and flow-rate at the top of each layer using a PLT. Kuchuk et al. (1986b) applied this multi-layer test technique to a real two-layer reservoir without cross-flow. Ehlig-Economides and Joseph (1987) presented an analytical solution for the layer permeability, skin factor and effective interlayer vertical permeability in multiple, commingled or cross-flow reservoirs providing the transient flow rates from all layers were monitored simultaneously. Their approach was not favoured in the field because of the difficulties of having to measure the downhole flow rates simultaneously at multiple well locations. This was despite having the great advantage of only requiring a short duration test.

Shah et al. (1988) overcame this problem by proposing a multi-step, test procedure that required simultaneous downhole measurements of wellbore pressure and flow rate at only one depth at a time. They also extended the Kuchuk et al. (1986a) study to an arbitrary number of layers with potential cross-flow effects. The general analytical solution for a commingled layered reservoir without cross-flow was derived by Kuchuk and Wilkinson (1991). This solution can be applied to different:

- Wellbore configurations (vertical, horizontal, inclined, fractured or partially penetrated)
- Individual layer properties (homogeneous, heterogeneous or fractured)
- Initial and/or boundary conditions (infinite acting, constant pressure, no flow or mixed)

Later studies extended the multi-layer transient test techniques to more complex reservoir and wellbore configurations (Spath et al., 1994, Larsen, 1999, Prats and Vogiatzis, 1999). Jatmiko et al. (1996) proposed a multi-layer test interpretation for a two-layer oil reservoir when the reservoir pressure falls below the bubble point pressure. Jackson and Banerjee (2000) incorporated numerical reservoir simulation and an automated history matching procedure for the purpose of multi-layer testing. Such an integrated workflow permits the numerical estimation of the layer permeabilities and skin factors using transient pressure and flow rate data from sequential PLT flow tests. Finally Spivey (2006), Poe et al. (2006) and Manrique and Poe (2007) showed how to calculate transient zonal flow rate and estimate zonal properties from various combinations of production and PLT data. An alternative workflow by Aly (1994), Ahmed and Lee (1995) and Aly and Lee (1996) identifies individual layer properties by monitoring the wellbore pressure caused by cross-flow between the layers prior to producing the well (i.e. pre-production well testing).

Published workflows for analysing multi-layer, transient flow data characterise the individual zone/layer properties. All these techniques necessitate the acquisition of wellbore transient pressure and zonal flow rate data. Such traditional multi-layer transient tests have the drawback of significant uncertainties related to the need for zonal flow rate measurements. Multi-zone intelligent well completion (IWC) in multi-layer reservoirs allows data acquisition via PDGs installed on either side of the ICVs.

2.5.2 Multi-phase Flow Metering from Indirect Measurements

Multiple, in-well, multi-phase flow meters, in principle, can be used for direct measurements of surface and downhole flow rates. However, current multiphase flow meters are either expensive, or accurate only within a restricted operating range, or cannot be always used downhole due to the installation risks or access problems (Leskens et al., 2008, Lorentzen et al., 2010a). Adjusting production flow by shutting-in (fully or partially) one or more zones (or wells) is the common practice to obtain the single zone (or well) parameters. This approach may result in production losses and inaccurate estimation of properties of connected zones. PLTs are also used in wells to profile the inflow rates; however they cannot provide the real-time production monitoring. Beside these approaches, the so called “soft-sensors” have been developed to calculate zonal multi-phase flow rates using passive indirect measurements such as temperatures, pressures and well rates.

Many soft-sensors have been suggested in the petroleum industry focusing on reservoir and well applications. Some of them apply the soft-sensing technique to estimate the reservoir properties for updating the reservoir monitoring and reservoir simulation model (Nævdal et al., 2002, Nævdal et al., 2003, Wen and Chen, 2005) while there exists other soft-sensors used for gas-lifted wells (Bloemen et al., 2006), underbalanced drilling (Lorentzen et al., 2001), conventional and multi-lateral wells (Leskens et al., 2008, Kruif et al., 2008), gas cone allocation in multi-zone reservoirs (Gryzlov et al., 2009) and well-testing optimisation and automation (Cramer et al., 2006).

A multi-phase soft-sensing method consists of an estimation technique, a multi-phase flow model and measurements. The multi-phase flow model relates the measurements to the parameters required for the estimation of downhole flow rates. The estimation technique is used to compute the parameters by minimisation of the mismatch between measured information and predicted ones. Two distinct groups of estimation techniques can be recognized in the published work on soft-sensors (1) stochastic based optimisation methods and (2) deterministic based optimisation method. Kalman Filter (KF) (Kalman, 1960), the statistically optimal state estimator for linear systems, and its extension to nonlinear problems such as Extended Kalman Filter (EKF), Ensemble Kalman Filter (EnKF) and Unscented Kalman Filter (UKF) are the most well-known approaches of the first group to find the optimum solutions of the multi-phase flow rate allocation problems. Initial work performed by Lorentzen et al. (2010a) and Lorentzen et al. (2010b) developed the framework for a transient well model and EnKF to estimate the flow rates using high frequency measurements of pressure and temperature. Later, Lorentzen et al. (2014) used a more sophisticated method called Auxiliary Particle Filter (APF) which was suitable for prediction of both discreet and continuous variables in a Bayesian framework and preserved the physical properties of the well model. They also employed Markov jump model to capture the potential abrupt changes in the flow rates. Luo et al. (2014) adopted the same framework as Lorentzen et al. (2014) with the addition of two methods to calculate the optimal variances of the process noise in Markov jump model rather than choose them manually. Li and Zhu (2009) interpreted P/T data to obtain a flow rate profile along horizontal wells using the traditional Markov Chain Monte Carlo method.

Newton-Raphson and Levenberg-Marquardt (LM) are common deterministic based optimisation algorithms proposed for data mismatch minimisation (Kabir et al., 2008, Yoshioka et al., 2009). Muradov and Davies (2009b) developed an automatic zonal flow

rate allocation algorithm for I-wells using real-time downhole (P/T) measurements. They tested three well-known numerical optimisation algorithms (steepest descent, Gauss-Newton algorithm (GNA) and LM algorithm) and EKF together with a comprehensive physical model to describe pressure and temperature changes across the IWC. Muradov and Davies (2011a) later demonstrated the application of distributed temperature sensing data for zonal flow rate and pressure allocation in I-wells. Several classical distributed temperature interpretation methods were employed in addition to an extension of the temperature tangent analysis technique to IWCs for "soft" multi-phase flow rate profiling in I-wells.

Saputelli et al. (2011) provided a comprehensive review of the application of ICVs and P/T data in intelligent wells for zonal flow rate allocation. They also provided an automated workflow for continuous multi-zone intelligent well production allocation. The workflow identifies reservoir and well performance parameters such as the reservoir pressure, productivity index, gas-oil ratio and water-cut consistently as a result of minimisation of the mismatch between the calculated variables and measured surface well-test rates and downhole "triple-gauge" data. The "triple gauge" system consists of two gauges that measure the upstream P/T of each ICV with the third gauge measuring the commingled fluid's P/T inside the tubing. They are often installed in two-zone I-wells. Sun et al. (2011) proposed a "triple-gauge-and-valve" numerical simulator to upgrade the two-zone, I-well triple-gauge P/T data into a real-time, flow-allocation data stream. The simulator provided continuous multi-zone flow rate estimation based on choke pressure drops (position of ICV). Ajayi et al. (2012) described a technique to estimate flow rates in a real two-zone intelligent well. They combined real time data from the installed downhole gauges with analytical choke flow equations, tubing performances and nodal analysis with reservoir data to provide a reliable estimate of zonal flow rates.

All the above soft-sensing techniques are subjected to multi-phase flow model errors and uncertainties in the measured data. The latter refers to the variance of the values attributed to a measured quantity. Therefore a new approach to overcome the inherent limitations of current passive soft-sensing techniques used to allocate downhole flow rates is required. We classify them as being "passive" since they employ existing data. Here we introduce an active multi-phase flow rate soft-sensing method to design optimum number of flow tests. The "Deformed Configuration" (DC) optimisation method (Rykov, 1983) is used in the active soft-sensing technique to design future flow

tests that minimises the uncertainties of the integrated surface and downhole measurements to estimate the most accurate zonal properties. The derivative optimisation techniques are not attractive to design further flow tests as the mathematical relationship between control variables (e.g. ICVs position) and objective function in the active soft-sensing formulation is not well-defined. The DC approach as a gradient free optimisation method is preferred to find the optimum solution using direct values of the objective function. The DC optimisation method consists of sequential simplexes which their geometrical shape may deform through several iterations to converge to the optimum solution. Hence, this method can avoid the noisy values by deformation of sequential simplexes. Details of the DC method are comprehensively discussed in Appendix B.

To my knowledge, this work is the first publication that demonstrates the applicability of DC optimisation method in flow rate soft-sensing problems. Rahmawati et al. (2012) implemented Nelder-Mead simplex (Nelder and Mead, 1965) method to optimise the production strategies using several control variables (combination of surface facility and reservoir parameters) and field operational constraints. Here, the control criterion of the flow tests are either the ICVs fractional flow area in the case of a multi-zone I-well or of the wellhead chokes of a number of conventional wells.

Chapter 3 Active Multi-phase Flow Rate Soft-sensing Algorithm

3.1 Introduction

Chapter 3 introduces active soft-sensing as an alternative approach to the published passive soft-sensing techniques. This active soft-sensing algorithm requires two optimisation steps to estimate the zonal reservoir properties and design the optimum multi-rate flow tests simultaneously. Two optimisation methods are introduced to perform each step. A gradient-based method available in Microsoft Excel Solver is used in the first step to calculate the zonal properties while a gradient-free optimisation technique coded in Microsoft Excel is applied to design the multi-rate flow tests. The justification for choosing these methods is highlighted by explaining what methods are available to solve these problems and why these proposed methods are preferred in this study. Additionally, a multi-phase flow model is used in the algorithm to relate the indirect measurements including well rates, pressure and temperature, to unknown reservoir parameters. The type of analytical equations used in the model is discussed here and their mathematical formulations and assumptions are addressed in Appendix C.

This chapter discusses the methodology and workflow of the algorithm to describe the links between the two optimisation steps and five different levels of active soft-sensing. These levels are proposed based on availability of pressure, temperature and well rate measurements. Then, individual levels are explained in terms of calculated results and additional required fluid and rock reservoir properties to perform the flow rate soft-sensing.

3.2 Active MPFR Soft-sensing Methodology

The Active Multi-phase Flow Rate (MPFR) soft-sensing proposes a general algorithm to satisfy either monitoring or controlling purposes in the commingled production system specifically a multi-zone I-well in this study. The algorithm provides simultaneous estimation of zonal properties and minimum number of sequential flow tests to optimise one of the following objective functions:

- Maximise reliability of estimated zonal properties
- Maximise the oil production

- Minimise the water production
- Minimise the gas production
- Minimise the producing GOR

This chapter will only focus on the formulation of the first objective function from the list above in the active soft sensing algorithm while the possibility of using the other objective function e.g. maximising the oil production will be discussed in Chapter 5. Here, the Active Multi-phase Flow Rate (MPFR) soft-sensing is a strategy to produce the most reliable estimate of reservoir properties and zonal flow rates during a series of multi-zone, multi-rate tests by changing the ICV positions in an optimum manner. This strategy advises the minimum sequence of tests with an optimum combination of zonal ICV positions in each test. This is important because it is essential to minimise the test time and any resulting production loss in addition to excessively reducing the number of future ICV movements that can be made during the remainder of the completion's lifetime. Figure 3-1 illustrates a schematic of a multi-zone I-well in which well rates are usually available through surface measurement but the contribution of phase production from individual zones is required to be determined through other approaches.

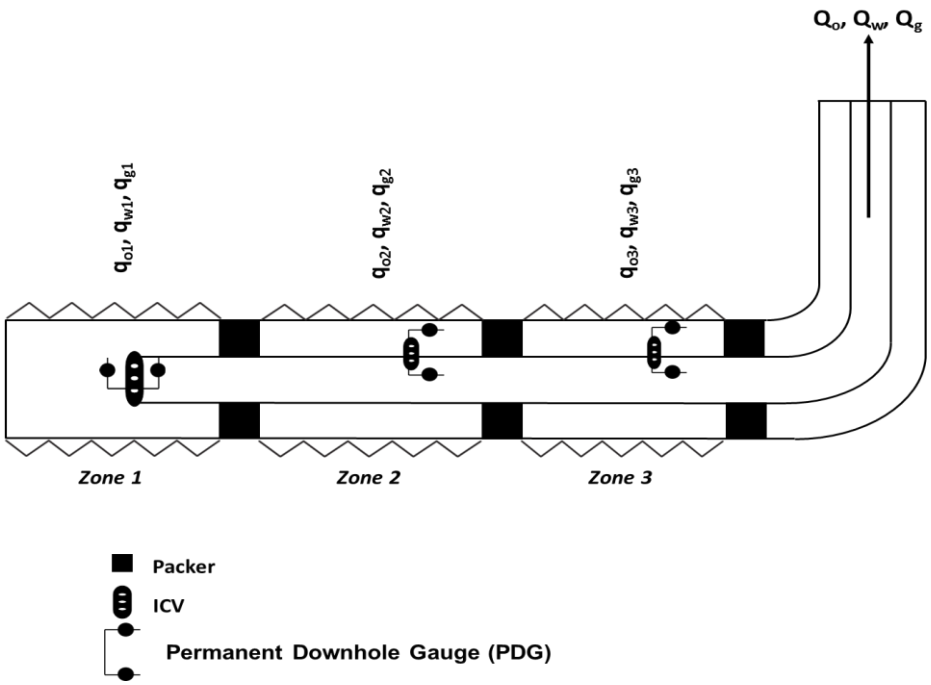

Figure 3-1 A schematic of a multi-zone I-well

An example sequence of ICV position in a multi-rate test conducted in a 2-zone IW is shown in Table 3-1. Each combination of ICV positions within a sequence of tests is called a "Flow Test".

Table 3-1 Sequential multi-rate test in a 2-zone IW

Flow Test Number	**ICV_1 Position***	**ICV_2 Position***
1	1	1
2	0	1
3	1	0

- Fraction of ICV area open to flow

Two optimisation steps are required to solve this problem:

1) Zonal properties such as reservoir pressure, productivity index, water-cut, gas-liquid ratio and in-situ gas mass fraction are traditionally calculated by minimising the TOTAL mismatch between the measured data and the values predicted by the multi-phase flow model. It is a constrained optimisation problem that was solved using a commercial Generalised Reduced Gradient (GRG) nonlinear optimisation method.
2) The optimal sequence of ICV positions in the multi-rate test is then found with a gradient- free optimisation method, the "Deformed Configuration" techniques (Rykov, 1983, Rykov, 1995). *Note that Step 2 identifies the next flow test that is with a **higher mismatch** in order to better explore the search space.*

These two optimisation steps are implemented in a sequential manner that estimated zonal properties from step 1 are used to calculate the objective function in each flow test. The minimisation of the mismatch can be performed in different levels based on the measurements availability. The main outputs of this minimisation are the zonal properties required to estimate the zonal flow rates. Then step 2 attempts to design the ICVs position of the next flow test using direct values of objective functions. This is repeated until the algorithm meets the stopping criteria. More details of the active soft-sensing workflow will be discussed in the next sections.

The uncertainty in the downhole PDG measurement, δ, is the measurement's scatter around its true value over the instrument's operational range (Da Silva et al., 2012). It is the critical value for determining the accuracy of the reservoir and production monitoring, as shown by the following mismatch formulae:

- Total oil production rate:

$$\text{Mismatch}_1 = \frac{(\text{Q}_{\text{o,measured}} - \text{Q}_{\text{o,calculated}})^2}{(\delta \text{Q}_\text{o})^2} \quad 3\text{-}1$$

- Total water production rate:

$$\text{Mismatch}_2 = \frac{(\text{Q}_{\text{w,measured}} - \text{Q}_{\text{w,calculated}})^2}{(\delta \text{Q}_\text{w})^2} \quad 3\text{-}2$$

- Total gas production rate:

$$\text{Mismatch}_3 = \frac{(\text{Q}_{\text{g,measured}} - \text{Q}_{\text{g,calculated}})^2}{(\delta \text{Q}_\text{g})^2} \quad 3\text{-}3$$

- Pressure drop across ICVs:

$$\text{Mismatch}_4 = \frac{(\Delta\text{p}_{\text{ICVi,measured}} - \Delta\text{p}_{\text{ICVi,calculated}})^2}{(\delta \Delta\text{p}_{\text{ICVi}})^2} \quad 3\text{-}4$$

- Mixture's average temperature downstream the ICVs:

$$\text{Mismatch}_5 = \frac{(\text{T}_{\text{mix}_\text{i},\text{measured}} - \text{T}_{\text{mix}_\text{i},\text{calculated}})^2}{(\delta \text{T}_{\text{mix}_\text{i}})^2} \quad 3\text{-}5$$

- Zonal build-up pressure drop if any zone is completely closed during a multi-rate flow test:

$$\text{Mismatch}_6 = \frac{(\Delta\text{p}_{\text{BUi,measured}} - \Delta\text{p}_{\text{BUi,calculated}})^2}{(\delta \Delta\text{p}_{\text{BUi}})^2} \quad 3\text{-}6$$

In above formulas, i represents the corresponding measured and calculated information for each zone. The quadratic mismatch function is preferred in this study as it reflects a common approach to define the difference between measured and estimated information. The total mismatch and mismatch equation of individual flow tests may involve all or some of the above mismatch types depending on the number of the open and close ICVs. For instance, *Mismatch₄* is not applicable when the ICV is closed or *Mismatch₆* is only relevant if any ICV is closed in the flow test. Equations 3-7 and 3-8 are used to calculate mismatch of individual flow test and the total mismatch of all flow tests respectively.

$$\text{Mismatch of Individual Flow Test} = (A_1 Mismatch_1 + A_2 Mismatch_2 + A_3 Mismatch_3 + A_4 \sum_{\text{j=1}}^{\text{n}} Mismatch_4 + A_5 \sum_{\text{j=1}}^{\text{n}} Mismatch_5 + A_6 Mismatch_6)^{0.5} \quad 3\text{-}7$$

$$\text{Total Mismatch} = \left(B_1 \frac{\sum_{i=1}^{K} \text{Mismatch}_{1,i}}{K} + B_2 \frac{\sum_{i=1}^{K} \text{Mismatch}_{2,i}}{K} + B_3 \frac{\sum_{i=1}^{K} \text{Mismatch}_{3,i}}{K} + B_4 \sum_{j=1}^{n} \frac{\sum_{i=1}^{K} \text{Mismatch}_{4,i,j}}{K} + B_5 \sum_{j=1}^{n} \frac{\sum_{i=1}^{K} \text{Mismatch}_{5,i,j}}{K} + B_6 \frac{\sum_{i=1}^{K} \text{Mismatch}_{6,i}}{K}\right)^{0.5} \quad 3\text{-}8$$

where K and n are the number of flow tests and zones respectively. A and B represent the weight factors corresponding to each mismatch however this study has assumed the equal weight factor for all mismatches.

3.3 Active MPFR Soft-sensing Workflow

Figure 3-2 charts the sequence of steps required by the active soft-sensing technique to calculate the zonal multi-phase flow rates. First well rate and zonal annular/tubing pressure and temperature data are taken from the multi-rate test measurements. It should be noted that this information may contain errors. Optimisation Step 1 is performed until minimum mismatch is achieved between measurements and estimated values. The estimation of zonal properties is based on all the number of flow tests in this step. Then optimisation step 2 is initiated by DC technique to design the next flow test which provides new set of measurement to recalculate the zonal properties. A comparison between the first and second sets of estimated zonal properties determines whether the workflow is continued to the optimisation step 2 or the algorithm is stopped.

The deformed simplex method requires (n+1) flow tests to form the first simplex for an n-zone intelligent well (see section 3.4.2). As discussed, one design for the initial (n+1) flow tests is to sequentially close one of the ICVs in each test while fully opening the other zones. The act of closing an ICV initiates a Pressure Build-Up (PBU) test, providing high quality information on zonal reservoir properties. Table 3-2 lists the initial flow tests required to construct the first simplex for a 3-zone I-well test.

The active soft-sensing procedure is used to design one or more further multi-rate tests to measure the required data (Explained in next section) when the deformed simplex method is used to obtain the new ICV positions. This procedure predicts the zonal properties (*zonal reservoir pressures, productivity indices, water-cuts and gas mass fractions)* by minimizing the normalised mismatch between measured data and calculated values with an optimal sequence of ICV positions.

The optimization method proposes the new valve positions to be implemented in a further flow-rate test. These positions are chosen so as to improve the accuracy of the estimated zonal flow-rates from the initial (n+1) tests. These measurements from this (single) flow rate measurement are then added to the measured data set followed by recalculation of the zonal properties.

The second series of calculated zonal properties values is compared with the initial obtained values. Comparison of the two sets of results provides an estimate of the uncertainty in the values of the reservoir and zonal parameters.

Repetition of the above workflow followed by a further (single) flow rate test yields a third set of calculated values of zonal properties. It should now be possible to estimate the accuracy of the soft-sensing workflow by comparing the three values for each of the calculated parameters. It can also now be decided whether a further repetition of the workflow is likely to generate significant improvement in the observed results. Specific assumptions are considered during the design of multi-rate flow tests:

- Each flow test will take time until measured well rates, pressure and temperature become stabilised. It's not applicable for low permeability reservoirs with longer stabilisation time. This is not the case for transient annular pressures when a zone production is closed.
- The multi-rate flow tests are completed during a limited time period while the zonal properties are not expected to change significantly. It is assumed these parameters are constant values in the calculations.

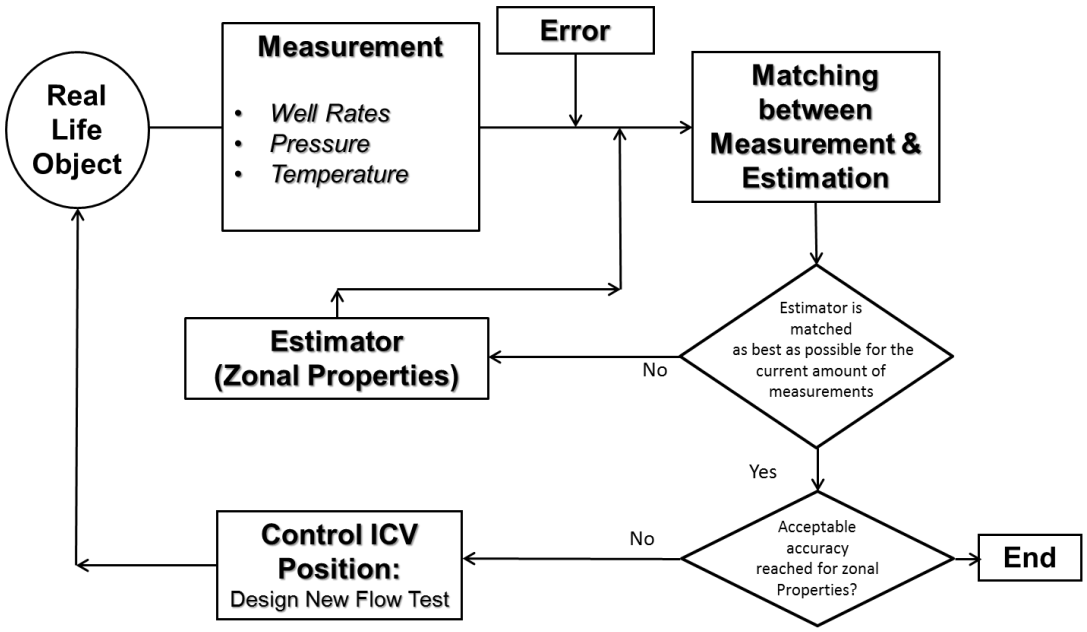

Figure 3-2 Active MPFR soft-sensing

Table 3-2 First (n+1) ICV position combinations in a 3-zone intelligent well

No. of Flow Test	ICV1 Position	ICV2 Position	ICV3 Position
1	1	1	1
2	0	1	1
3	1	0	1
4	1	1	0

3.4 Optimisation Problems of Active MPFR Soft-sensing

All optimisation problems require the definition of the

- Objective function
- Control variables
- Constraints to define the feasible values of control variables

Optimisation problem searches for feasible values of the control variables that correspond to the optimum (either a minimum or a maximum) value of the objective function. Minimisation problems are preferred since traditional optimisation theory deals with the minimisation problem and maximisation problems can be easily reformulated as minimisation ones by simple reverse sign of the objective function. They can be represented as finding x^* such that:

$$x^* = argminf(x), \quad x \in X \tag{3-9}$$

$$X = \{x: x \in R^n, g_i(x) \geq 0, i = \overline{1, m_1}, g_i(x) = 0, i = \overline{m_1 + 1, m}\} \tag{3-10}$$

where the objective function $f(x)$ and the constraint functions $g_i(x)$, $i = \overline{1, m}$, are real scalar ones. The optimisation problem can be classified as linear, quadratic, non-linear, semi-infinite, semi-definite, multiple-objective, discrete optimization problem etc. depending on the description of the objective function $f(x)$ and the feasible values of control variables. Table 3-3 lists the details of optimisation problems in steps 1 and 2 of the active soft-sensing algorithm in which the algorithm attempts to maximise the reliability of estimated zonal properties.

If step 2 is performed to design flow tests to optimise alternative objective functions the flow test mismatch is replaced by total oil, water or gas production. This implies that next flow tests are designed to increase the oil production or decrease the unwanted fluid production.

Table 3-3 Optimisation problems in active soft-sensing

	Step 1	Step 2
Objective Function	Total Mismatch Eq. (3-8)	Flow Test Mismatch Eq. (3-7)
Control Variables	• Zonal Reservoir Pressures • Zonal Productivity indices • Zonal Water-cuts • Zonal Annular Gas Mass Fraction	Fraction of ICVs' area open to flow
Constraints	Feasible Values of Zonal Reservoir Parameters	Variation of Fraction of ICVs' flow area between 0 and 1
Optimisation	Minimisation	Maximisation
Optimisation Method	Generalised Reduced Gradient (GRG)	Deformed Configuration (DC)

3.4.1 Algorithm to Estimate Zonal Properties

Step 1 of the active soft-sensing is the constrained optimisation of a system of nonlinear equations involving multiple control variables. Iterative methods are frequently employed to solve the resulting non-linear equations. These suffer from the problem that a suitable starting solution (point) plays an important role especially for multiple solution problems. The convergence to a satisfactory solution relies on the algorithm used and the starting solutions. For constraint problems the three methods that have been more successful in comparison studies on industrial problems are successive linear and quadratic programming (SLP and SQP) and GRG. In addition to deterministic optimisation methods, stochastic approaches have been proposed to solve these problems, even though their movement is slow to the optimum solution (Pike, 1986). GRG method is preferred in this study as it is available in Microsoft Excel Office.

Microsoft Excel Solver and MATLAB may also be used to solve the nonlinear equations in this study. Microsoft Excel Solver is an add on to Microsoft Excel Office. It uses Generalised Reduced Gradient (GRG) nonlinear optimisation technique (Lasdon et al., 1974) while MATLAB offers various methods to solve non-linear equations via their Optimisation Toolbox™ (interior point, successive quadratic programming (SQP), active-set and trust-region reflective). The Optimisation Toolbox™ also includes the Levenberg-Marquardt algorithm using a trust-region method to solve both constrained and unconstrained nonlinear, least-square problems. Microsoft Excel Solver is

recommended in this work since widely available and can be easily set up to solve optimisation problems involving a limited number of control variables. Here a brief description of the GRG algorithm is provided in the next sections together with an explanation of how such optimisation problems can be coded in Microsoft Excel Office.

3.4.1.1 Microsoft Excel Solver

Microsoft Excel Solver 2010 offers three optimisation techniques, simplex linear programming (LP), GRG non-linear and revolutionary methods to solve linear (first order) equations, non-linear, smooth functions and non-smooth functions respectively. The objective functions, control variables and constraints are coded as cells whose values change in the spread sheet via a graphical user interface (GUI) (Figure 3-3).

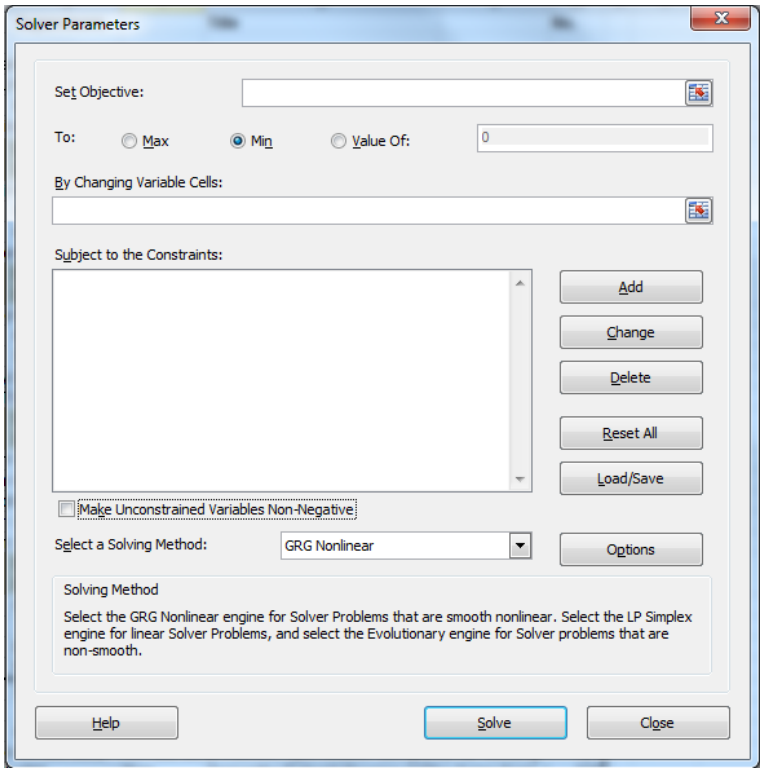

Figure 3-3 Excel Solver's GUI

The GRG non-linear method is selected from the available solving methods in the Excel Solver 2010 to minimise the objective function given by Equation 3-8 which is both differentiable and non-linear. Details of GRG method is explained in 0. The control variables are individual zonal properties including reservoir pressure, productivity index, water-cut, gas mass fraction. For example, there are 12 control variables to optimise the objective function in a 3-zone I-well. Constraints are defined for each

control variable in order to obtain the feasible values of zonal properties. Table 3-4 lists the lower and upper bounds of the zonal properties required to be set up in the Excel Solver's GUI. Available information from multi-rate flow tests are used to define the feasible range of zonal reservoir pressures according to zonal annulus and tubing pressure measurements.

Table 3-4 Lower and upper boundaries of zonal reservoir properties

Control variable	**Lower Bound**	**Upper Bound**
Reservoir Pressure, psi	From multi-rate flow test	From multi-rate flow test
Productivity index, STB/D/psi	Greater than zero, e.g. 10^{-10}	-
Water-cut, fraction	0	1
Gas Mass Fraction	0	1

There are two main challenges associated with estimation of zonal properties using Microsoft Excel's GRG non-linear solver:

1) Uniqueness: there is more than one set of zonal properties that can give the minimum objective function within the constraint intervals. A way to overcome this problem is by using as many sets of measurements as possible. Next section introduces a method to optimise multi-rate flow tests required to estimate the most accurate zonal properties.
2) Convergence: The GRG non-linear may not converge to the best possible set of parameters. This problem happens because of convergence to a local minimum rather than a global minimum (**Error! Reference source not found.**). The simple solution is to attempt the GRG non-linear solver using different initial guesses and select the result corresponding to the lowest value of the objective function. The Excel Solver 2010 includes the "Multistart" option which runs the GRG solver a number of times and randomly selects a different set of initial values for the control variables. Then the solver presents the best of all of the local optimal solutions that it has found.

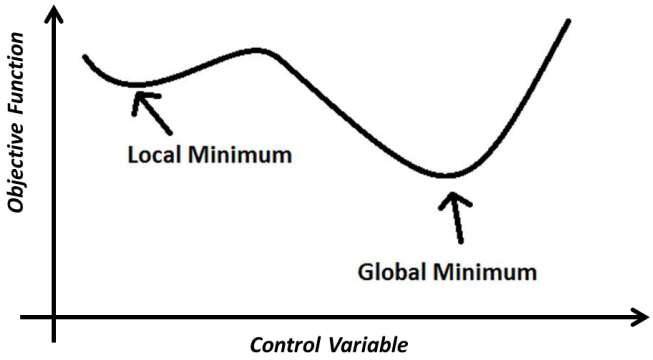

Figure 3-4 Global and local optimum solutions

Production and well testing history data may be used to define smaller search space. As a result, the GRG optimiser would search for the solution efficiently within the search space. The estimated zonal properties from other studies may also be used as initial guesses in the GRG algorithm resulting in faster estimation of zonal properties which are close to the solution of the interest.

3.4.2 Method to Optimise Multi-Rate Flow Tests

Step 2 of the active soft-sensing is a multivariate, constrained optimisation problem where the objective function (Eq. 3-7) is the mismatch of each flow test and the control variables are the fraction of ICVs area open to flow (between 0 and 1). This step uses a direct search optimisation technique, "Deformed Configuration" (DC) to design the optimum flow tests. This class can be considered as a generalisation of the method of Spendley et al. (1962) for regular simplexes, the method of Nelder and Mead (1965) for deformed simplexes, the method of Box (1965) for complexes. Although DC method is still traditionally considered as a heuristic technique, the convergence of the whole class for convex functions has been proved by Rykov (1980) using the general relaxation theory. Computational experiments confirmed the convergence rate obtained for methods of Spendley et al, Nelder-Mead and Box is relatively lower than one appeared for the generalised DC method (Kuznetsov, 1992). The DC method is a deterministic optimisation method with the following features:

1) The direct search algorithm or does not use derivatives of the objective function
2) It adapts to the function's topology (valleys, ridges etc.)
3) It is flexible (the user can change the local optimality criteria and mapping types while the method is running)

4) It is robust to errors in objective function evaluation

It is difficult or sometimes impossible to relate the objective functions of the interest to the ICVs position mathematically. Since the objective function is non-smooth and non-differential the direct search methods are the most appropriate approach to solve optimisation problems defined by functions for which derivatives are unavailable or available at a prohibitive cost. Conn et al. (2009) comprehensively reviewed the derivative-free optimisation algorithms by extracting and emphasizing the common theoretical features used by these algorithms, as well as highlighting the differences. Based on their work, increasing complexity in mathematical modelling, higher sophistication of scientific computing and abundance of legacy codes are the main reasons of using derivative-free optimisation methods. The DC technique involves calculations of function values in separate points at each step followed by spatial mapping of control variables leading to optimise the function value. The basic feature of the DC method is augmented by introducing the search control which consists of choosing the locally optimal direction, mapping the configuration vertices, the centroid, and the step-size as explained in Appendix B. Since there are several mapping of vertices and deforming the simplexes (or complexes) from step to step within the optimisation technique, this method has relatively fast convergence and is less sensitive to noise corruption than the computation of the objective function at any instant (Veres et al., 2004).

3.5 Active MPFR Soft-sensing Levels

A wide range of measurement sources can be potentially incorporated in the active soft-sensing workflow. These measurements differ in the methods by which they are interpreted i.e. by the type of the well and reservoir model used. Models are available for (1) stabilised well production, (2) pressure drops across the ICV flow restrictions (3) transient pressure changes during zonal PBU tests and (4) temperature distribution in the well (5) temperature changes across the ICV flow restrictions and (6) tubing and annular fluids mixing temperature. It is convenient to categorise the complexity of I-well measurements and analysis into five levels:

- Level 0: Well production flow rates (oil, water and gas) and a single stabilised pressure measured in the upper well completion.

- Level I: Well production rates and the stabilised zonal annular pressures are measured.
- Level II: Level I data plus stabilised zonal tubing pressures and annulus temperatures
- Level III: Level II data plus stabilised tubing temperatures
- Level IV: Level II data plus transient zonal annulus pressures of any PBU test.

Five different data set options will be discussed that combine the P/T downhole gauge readings and well production flow rate measurements. These measurements form the basis of the objective functions used in the optimisation steps 1 and 2 of the active soft-sensing algorithm. It should be noted that these objective functions include one or several mismatch terms between the measurements and estimated values depending on the available measured information.

The first one is the simplest in terms of downhole data measurements. The later ones benefit from an increased understanding of the reservoir and reservoir fluid properties plus a richer downhole data set. This allows more complex models to be used and a greater spectrum of reservoir parameters estimated. For example, annular T/P measurements are combined to calculate fluid properties such as density, formation volume factor, viscosity and compressibility for all the phases that contribute to the pressure drop estimate across the ICVs (level II) and model transient PBU (level IV).

All levels result in the calculation of zonal parameters (e.g. reservoir pressure, productivity index, water-cut and in-situ gas mass fraction in the annulus) that are then used to estimate the multi-phase flow rates. However, addition of level IV data adds value to the active soft-sensing workflow via estimation of the skin value as well as the zonal permeability (both vertical and horizontal, providing the appropriate flow regimes are identified in the PBU analysis). Table 3-5 summarises the reservoir and well properties which can be estimated by each of the measurement levels.

Table 3-5 Results obtained from different active soft-sensing levels

	Zonal Reservoir Pressure	Zonal Productivity Index	Zonal Water-cut	Zonal In-situ Gas Mass Fraction	Zonal Permeability	Zonal Skin
Level 0	√	√	√	√		
Level I	√	√	√			
Level II	√	√	√	√		
Level III	√	√	√	√		
Level IV	√	√	√	√	√	√

3.5.1 Level 0 Data Set

Stabilised bottomhole pressure in the upper well completion and well production flow rate are measured in this level. The produced fluid's bubble point pressure is also required not only for Level 0 but also for the other Levels to interpret whether free gas is being produced during zonal inflow periods or evolved from the produced oil solution as a result of pressure drop occurring across the production tubing or at surface facility. Multi-phase flow models are used to relate the bottomhole pressure to individual zonal phase rates. These model equations will account for the pressure drop along the tubing, ICVs and reservoir due to multi-phase fluid flow. Table 3-6 lists the required measured data set for initial (n+1) flow tests in a 3-zone I-well.

Table 3-6 Required Measurements for Level 0

	ICVs Position			Well Production Rate			Stabilized Bottomhole Pressure
NO. of Exp.	**ICV_1**	**ICV_2**	**ICV_3**	**Qo**	**Q_g**	**Qw**	**$P_{bottomhole}$**
1	-	-	-	-	-	-	-
2	-	-	-	-	-	-	-
3	-	-	-	-	-	-	-
4	-	-	-	-	-	-	-

Level 0 uses the least downhole measured data among the active soft-sensing levels. However, other information in addition to the Table 3-6 measurements is required. These relate to the fluid properties for each zone to calculate pressure drops along the tubing and across the ICV:

- Oil density at standard conditions
- Gas density at standard conditions
- Produced (formation, injected or mixed) water density at standard conditions
- Gas-Oil-Ratio (GOR)
- PVT correlation
- ICV flow coefficients for each position
- Tubing roughness

It should be noted that GOR and PVT correlations are not required if fluid density and formation volume factor measurements are available at the downhole, zonal flow-conditions.

3.5.2 Level I Data Set

Zonal, downhole, pressure gauge measurements are recorded once the flow has stabilised after altering the ICV position. The zonal multi-phase rates may then be calculated once knowledge of the surface flow rates is added. Table 3-7 lists the data that should be recorded during the four flow-rate tests required for application of the technique to a 3-zone I-well. The estimated accuracy of the flow rate and pressure measurements "Adds Value" by estimating the accuracy of the analysis. Inflow performance relationship (IPR) equations are used to calculate the zonal properties. The main limitation of this Level is that the in-situ gas mass fraction in the annulus intervals is not estimated using the measurements in Table 3-7. Alternatively, the zonal gas-liquid ratio may be calculated by assuming no free gas is being produced from the gas cap.

Table 3-7 Required Measurements for Level I

	ICVs Position			**Well Production Rate**			**Stabilized Annulus Pressure**		
NO. of Exp.	**ICV_1**	**ICV_2**	**ICV_3**	**Qo**	**Q_g**	**Qw**	**Pan_1**	**Pan_2**	**Pan_3**
1	-	-	-	-	-	-	-	-	-
2	-	-	-	-	-	-	-	-	-
3	-	-	-	-	-	-	-	-	-
4	-	-	-	-	-	-	-	-	-

3.5.3 Level II Data Set

Level II Data Set is an extended version of Data Set I in which the ICV performance relationship (as supplied by the equipment manufacturer) is added to provide additional data that will allow the soft-sensing technique to calculate free gas in the annulus intervals and improve its estimates of the zonal flow rates. Table 3-8 indicates the required data to start the workflow for the case of a 3-zone I-well. Fluid properties listed in Level 0 are required to estimate the pressure drop changes across the intelligent well completion.

Table 3-8 Required Measurements for Level II

	ICVs Position			**Well Production Rate**			**Stabilized Annulus Pressure**			**Stabilized Tubing Pressure**			**Stabilized Annulus Temperature**		
NO. of Exp.	**ICV_1**	**ICV_2**	**ICV_3**	**Qo**	**Q_g**	**Qw**	**Pan_1**	**Pan_2**	**Pan_3**	**$Ptub_1$**	**$Ptub_2$**	**$Ptub_3$**	**Tan_1**	**Tan_2**	**Tan_3**
1	-	-	-	-	-	-	-	-	-	-	-	-	-	-	-
2	-	-	-	-	-	-	-	-	-	-	-	-	-	-	-
3	-	-	-	-	-	-	-	-	-	-	-	-	-	-	-
4	-	-	-	-	-	-	-	-	-	-	-	-	-	-	-

3.5.4 Level III Data Set

The main objective of Level III is to use the potential of downhole temperature measurements to estimate zonal multi-phase rates. In previous Levels, well production rates and pressure measurement played a key role in determination of zonal properties while temperature measurements and its associated mismatch function will add the value to the active soft-sensing by improving the accuracy of the estimated zonal properties. Models available for temperature distribution in the well, temperature changes across the ICVs and annular and tubing fluids mixing temperature create the relation between temperature/pressure measurements and zonal properties. The required measured data set in Level III is shown in Table 3-9 for initiation of active workflow in a 3-zone I-well. It is essential that the temperature data is recorded during multi-rate flow tests at a resolution of $0.01^{o}C$.

Table 3-9 Required Measurements for Level III

	ICVs Position			Well Production Rate			Stabilized Annulus Pressure			Stabilized Tubing Pressure			Stabilized Annulus Temperature			Stabilized Tubing Temperature		
NO. of Exp.	**ICV_1**	**ICV_2**	**ICV_3**	**Qo**	**Q_g**	**Qw**	**Pan_1**	**Pan_2**	**Pan_3**	**$Ptub_1$**	**$Ptub_2$**	**$Ptub_3$**	**Tan_1**	**Tan_2**	**Tan_3**	**$Ttub_1$**	**$Ttub_2$**	**$Ttub_3$**
1	-	-	-	-	-	-	-	-	-	-	-	-	-	-	-	-	-	-
2	-	-	-	-	-	-	-	-	-	-	-	-	-	-	-	-	-	-
3	-	-	-	-	-	-	-	-	-	-	-	-	-	-	-	-	-	-
4	-	-	-	-	-	-	-	-	-	-	-	-	-	-	-	-	-	-

Thermal properties including heat transfer coefficient, latent transformation enthalpy, mass heat capacity and Joule-Thompson coefficient in addition to fluid properties given in Level 0 should be known to calculate temperature distribution in the wellbore and intelligent well completion.

3.5.5 Level IV Data Set

Data Set IV adds transient pressure measurements to the Table 3-7, Table 3-8 or Table 3-9 data. At least one ICV is closed, halting production from that zone & initiating a pressure build-up test. The following extra information is now required:

- PVT measurements as listed in Level 0 data set
- Fluid viscosity and compressibility: either measurements at the downhole conditions or at surface conditions plus the appropriate correlations
- Reservoir thickness
- Reservoir porosity
- Zonal production interval length
- Preferred correlation to calculate productivity index

Build-up tests duration should be designed so that at least one flow regimes (vertical radial, linear or pseudo radial flow) is observed as well as being long enough to provide a sufficiently accurate estimate of the reservoir pressure. Frequent accurate pressure measurements are required for well test interpretations. Typical permanent downhole pressure/temperature gauges record the pressures with resolution of 0.01 psi and a similar data point frequency to that required for transient well testing.

Adding data set IV into the workflow increases the complexity of the zonal inflow calculations and potentially affects the accuracy of the results. However, it adds value

by estimating the zonal skin value as well as the zonal permeability (both vertical and horizontal for each phase, depending on whether the flow regimes were identified by the pressure build-up tests).

The measured transient pressure data is integrated into the active soft-sensing method using relevant well testing equation to model the observed flow regime. Vertical and horizontal permeabilities and skin are the main parameters to be calculated in the optimisation step 1 along with other zonal properties including reservoir pressure, water-cut and annular gas mass fractions while the total mismatch objective function is minimised. The optimum values of vertical and horizontal permeabilities and skin are converted to zonal productivity indices using appropriate horizontal well model.

3.5.6 Accuracy of MPFR Soft-sensing from Different Levels

The richness of measured information used in the active soft-sensing algorithm increases from level zero to level four. Higher levels provide greater understanding of zonal properties with higher accuracy. For instance, level one cannot calculate the zonal in-situ gas flow due to the equations used to relate measured well rates and zonal annulus pressure. While the addition of ICV performance equation to estimate the pressure drop across ICVs results in the calculation of in-situ gas inflow rates from individual zones. Level four is able to estimate the zonal permeabilities and skin directly from the algorithm which in turn used to calculate the zonal productivity indices. Permeability and skin are control variables of optimisation step 1 in this level data set while the value of the productivity index is used directly as a control variable in levels zero to three. It will be shown in Chapter 4 that the addition of Level 4 into the active soft-sensing of zonal flow rates in a real 2-zone I-well provides more accurate estimation of zonal properties compared to the case in which these properties are estimated using level one.

The implementation of higher levels requires the knowledge of reservoir fluid and rock properties. The accuracy of estimated zonal properties is affected by the uncertainties related to this information. However, the estimation of zonal properties is highly sensitive to typical errors which take place in the well rate, pressure and temperature measurements. Details of these influences on the zonal flow rates estimation will be discussed in Chapter 6.

The multi-level option of active soft-sensing algorithm facilitates use of different sets of measurement. This option makes the algorithm being applicable in cases that some

types of measurements are unavailable or unreliable due to noisy measurement tools. This beneficial feature of the algorithm is also discussed in a real 2-zone I-well case where zonal tubing pressures are discarded due to the possible gauge drift error and transient zonal annulus pressures are alternatively used to add level 4 into the active soft-sensing algorithm.

3.6 Active MPFR Soft-sensing Formulation

Both static and dynamic flow models are used to relate the zonal inflow rates to pressure measurements. These flow models are discussed in detail in the example of multi-zone intelligent oil well. However, the models can be updated if the active monitoring is implemented in a multi-zone intelligent gas well without changing the active soft-sensing methodology. Figure 3-5 is the schematic of a multi-zone intelligent well indicating the path that fluid flows from the reservoir up to the surface. Pressure and temperature changes across reservoir and ICVs as well as the temperature distributions along the well are the main sources providing information about the zonal inflow rates. Well testing equations, (semi-)steady state IPR, ICV performance relationship and temperature model are used to estimate the measured well flow rate, annulus and tubing pressure and temperature. The multi-phase flow model including analytical equations to predict the pressure and temperature changes across the reservoir, wellbore and intelligent well completions are discussed in Appendix C.

Fluid properties such as density, viscosity, compressibility and thermal properties required in the flow models are calculated either from black oil correlations or compositional models. These properties must be evaluated at downhole conditions (measured pressure and temperature) in order to be used in the flow model equations.

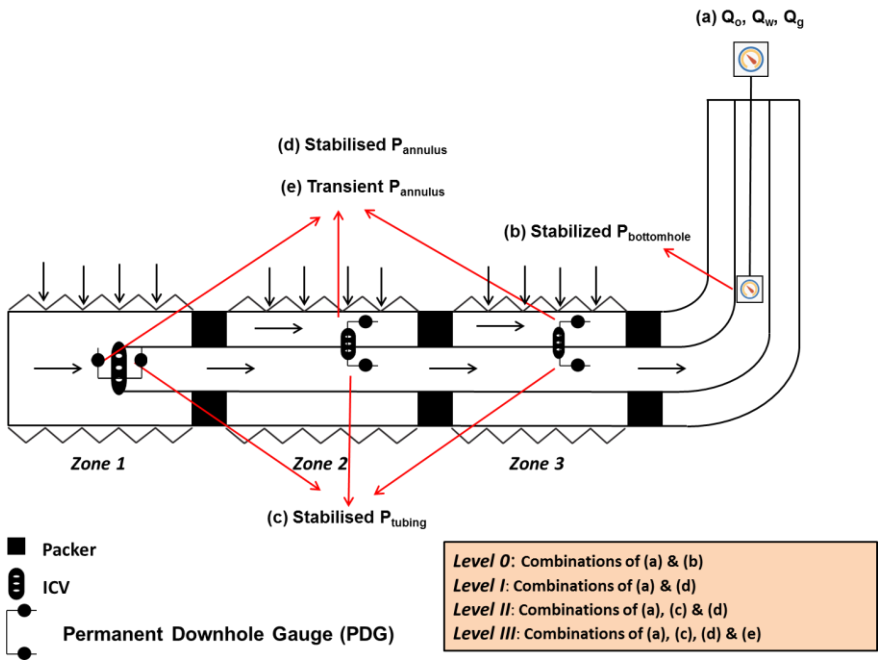

Figure 3-5 An I-well's gauges and the resulting analysis levels

3.7 Applications of MPFR Active Soft-sensing Algorithm

Various parts of the active soft-sensing algorithm were discussed in the previous sections. The control part differentiates the active soft-sensing from the passive ones. The active soft-sensing algorithm is originally developed for the purpose of monitoring zonal inflow rates where the reliability of the estimated zonal properties is improved. There are other applications that active soft-sensing can be employed without changing its methodology:

- The algorithm can update the estimated zonal properties from passive soft-sensors through design of further flow tests. This is important when the estimate is affected by erroneous measurements.
- The optimisation objective function may also be specified as oil production. This is particularly useful when the algorithm is applied to maximise oil production or speed up the well start-up procedure. Details are discussed in Chapter 5.
- Other sophisticated multi-phase flow model can be incorporated in the algorithm in order to account for more complicated downhole flow conditions in the reservoir, wellbore and intelligent completion. The control part updates the important parameters required for estimation of flow rates by advising on additional measurements.

- The algorithm's universality also allows applying it to real-time, multi-rate flow test design in conventional wells.

3.8 Summary

This chapter discussed the methodology behind the active MPFR soft-sensing technique that involves performing two sequential optimisation steps. The optimisation workflow for calculating the zonal properties (reservoir pressure, productivity index, water-cut and annular gas mass fraction) by minimising the mismatch between the observed information and their estimated values from the multi-phase flow model equations is presented. A second workflow that designs further multi-rate flow tests by regulating the ICVs to measure well rate, pressure and temperature required for zonal properties estimations. The GRG non-linear method available in Microsoft Excel Solver is used in the first optimisation step while the deformed configuration method is applied to solve the second optimisation problem. These solutions were selected based on the type of optimisation problem. They have been found to be the most suitable techniques; being widely available and simple to set up the optimisation problems.

Five versions, or levels, of the active MPFR soft-sensing algorithm are available depending on the complexity and of the measured downhole data. These levels suggest several types of data acquisition and analysis model to estimate measurements through performing an inverse modelling. The difference between measured information and model predictions are used to form the mismatch objective functions of steps 1 and 2 of the algorithm.

It was discussed that a multi-phase flow model is formulated in the algorithm to predict the well rates, annular and tubing pressures and temperatures. The equations used in the multi-phase flow model account for pressure drop in the reservoir, across the ICV and along well and temperature changes along the well, across the ICV and after commingle point of annular and tubing fluids (see Appendix C).

The next chapter will explore the validity of the active MPFR soft-sensing algorithm by applying it to estimate the zonal multi-phase flow rates in both synthetic and real examples.

Chapter 4 Active MPFR Soft-sensing Algorithm Validation & Case Studies

4.1 Introduction

This chapter explores the validity of the developed active MPFR soft-sensing algorithm. Synthetic, multi-zone I-wells and a real example of 2-zone I-well are used to investigate the applicability of the algorithm to estimate the zonal, multi-phase flow rates from individual zones of a multi-zone I-well. The synthetic examples are modelled using commercial OLGA/ROCX^{TM} simulator. It is addressed why such a dynamic simulator is suggested to model the multi-zone I-wells. These examples verify the applications of the algorithm in oil and gas reservoirs and I-wells with cross-flow problems or equipped with faulty ICVs and noisy sensors. The results are presented to explore the optimum number of flow tests required to estimate the zonal flow rates. It is also discussed that the design of multi-rate flow tests are affected by the multi-phase flow model and the number of zonal properties to be estimated through the algorithm.

Several steps are proposed to estimate zonal oil and water flow rates in a real 2-zone I-well based on the provided multi-rate flow test and well build-up test information. The quality of these measurements to apply the individual levels of the algorithm is also tested. Then the most accurate zonal properties are estimated through the sequential steps and further flow test is proposed to improve the accuracy of the estimated zonal properties.

Finally, the impact of noisy measurements on the algorithm's robustness is observed by generating random errors in the synthetic measurements. Confidence interval is used to yield the interval estimation of zonal properties with a high confidence while errors are introduced in the measurements.

4.2 Reservoir/Wellbore Model in OLGA/ROCX

A reservoir/wellbore model is required to simulate the pressure and temperature distributions during multi-rate flow tests. The output results are then to be used as the input information for the multi-phase flow meter algorithm testing. A commercial, dynamic reservoir/well flow simulator (OLGA/ROCX^{TM}) is used in this study to model synthetic, multi-zone I-wells. It is important to use this simulator to capture the transient

effects of hydraulic and thermal interaction between reservoir, wellbore and intelligent well completions during active monitoring in the situations such as:

- Multi-branch flow
- Shut-in/start-up
- Well testing
- Water and gas coning
- Cross flow

The study by Muradov and Davies (2009a) indicates that OLGA simulator allows building a model capable of correct flow rate performance prediction for advanced completion design. They tested several simulators (steady-state well flow simulator, reservoir simulator and dynamic well flow simulator) on their ability to predict the accurate flow rates using the temperature data. The dynamic well flow simulator OLGA was proved to provide with independent, reference well temperature and pressure profiles. The important process of heat exchange between the tubing and annulus is not captured by the steady state well flow simulators. Although the reservoir simulator is able to model the thermal effects between the tubing and annulus, it has limited use to simulate temperature distribution since any flow rate change has to be reflected by manual changes in the heat transfer coefficients for each well segment. The dynamic well flow simulator considers the thermal interaction present in intelligent wells between the tubing and annulus using the annular thermal coupling. Additionally, the required heat transfer coefficients are calculated in-situ. Examples of similar temperature profile between Muradov and Davies (2008) semi-analytical model and OLGA simulator for more complex cases (multi-zone I-well with multi-phase flow) can also be found in the published literature (Muradov and Davies, 2009b). As a result, OLGA simulator is suggested as a suitable tool for providing accurate and realistic data for a synthetic case study of multi-zone I-wells.

The OLGA/ROCX^{TM} simulator consists of two flow models, one for the wellbore and one for the reservoir. These flow models are then integrated to allow the calculation of pressure and flow rates at the sandface. Table 4-1 lists the number of cases published in the literature to verify the performance of the integrated wellbore/reservoir dynamic simulation in OLGA/ROCX. To my knowledge, this study is the first work on coupling OLGA and ROCX to demonstrate the added value from I-wells

Table 4-1 Publication on OLGA/ROCX

Author, Year	Case	Synthetic/Real
(Sagen et al., 2007)	1) Start-up with gas coning and slugging 2) Start-up and shut-in of horizontal well	Synthetic
(Hu et al., 2007)	1) Well shut-in/start-up 2) Gas-lift casing heading 3) Dynamic gas coning 4) Cross-flow	Synthetic
(Hu et al., 2007)	1) Well testing	Real
(Chupin et al., 2007)	1) Gas storage reservoir 2) Well loading in a two-layer reservoir	Real
(Hu et al., 2010)	1) Liquid-loaded gas wells	Real
(Sagen et al., 2011)	1) Chemical placement operation 2) Load on sandface during well bean-up	Real

4.2.1 Wellbore Model

The (OLGA) wellbore model proposed by Bendiksen et al. (1991) simulates transient, three-phase flow in pipes. At each time step, the model solves the following equations along with the relations describing the friction at the wall and the fluid interface, the droplet and bubble entrainment and the droplet deposition:

- Five coupled mass conservation equations for the gas phase, the water droplets, the oil droplets, the oil film and the water film
- Three momentum equations for the gas/droplet field, the oil film and the water film
- One single energy balance equation for the fluid mixture

The flow model can be used for complex well trajectory and completion type such as undulating, multi-lateral and intelligent wells. It accounts for transient heat transfer between the tubing and the annulus and between the annulus and the formation. The effects of frictional cooling/heating of the flow in the wellbore together with Joule-Thomson effect of the flow from the reservoir to the wellbore are considered in the model.

4.2.2 Reservoir Model

The reservoir model (ROCX) developed by (Sagen et al., 2007) is used to simulate the three-phase Darcy flow in porous medium. The model solves fully implicitly the oil, water and gas mass conservation equations plus the energy balance equation using the Newton-Raphson method at each time step. Appropriate set of closure formula is also used to describe the volume balance for the phases. Rock porosity and permeability, fluid transport properties and thermal properties of the rock and fluid are combined to build the numerical reservoir model with either a radial or a rectangular grid system. The initial conditions of the phase pressures and saturations at each grid block together with constant or time dependent boundary conditions at both the well and the outer boundaries of the reservoir must be defined prior to simulation.

4.2.3 Integrated Model

The integrated simulation is controlled by OLGA's wellbore model in OLGA. It provides the pressure boundary for the reservoir model while the reservoir model calculates the flow rates of the phases flow into the wellbore. Figure 4-1 illustrates the steps of numerical coupling between the two models implemented in an implicit scheme. The sensitivity coefficients "a" and "b" are calculated using the Jacobian matrix of the reservoir model at the last iteration (Hu et al., 2007).

$$a_P^n = \frac{dM_P^n}{dP_P^n} \tag{4-1}$$

$$b_P^n = M_P^n - a_P^n P_P^n \tag{4-2}$$

where P_P and M_P are the wellbore pressure and mass flow rates respectively and the subscript P refers to the phases, i.e. oil, water and gas. The Equation 4-2 can be analytically calculated from the reservoir model given by (Sagen et al., 2007). This implicit integrated reservoir model provides stable numerical simulation runs even with relatively large time steps.

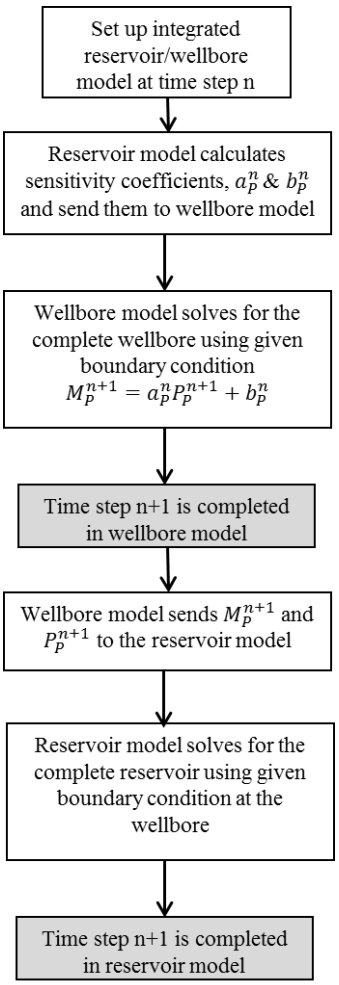

Figure 4-1 Steps of implicit coupled reservoir/wellbore model in OLGA/ROCX^{TM} (Hu et al., 2007)

The wellbore and reservoir models use a common PVT description of the reservoir fluid's properties, ensuring the PVT consistence across the sandface. There are three options to model PVT fluid properties in OLGA: 1) black oil tracking, 2) look up tables and 3) compositional tracking. Black oil tracking uses correlations for phase behaviour and physical property calculations according to the concentrations of the oil, gas and water components. Look up tables are pre-calculated tables which stores the calculated fluid properties in a table as a function of temperature and pressure for a fixed composition. Selected equation of state is used in the compositional tracking option where detailed fluid compositions are available to compose different fluids. A combination of options 1 and 2 was used in this study as the complicated third option was not suitable to model the fluid properties.

OLGA/ROCX can be initialised with either user-specified initial condition or use the simulation snapshot from a previous run. This snapshot can be from a previous (OLGA)

integrated simulation or from a standalone wellbore and reservoir simulations of the individual wellbore and reservoir models. This latter approach can lead to a significant improvement in the simulation's run time efficiency. For instance, standalone reservoir simulation may be run separately until condition of interest is reached. It's then coupled to the wellbore model and the simulation continued. Much greater computational resources are required of the coupled model is employed from the very beginning due to the integrated simulation selecting a smaller time step than the either wellbore or the reservoir models. Hence its speed is considerably less than the one for standalone simulation of two models.

4.3 Synthetic Case Studies

Six cases were built with both the OLGA (steady-state fluid inflow) and the coupled OLGA/ROCX (transient fluid inflow simulation) to study the applicability of the active soft-sensing technique. The use of different levels of data analysis, which depends on the measurement availability, was tested in order to estimate the individual zonal properties required to calculate multi-phase zonal flow rates.

4.3.1 3-zone Intelligent Well in an Oil Reservoir (Oil and Water Production)

A synthetic reservoir simulation model containing a three-zone, horizontal I-well was used (Figure 4-2). Three isolated reservoir zones have the same fluid properties, size and fluid saturations with different reservoir pressures and horizontal and vertical permeabilities (Table 4-2).

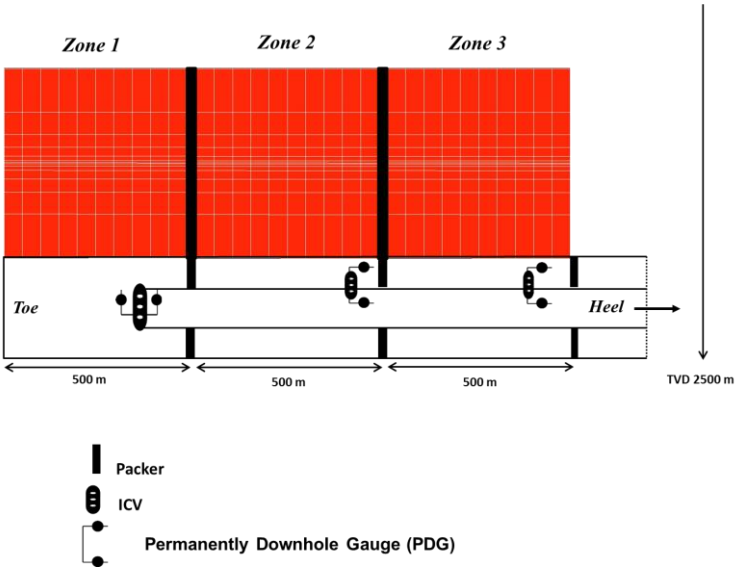

Figure 4-2 A schematic view of 3-zone I-well

Each zone was modelled as a separate, rectangular reservoir with 10x27x13 grid blocks in the x, y and z directions respectively. The zones contain both oil and water. Zonal reservoir inflow was distributed along the horizontal wellbore with multiple inflow points. Near-wellbore grid refinement was employed in the y and z directions to acquire high quality, transient pressure data. The transient pressure data was analysed with commercial, PBU interpretation software to validate the applicability of the analytical PBU model to be used later. Figure 4-3, Figure 4-4 and Figure 4-5 illustrate the zonal PBU test interpretation of the measurements produced by the two simulation models. Table 4-3 indicates a reasonable match between the input permeabilities in the simulator and the ones estimated from the PBU tests. This confirms the compatibility between the well/reservoir simulation model and the selected data interpretation models.

Table 4-2 Properties of individual zones

Property / Zone	Pr (psia)	PI_o (STB/D/psia)	$K_{v,o}$ (md)	$K_{h,o}$ (md)	$K_{v,w}$ (md)	$K_{h,w}$ (md)	Water-cut (fraction)
Zone-1	5801	1.5	3.3	0.33	1.24	0.124	0.33
Zone-2	5729	1.2	2.47	0.247	0.93	0.093	0.33
Zone-3	5656	0.8	1.65	0.165	0.62	0.062	0.33

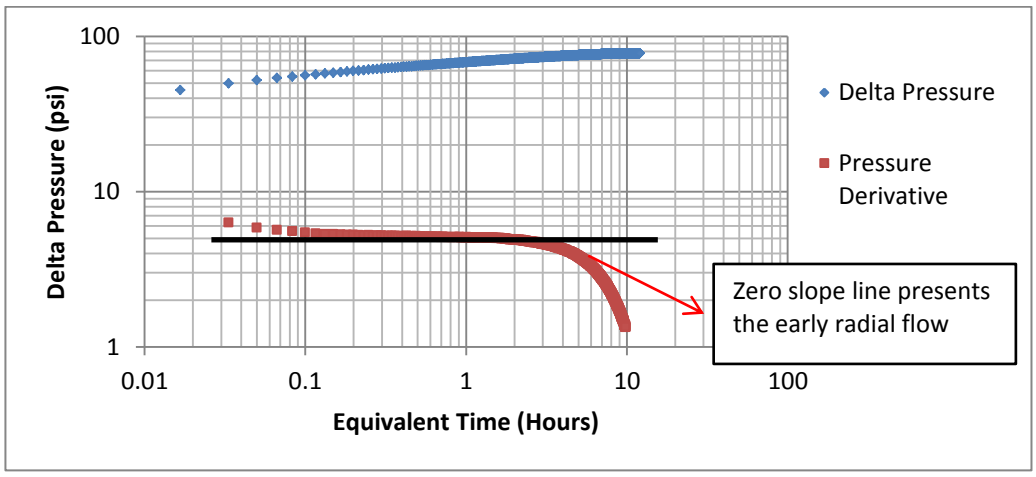

Figure 4-3 Pressure transient analysis performed on zone-1 pressure build-up test

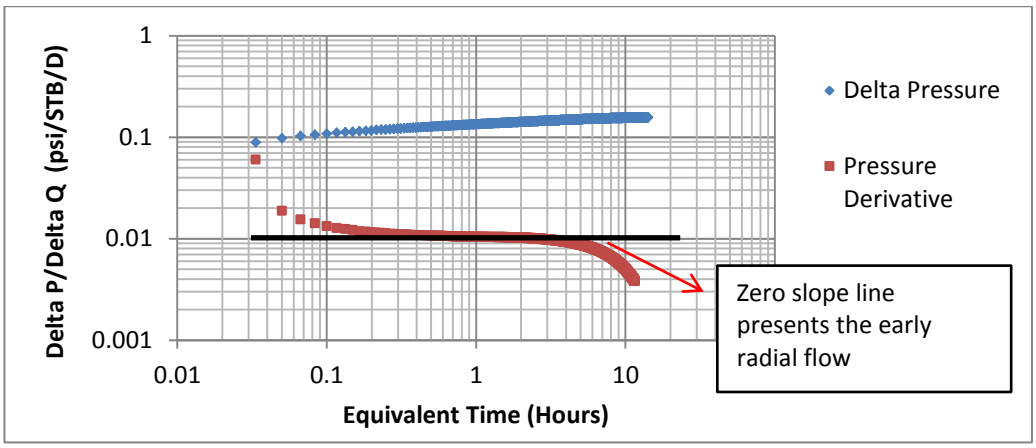

Figure 4-4 Pressure transient analysis performed on zone-2 pressure build-up test

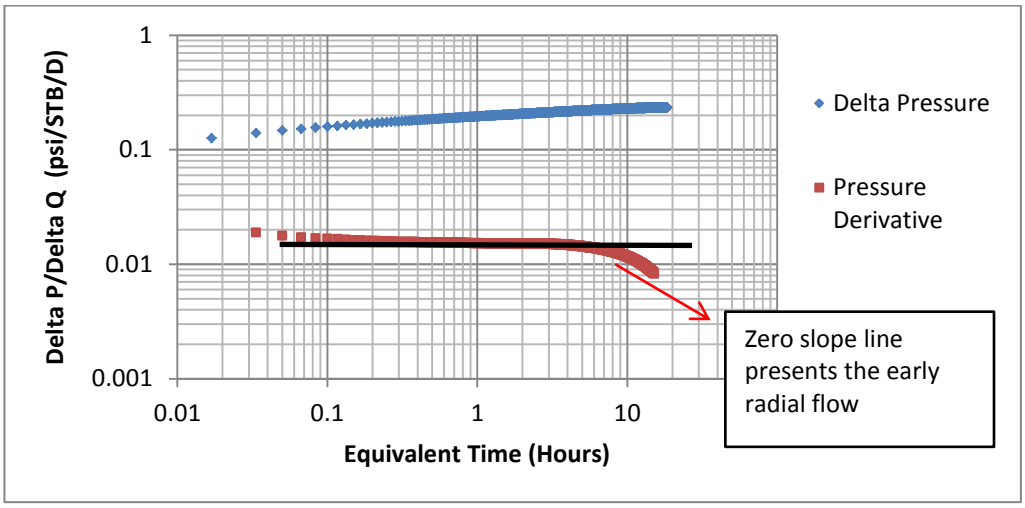

Figure 4-5 Pressure transient analysis performed on zone-3 pressure build-up test

Table 4-3 Comparison of Input and PBU derived reservoir zone permeability

	Input Values (md)			**Values obtained (md)**	
	K_h	**K_v**	**K_{bar}***	**K_{bar}**	**Relative Error (%)**
Zone-1	20	2	6.3	5.7	9.5
Zone-2	15	1.5	4.7	4.2	10.6
Zone-3	10	1	3.2	2.9	9.4

*$K_{bar} = \sqrt{K_h K_v}$

The ICV position combinations listed in **Error! Reference source not found.** formed the first 4 flow tests. The zonal properties (reservoir pressure, productivity index and water-cut) were estimated by minimising the total mismatch function in optimisation

step 1. The synthetic measurements are the well oil and water production rates, the stabilised annulus and tubing pressures across each zone and the transient annulus pressures of the shut-in zones. Our synthetic case study employed Level I, II and IV data analysis. The highest levels include the response of the reservoir/well system to alterations in the ICV positions – the pressure drop from the reservoir to the annulus (reservoir response, level I and IV) and the pressure drop across an ICV (level II).

Figure 4-6 summarises three iterations to find the extra flow tests required to estimate the multi-phase flow rates. These flow tests are designed in the optimisation step 2 in order to maximise the mismatch of individual flow tests. The first iteration corresponds to the first simplex whose vertices are initial four flow tests. Fifth flow test placed the flow test with least mismatch to form the second simplex in the second iteration. Flow tests 1, 3, 4 and 5 are the vertices of the second simplex. The flow test is discarded at each iteration is highlighted with red colour. Fifth flow test has the least mismatch among the other vertices of the second simplex and replaced with the sixth flow test in the next iteration as shown in Table 4-4. The values of the mismatch from individual flow tests change due to the update of the estimated zonal properties at each iteration.

Iteration #1					
NO. Simplex	NO. Flow Test	ICV_1 Opening (fraction)	ICV_2 Opening (fraction)	ICV_3 Opening (fraction)	Mismatch Eq. (3-7)
1	1	1	1	1	0.30
	2	0	1	1	0.27
	3	1	0	1	1.63
	4	1	1	0	0.37

Iteration #2					
NO. Simplex	NO. Flow Test	ICV_1 Opening (fraction)	ICV_2 Opening (fraction)	ICV_3 Opening (fraction)	Mismatch Eq. (3-7)
2	1	1	1	1	0.27
	3	1	0	1	1.64
	4	1	1	0	0.27
	5	1	0.3	1	0.109

Figure 4-6 How DC optimisation method designs the next flow test

Table 4-4 lists the ICV opening fractions for flow tests 5 and 6, required by the Level I, II and IV analysis; while Figure 4-7 presents the annular PBUs used in the level IV analysis.

Table 4-4 ICVs opening fraction corresponding to each flow test

NO. Simplex	NO. Flow Test	fraction of area open to flow			Q_o (STB/D)	Q_w (STB/D)	P_{an1} (psia)	P_{an2} (psia)	P_{an3} (psia)	P_{tub1} (psia)	P_{tub2} (psia)	P_{tub3} (psia)
		ICV_1	ICV_2	ICV_3								
1	1	1	1	1	518	260	5613	5586	5575	5573	5573	5573
	2	0	1	1	518	260	5800	5445	5412	5395	5395	5395
	3	1	0	1	518	260	5548	5724	5486	5478	5478	5478
	4	1	1	0	518	260	5589	5559	5651	5541	5541	5541
2	5	1	0.3	1	518	260	5598	5625	5556	5553	5553	5553
3	6	1	0.6	1	518	260	5609	5598	5571	5569	5569	5569

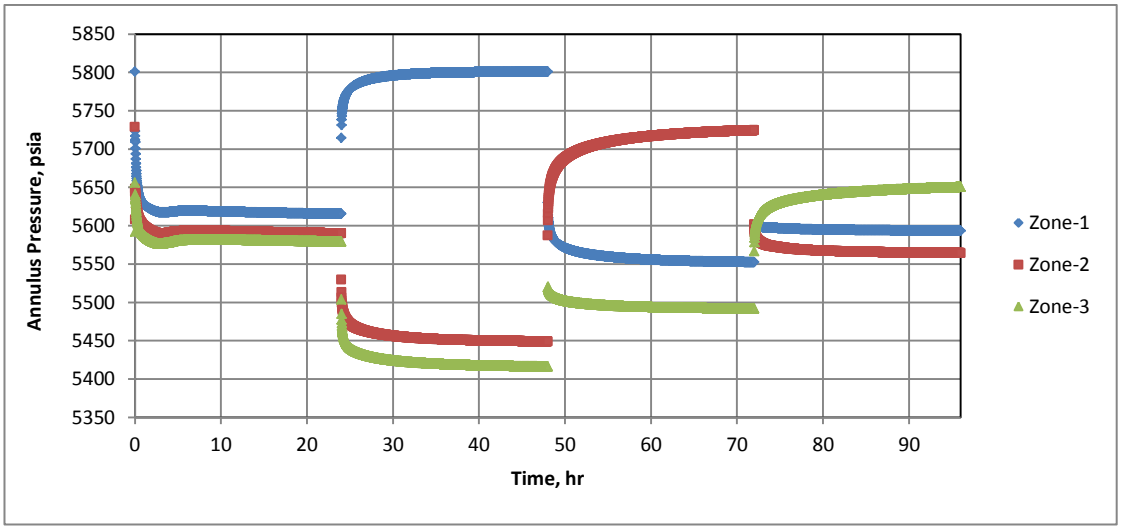

Figure 4-7 PBU tests performed on the individual zones during the initial four flow tests

The boundary condition at heel section was a constant liquid production of 800 STB/D. However, results indicate that OLGA simulator meets the constraint rate with a numerical error of 22 STB/D. Figure 4-8 shows that around 800 STB/D oil phase is produced at early time steps then it is reduced to 518 STB/D while water breakthrough occurs and its production increases to 260 STB/D. This trend is continued for the remaining simulation time in which ICVs position are regulated.

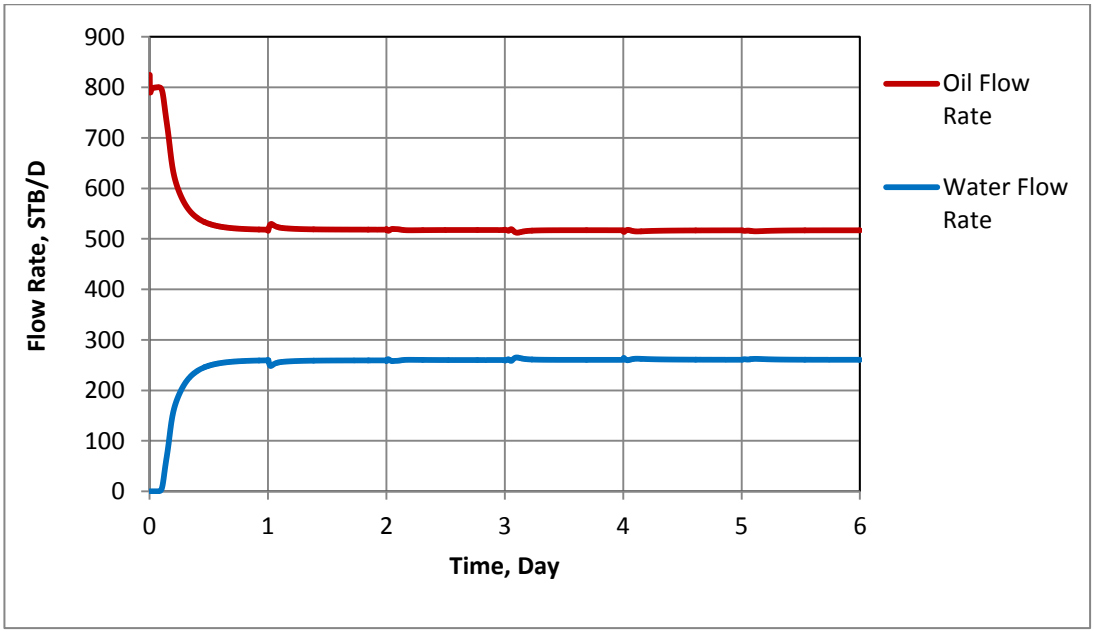

Figure 4-8 Well oil and water production during individual flow tests

The workflow continued by estimating the zonal properties using the optimisation Steps 1 and 2 (discussed in Chapter 3) until the estimated properties start converged near their true values. Figure 4-9 illustrates this convergence for the zonal reservoir pressures, productivity indices and water-cuts. The equation used to calculate the total misfits of estimated zonal parameters is:

$$\text{Total Misfit} = \sqrt{\sum_{i=1}^{n} \left(\frac{\text{estimated value} - \text{true value}}{\text{true value}} \right)^2_{\text{zone}_i}} \qquad 4\text{-}3$$

where n stands for the number of the zones completed along the I-well. The total misfit is a dimensionless parameter used to compute the relative error (misfit) of the estimated individual properties of all production intervals. The active soft-sensing algorithm stops when one of the following conditions occurs:

1) No changes are observed in all estimated reservoir parameters. Here, It is assumed that the optimisation process stops when the difference between the two last total misfits (see Equation 4-3) is less than or equal to 0.01 for all zonal properties. This corresponds to that part of Figure 3-2 where the acceptable accuracy is reached for zonal properties.
2) The deformed simplex optimisation method results in the same ICV configuration as those in the previous flow test (i.e. a new flow test with a higher mismatch cannot be found).

In this case, the test stopped after the sixth flow test, requiring a total of three simplex designs. The number of total flow tests and simplexes required to achieve the optimum estimation of zonal properties is equal to $n + x$ and $x + 1$ in a n-zone I-well where x corresponds to those additional flow tests obtained by DC algorithm. This is valid if step $\alpha = 2$ is sufficient to design a next flow test with mismatch higher than the arithmetic average of the mismatch at each optimisation step for the previous flow tests. If step with $\alpha = 2$ maximised the objective function, the steps with $\alpha > 2$ were not applied to achieve a higher maximisation in the objective function as it was planned to keep the number of flow tests as minimum as possible. α is the simplex size coefficient that is discussed in more details in Appendix B. By varying its value one can expand or contract the simplex in a selected direction of simplex centroid displacement, adapting the simplex form and size, in the best possible manner, to the optimised function topology. The design of next simplex may require the definition of α when the simplex algorithms is utilised for optimisation of nonlinear functions (Rykov, 1983).

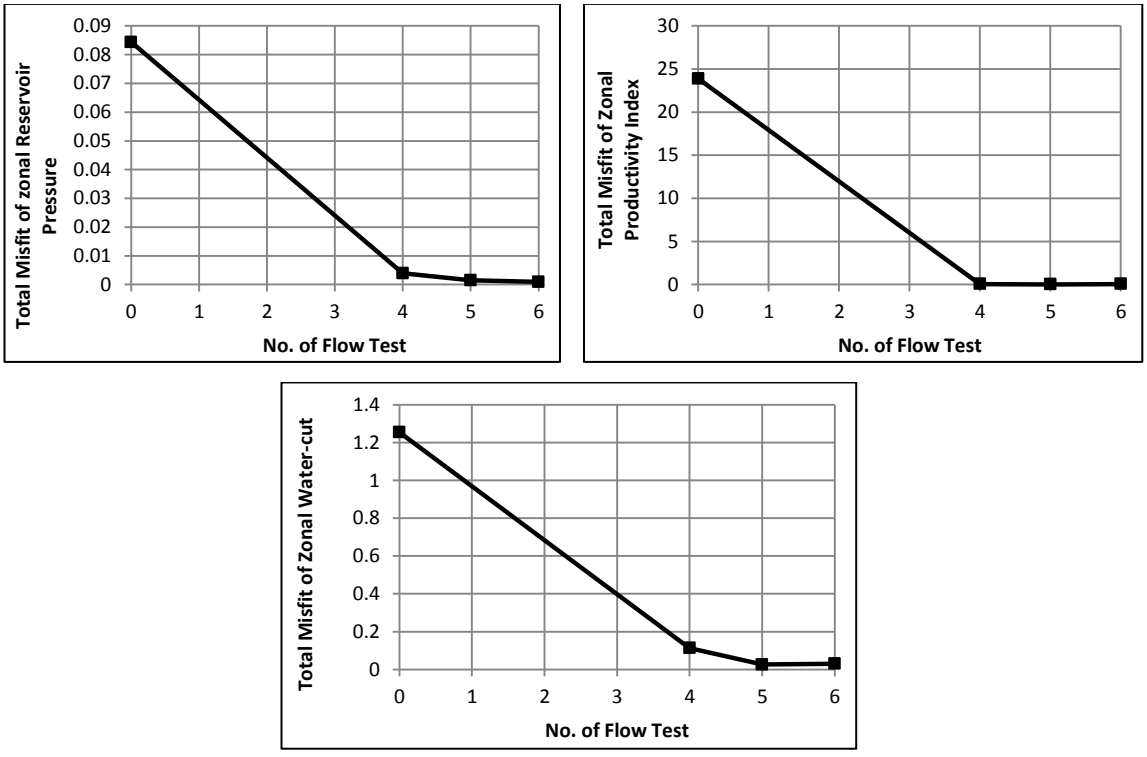

Figure 4-9 Trend of total misfit of zonal properties

4.3.2 3-zone Intelligent Well in an Oil Reservoir (Oil, Water and Gas Production)

This synthetic example is a 3-zone intelligent well in OLGA simulator with steady-state inflow rate where three phases: oil, water and gas are present (Figure 4-10). It was

assumed that both pressure and temperature are measured in the annulus and tubing sections via downhole P/T gauges installed on either side of the ICVs. The Table 4-5 level I, II and III measurements were applied to calculate zonal properties (reservoir pressure, productivity index, water-cut and annular gas mass fraction) and estimate the oil, water and gas flow rates across each producing interval. A reasonable reduction in the objective function mismatch was observed for all properties at the end of the eighth flow test (fifth simplex) which shows that all zonal properties have converged to the true values (Figure 4-11).

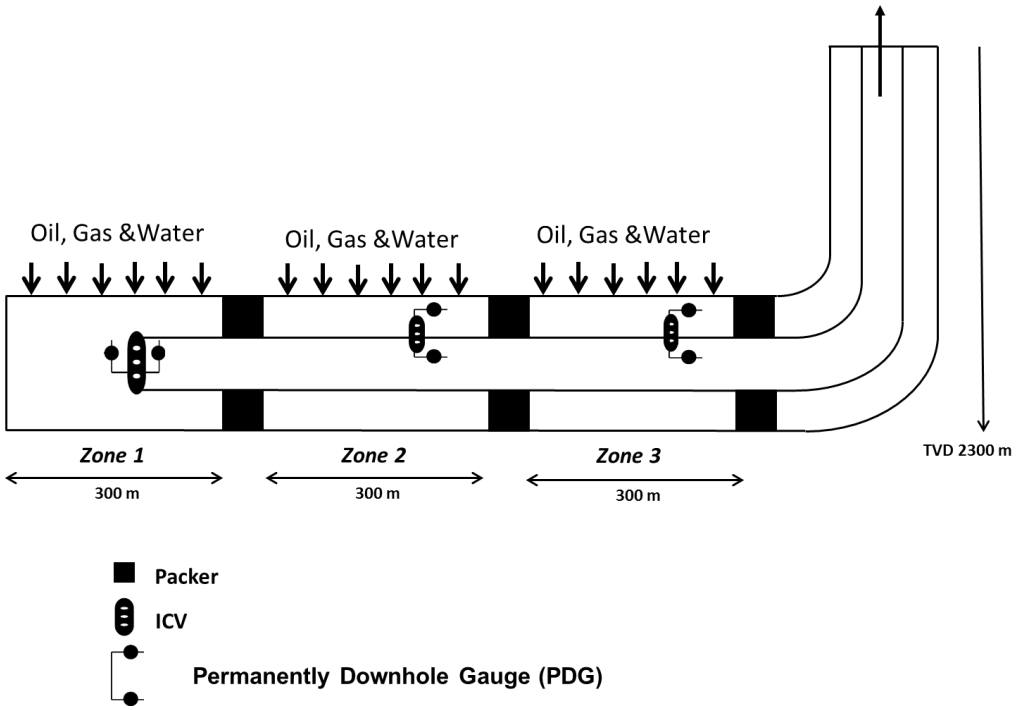

Figure 4-10 A schematic view of modelled 3-zone I-well in OLGA

Table 4-5 Temperature, pressure and well rates measurements in a 3-zone I-well

Exp. No.	P_{an1}	P_{an2}	P_{an3}	P_{tub1}	P_{tub2}	P_{tub3}	T_{an1}	T_{an2}	T_{an3}	T_{tub1}	T_{tub2}	T_{tub3}	T_{mix2}	T_{mix3}	Q_{liquid} (STB/D)	Q_{oil} (STB/D)	Q_{Water} (STB/D)	Q_{gas} (MSCF/D)
1	3324.33	3320.68	3308.59	3323.77	3320.63	3308.58	74.95	73.50	71.38	74.82	74.04	73.07	74.01	72.99	10507.89	5397.63	5110.26	6590.45
2	3399.99	3244.53	3237.32	3244.25	3244.27	3237.27	75.00	72.97	70.78	72.97	72.97	71.68	72.97	71.63	10282.42	7576.51	2705.91	9287.70
3	3299.37	3379.98	3284.56	3298.37	3292.84	3284.54	74.94	73.76	71.50	74.87	74.62	73.19	74.57	73.10	10283.31	4611.86	5671.45	4804.41
4	3313.59	3308.85	3359.76	3312.86	3308.78	3292.76	74.94	73.51	71.62	74.83	74.05	73.47	74.02	73.37	10405.39	4872.18	5533.21	6573.12

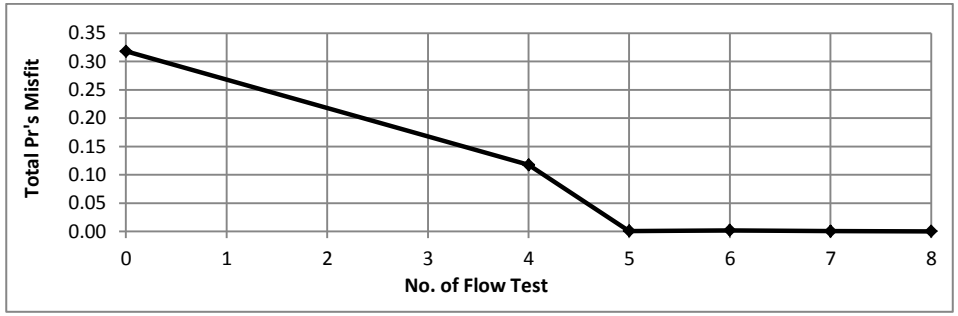

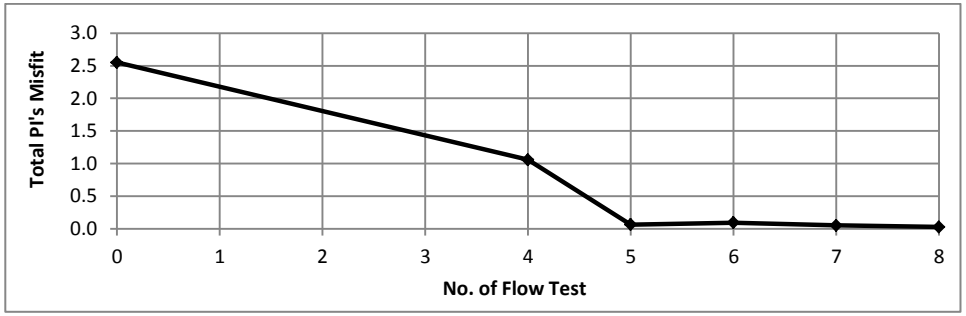

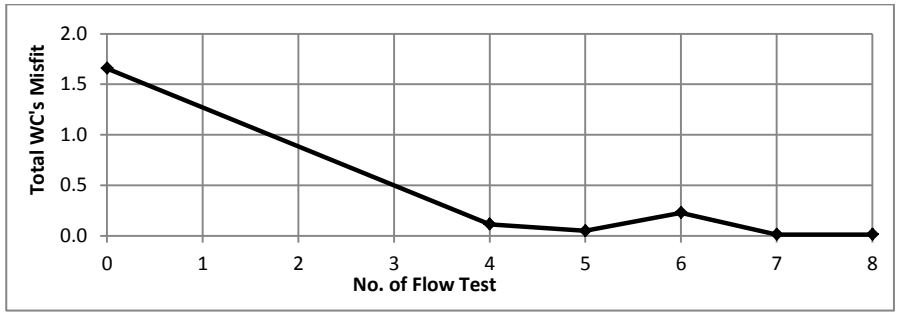

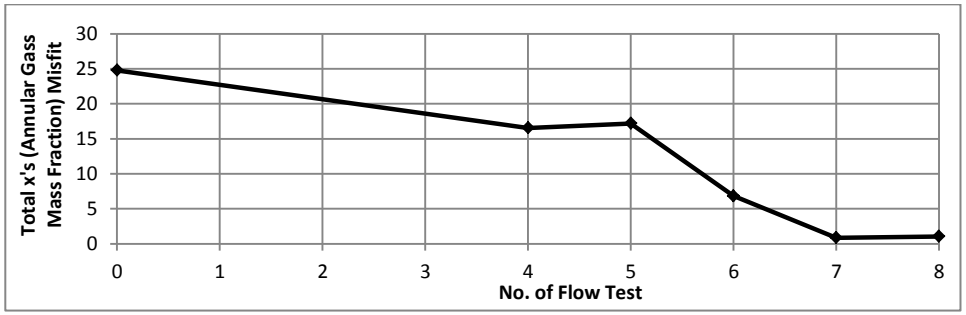

Figure 4-11 Trend of total misfit of zonal properties

4.3.3 3-zone Intelligent Well in a Gas Reservoir (Gas and Water Production)

The proposed active soft-sensing technique can be used to determine the downhole flow rates in a commingled gas production system provided an appropriate multi-phase flow model is used. In this study, backpressure (Fetkovitch) model (Rawlins et al., 1935) is used to describe the zonal gas inflow into the horizontal wellbore (Equation 4-4).

$$q_g = C(P_R^2 - P_{wf}^2)^n \quad 4\text{-}4$$

where C and n define the performance coefficient and the equation's exponent. Coefficient C accounts for the reservoir rock properties, fluid properties and reservoir flow geometry; while n considers the additional pressure drop due to high-velocity gas flow as it varies from 1 (laminar flow) to 0.5 (fully turbulent flow).

In this case study, water and gas well rates measurements together with the annular and tubing pressures at each ICV are considered so that Levels I and II of the active soft-sensing algorithm can be implemented.

Individual zones were modelled with different values of C, n and water-gas ratio (WGR), representing a range of the different gas and water flow conditions for each producing interval (Figure 4-12). Figure 4-13 shows the convergence of the estimated zonal properties with the number of flow tests. Convergence of the zonal properties was slower than for the simpler, all oil case due to nonlinearity and the extra unknowns in the backpressure equation. A higher number of flow tests and measurements are thus required to estimate the zonal, multi-phase flow rates reliably.

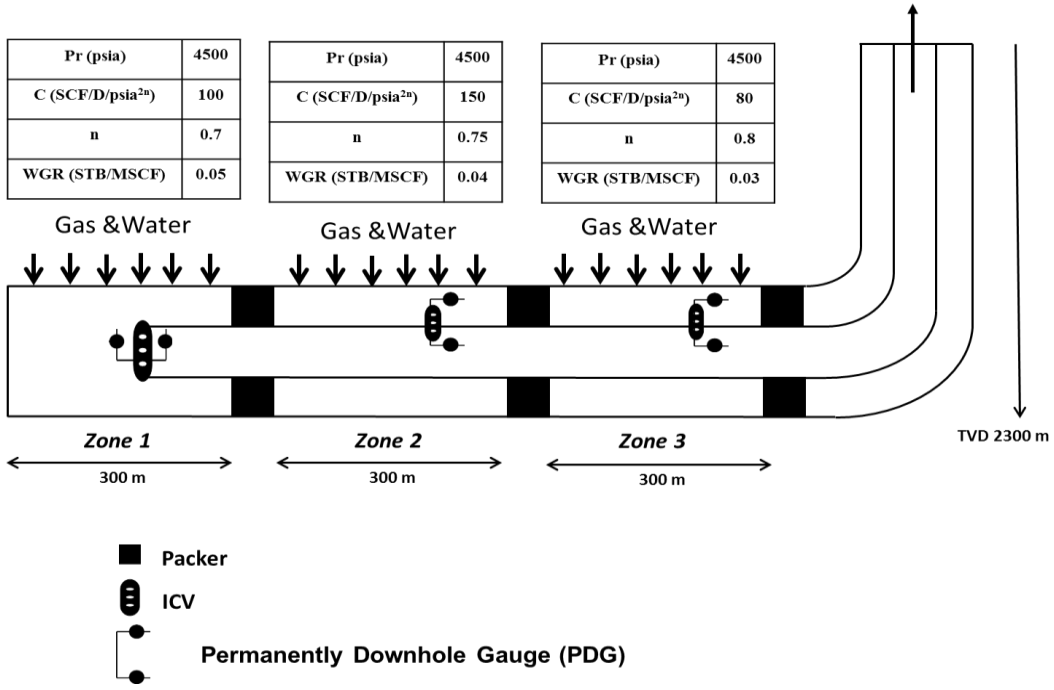

Figure 4-12 A schematic of I-well together with zones properties in a gas reservoir

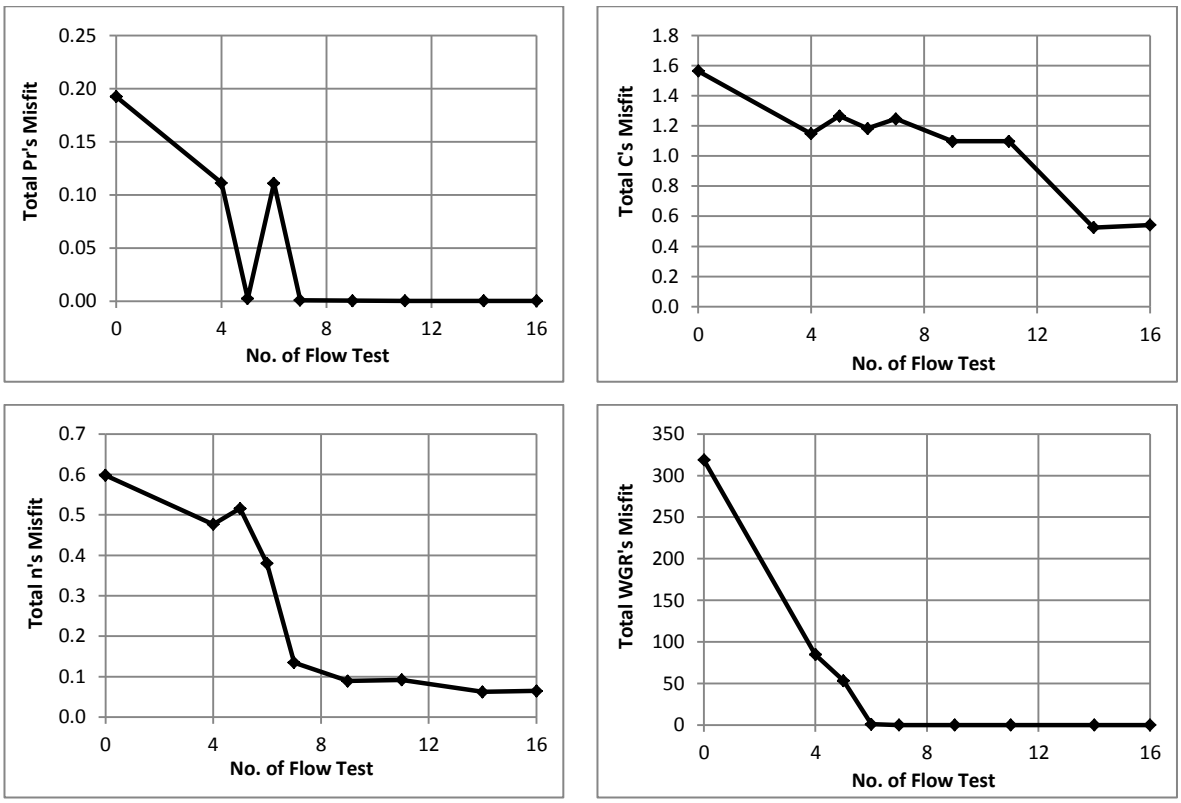

Figure 4-13 Convergence trend of zonal properties to their true values for a gas reservoir

4.3.4 5-zone Intelligent Well with Cross-flow in Oil Reservoir

A 5-zone intelligent well was built in OLGA and steady-state inflow was assumed across individual zones. All zones were modelled with different reservoir pressures to simulate the cross flow phenomena inside the wellbore. Figure 4-14 shows the 5-zone intelligent well model in the OLGA GUI together with details of the zonal characteristics. It was assumed only oil and water phases flow inside the wellbore and the intelligent well completion and zonal annulus and tubing pressures are measured in addition to well oil and water production rates. These measurements are sufficient to apply levels I and II of the active soft-sensing technique.

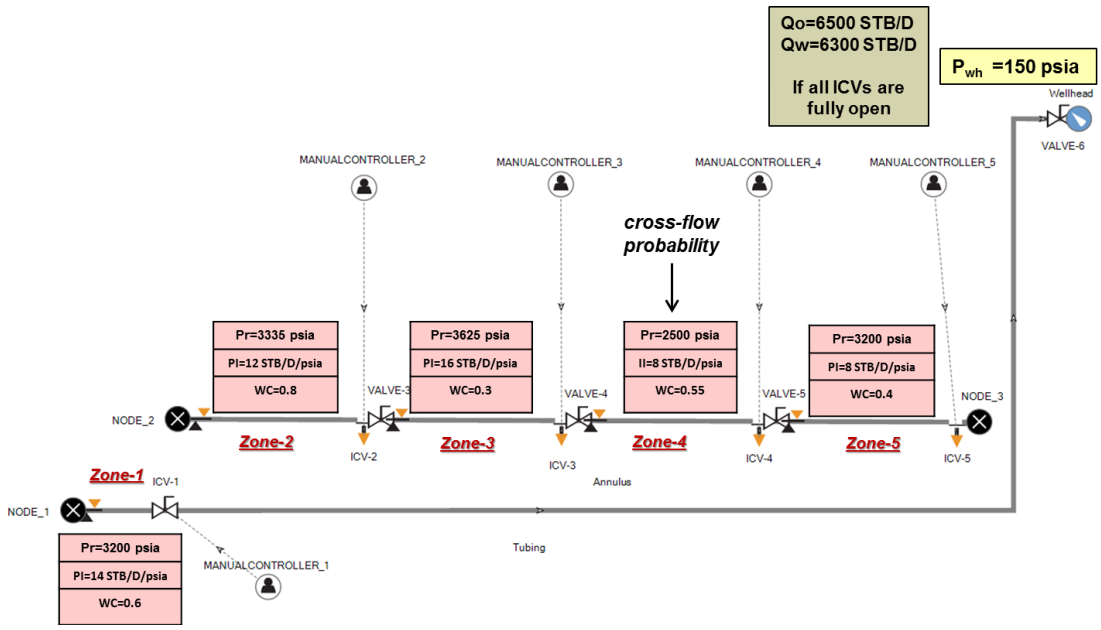

Figure 4-14 A schematic of 5-zone intelligent well in OLGA GUI

Zone 4 has the low pressure and causes cross-flow from the other zones (Figure 4-15). The zone liquid injectivity index (II) was set to 8 STB/D/psi and the ratio of the water phase to total liquid injected into zone 4 was 0.55. The active soft-sensing algorithm was implemented using levels I and II and results showed that the minimum misfit of zonal properties can be obtained after designing eight flow tests. Figure 4-16 shows that the active soft-sensing algorithm has been terminated at the end of eighth flow test to confirm all zonal properties converge to their true values.

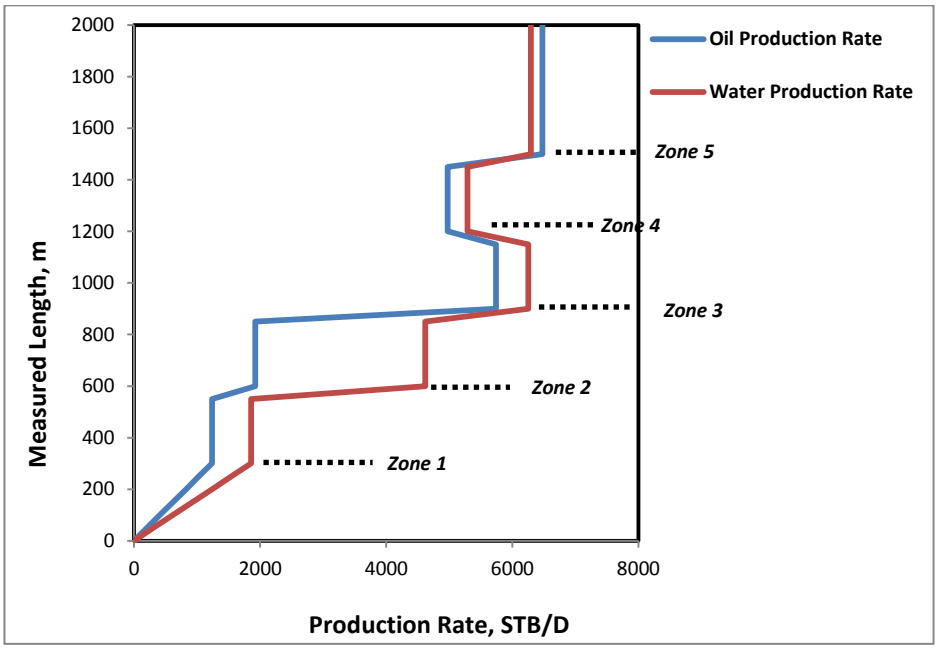

Figure 4-15 Inflow profile of oil and water production along individual zones

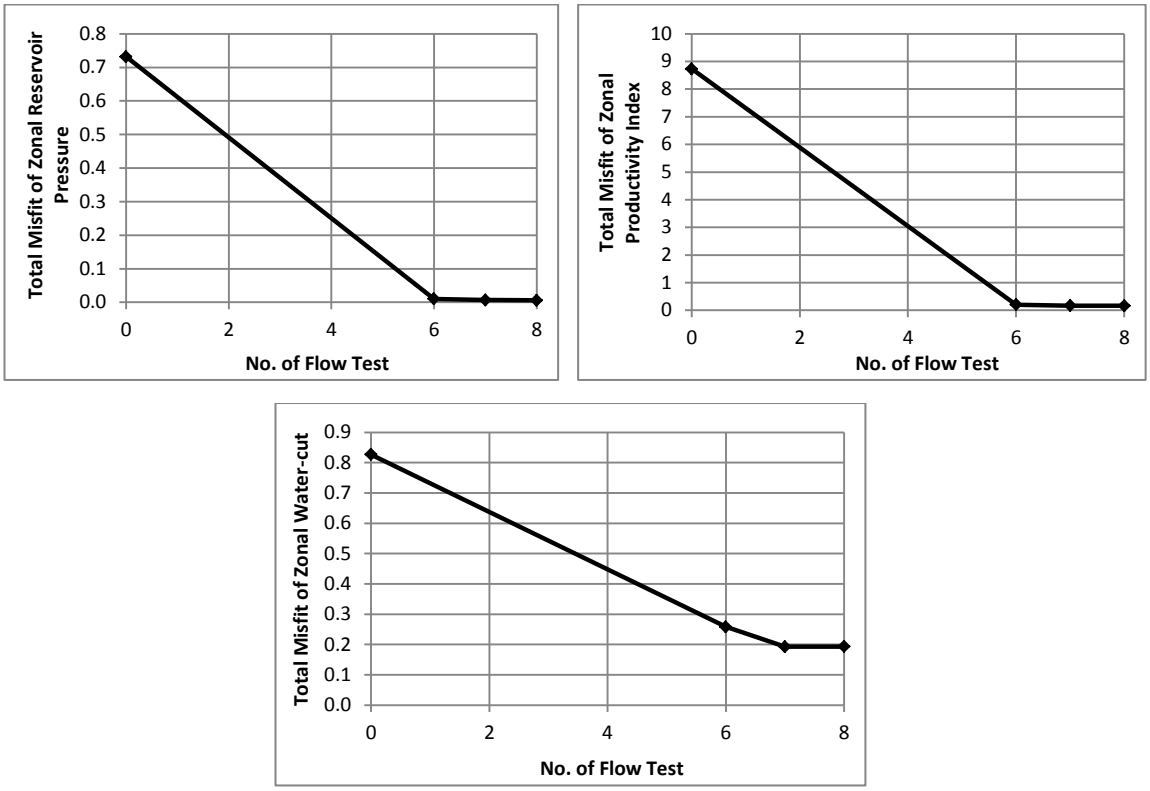

Figure 4-16 Trend of the total misfit of zonal properties

4.3.5 Optimisation of Wellhead Choke and ICV Position during Flow Rate Allocation in a 3-zone I-well

A 3-zone I-well modelled in OLGA^{TM} was used for this study. The well is 2300 m TVD deep and the 900 m horizontal completion produces 30^{o} API oil and water. The zonal properties for zones 1, 2 and 3 are; reservoir pressures of 4350 psi, 4050 psi, and 3625 psi, oil productivity indices of 9 STB/D/psi, 7 STB/D/psi, 4 STB/D/psi with a water-cut of 20%, 5%, and 30% respectively. The reservoir zones are separated by packers and the inflow into the tubing is controlled by ICVs. The well is operated at the wellhead pressure of 150 psi (see Figure 4-17).

The wellhead choke may be accepted as an extra control variable in the active soft-sensing algorithm while one of the ICVs can now be constrained to be fully open and the wellhead pressure or the well production rate is controlled by the surface choke. This practical scenario is important when ICV control is determined by operational reasons or operators are interested in maintaining production from a high productivity zone with fully opened ICV. Here, it is assumed that ICV_3 is non-operational (i.e. it cannot be moved) but all the PDG gauges measure the accurate pressure and

temperature either side of the ICVs. There is no need to consider the effect of vertical lift performance (VLP) in this example neither controlling nor objective function mismatch minimisation parts of the active soft-sensing. The DC optimisation method controls the ICVs and wellhead opening area based on the direct values of the objective function and the GRG method attempts to minimise the mismatch between the estimated information and those measured by the downhole gauges installed either side of the ICV's choke.

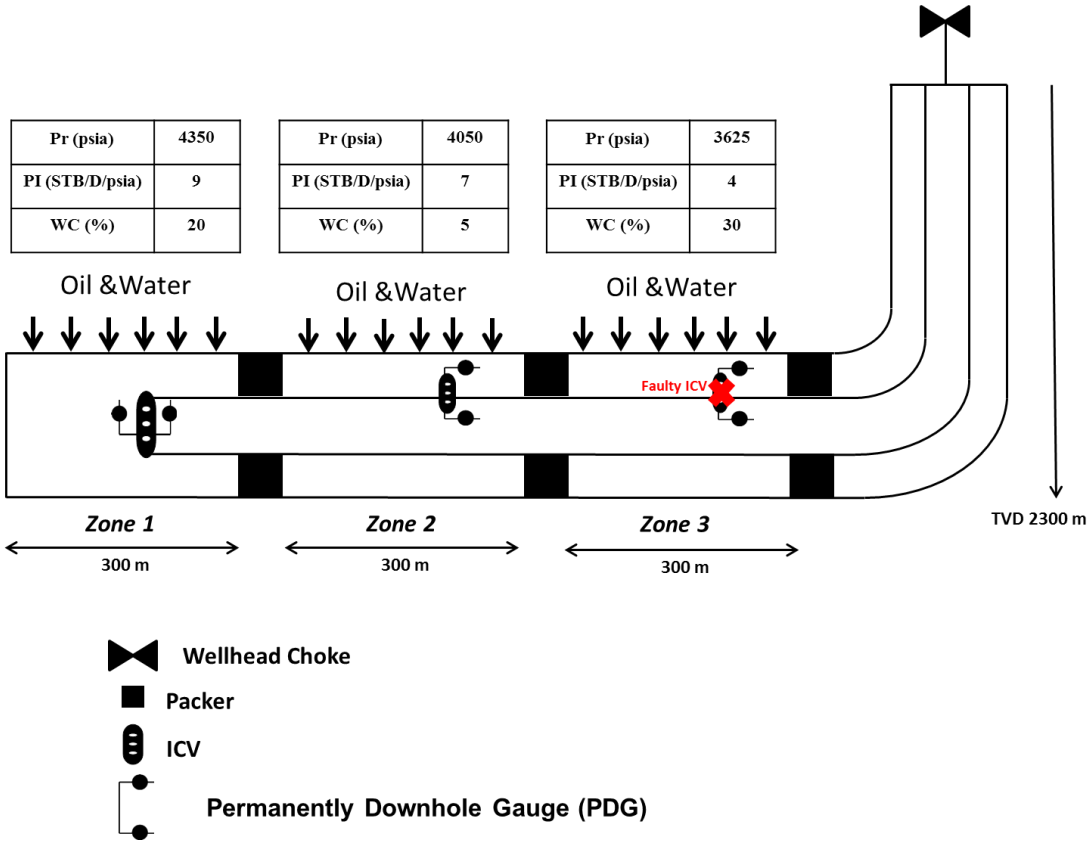

Figure 4-17 A schematic view of a 3-zone I-well equipped with non-operational ICV

The algorithm is initiated with four flow tests since two ICVs (ICV_1 and ICV_2) and the wellhead choke form the control variables of the DC optimisation problem. Table 4-6 lists the initial four flow tests where zones one and two are shut-in during the second and third flow tests respectively and the wellhead is choked during the fourth flow test. DC simplex optimisation suggests the ICV's opening area fraction and the wellhead choking for the next flow tests in order to achieve the best estimation of the zonal properties.

Table 4-6 ICVs and wellhead configuration during multi-rate flow tests

NO. Simplex	NO. Flow Test	fraction of area open to flow		
		ICV_1	ICV_2	Wellhead Chock
1	1	1	1	1
	2	0	1	1
	3	1	0	1
	4	1	1	0.5
2	5	1	0.3	0.7
3	6	1	0.9	0.9
4	7	1	0	0.9

Figure 4-18 summarises the satisfactory results obtained at the end of seventh flow test. Results show four simplexes are required to obtain the most accurate estimations for zonal reservoir pressure, zonal productivity index and zonal water-cut respectively.

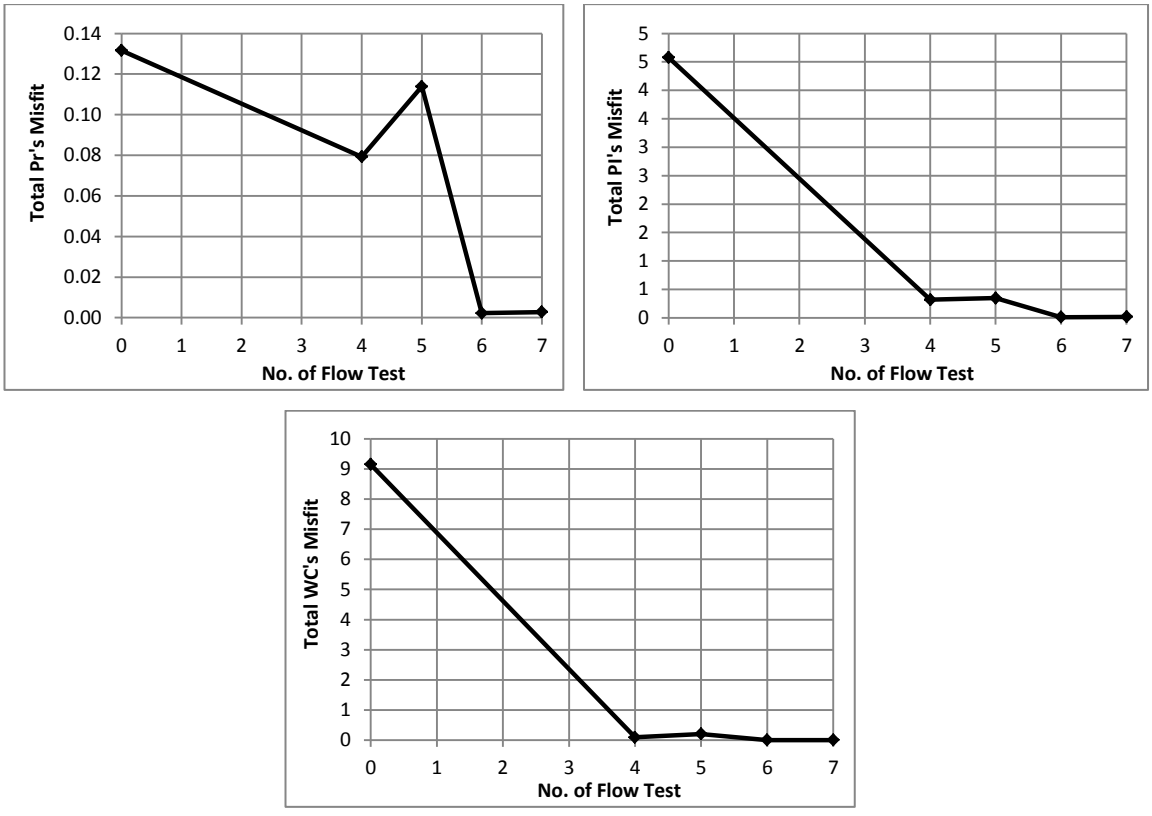

Figure 4-18 Trend of total misfit of zonal properties

4.3.6 Evaluation of Differential Drift of Pressure Sensors in a 3-zone I-well

The model presented in section 4.3.2 was used to test whether the active soft-sensing algorithm could identify measurable drift errors of downhole gauges. It was assumed

that the PDG pressure measurements installed on ICV_2 and ICV_3 had constant drift error of +15 and +25 psi respectively. The upstream (annulus) pressure of ICV_2 and ICV_3 is lower than the downstream (tubing) pressure when the zone is producing. This is against the expectation that the zonal annulus pressure must be higher than the zonal tubing pressure at the time of production from individual zones. These errors are added to the active soft-sensing algorithm as two extra control variables in addition to zonal properties. The algorithm can also be modified to recognise that the downhole gauges have a constant drift rate (e.g. X psi/year).

The results indicate that an accurate estimation of the zonal properties is feasible (see Figure 4-19). The algorithm could have been terminated at the end of tenth flow test however it continued to recommend further flow tests to estimate more accurate values of the zonal water-cuts and annular gas mass fractions. Figure 4-20 illustrates how the gauge's drift error is found more quickly than the zonal properties. This occurs because the latter ones have a nonlinear relationship with the measurements in the multi-phase flow model while the former are related to annular and tubing pressures through a linear equation:

$$\text{Estimated } \Delta P_{ICV} = \text{Measured } P_{annulus} - (\text{Measured } P_{tubing} - \text{Drift Error}) \qquad 4\text{-}5$$

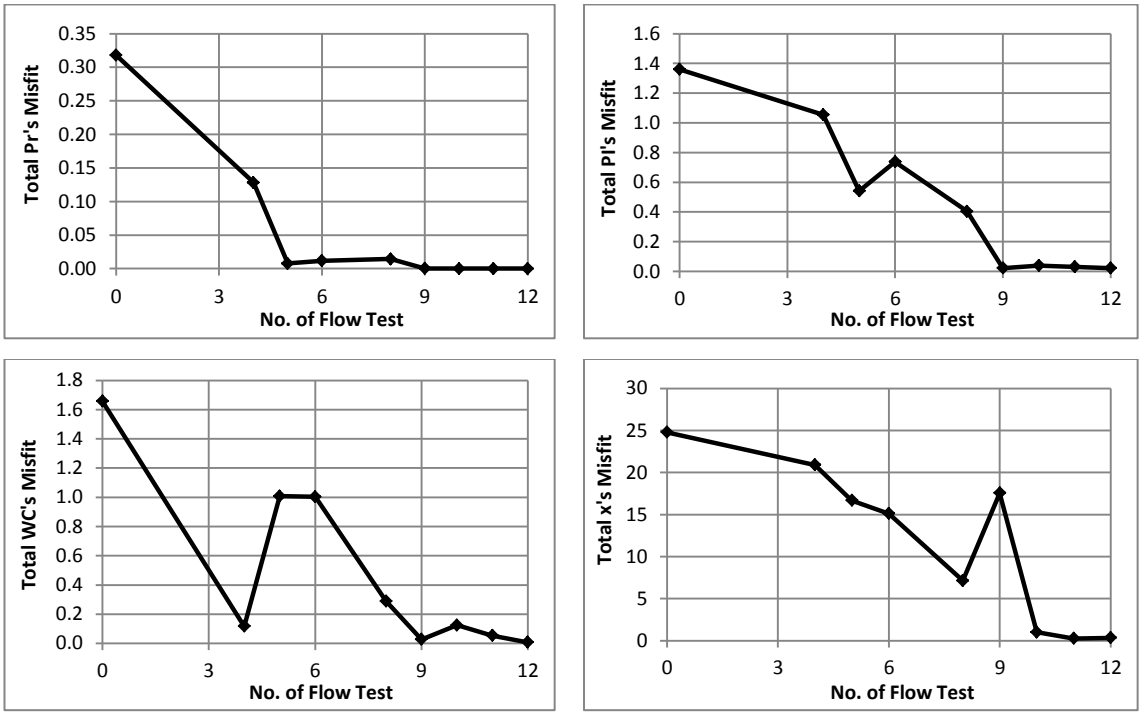

Figure 4-19 Trend of total misfit of zonal properties

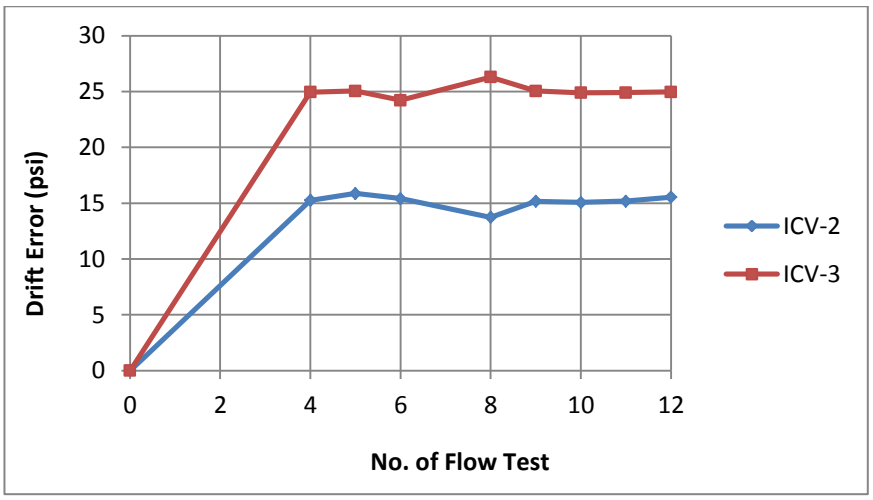

Figure 4-20 Estimated gauges drift error with number of flow tests

4.4 2-zone Intelligent Well (Real Example)

This section demonstrates how active soft-sensing algorithm can be applied to the management of a real two-zone intelligent well in an oil field. Figure 4-21 shows the well completion schematic of a horizontal wellbore producing from two zones, each of which is managed by a four position ICV. In addition, two permanent downhole gauges (PDG's) have been installed on either side of the ICV's flow restriction to measure the annulus and tubing pressure and temperature. Figure 4-22 shows the measured annulus pressure for each zone during the period 17th January to 29th March 2013 while Figure 4-23 records the measured annulus pressures during a multi-rate test including flow tests 1 to 5. The zonal temperature measurements were not used in this study as the measurement resolution was too low (1^{o} C) to detect meaningful temperature changes in the well and across the ICV.

Table 4-7 summarizes the data from Figure 4-23 for five flow tests during which the ICV position changed. A flow test is a production period with a specified ICV position. The annulus and tubing pressure, oil and gas production rates at the surface and the well water-cut were measured during each flow test.

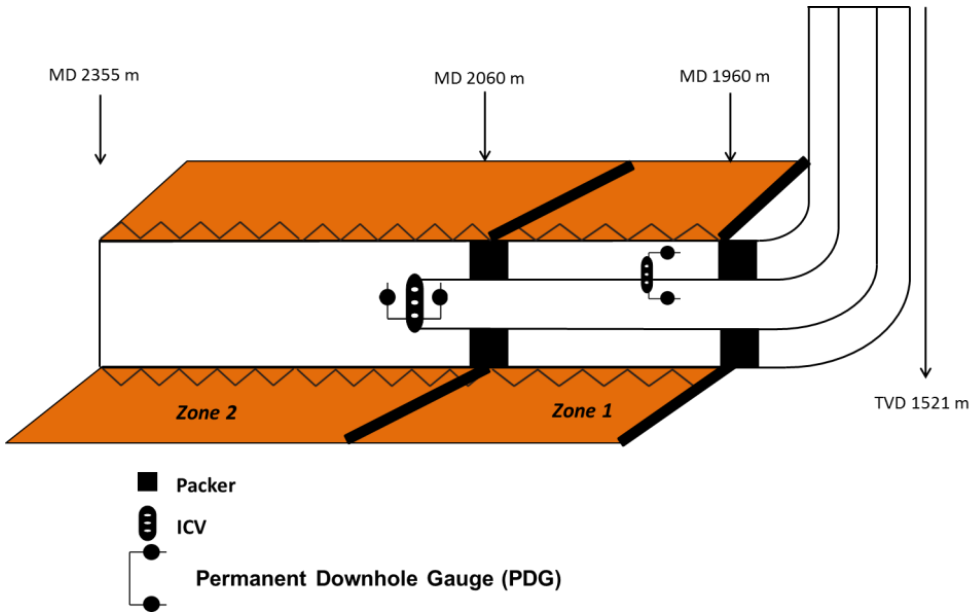

Figure 4-21 Schematic view of the real I-well

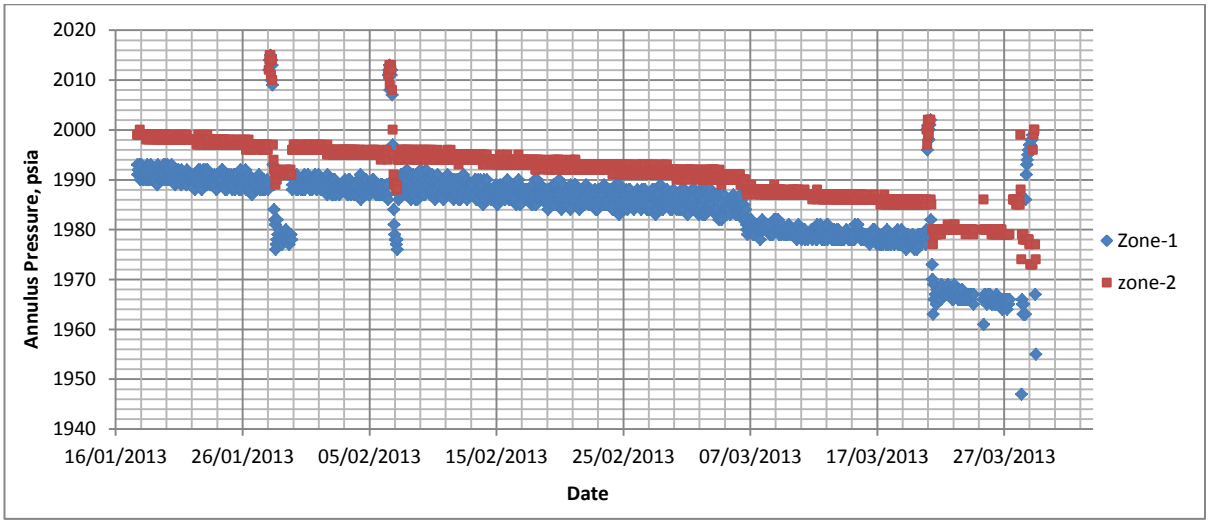

Figure 4-22 Measured Annulus pressure of zone 1 and 2, 17th January to 29th March 2013

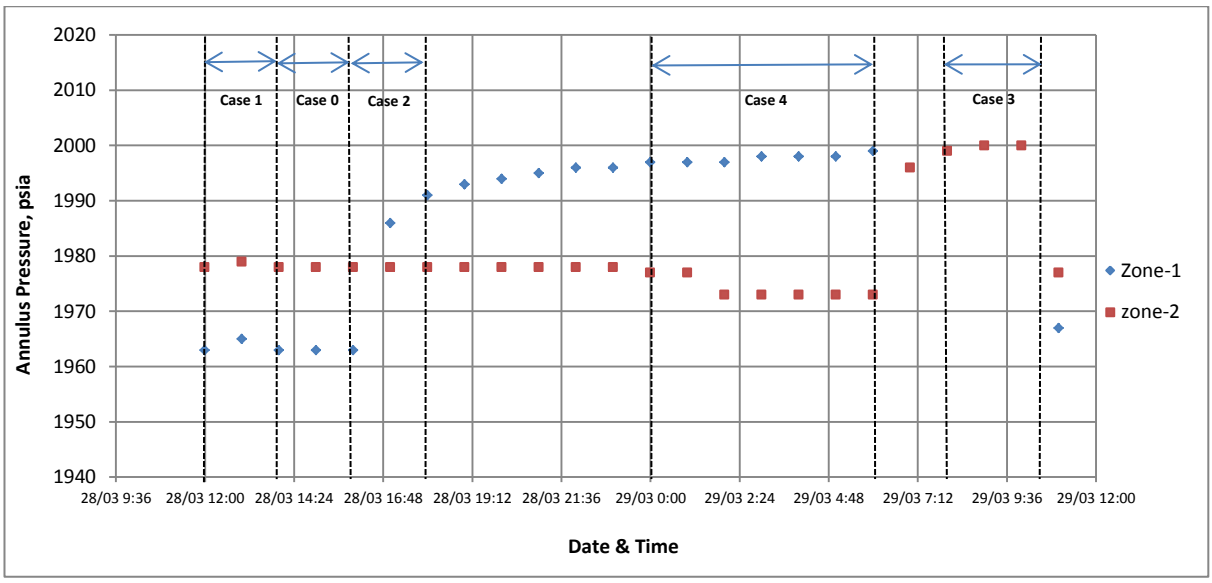

Figure 4-23 Measured Annulus Pressure of zone 1 and 2, flow test 1 to 5

Table 4-7 ICV positions and measurements from two-zone intelligent well during a multi-rate test

			PDG data						MPFM. Test for 2 hours.					
	% opening		psia						Rate (BLPD)	Water-cut %	Gas rate (MMscfd)	date	hrs	
			Z1			Z2								
	Zone 1	Zone 2	Tubular	Annulus	Delta P	Tubular	Annulus	Delta P					time start	time end
Flow Test 1	33	100	1966	1963	3	1979	1979	0	2251.2	13	3195.37	28-03-13	14:04	16:05
Flow Test 2	67	100	1966	1964	2	1978	1979	1	2309.4	12.94	3043.58	28-03-13	11:53	13:54
Flow Test 3	100	100	1965	1965	0	1979	1979	0	2236.5	12.9	3213.06	28-03-13	16:07	18:09
Flow Test 4	100	0	1286	1283	3	1285	2000	715	667.28	12.86	24.34	29-03-13	08:38	10:40
Flow Test 5	0	100	1954	1998	44	1973	1973	0	2182.9	13.16	3986.99	28-03-13	23:45	05:27

4.4.1 Which Active Soft-sensing Levels Can Be Applied to This Dataset

The active soft-sensing level depends on the data available. The transient and steady-state pressure measurements were analysed to determine if one or more of the active soft-sensing levels could be applied. Three levels of data analysis will be discussed:

Level I: The data in Table 4-7 indicates an unrealistically high gas production rate of 3000 MMSCF/D due to an erroneous gas measurement at the multi-phase flow meter. This data will be ignored since the annular and tubing pressures are higher than the produced fluid's bubble point. Hence, only liquids are present downhole. Level I can be potentially applied to all flow tests (1 to 5).

Level II: Flow tests 1 and 2 are candidates to perform level II as ICV_1 is choked during these tests. The measured tubing pressure is often greater than the annulus pressure

when the well is producing (Table 4-7). This indicates a gauge drift problem and Level II cannot be applied since the available data does not allow correction of gauge drift.

Level IV: Flow tests 4 and 5 (Table 4-7) are build-up tests for zones two and one respectively which can be used to apply level IV. Unfortunately the resolution and frequency with which the annulus pressure and the time interval were recorded was insufficient. Figure 4-24 and Figure 4-25 illustrate the trend of annulus pressure for individual zones. Figure 4-24 does show that the annulus pressure for zone 1 increases once the ICV has been shut-in, but there are insufficient data points and the pressure resolution is too low for a well test-style interpretation of this pressure build-up. The same conclusion is reached when analysing the zone 2 data (Figure 4-25). Figure 4-26 and Figure 4-27 present the log-log delta pressure and derivative pressure plots for zones 1 and 2 respectively. Although these figures confirm that well test analysis cannot be applied especially for zone 2, there is insufficient zone 1 pressure build-up data used to perform Level IV active soft-sensing.

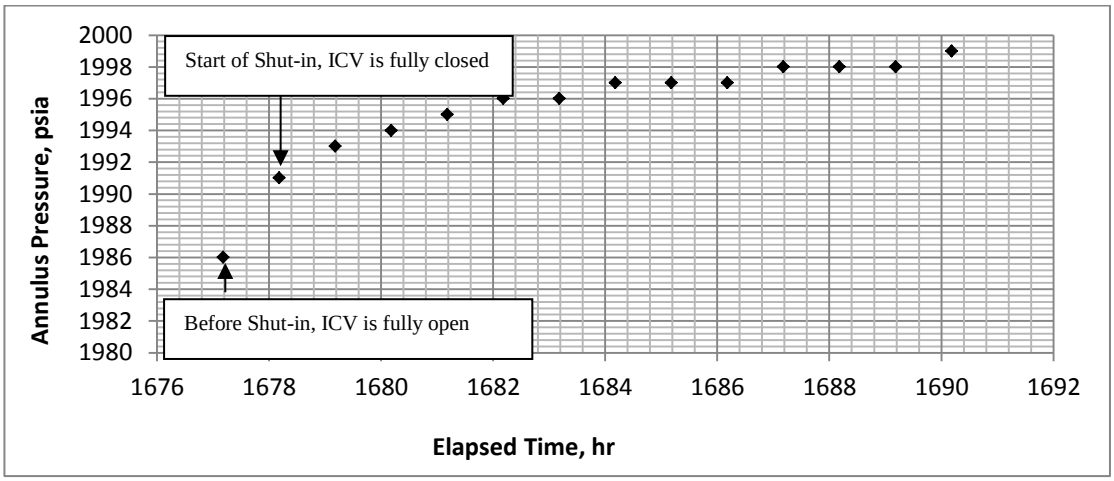

Figure 4-24 Measured annulus pressure (zone 1), flow test 5

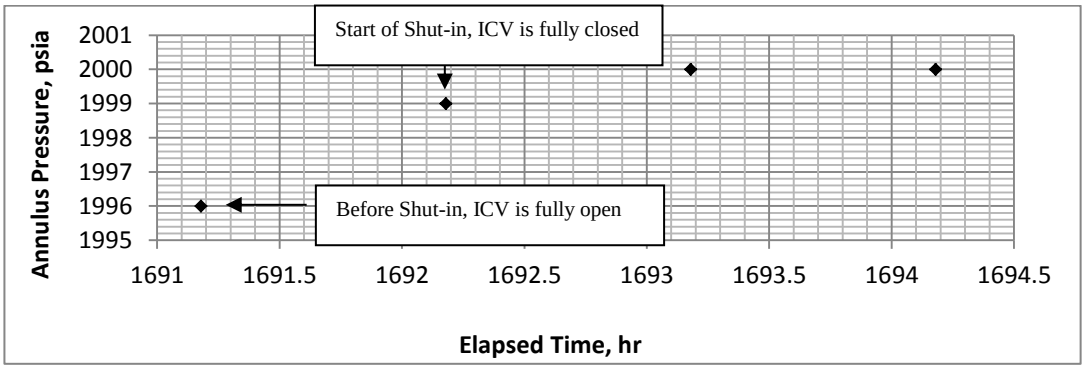

Figure 4-25 flow test 4, measured annulus pressure (zone 2)

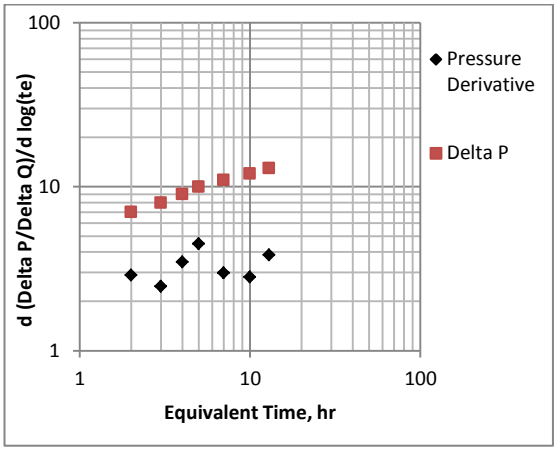

Figure 4-26 Log-log plot of the pressure derivative for zone 1, flow test 5

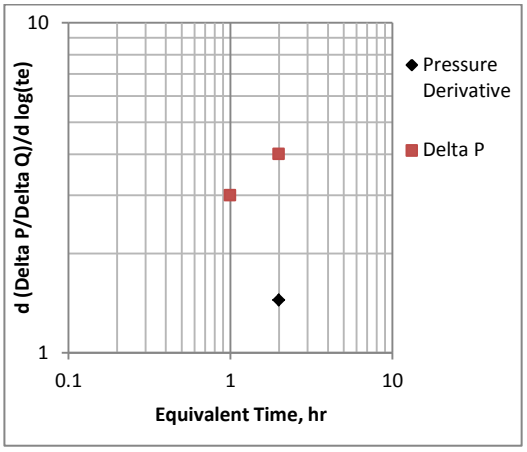

Figure 4-27 Log-log plot of the pressure derivative for zone 2, flow test 4

4.4.2 Implementation of Active Soft-sensing

It was discussed why the measured data sets only allow implementation of the Level I and IV active soft-sensing approach. A Level I analysis of the Table 4-7, flow tests 4 and 5, data derives the zonal reservoir pressures and the zonal oil productivity indices using the liquid inflow performance relationship (Equation C- 11) as shown in Table 4-8. Note that the measured (surface) water-cut at the time of the flow tests 4 and 5 have been assumed as estimated zonal water-cuts for zones 1 and 2 respectively.

Table 4-8 Zonal pressure, productivity index and water-cut using data from flow tests 4 and 5

	Estimated Reservoir Pressure (psia)	**Estimated Oil Productivity Index (STB/D/psia)**	**Estimated Water-Cut (%)**
Zone-1	1998	0.93	12.9
Zone-2	2000	80.8	13.2

The parameters in Table 4-8 were used to calculate the well oil production rate at surface and the water-cuts of flow tests 1, 2 and 3 indicates 22 - 25 % and 1.2 - 2 % relative error for oil production and water-cut respectively as shown in Table 4-9.

Table 4-9 Comparison of measured and estimated oil production rates and water-cut for flow test 1, 2 and 3

	Measured		Estimated		Relative Error (%)	
	Well Oil Rate (BLPD)	**Well Water-cut (%)**	**Well Oil Rate (BLPD)**	**Well Water-cut (%)**	**Well Oil Rate**	**Well Water-cut**
Flow Test 1	2251	13	1730	13.2	23	1.3
Flow Test 2	2309	12.9	1729	13.2	25	1.7
Flow Test 3	2236	12.9	1728	13.2	22	2.0

Flow tests 3, 4 and 5 in Table 4-7 form the three flow tests to initiate the active soft-sensing algorithm. The zonal productivity indices and water-cuts are considered as estimated variables. It was assumed that the zonal reservoir pressures can be estimated at the end of the shut-in period in flow tests 4 and 5. Table 4-10 summarizes the updated parameters of Table 4-8 after applying Level I active soft-sensing. Comparison between the measured and the estimated well oil production rates and water-cuts shows a significant improvement in the relative error after this updating of the zonal productivity indices and the water-cuts (see Table 4-11). The relative errors in the production rate have reduced by 40% from an average of 24 % to 15% for the oil rate and from an average of 1.6 % to 0.9 % for the water-cut (compare Table 4-9 and Table 4-11).

Table 4-10 Updated parameters after addition of flow test 3 data (see Table 4-8)

	Reservoir Pressure (psia)	**Oil Productivity Index (STB/D/psia)**	**Water-Cut (%)**
Zone-1	1998	0.94	12.9
Zone-2	2000	89.7	13.1

Table 4-11 Relative Errors of oil production rate and water-cut after updating estimated parameters

	Measured		Estimated		Relative Error (%)		Improvement due to Updating (%)	
	Well Oil Rate (BLPD)	**Well Water-cut (%)**	**Well Oil Rate (BLPD)**	**Well Water-cut (%)**	**Well Oil Rate**	**Well Water-cut**	**Well Oil Rate**	**Well Water-cut**
Flow Test 1	2251	13	1916	13	15	0.6	35	54
Flow Test 2	2309	12.9	1915	13	17	1.1	32	35
Flow Test 3	2236	12.9	1915	13	14	1.4	36	30

It will now be shown that there will be a further reduction in this error if transient pressure measurements (Level IV) is combined with the flow test 1 and 2 measurements are used in the active soft-sensing workflow. Figure 4-28 shows the semi-log plot of pressure for a well build-up test performed in the same field three years earlier than flow tests in Table 4-7. Interpretation of well build-up test indicated an average reservoir pressure of 2155 psia that suggests the zonal reservoir pressure has been underestimated, i.e. the zonal build-ups during the multi-rate tests were of an insufficient duration. The addition of other flow test history, such as well build-up test thus adds add value by providing a more accurate zonal reservoir pressure and more realistic productivity indices via Level I active soft-sensing.

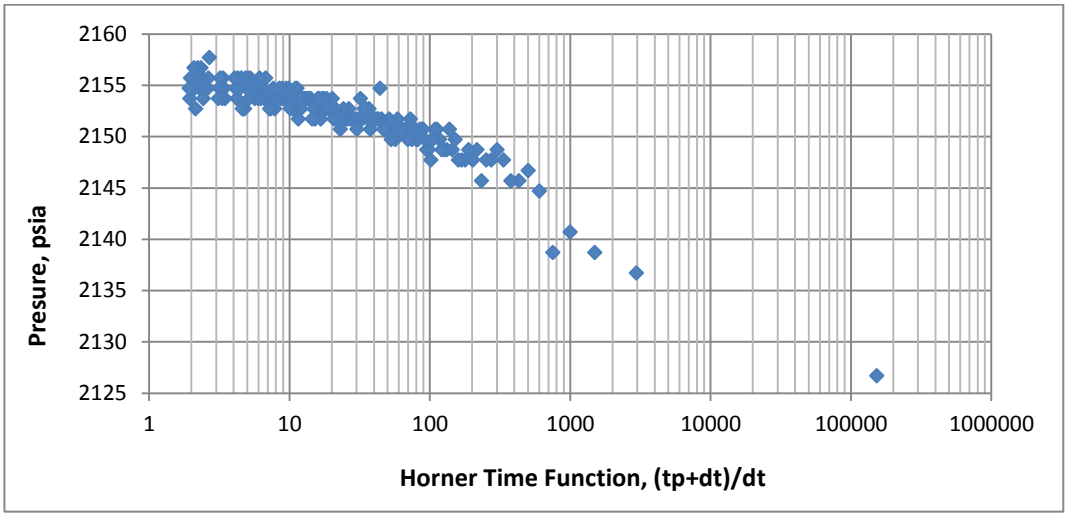

Figure 4-28 Semi-log plot of well build-up pressure versus Horner time function

The above estimated average reservoir pressure, build-up transient pressure analysis of zone 1 and the extra two flow tests (flow tests 1 and 2), may be used to sequentially update the zonal properties using the workflow listed in Table 4-12.

Figure 4-29 illustrates how the relative errors for the well's oil and water production rates decrease step by step when zonal parameters are updated using further measurements. Optimum zonal water-cuts are achieved after step 3 despite the zonal reservoir pressures and productivity index trends not converging to a constant value due to the measurement error (Figure 4-30 to Figure 4-32).

Table 4-12 Summary of different steps to implement active soft-sensing

Step No.	**Number of Flow Tests**	**Level No. of Active soft-sensing**	**Search Variables**
1	2	*Zonal build-up tests analysis using linear liquid PI equation*	---
2	3	Level 1	PI_1, PI_2, wc_1, wc_2
3	3	Level 1	Pr_1, Pr_2, PI_1, PI_2, wc_1, wc_2
4	3	Level 1 & Level 4	Pr_1, Pr_2, PI_2, wc_1, wc_2, S_1, kh_1, kv_1
5	4	Level 1 & Level 4	Pr_1, Pr_2, PI_2, wc_1, wc_2, S_1, kh_1, kv_1
6	5	Level 1 & Level 4	Pr_1, Pr_2, PI_2, wc_1, wc_2, S_1, kh_1, kv_1

The relative errors come from uncertainties in both measured pressures and well rates in the field and models incorporated in the algorithm. Analytical equations including well testing, inflow performance relationships (See Appendix C) and productivity index correlation (Joshi, 1988) are used to estimate zonal properties. These equations are derived through simplified assumptions that may not truly model the fluid flow within the reservoir. It is assumed that steady-state liquid inflow occurs from individual zones in the absence of gas phase in order to use a simplified liquid inflow performance relationship to relate the oil rates into zonal annular pressures in all flow tests.

The early radial flow regime is also assumed to interpret zone 1 pressure transient data. This provides the use of more measured data which allows performing extra level 4 in addition to level 1. Furthermore, a pressure drop is normally expected across a choked ICV for a producer zone in which annulus pressure is higher than tubing pressure. However, level 2 is discarded in the study as the measured tubing pressure does not meet the above assumption. Further discussions related to effects of model and measurement uncertainties on the estimated zonal flow rates will be addressed in Chapter 6.

Future field data is required to confirm this result; that the zonal reservoir pressures and productivity indices can be estimated accurately using the active soft-sensing.

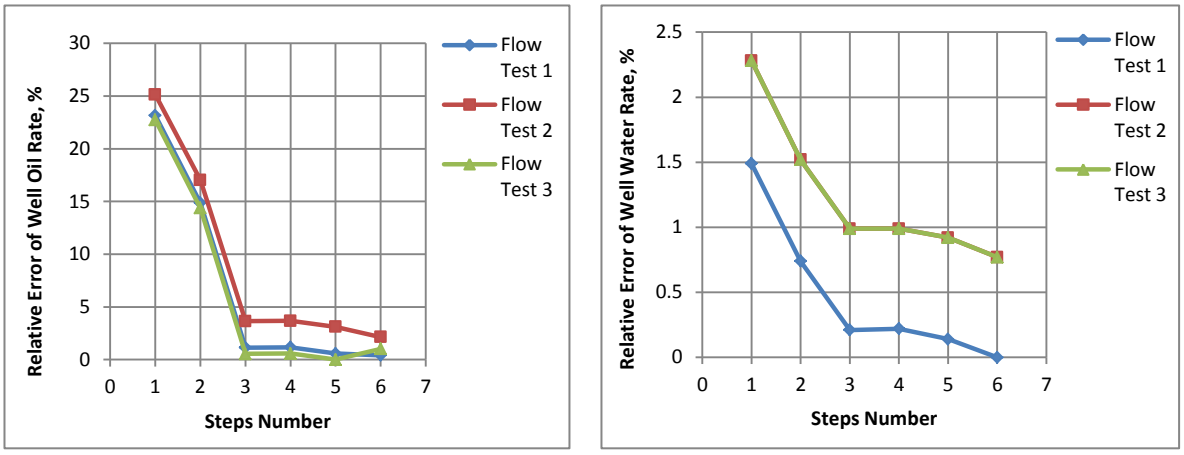

Figure 4-29 Relative error of well rates versus step number for active soft-sensing

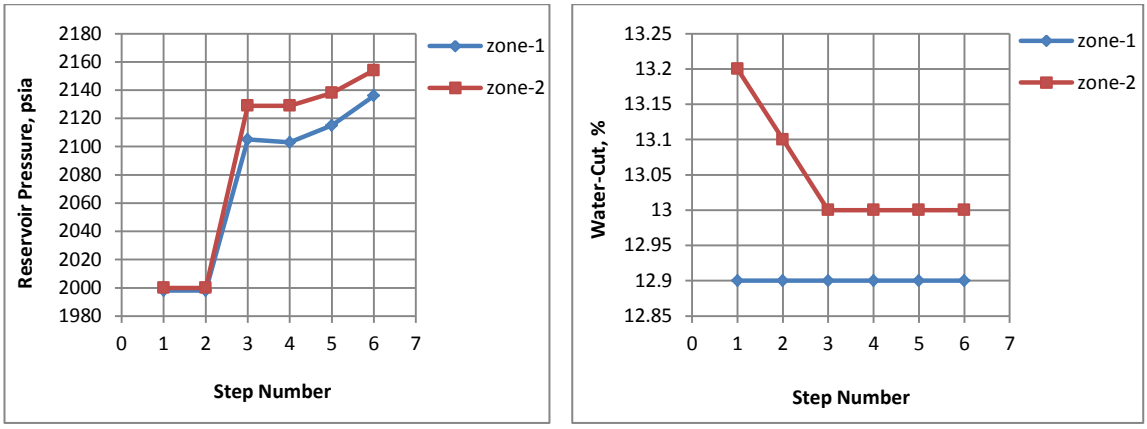

Figure 4-30 Error of zonal reservoir pressure and water-cut versus step number for active soft-sensing

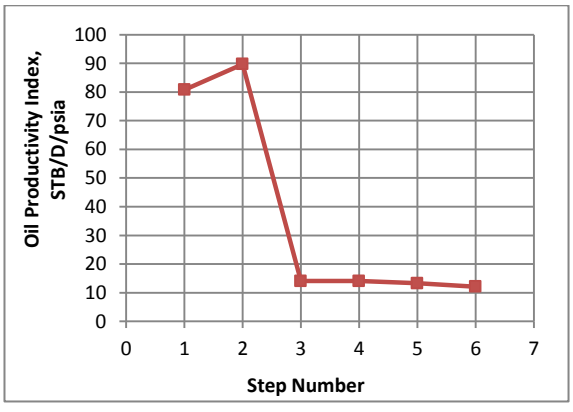

Figure 4-31 Error of zone 2 productivity index versus step number for active soft-sensing

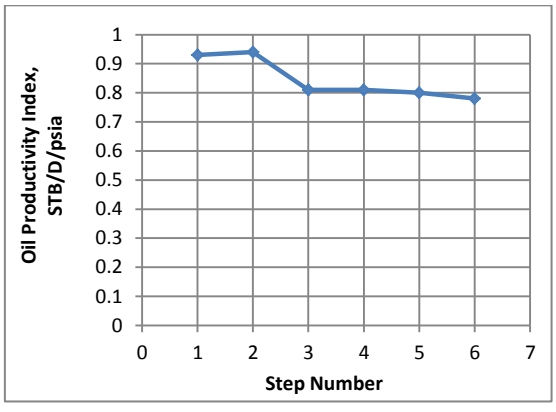

Figure 4-32 Error of zone 1 productivity index versus step number for active soft-sensing

The pressure drop across each ICV can thus be calculated from the active soft-sensing workflow. Figure 4-33 shows that the pressure drop on choking ICV_2, unlike ICV_1, is sufficiently large to supply meaningful data. Therefore, Zone 1 choking data was not included when applying Level II. However, Level II analysis can only be applied to zone 2 if the drift problem is resolved with a calibration test e.g. measure the pressure difference between the annulus and the tubing when ICV_2 is open and the well is not producing.

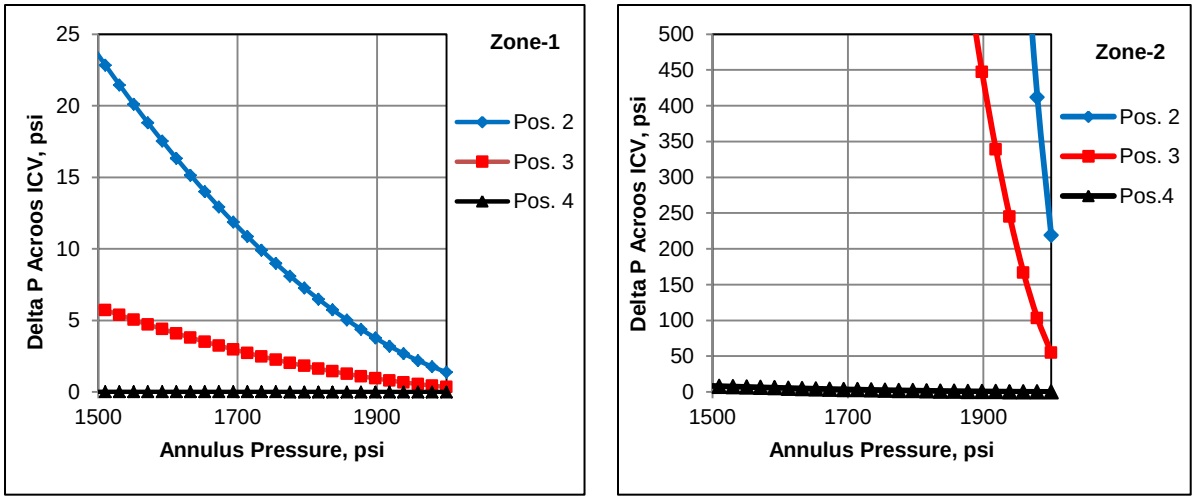

Figure 4-33 Pressure drop across ICVs corresponding to each ICV opening

4.4.3 Designing the Next Flow Test

If someone wants to design the next flow test using the DC optimisation method, three initial flow tests are required as the method is applied in a two-zone I-well. Table 4-13 describes three initial flow tests and suggested the next ICVs position. The second flow test with the lowest mismatch is discarded and the fourth flow test is replaced to form the new set of ICV positions for the continuation of active soft-sensing algorithm. The total mismatch values represent the relative error between the measured information and estimated ones using the multi-phase flow model within the active soft-sensing algorithm.

Table 4-13 Proposed ICVs configuration of next flow test

	ICVs Opening		Total Mismatch
Flow Test NO.	**ICV1**	**ICV2**	
1	**100%**	**100%**	**0.213 (Well Oil & Water Flow Rates)**
2	**100%**	**0%**	**0.006 (Well Oil & Water Flow Rates)**
3	**0%**	**100%**	**0.098 (Well Oil & Water Flow Rates + Zone 1 Annulus Transient Pressure)**
4	**33%**	**67%**	**Recommend ICV configuration for next test**

4.5 Active MPFR Soft-sensing Algorithm Robustness under Uncertainty

In general, the total uncertainty of the active soft-sensing algorithm is related to the measurement uncertainty of each measured input plus the error associated with the model used to analyse the measurements. Measurement uncertainty has a probabilistic nature and reflects the variance of the values attributed to a measured quantity. Both systematic and random errors contribute to the total measurement uncertainty. The multi-phase flow model includes various analytical equations to estimate well production rate, pressure drop across ICVs, pressure transient during PBU test and temperature distribution along the wellbore and across the ICVs. These equations are accepted based on the assumptions addressed in Chapter 3. It should be noted that the model's estimation error increases when these assumptions are not met during active soft-sensing of the multi-phase flow rates in the wellbore.

The reliability of the estimated zonal properties using active soft-sensing is affected by the measurement uncertainties. It has been shown that deformed simplex method is less sensitive to the error associated with the objective function due to the mapping of several configuration (simplex) vertices whose numbers are automatically justified from step to step (Rykov, 1983). The confidence interval may thus be used to evaluate the robustness of the active soft-sensing algorithm (see Appendix E for more details).

Table 4-14 summarises the true and estimated values of zonal reservoir pressures, productivity indices and water cuts and their associated uncertainty. The total uncertainty (the sum of model and measurement uncertainties) of the pressure and flow rate estimates has a standard deviation value of ± 10 psia and $\pm 10\%$ respectively.

These, not untypical, values were selected as examples to prove the algorithm's robustness. It was assumed that the measurement's added noise was normally distributed {the detail of how a random noise was added to the measurements is discussed in Chapter 5}.

Table 4-14 Estimated zonal parameters using active soft-sensing method

Property / Zone	Pr (psia)			PI_o (STB/D/psia)			wc (Fraction)		
	True value	***Estimated Value***	***Uncertainty***	***True value***	***Estimated Value***	***Uncertainty***	***True value***	***Estimated Value***	***Uncertainty***
Zone-1	5801	5799	±18	1.5	1.59	±0.27	0.33	0.36	±0.03
Zone-2	5729	5724	±18	1.2	1.18	±0.20	0.33	0.32	±0.03
Zone-3	5656	5635	±14	0.8	0.94	±0.20	0.33	0.32	±0.03

We are thus 90% percent confident that the true values of the zonal reservoir pressures, productivity indices and water-cuts are within the interval of:

$$Estimated\ Value - 1.645 \times Uncertainty < True\ Value < Estimated\ value + 1.645 \times Uncertainty$$

For example, if the estimated value of the reservoir pressure of zone 1 is 5799 psia with uncertainty of ±18 psia, its true value (5801 psia) lies within the interval [5769,5828] with a confidence of 90%. This confidence interval was obtained based on the measurements and estimated zonal properties at the last flow test designed by the active soft-sensing algorithm.

The interpretation of confidence interval is: if an infinite number of random samples are collected and *A* percent confidence interval is computed for each sample using the formula in Appendix E (Equation E- 1) , then *A* percent of these intervals will contain the true value (Montgomery and Runger, 2011). Here, I only obtained one random sample and calculated one confidence interval. Since this interval will or will not contain the true values of the zonal properties, it is not reasonable to attach a probability level to this specific event. The appropriate statement would be that the observed interval includes the true value of zonal properties with confidence of 90%. This statement has a frequency-level interpretation that it is not known if the statement (90% confidence interval) is true for this specific sample, but the method used to obtain the interval yields correct statement, 90% of the time.

4.6 Summary

The active soft-sensing algorithm was successfully tested on several synthetic cases and one real I-well case. The algorithm proved applicable to estimate zonal properties and multi-phase flow rates regardless of the well deviation completed in either oil or gas field if appropriate multi-phase flow equations are available. In addition, the algorithm's robustness was verified against model and measurement uncertainties. A real well study involved field measurements that were not only contaminated with the errors, but also biased by incorrect modelling during the common practice in which a shut in production, either fully or partially, is carried out in one or more zones to test the individual well zones. The soft-sensing monitoring approach using real well highlighted some practical lessons as:

1. Access to full production and well tests (including build-up or drawdown) history data help the active monitoring approach in determining range of possible zonal property values that are input as search variables in the optimisation workflow. These data add value to the study by forming another source of zonal property data when the information acquired from multi-rate flow tests is not sufficient to satisfactorily calculate the parameters.
2. An improved estimate of zonal properties is achieved by adding more flow tests. However, it also requires an additional understanding of the reservoir rock and fluid properties.
3. The algorithm can also manage gauge measurement issues such as gauge drift or resolution. These additional constraints form an extra control variable in the optimisation workflow.
4. The workflow described here offers a number of possible levels to apply the monitoring algorithm based on different types of the measurements with an acceptable resolution.
5. Use of active soft-sensing to predict the preferred ICV positions must be carried out reasonably quickly after the previous test since it is assumed that zonal properties are constant during the multi-rate flow tests.

Chapter 5 Integrated Zonal, Control and Monitoring in Multi-zone I-wells

5.1 Introduction

This chapter explains the approach in which reservoir properties are monitored and well production is controlled in a reactive manner simultaneously. The active MPFR soft-sensing discussed in Chapter 3 and Chapter 4 is based on initial (n+1) flow tests in an n-zone I-well. This requirement implies the availability of multiple initial flow tests which are further used when the soft-sensing algorithm is applied for the estimation of flow rates in the I-wells completed in a large number of zones (e.g. 5-zone I-well). In Chapter 4, the required initial flow tests were chosen arbitrarily. The first part of this chapter proposes an alternative approach to the design of the initial flow tests. It is followed by the DC technique which is used to define the ICV's configuration for the next flow tests. The design of the initial flow tests is based on the maximisation of oil production by manipulation of the ICV positions.

The second part of the chapter proposes a generalised workflow called integrated control and monitoring (ICM) to design the multi-rate flow test and estimate the zonal properties using two strategies that define different objective functions used in the DC optimisation method: 1) maximise the reliability of the estimated zonal properties or 2) maximise the oil production (Figure 5-1).

The main difference between the optimisation processes of ICM workflow described in Chapter 5 and the active soft-sensing presented in Chapter 3 and Chapter 4 is the addition of an in-house optimiser to design the initial (n+1) flow tests. The workflow described by Figure 3-2 is used in this chapter by changing the objective function criteria after the initial flow tests have been designed. ICM workflow uses optimisation step 1 to estimate the zonal properties while the total mismatch objective function is minimised. The optimisation step 2 is performed simultaneously to design further flow tests while the individual mismatch function (corresponding to the reliability of the estimated zonal properties) or total oil production is maximised depending on which of above two strategies is selected in the ICM workflow.

Last part of the chapter demonstrates the convergence rate of the ICM workflow regarding the two objective function optimisations. The number of required flow tests to

optimise individual objective functions and the accuracy of estimated zonal properties are compared and a hypothesis test is applied to verify the comparison statements. The comparison is conducted for ten data sets each containing random errors in the measured well rate and pressure.

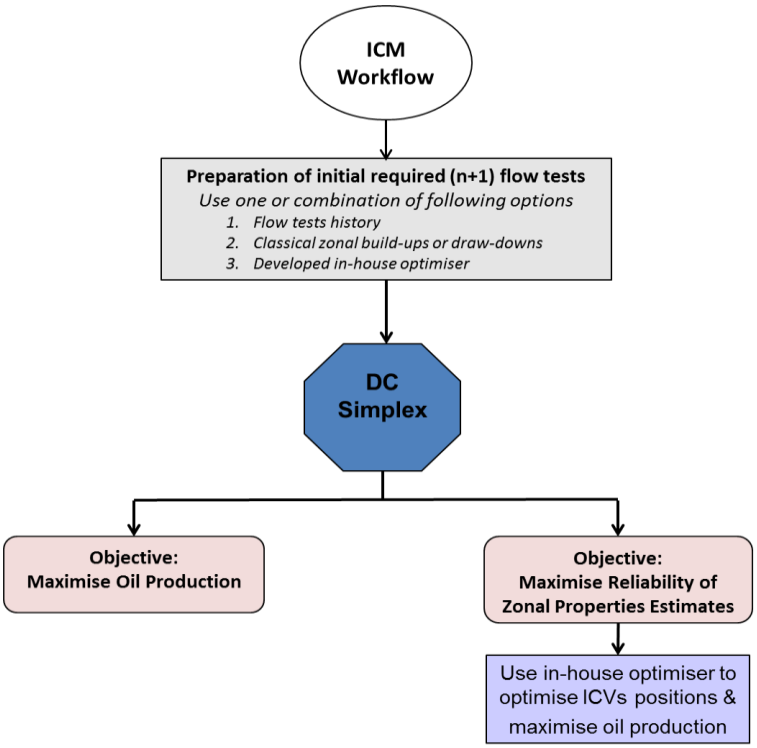

Figure 5-1 Different objective functions for the DC simplex algorithm

5.2 Design of (n+1) Initial Flow Tests

The design of the initial flow tests is important when applied to I-wells with a large number of zones (Skilbrei et al., 2003, Knabe et al., 2014). Zonal pressure build-up or flow rate tests result in lost production; reducing the incentive to carry them out despite them being necessary to provide the information to efficiently manage the well's and or reservoir's production. Moreover, restarting I-wells after a shut-in period can be problematic due to the hydrostatic head of the column of "dead" liquid in the tubing. Further factors, such as pressure depletion, cross-flow between the zones and high water-cut production, all accentuate this problem.

The (n+1) initial flow tests are designed in a way to maximise the oil production after each flow test. It is essentially the same as reactive control mode (Grebenkin and Davies, 2012) where production from zones with a higher level of unwanted fluid production or zones experiencing cross-flow is limited in order to maximise the total

production. This approach can be applied as an alternative solution to design the required initial flow tests for active soft-sensing monitoring.

5.2.1 Problem Formulation

The approach to design of initial (n+1) flow tests is implemented in two different optimisation steps (Figure 5-2). With Microsoft Excel's Solver being used to optimise each step's objective functions Equation 3-8 presents the objective function of the first optimisation step (monitoring) that is minimised to calculate the zonal properties. In the second optimisation step (production maximisation), the objective function is based on nodal analysis to predict the well's production rates by simultaneous solution of the well's inflow (IPR) and outflow (VLP) equations (Brown and Lea, 1985). This workflow uses the heel section or upper part of the completion as the operating point and performs the nodal analysis as described below.

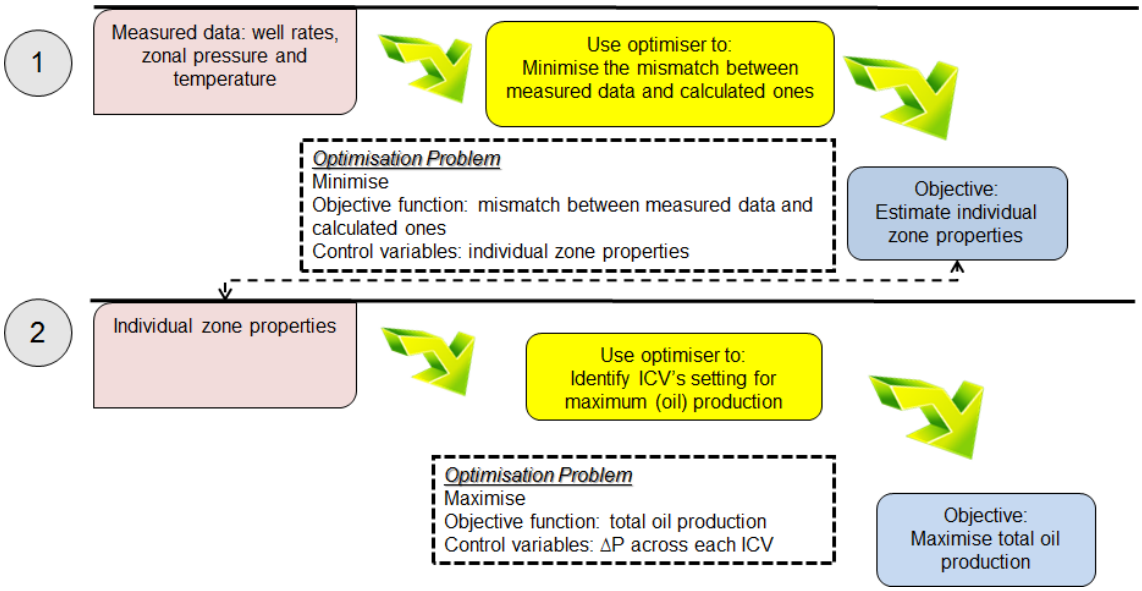

Figure 5-2 Comparison between optimisation problems

The well inflow relation describes the inflow production rate as a function nodal pressure. Let's assume an n-zone I-well, in which individual zones are characterised by different reservoir pressures (P_r), linear liquid productivity indices (PI_l), water-cuts (wc) and gas-oil-ratios (GOR). The schematic of the n-zone I-well is presented in Figure 5-3.

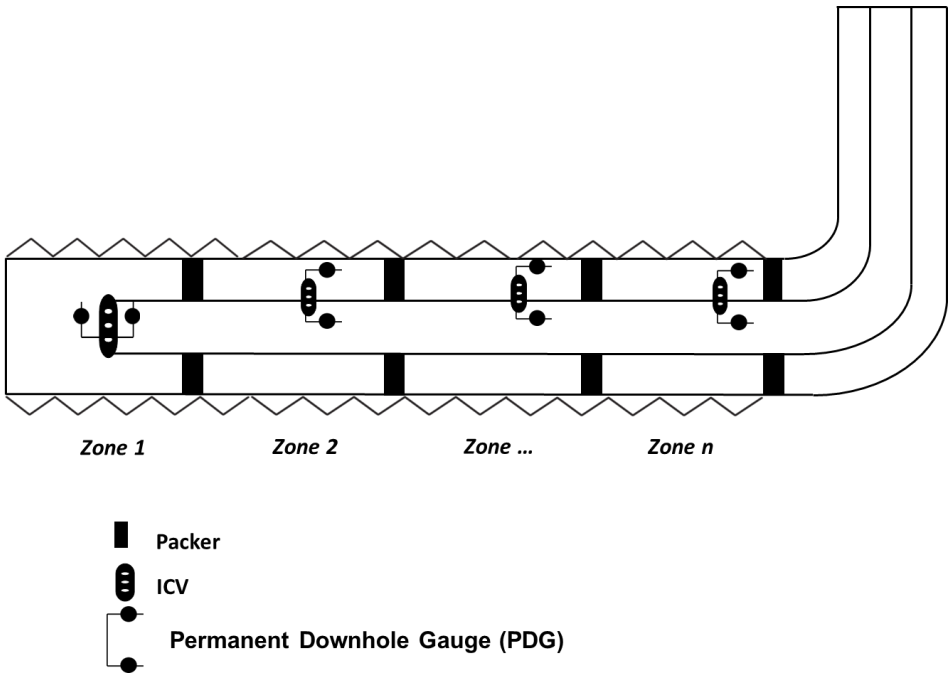

Figure 5-3 A schematic of n-zone I-well

The zones at the toe and heel are numbered as 1 and n respectively and the well inflow rate is calculated using a combination of inflow productivity equations and flow correlations.

$$Q_l = \sum_{i=1}^{n} (PI_{li}(P_{ri} - P_{bhp} - \Delta P_{fin} - \Delta P_{gin} - \Delta P_{ICVi}) \quad 5\text{-}1$$

$$Q_w = \sum_{i=1}^{n} wc_i(PI_{li}(P_{ri} - P_{bhp} - \Delta P_{fin} - \Delta P_{gin} - \Delta P_{ICVi}) \quad 5\text{-}2$$

where

P_{bhp} = Bottomhole pressure at the heel,

ΔP_{ICVi} = Pressure drop across each ICV,

ΔP_{fin} = Pressure drop in the tubing due to friction between zone i and n,

ΔP_{gin} = Pressure drop in the tubing due to elevation between zone i and n.

Vogel's correlation is substituted if the average reservoir pressure is below the bubble-point pressure.

$$Q_o = \sum_{i=1}^{n} q_{o_{i_{max}}}(1 - 0.2\left(\frac{P_{an_i}}{P_{ri}}\right) - 0.8\left(\frac{P_{an_i}}{P_{ri}}\right)^2) \quad 5\text{-}3$$

$$Q_w = \sum_{i=1}^{n} \frac{wc_i q_{o_{i_{max}}}(1 - 0.2\left(\frac{P_{an_i}}{P_{ri}}\right) - 0.8\left(\frac{P_{an_i}}{P_{ri}}\right)^2)}{(1 - wc_i)} \quad 5\text{-}4$$

$$P_{an_i} = P_{bhp} + \Delta P_{fin} + \Delta P_{gin} + \Delta P_{ICVi} \quad 5\text{-}5$$

Equations 5-1 through 5-4 describe the liquid inflow rates versus bottomhole pressure. The acceleration term has been ignored in the calculation of pressure drop in the tubing and annulus.

The well outflow expression, relating the bottomhole pressure to the rate flowing through tubing, depends on fluid properties, well depth, tubing size, surface pressure, water-cut and GOR. Various multi-phase correlations (Hagedorn and Brown, 1965, Duns and Ros, 1963, Fancher and Brown, 1963, Beggs and Brill, 1973) have been proposed to model the VLP. They all have the similar expressions for calculation of the frictional pressure loss; while using different equations for multi-phase friction and gas/liquid holdup fractions.

5.2.2 Problem Solution

Multi-rate flow tests require regulating one or more ICVs position in a multi-zone I-well. Zonal properties are provided via passive soft-sensing (Chapter 3) to maximise the oil rate at a given time. Reactive maximisation of oil production requires a methodology that is a combination of nodal analysis and the optimisation algorithm:

Maximise $Q_o = f(\Delta P_{ICVi})$ 5-6

Subject to $0 \leq \Delta P_{ICVi} \leq inf, \qquad i = \overline{1,n}$ 5-7

$0 \leq ICV_i\ Opening \leq 1, \qquad i = \overline{1,n}$ 5-8

The pressure drop across each ICV is the control variable. An interval with lower and upper bound is specified to vary the pressure drop between a fully open and a fully closed position. Zero in Equation 5-7 indicates the fact that a negligible pressure drop is observed across the ICVs if they are fully open. The upper bound can be any large number since it ensures that the ICV is fully closed at given pressure drop. The optimum ICV pressure drop is then converted to an ICV opening expressed as a fraction of the maximum flow area. ICV pressure drop has been selected as the control variable because the oil production rate (Equation 5-6) is calculated using nodal analysis which is in turn based on the nodal pressure. The bottomhole pressure and oil production rate corresponding to optimum ICV openings are calculated using nodal analysis for each trial. The optimum combination of ICVs openings may then be used as a new flow test and added to the previous flow tests and thus the zonal properties recalculated.

This approach is found very efficient in the intelligent wells completed in large number of zones. However, zonal build-ups or drawdowns may still be favoured to operators to initiate (n+1) flow tests when the soft-sensing problem is solved for a 2-zone or 3-zone I-well. It should be noted that the proposed approach may be stopped when the flow tests are less than (n+1) if one of the two stopping criteria mentioned in Chapter 4 occurs. It implies that is 1) the predefined accuracy has reached for the zonal properties or 2) the optimiser has resulted in the same ICVs position while maximising the oil production. This reflects the benefit of using in-house optimiser to design less than (n+1) flow tests to estimate the zonal flow rates and maximise oil production simultaneously.

5.3 Integrated Control and Monitoring (ICM) Workflow

Well Monitoring is designed to estimate the zonal properties and downhole flow rates while Well Control attempts to increase the oil production and reduce the production of unwanted fluids. Accurate estimation of zonal properties is an essential part of optimising the oil recovery from each interval's production. The Figure 5-4 workflow provides a fast and informed production control in multi-zone I-wells by optimising the ICVs configuration when the zonal properties are unknown. Note that the workflow can be applied to all commingled production systems, including multiple conventional wells where the wellhead choke settings are optimised.

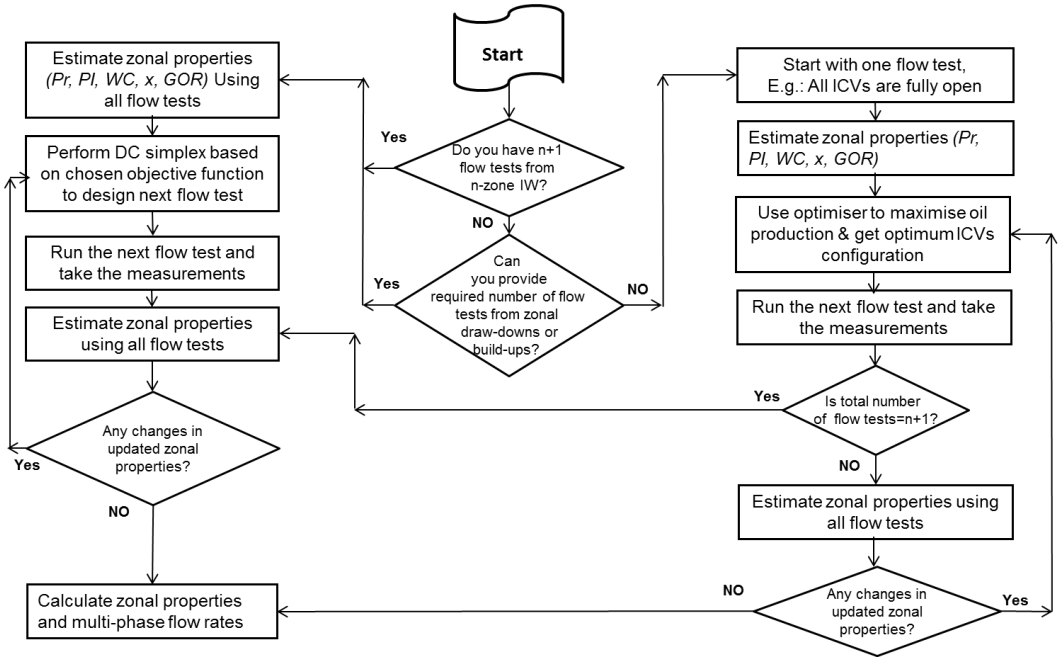

Figure 5-4 Integrated control and monitoring workflow in multi-zone I-well

The workflow described above is divided into two parts. The right-hand side of the workflow explains the design of initial flow tests required to perform the DC optimisation method; while the left-hand side presents the active MPFR soft-sensing methodology. The initial flow tests can also be obtained from classical zonal testing (either a draw-down or build-up), even when they are not suitable for estimating the zonal properties due to the measurements not being of sufficient quality.

5.4 ICM Workflow Validation

A synthetic 5-zone horizontal I-well model was built in the commercial simulator OLGA^{TM}. The I-well was completed with 5 ICVs equipped with PDGs to monitor the zonal pressure and temperature. Each zone was modelled with different values of the reservoir pressure, productivity index and water-cut (See Table 5-1). One zone has a high water-cut (zone-2) and another zone had a sufficiently low reservoir pressure (zone-4) that cross-flow occurred in the wellbore.

Table 5-1 Zonal properties in a 5-zone I-well

Property	**Zone-1**	**Zone-2**	**Zone-3**	**Zone-4**	**Zone-5**
Reservoir Pressure (psia)	3200	3335	3625	2500	3200
Liquid Productivity Index (STB/D/psia)	14	12	16	8	8
Water-cut (Fraction)	0.6	0.8	0.3	0.55	0.4

It was assumed that the wellbore has been shut-in for several days and no information is available regarding the zonal properties. Figure 5-5 shows the well oil and water production after a five-day shut-in period when the well is returned to production with fully open ICVs. The options for controlling the production are:

1) Active soft-sensing to estimate the zonal properties followed by reactive control. This requires designing one extra flow test to maximise the oil production (i.e. separate the control and monitoring workflows).
2) ICM workflow to find the optimum ICVs position after the 6th day which results in the estimation of unknown zone properties and maximising the total oil production at the same time (simultaneous control and monitoring)

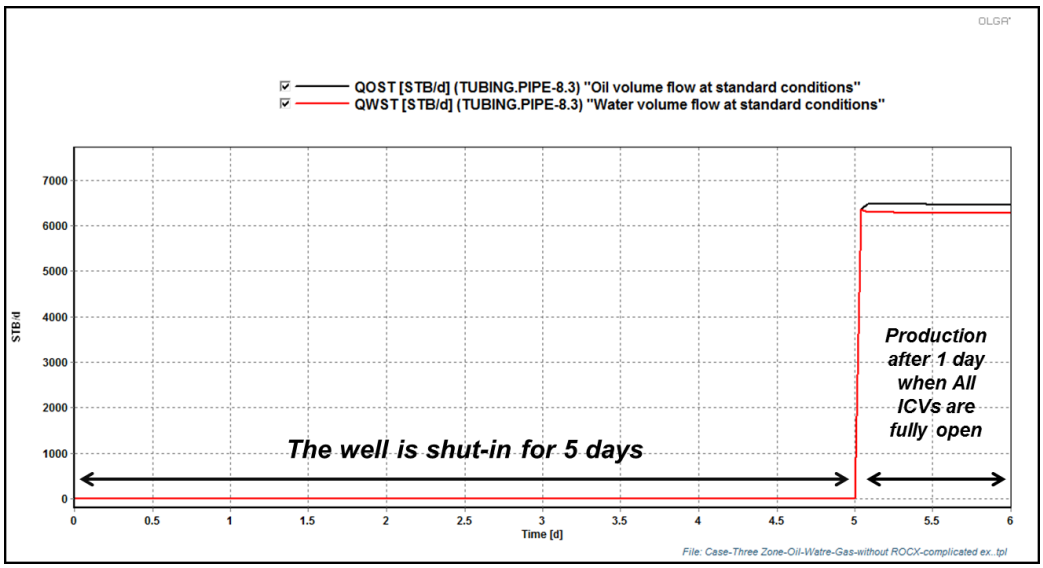

Figure 5-5 Well oil and water production from a 5-zone I-well

The DC simplex optimisation methods require six initial flow tests to implement active soft-sensing (Table 5-2). Finally the, 7th and 8th flow test are designed by the DC approach to increase the accuracy of the zonal property estimates.

Table 5-2 ICV configuration in multi-rate flow tests

Simplex No.	Flow Test No.	ICV1	ICV2	ICV3	ICV4	ICV5
1	1	1	1	1	1	1
	2	0	1	1	1	1
	3	1	0	1	1	1
	4	1	1	0	1	1
	5	1	1	1	0	1
	6	1	1	1	1	0
2	7	1	0.6	0.6	0.6	0.6
3	8	1	0.4	0.4	0.8	0.4

Figure 5-6 describes the convergence trend of zonal properties to their true values. The y-axis represents the ratio of total zonal property misfit at every simplex step to initial total zonal property misfit calculated by the following equation:

$$\frac{\text{Total Misfit of Zonal Property}}{\text{Initial Total Misfit of Zonal Property}} = \frac{\sqrt{\sum_{i=1}^{n}\left(\frac{\text{estimated value} - \text{true value}}{\text{true value}}\right)^2_{\text{zone}_i}}}{\sqrt{\sum_{i=1}^{n}\left(\frac{\text{Initial value} - \text{true value}}{\text{true value}}\right)^2_{\text{zone}_i}}} \quad 5\text{-}9$$

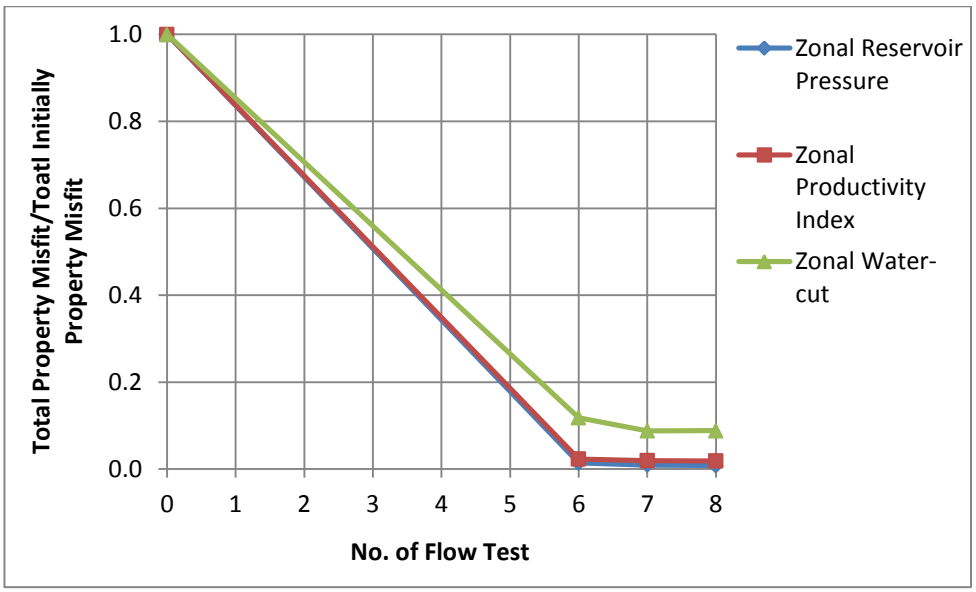

Figure 5-6 Reduction of total property misfit with increasing number of flow tests

The estimated zonal properties are then used by Excel Solver to design the optimum ICVs configuration that maximises the oil production. As expected, the optimiser suggests zones 2 and 4 are closed. Figure 5-7 illustrates that maximum oil production is achieved after nine flow tests with the flow tests 1 to 8 used for estimating the zonal property values as accurately as possible while the 9th flow test is designed to maximise the total oil production (separate control and monitoring workflow).

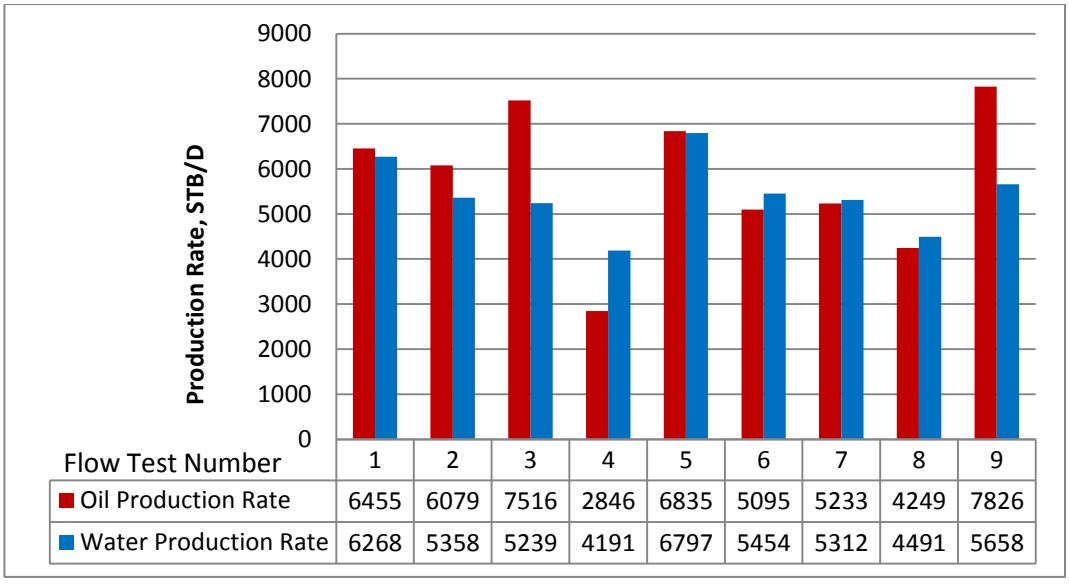

Flow Test Number	1	2	3	4	5	6	7	8	9
Oil Production Rate	6455	6079	7516	2846	6835	5095	5233	4249	7826
Water Production Rate	6268	5358	5239	4191	6797	5454	5312	4491	5658

Figure 5-7 Comparison of oil and water production rate from different flow tests for the (separate control and monitoring) workflow

The oil production may reach its maximum value at an earlier flow test if the ICM workflow is applied to the same model (Figure 5-8). Since the ICM workflow includes maximising oil production as the objective function.

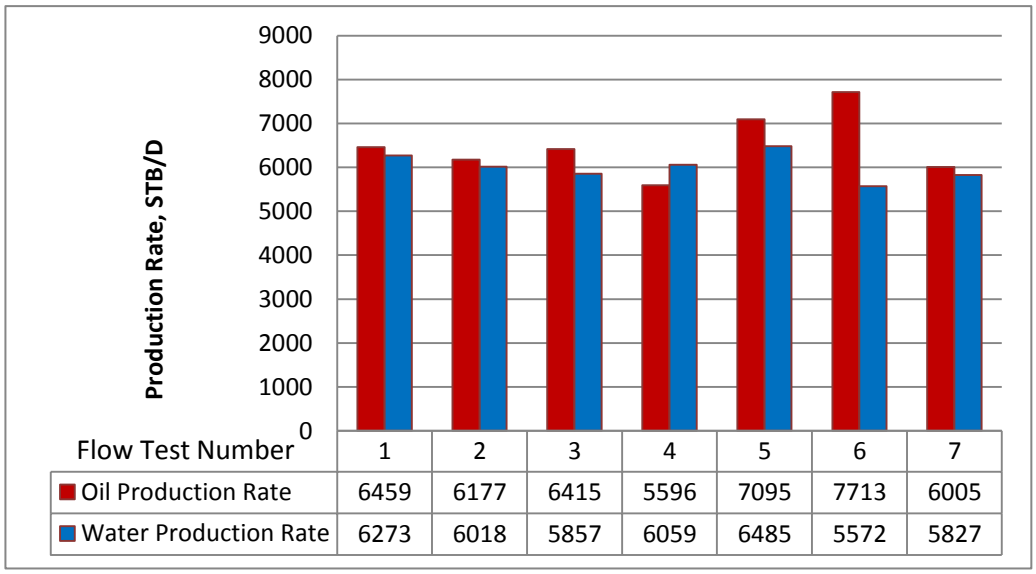

Flow Test Number	1	2	3	4	5	6	7
Oil Production Rate	6459	6177	6415	5596	7095	7713	6005
Water Production Rate	6273	6018	5857	6059	6485	5572	5827

Figure 5-8 Comparison of oil and water production rate from different flow tests for the ICM workflow

Table 5-3 lists the designed flow tests and their corresponding ICVs configuration by the ICM workflow. The ICM workflow was started with two arbitrary flow tests (1st and 2nd Flow tests). The next four flow tests were designed sequentially by Excel Solver to maximise the oil production and the 7th flow test is obtained by DC optimisation technique in which the maximum reliability of the zonal properties estimates is considered as an objective function criterion. The objective function criterion of DC algorithm can be selected either from maximum reliability of zonal properties estimates or maximum total oil production, as will be discussed in the next section. The trend for estimation of the zonal properties is shown in Figure 5-9.

It was observed that both workflows achieve satisfactory estimates of the zonal properties; however the ICM workflow attempts to achieve the maximum oil production with a reduced number of flow tests.

Table 5-3 ICVs configuration in multi-rate flow tests

Simplex No.	Flow Test No.	ICV1	ICV2	ICV3	ICV4	ICV5
1	1	1	1	1	1	1
	2	0.9	0.9	0.9	0.9	0.9
	3	0	1	1	0	1
	4	1	1	1	0	0
	5	1	0.6	1	0	1
	6	1	0	1	0	1
2	7	0.6	1	1	0.8	0.6

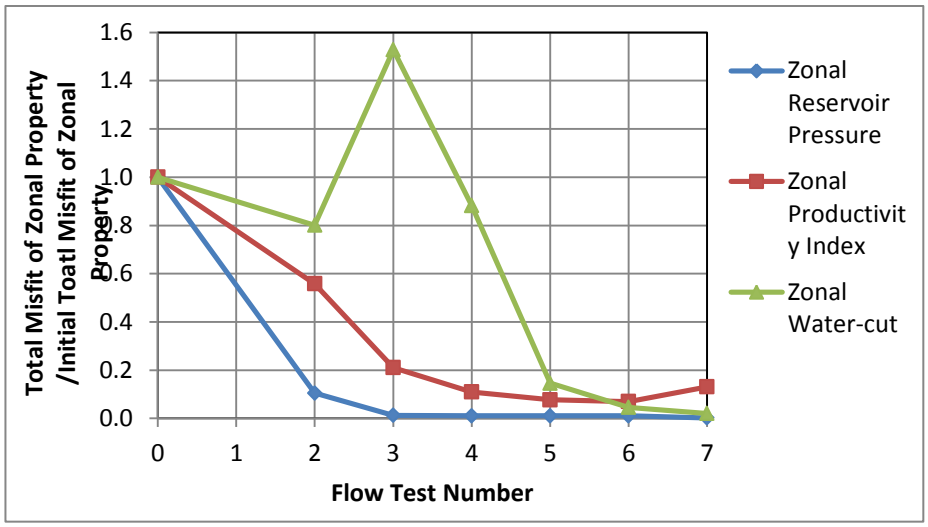

Figure 5-9 Estimation of different zonal properties versus flow tests

Two different approaches were used to design the multi-rate flow tests in Table 5-2 and Table 5-3. Optimisation process (step 1 and 2) discussed in Chapter 3 and Chapter 4 was applied to design the optimum ICVs position in Table 5-2 where the 6 initial flow tests were selected manually from the choice of zonal build-up tests together with a flow test in which all zones are fully open and the objective function was maximising the reliability of zonal property estimates. While the multi-rate flow tests in Table 5-3 were obtained using the ICM workflow. As part of this workflow, two arbitrary flow tests are initially chosen, then the in-house optimiser is used to design the next four flow tests to maximise the oil production. Finally the optimisation process is continued to design further flow tests in order to maximise the reliability of the zonal property estimates.

Figure 5-6 and Figure 5-9 compares the results between separated control and monitoring workflows and simultaneous control and monitoring approach. It is shown that higher accurate zonal properties are estimated through the separated control and

monitoring workflows however it requires higher number of flow tests to be designed (see Figure 5-6). On the other hand, simultaneous control and monitoring approach provides lower number of flow tests required to maximise the oil production (Figure 5-8) as the in-house optimiser designed the initial flow tests based on the oil production maximisation. This approach may result in the estimation of zonal properties with lower accuracies as shown in Figure 5-9.

5.5 Convergence Rates in Monitoring and Control Approaches

The earlier sections of this chapter discussed the general guideline for the design of multi-rate tests design using the ICM workflow. Inclusion of the DC optimisation method in the workflow provides the possibility to select a different objective function. The two criteria: 1) maximising the reliability of the zonal property estimates or 2) maximising the total oil production rate will now be considered.

Figure 5-1 described two different search routes of multi-rate flow test design once (n+1) flow tests are available in a n-zone I-well. The choice of these criteria becomes important when errors are included in the measurements and more than (n+1) flow tests might be required for the most accurate estimation of the zonal properties.

The objective functions used in the DC simplex algorithm depends on the search criteria with the ICV positions being the control variables in the optimisation problem for all search criteria. The DC algorithm is a derivative-free optimiser which uses the values of the objective function directly. Hence other scenarios can be defined; such as minimising the water production, gas production or GOR instead of maximising the oil production. This advantage makes the DC applicable to cases when it is complicated, or even impossible, to relate the objective functions mathematically to the control variables.

The estimation of zonal properties is based on the number of measurements from multi-rate flow tests. Section 5.5 attempts to answer the following questions in order to compare the search performances during the implementation of the active soft-sensing approach:

1) How do the results of active soft-sensing change if the errors are added to the measurements?
2) Which search criterion meets the optimum objective function fastest?
3) Which search criteria estimates more accurately the zonal multi-phase flow parameters?

5.5.1 Modelling of Noisy Measurements from Multiple sensors

A 3-zone I-well was modelled in the OLGA^{TM} simulator with all three phases being present (see Figure 5-10). The input values for the active soft-sensing algorithm was limited to the well rates and zonal annulus and tubing pressures in this study. It is assumed that the flow meter (installed either at surface or in the upper part of well completion) and PDGs systematically yield data with random errors of ±X%. The well test schedule is designed to either maximise either oil production or estimate reliability from this non-ideal data.

The following function is used to generate random errors in the measured data:

$$\text{Noisy Measurement} = \text{True Measurement} + (1 - 2 \times \text{rand}) \times \delta \qquad 5\text{-}10$$

where δ is the measurement uncertainty and Rand represent the random function in Microsoft Excel which returns an evenly distributed random real number greater than or equal to 0 and less than 1.

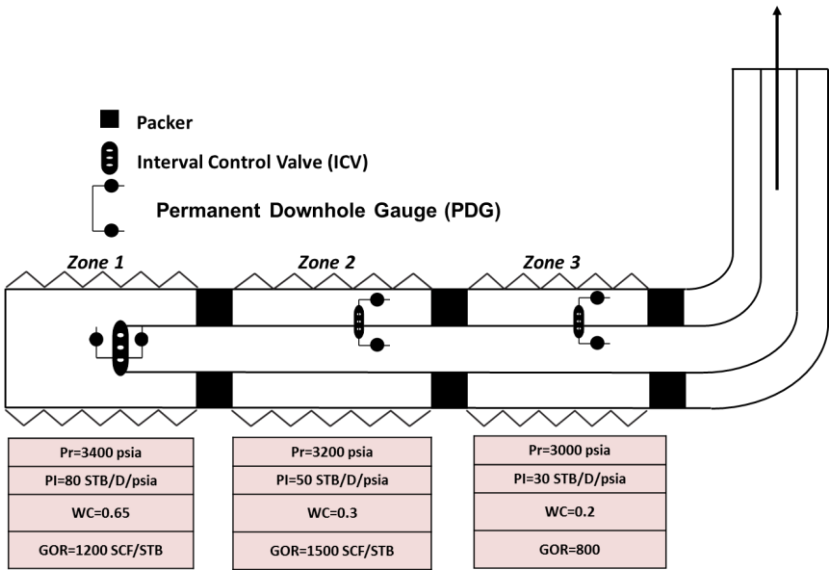

Figure 5-10 A synthetic 3-zone I-well modelled in OLGA^{TM}

A sensitivity analysis when operating the ICVs with an ON/OFF control strategy (Grebenkin and Davies, 2012) showed that the maximum oil production is obtained when zone-1 is closed and the other zones are on production (see Figure 5-11). The same ICV configuration is also obtained by our in-house, Excel based optimiser if the true values of the zonal properties are entered into the optimisation algorithm. The in-house optimiser combines the nodal analysis and Excel Solver to solve Equations 5-6 to 5-8. This specific ICVs configuration was therefore excluded from the initial flow tests used in this study exploring how fast the active soft-sensing workflow approaches

the optimum ICV configuration. The following steps are proposed to initialise 4 sets of ICVs configuration:

1) Design n of zonal draw-down tests and estimate zonal properties from individual tests. Ideally, these flow tests should be sufficient to estimate the most accurate zonal properties if the measured well rates and pressures are 100% accurate. The optimum ICV configuration to maximise oil production is shown in Figure 5-11.
2) Add a low value of measurement uncertainty (e.g. ± 5 psi for pressure measurements and $\pm 5\%$ for flow rates). It is assumed that measurement uncertainty value is a combination of different parameters including accuracy, resolution, sensitivity and gauge drift.
3) Repeat the estimation of the zonal properties. The estimates are now different from the ones in step 1 values with the difference depending on the value of the uncertainties.
4) Use the step 3 results as input to the Excel optimiser to identify the ICV configuration that maximises the oil production.
5) Repeat step 2 to 4 with increasing the values of measurement uncertainty until the resulting ICV configuration is different from the optimum one calculated in step 1.

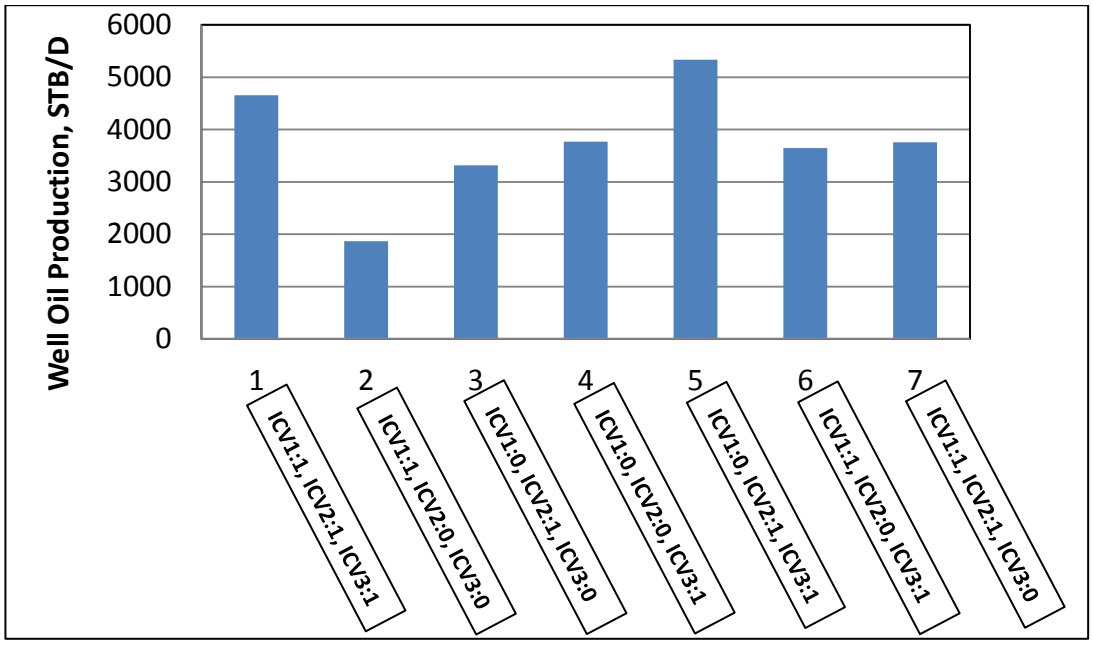

Figure 5-11 Well oil production at different combinations of ON/OFF ICV position

According to the above steps, ICVs opening combinations in Table 5-4 is selected as the initial flow tests to implement the active soft-sensing algorithm considering two different optimisation criteria. Uncertainty values of ± 5, ± 10, ± 15, ± 20 psi and ± 5, ± 10, ± 15, $\pm 20\%$ are added to pressure and flow rate measurements respectively in this study. The pressure and well rate measurements with ± 20 psi and $\pm 20\%$ measurement uncertainty are the first data set measurements that resulted in different ICV positions. These positions are used to design flow test number 4 in Table 5-4.

Table 5-4 Initial four ICVs position combinations

No. of Flow Test	ICV_1 Opening (fraction)	ICV2 Opening (fraction)	ICV3 Opening (fraction)
1	1	0	0
2	0	1	0
3	0	0	1
4	0.3	1	0.9

10 sets of random numbers are generated to yield random errors in the measured well rates and pressures. Figure 5-12 and Figure 5-13 present a typical multi-rate flow test and its associated noisy measurements. These flow tests have been designed by the DC optimisation method to maximise the reliability of the estimated zonal properties when noise was included in well rates and pressure measurements.

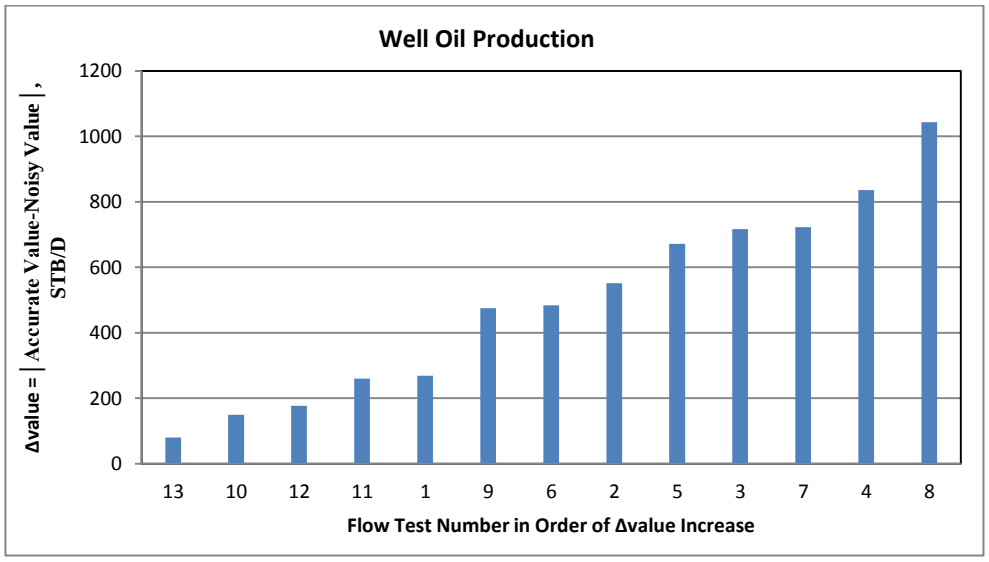

Figure 5-12 Comparison between accurate and inaccurate measured oil flow rate during multi-rate flow test

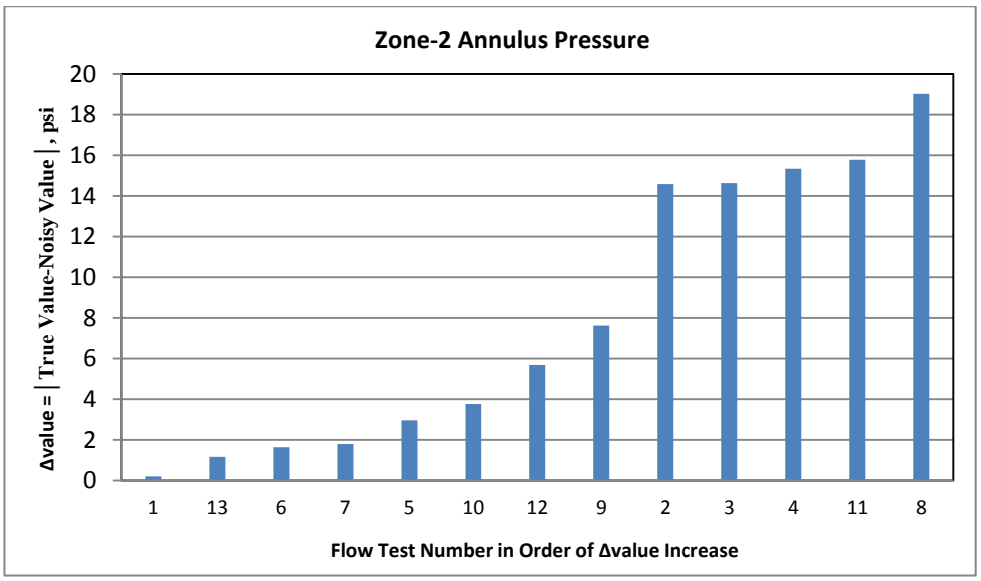

Figure 5-13 Comparison between accurate and inaccurate measured zonal annulus pressure during multi-rate flow test

5.5.2 Impact of Erroneous Measurements on Optimum ICV Configurations to Maximise Oil Production

Measurement uncertainties affect the optimum ICVs configuration required to maximise the oil production. The DC optimisation method uses direct values of erroneous objective function to search for the optimum ICVs position as errors are included in the well rates measurements. Results verify the robustness of the DC Simplex optimisation algorithm that finds the ICV positions in the vicinity of optimum one, even the optimisation is based on a noisy objective function. Table 5-5 compares the true optimum ICV positions to maximise the oil production with those obtained when erroneous measurements are used in DC optimisation method. This comparison has been listed for 10 cases of synthetic 3-zone IW described in 5.5.1 where random functions repeated 10 times to generate the noisy measurements using Equation 5-10 (measurement uncertainty of ± 20 psi and $\pm 20\%$ for pressure and well rate measurements respectively). The true optimum ICV positions are ICV_1 is closed and ICV_2 and ICV_3 are fully open (case 0). This is also found in most Table 5-5 cases. Figure 5-14 shows that the true oil production (without any random errors) from a well with estimated optimum ICVs position in Table 5-5 is still close to the true maximum oil production. However, the estimated maximum oil production differs from the true maximum oil production as noise is also added to the measured well oil rate.

Table 5-5 Optimum ICV positions calculated to maximise oil Production

	ICVs Open Area Fraction		
	ICV_1	ICV_2	ICV_3
Case 0	0	1	1
Case 1	0	1	1
Case 2	0	1	1
Case 3	0.1	0.9	1
Case 4	0	1	1
Case 5	0.3	1	1
Case 6	0.3	1	0.9
Case 7	0	1	1
Case 8	0.5	1	1
Case 9	0.3	1	1
Case 10	0.3	1	0.9

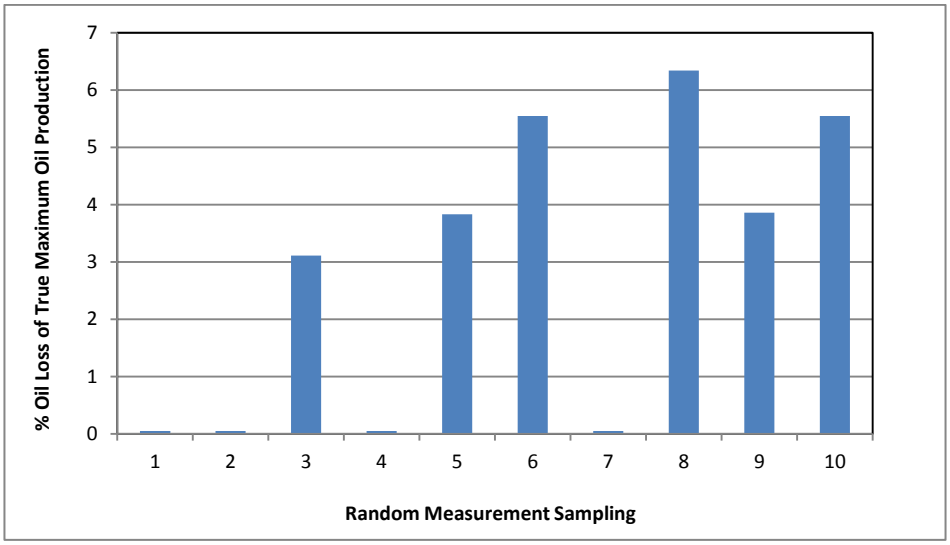

Figure 5-14 Oil loss percentage of true maximum oil production at different optimum ICV positions

5.5.3 Comparison of Results between two optimisation objective functions of "maximising oil production" or "reliability of zonal properties estimates"

Initial flow tests in Table 5-4 together with noisy measurements generated in 5.5.1 were used in the DC optimisation method to find the optimum ICV positions for either maximum oil production rate or reliability of zonal properties estimates. The DC

method was applied 10 times (referred to ten random numbers sampling) for both two routes of optimisation. The DC optimisation algorithm stops finding optimum ICVs configuration to maximise the oil production when the oil production from a new flow test is smaller than the arithmetic average oil production rate from all the flow tests forming the last simplex. An alternative stopping criterion would be to stop the DC algorithm when the new flow test results in a predefined small increase in oil production compared to the arithmetic average oil production rate from the vertices of the previous simplex. Other DC optimisation algorithm stopping criteria when attempting to maximise the reliability of the estimated zonal properties would be:

- Estimated zonal properties do not change with the new ICV configuration
- The DC designs an ICV configuration that was used in a previous flow test.

Table 5-6 illustrates that a different number of flow tests used to optimise the two objective functions. The number of flow tests required to maximise the oil production rate being less than when maximising the reliability of zonal property estimates. It also shows that the maximum oil production rate is achieved in earlier flow tests before the DC algorithm stops. The extra flow tests are required to improve the reliability of the zonal property estimates.

Table 5-6 Number of flow tests designed by the DC algorithm when different objective functions are used

Random Measurement Sampling		**1**	**2**	**3**	**4**	**5**	**6**	**7**	**8**	**9**	**10**
Flow Test Number	**To Maximise Oil Production (Objective Function: Maximise Oil Production)**	5	5	14	5	8	4	5	9	8	4
	Generate Best Zonal Properties Estimates (Objective Function: Maximise Oil Production)	13	5	17	11	12	12	12	10	11	10
	Generate Best Optimum Zonal Properties Estimates (Objective Function: Maximise Reliability of Zonal Properties Estimates)	12	8	17	11	11	14	12	13	11	11

The total zonal property misfit obtained at the end of the active soft-sensing algorithm is repeated for each set of random measurements. Figure 5-15 to Figure 5-18 compare the results between the two routes of optimisation where higher misfit of the zonal properties is observed in most cases when the objective function is maximisation of the

oil production. As expected the route corresponding to the objective function of maximising reliability of zonal properties estimates results in the best estimation of zonal properties, especially zonal reservoir pressures and productivity indices.

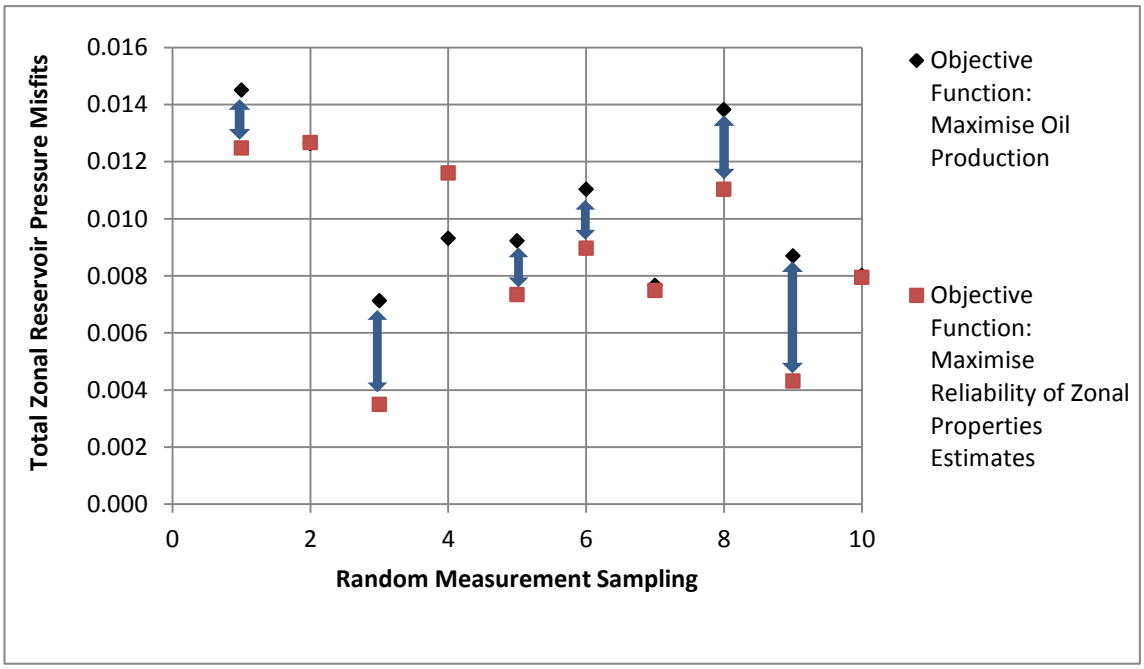

Figure 5-15 Total zonal reservoir pressure misfit for different objective functions

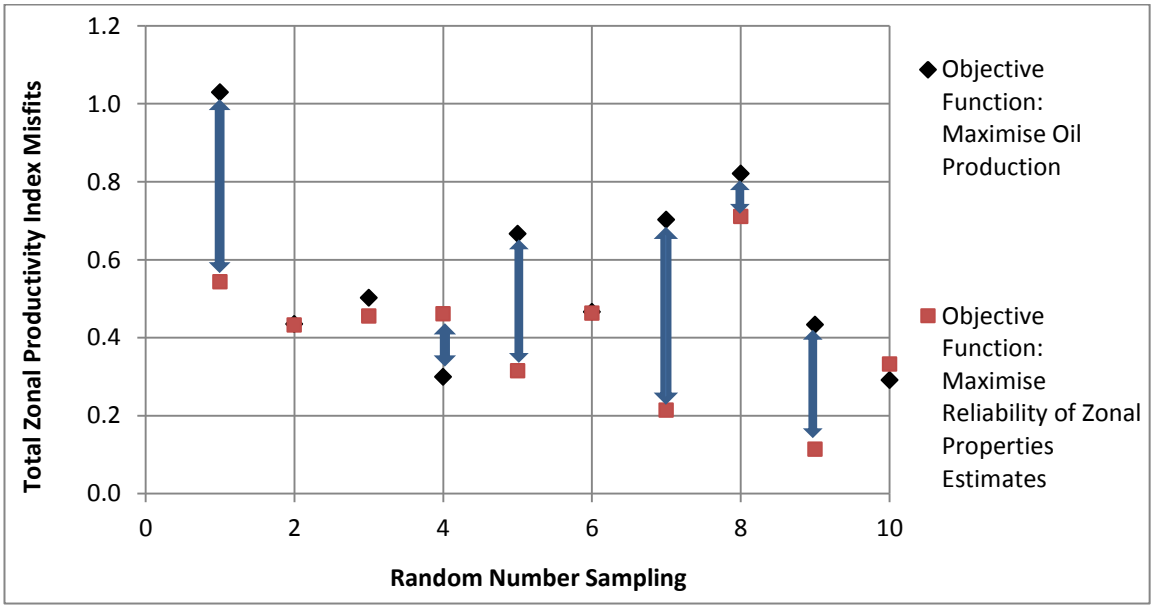

Figure 5-16 Total zonal productivity index misfit for different objective function

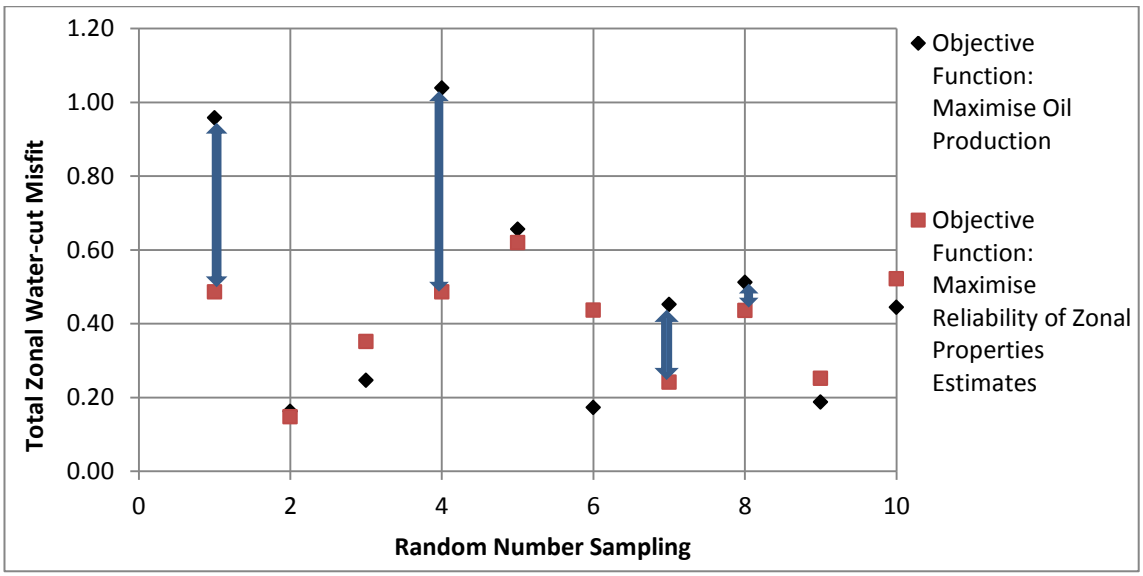

Figure 5-17 Total zonal water-cut misfit for different objective function

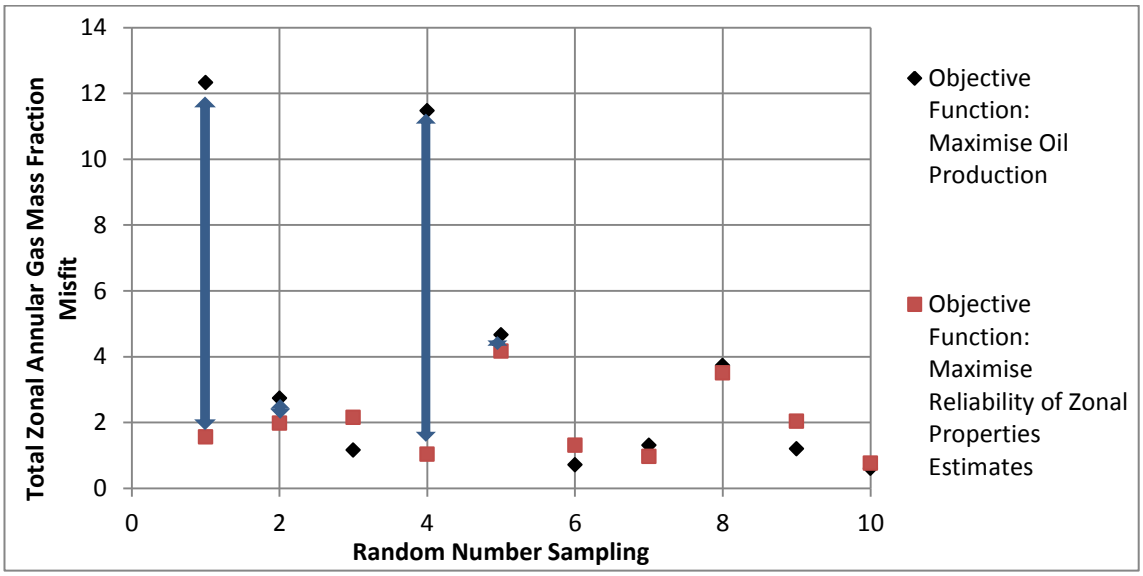

Figure 5-18 Total zonal gas mass fraction misfit for different objective function

A 3-D representation can be used to visualise the location of control variables within the search space (Figure 5-19 and Figure 5-20). The x, y and z axes represent the positions of ICV_1, ICV_2 and ICV_3 positions respectively. These 3-D plots present the control variables for one of the 10 noisy measurements (defined in 5.5.1) and describe the path followed by control variables towards the optimum solution. These figures illustrate the behaviour of DC optimisation algorithm under different objective function. Figure 5-19 used a smaller area of the search space that was mainly limited to the location of the optimum ICV position; while Figure 5-20 shows the DC algorithm uses a larger search space. When the search objective is the maximum total oil production, the DC algorithm

finds the optimum solution more easily and faster. Further flow tests are then designed close to the optimum one until the DC algorithm stops. This is not the case when the objective function criterion is changed to reliability of the estimated zonal properties. The DC algorithm finds the optimum solution more slowly, but it did use the search space efficiently by employing a larger space to obtain a more accurate estimation of the zonal properties.

More accurate estimations of zonal properties are obtained when the objective function is the maximum reliability of zonal properties estimates. However results confirm that the very accurate zonal properties are not required in order to find the optimum ICVs position to maximise oil production. Figure 5-20 shows satisfactory performance of the DC optimisation algorithm when the ICVs configuration is designed very close to the optimum one.

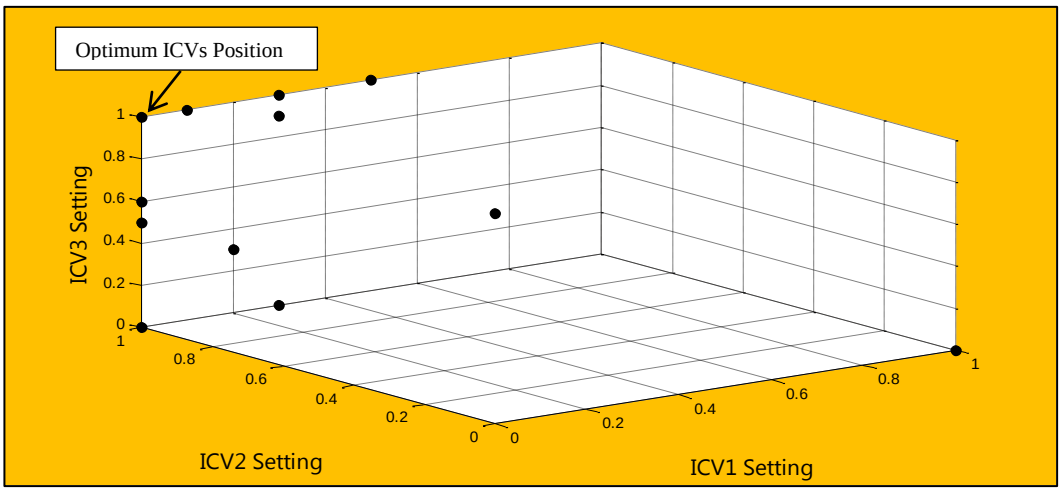

Figure 5-19 ICVs position combinations designed by DC when the objective function is the maximum total oil production

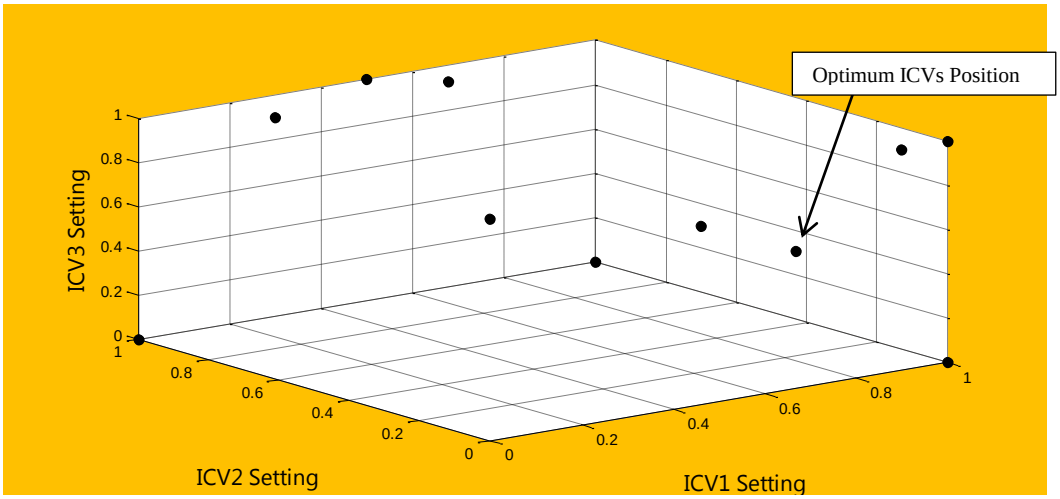

Figure 5-20 ICVs position combinations designed by DC when the objective function is the maximum reliability of zonal properties estimates

5.6 Test of Hypotheses

5.6.1 Concept Introduction

Many engineering, science and management problems need to decide whether to accept or reject a statement about some parameters. The comparison between the results of two optimisation routes lead to the statement that ***zonal properties are estimated more accurately when the objective function is the maximum reliability of zonal properties estimates than the maximum total oil production***. This statement or hypothesis requires testing to confirm whether it is 'true or not'. Statistical hypothesis testing is a method of testing a hypothesis about a parameter in a population, using data measured in a sample.

Here, the objective of the hypothesis testing is to verify the above statement. Hypothesis-testing procedure relies on using information in a random sample from the population of interest. If this information is consistent with the hypothesis, then it is concluded that the hypothesis is true. The truth or falsity of a particular hypothesis is evaluated with 100% certainty when the entire population is considered.

The hypothesis-test compares the null hypothesis (H_0) (the hypothesis which is tested) and an alternative hypothesis (H_1). H_0 specifies the exact value of the parameter. Rejection of the null hypothesis results in the acceptance of the alternative hypothesis that allows the parameter to hold several values. Three steps are required for a hypothesis test: 1) take a random sample, 2) compute test statistics from the sampled data and 3) use the test statistics to decide if the null hypothesis is true. Appendix F discusses how the test statistics are calculated and decision on the veracity of the null hypothesis is made.

A statistical hypothesis test may result in one of four different situations (

Table 5-7) to determine whether the final decision is true or involves error. The type I error probability is sometimes called the significance level or the size of the test. It implies the percentage of all random samples that would lead to rejection of the H_0 when H_0 is true.

Table 5-7 Decision in hypothesis testing

Decision	**H_0 is True**	**H_0 is False**
Accept null hypothesis, H_0	No Error	Type II Error (β)
Reject null hypothesis, H_0	Type I Error (α)	No Error

5.6.2 Hypothesis Tests on the Mean of Zonal Properties Estimates

Two different approaches were selected to estimate the zonal properties using the active soft-sensor. The test on the means of total misfits of the zonal properties is carried out to determine whether there is any difference in the mean of the misfit of the zonal properties between the two approaches. We have generated two populations using the same 10 noisy measured data set (well rate, zonal annulus and tubing pressures) samples defined in 5.5.1 but with different objective functions. Ten different values are obtained for the total misfit of each zonal property (reservoir pressure, productivity index, water-cut and annular gas mass fraction) which form an independent sample of size 10 from its population. Table 5-8 summarises the means and standard deviation of samples for each zones property obtained through two approaches. The number of random samples is small ($n_1 = n_2 = 10$) and the variance of the populations is unknown. A further assumption, that the data is normally distributed, is necessary to perform the hypothesis test using the t-distribution (Montgomery and Runger, 2011). The t-distribution role is preferred if the data set is small or the standard deviation of the population is unknown (which is often the case). The z-distribution is used when the number of the samples is high (≥ 30) and the population standard deviation can be assumed being equal to the sample standard deviation (Montgomery and Runger, 2011). Probability plotting is a graphical method for determining whether sample data conform to a normal distribution. The estimated misfits of a zonal property in the sample are first ranked from the smallest to the largest to construct a probability plot. Then they are noted as $x_{(1)}, x_{(2)}, \ldots, x_{(n)}$ where $x_{(1)}$ is the smallest estimated misfit and $x_{(n)}$ is the largest one. The vertical and horizontal axes of the normal probability plot are represented by the observed cumulative frequency $100(j - 0.5)/n$ and ordered observations $x_{(j)}$ respectively. The hypothesized distribution adequately describes the data if the plotted points fall approximately along the line. Alternatively, the distribution model is not appropriate if the plotted points deviate significantly from a straight line. A subjective visual examination of the data is frequently used to determine whether or not the plotted points fall along the straight line. A good rule of thumb is to draw the straight line approximately between the 25^{th} and 75^{th} percentile points since the focus should be more near the middle of the plot rather than emphasising the extreme points when drawing the straight line. Covering all the points by an imaginary "fat pencil" is used to assess the closeness of the points to the straight line (Montgomery and Runger,

2011). Since the points in Figure 5-21 pass the "fat pencil" test, it is concluded that a normal distribution is an appropriate model.

Table 5-8 Means and standard deviations of the calculated total misfit of each zonal property

		Approach	
		Maximise Oil Production	Maximise Reliability of Zonal Properties Estimates
Total Misfit of the Zones Reservoir Pressure	Mean	0.0102	0.0087
	Standard Deviation	0.0026	0.0032
Total Misfit of the Zones Productivity Index	Mean	0.5646	0.4041
	Standard Deviation	0.2365	0.1691
Total Misfit of the Zones Water-cut	Mean	0.4834	0.3982
	Standard Deviation	0.3180	0.1467
Total Misfit of the Zones Annular Gas Mass Fraction	Mean	3.9926	1.9451
	Standard Deviation	4.3815	1.1141

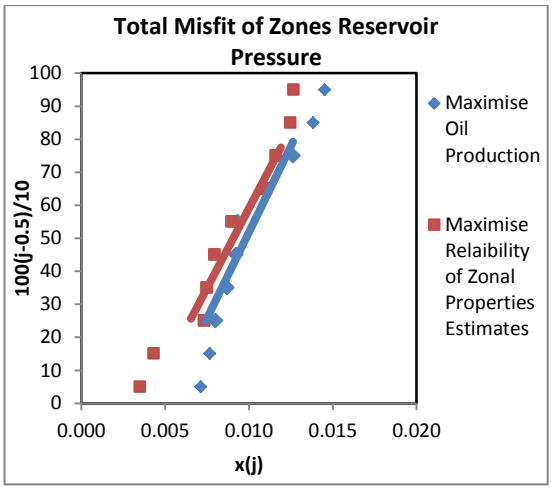

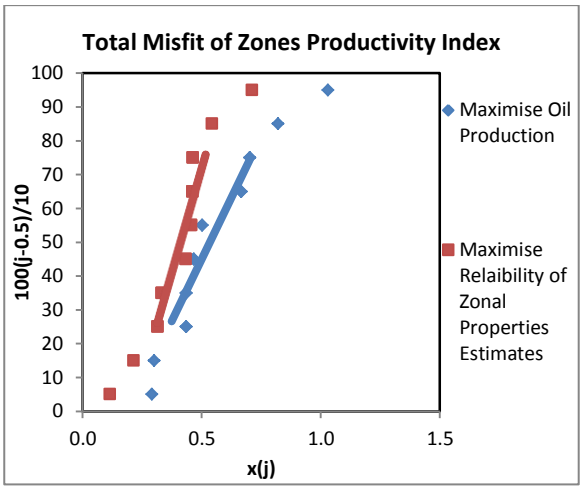

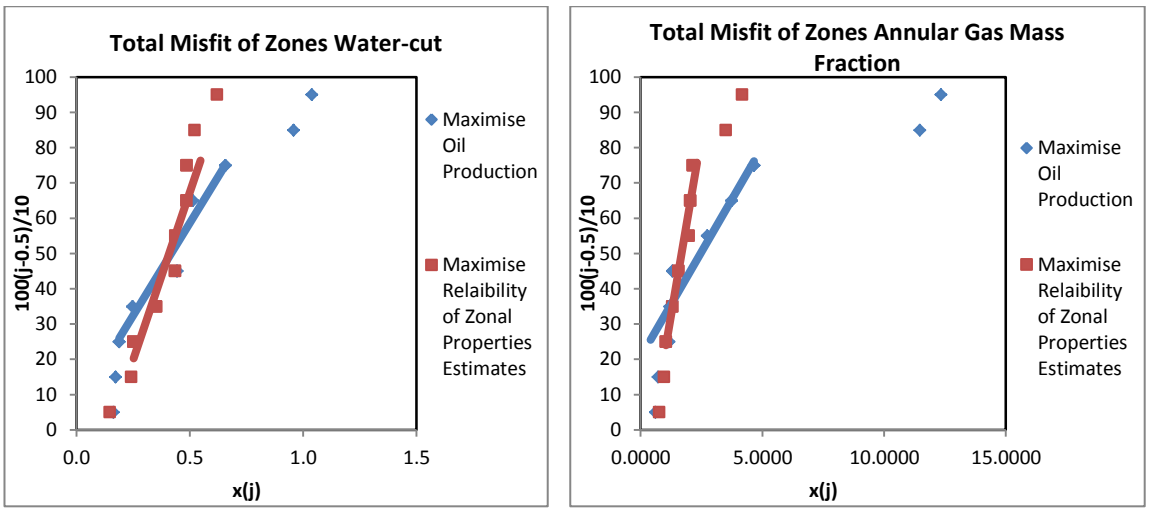

Figure 5-21 Normal probability plot of total misfit for zonal properties

μ_1 and μ_2 are the mean of the total misfit of zonal property obtained using the objective functions: (1) maximise oil production and (2) maximise reliability of the zonal properties estimates. The hypothesis test may now be applied to determine if there is any difference between the means of these two independent populations:

$$H_0: \mu_1 = \mu_2$$
$$H_1: \mu_1 > \mu_2 \qquad 5\text{-}11$$

Equation 5-11 is the hypothesis test for on the means of two samples where the alternative hypothesis is one-sided. If the null hypothesis is accepted, it means both approaches result in the estimation of zonal properties with equal accuracy under measurement uncertainty. Alternatively, then more accurate zonal property values are estimated when the optimisation is based on the maximising the reliability of the zonal properties estimates if it is rejected. We have chosen to assume the most difficult situation where the means and variances are not known and variances are not equal to each other to evaluate the hypothesis test on these normal populations,. Here, t_0^* and ϑ are computed as the test statistic and degree of the freedom (see Appendix F). It is assumed that t_0^* is distributed normally with degrees of freedom of ϑ (Montgomery and Runger, 2011).

$$t_0^* = \frac{\overline{X_1} - \overline{X_2}}{\sqrt{\frac{S_1^2}{n_1} + \frac{S_2^2}{n_2}}} \qquad 5\text{-}12$$

$$\vartheta = \frac{(\frac{S_1^2}{n_1} + \frac{S_2^2}{n_2})^2}{\frac{(S_1^2/n_1)^2}{n_1+1} + \frac{(S_2^2/n_2)^2}{n_2+1}} - 2 \quad \text{5-13}$$

$\overline{X_1}$, $\overline{X_2}$, S_1^2 and S_2^2 are the means and variances of the random samples of sizes n_1 and n_2 respectively. The null hypothesis is rejected if either $t_0^* > t_{\alpha/2,\vartheta}$ or $t_0^* < -t_{\alpha/2,\vartheta}$. Similarly, the rejection criterions $t_0^* > t_{\alpha,\vartheta}$ and $t_0^* < -t_{\alpha,\vartheta}$ are used to reject the H_0: $\mu_1 = \mu_2$ if the one-sided alternatives are $\mu_1 > \mu_2$ and $\mu_1 < \mu_2$ respectively.

The rejection criteria and decision for a range of significance levels α are listed in Table 5-9 to Table 5-12 where each table presents the results for each zones property.

It is found that at a low significance levels, α, (.0005 to 0.1) the null hypothesis is accepted. Therefore, it is expected to have the equal means of the total misfits from both optimisation approaches. However, at higher significance levels, α, (0.25 and 0.4) the null hypothesis is rejected. Hence maximising reliable zonal properties estimates provides a more accurate calculation of multi-phase flow rates during active soft-sensing.

Table 5-9 Inference for the difference in the means of the total misfit of the zones reservoir pressure

Total Misfit of the Zones Reservoir Pressure		
Significance Level, α	**Rejection Criteria, $t_{\alpha,\vartheta}$**	**Decision on H_0**
0.0005	3.883	Accept
0.001	3.579	Accept
0.0025	3.174	Accept
0.005	2.861	Accept
0.01	2.539	Accept
0.025	2.093	Accept
0.05	1.729	Accept
0.1	1.328	Accept
0.25	0.688	Reject
0.4	0.257	Reject
$t_0^* = 1.11$ & $\vartheta = 19$		

Table 5-10 Inference for the difference in the means of the total misfit of the zones productivity index

Total Misfit of the Zones Productivity Index		
Significance Level, α	**Rejection Criteria, $t_{\alpha,\vartheta}$**	**Decision on H_0**
0.0005	3.922	Accept
0.001	3.61	Accept
0.0025	3.197	Accept
0.005	2.878	Accept
0.01	2.552	Accept
0.025	2.101	Accept
0.05	1.734	Accept
0.1	1.33	Reject
0.25	0.688	Reject
0.4	0.257	Reject
$t_0^* = 1.746$ & $\vartheta = 18$		

Table 5-11 Inference for the difference in the means of the total misfit of the zones water-cut

Total Misfit of the Zones Water-cut		
Significance Level, α	**Rejection Criteria, $t_{\alpha,\vartheta}$**	**Decision on H_0**
0.0005	4.221	Accept
0.001	3.852	Accept
0.0025	3.372	Accept
0.005	3.012	Accept
0.01	2.65	Accept
0.025	2.16	Accept
0.05	1.771	Accept
0.1	1.35	Accept
0.25	0.694	Reject
0.4	0.259	Reject
$t_0^* = 0.77$ & $\vartheta = 13$		

Table 5-12 Inference for the difference in the means of the total misfit of the zones annular gas mass fraction

Total Misfit of the Zones Annular Gas Mass Fraction		
Significance Level, α	**Rejection Criteria, $t_{\alpha,\vartheta}$**	**Decision on H_0**
0.0005	4.587	Accept
0.001	4.144	Accept
0.0025	3.581	Accept
0.005	3.169	Accept
0.01	2.764	Accept
0.025	2.228	Accept
0.05	1.812	Accept
0.1	1.372	Reject
0.25	0.7	Reject
0.4	0.26	Reject
$t_0^* = 1.432$ & $\vartheta = 10$		

5.6.3 Hypothesis Tests on the Number of Flow Tests

The hypothesis test can also be applied to investigate the number of required flow tests to maximise either oil production or reliability of the estimated zonal properties. Following hypothesis is tested based on the findings in Table 5-6 where it was observed that smaller number of flow tests is required to maximise the oil production:

$H_0: \mu_1 = \mu_2$ 5-14

$H_1: \mu_1 < \mu_2$

μ_1 and μ_2 represent the mean of the number of required flow tests to maximise oil production and reliability of the estimated zonal properties respectively. If the null hypothesis is rejected, it is concluded that DC algorithm maximises the oil production by designing smaller number of flow tests. The normal probability plot shown in Figure 5-22 allows flow test numbers obtained in Table 5-6 are to be modelled using a normal distribution.

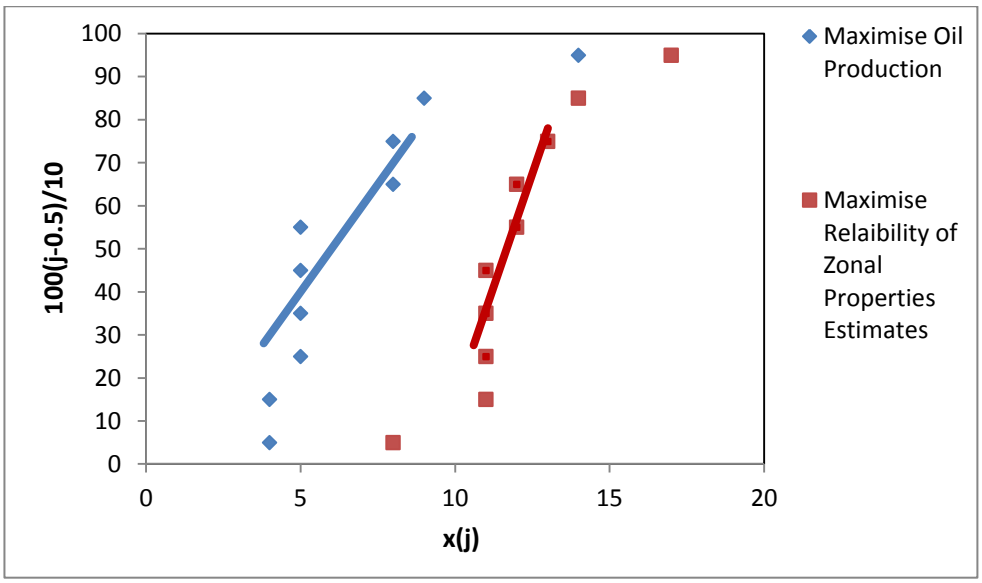

Figure 5-22 Normal probability plot for number of flow tests

Similar to the previous section, t_0^* and ϑ are calculated to test the hypothesis on the mean of the required number of flow tests to maximise the two objective functions assuming that means and variances of these two populations are unknown and the variances are not equal to each other. Table 5-13 summarises the decision on the null hypothesis corresponding to different values of significance level, α. The null hypothesis is rejected for all α values; confirming that a smaller number of flow tests are required for the DC algorithm to find the optimum ICVs configuration when maximising the oil production compared to when it is required to maximise the reliability of estimated zonal properties.

Table 5-13 Inference for the difference in the means of required flow test number

Number of Flow Tests		
Significance Level, α	**Rejection Criteria, $t_{\alpha,\vartheta}$**	**Decision on H_0**
0.0005	3.922	Reject
0.001	3.61	Reject
0.0025	3.197	Reject
0.005	2.878	Reject
0.01	2.552	Reject
0.025	2.101	Reject
0.05	1.734	Reject
0.1	1.33	Reject
0.25	0.688	Reject
0.4	0.257	Reject
$t_0^* = -4.28$ & $\vartheta = 18$		

5.7 Summary

The active multi-phase flow rate monitoring can be potentially combined with the production reactive control algorithm to develop the ICM workflow. The ICM workflow not only designs the required initial flow tests of the active soft-sensing workflow, but also provides simultaneous inflow rate monitoring and oil production control. The results reported in this chapter are promising as far as the application of ICM workflow to monitor the zonal properties and maximise the oil production for a 5-zone I-well.

The ICV positions are the key variables to achieve the purposes of monitoring and controlling in the ICM workflow. They are regulated to maximise the oil production during (n+1) flow rate tests in n-zone I-wells. Additional flow tests by further regulation of the ICVs are designed by the DC optimisation method. DC optimisation provides the flexibility of defining different objective functions such as optimising the ICV positions to achieve either maximum reliability of the zonal properties or maximum oil production.

The importance of the ICM workflow was highlighted in a study of the situation when the surface or/and downhole measurements are uncertain. Various noise levels were added to the accurate downhole measurements and modelled with the ICM workflow. The conclusions are:

1. The ICM workflow used to optimise the oil production is fast and finds the best ICV positions in the vicinity of optimum ICV configuration. This implies a small search space is required by the ICM workflow.
2. The ICM workflow used to maximise the reliability of the zonal properties estimates is slow, but uses a larger search space to design the multi-rate tests. This results in more accurate estimation of zonal properties, even in the presence of using measurements.
3. The hypothesis test was applied to investigate the behaviour of different optimisation strategies in terms of the accuracy of the estimated multi-phase flow rates and the design of the number of flow tests. A synthetic example was used to explore the application of the hypothesis test. The results confirmed that an ICM workflow based on the maximising the reliability of the estimated zonal property values did provide more accurate estimates, but also required more flow tests (N.B. This is not a general conclusion since only one example has been tested in the work).

Chapter 6 Extension of Active Soft-sensing in Well Monitoring System Design

6.1 Introduction

There are several types of surface and downhole sensors to assist the well performance monitoring. Every sensor, or measurement tool, is defined with metrological specifications in terms of accuracy, repeatability, reproductability, resolution, stability and measurement uncertainty which affect the monitoring of downhole multi-phase flow rates in the wellbore. Active flow rate soft-sensing allocates the phase rates in the commingled production systems by combining data from different types of measurement from multiple sensors. The estimated flow rates are influenced by the inherent uncertainty present in the incorporated multi-phase flow model and the sensor measurements. In this chapter, the uncertainty of the models used to predict the well rate and pressure and temperature changes in the wellbore is quantified by comparing the analytical results with outputs from OLGA simulator. Besides that, different cases are modelled to include random and drift errors in either single or multiple measurements.

This chapter will also consider the efficiency of zonal property characterisation based on model uncertainty and noisy measurements by multiple sensors. Results are discussed to find the influence of noisy measurement on estimation of individual zonal properties which helps to derive strategies to design a well monitoring system using flow meters together with pressure and temperature sensors.

6.2 Sources of Uncertainty in Active Soft-sensing

There are several sources of uncertainty that reduce the confidence associated with the active soft-sensing method's results (see section 4.5). The two key uncertainties identified are:

1) Measurement Uncertainty in:
    a) Pressure and temperature data: Examples include noise, drift, temperature effects and time shift.
    b) Well rate measurement: The equipment used and the accompanying uncertainty will depend on whether it is measured at the surface or downhole.

c) Well/reservoir response: A steady-state flow rate test is required to minimise the error in the stabilized annular and tubing pressure/temperature measurement. Also, a sufficiently long pressure transient test is needed to identify the flow regimes during the test.

2) Model Uncertainty in:
   a) Fluid and rock properties: Phase densities and formation volume factors. These are used in the pressure drop calculation across the ICVs and flow lines. The parameter values must be calculated at downhole pressure and temperature. Also, the estimates of the reservoir properties from well test analysis depend on the knowledge of fluid and rock properties such as viscosity, compressibility and porosity. These properties are often not well known, and are calculated from industry standard models.
   b) Analytical equations used to form the multi-phase flow model: All analytical solutions should be derived based on valid assumptions. The estimated zonal properties will be inaccurate if the analytical model incorrectly describes fluid flow through porous media, the wellbore and IWC.
   c) The estimation of zonal properties: Analysis of the results from optimisation methods (either deterministic or probabilistic) confirmed that the estimation of optimum zonal properties is difficult when the flow models are nonlinear and/or consists of high number of control variables.

These sources of uncertainties differ from each other in terms of their origin, their degree of importance and whether the resulting level of uncertainty has a significant effect on the estimated zonal properties.

Advances in I-wells and information technology can provide a very high frequency data from each well. The data typically undergo a series of steps that includes data acquisition, pre-processing, post- processing and interpretation to transform data into the knowledge for making reliable decisions (Figure 6-1).

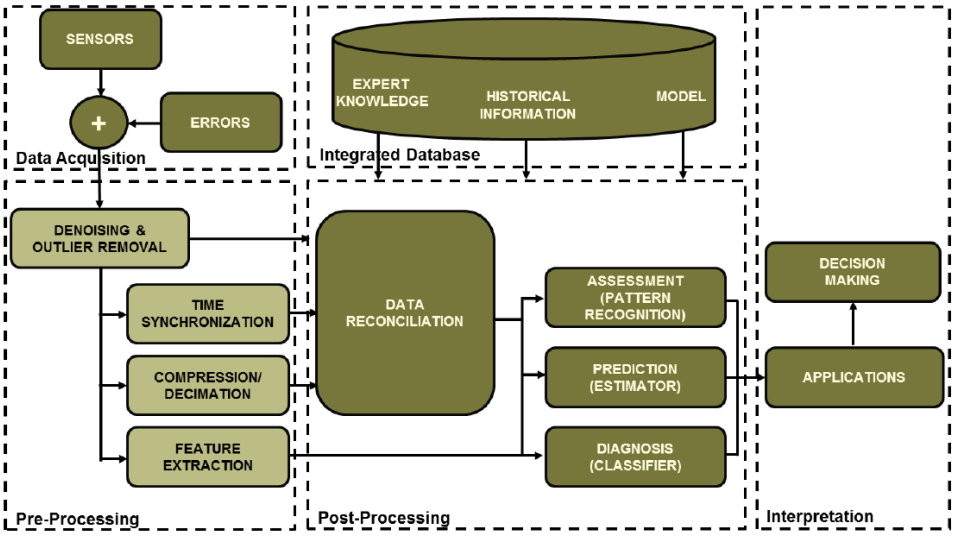

Figure 6-1 Data analysis framework (Da Silva et al., 2012)

Measured data acquired by the supervisory control and data acquisition (SCADA) system are transmitted from the field to the operator's office where the data pre-processing steps (sampling, denoising, outlier removal, compression and time synchronisation) reduce noise, but may also add another source of uncertainty. Missing data, filtering, time synchronisation, limited storage capacity and different sample rates must all be managed to prevent noise generated by the sensors and transmission system appearing on the engineer's desktop (Da Silva et al., 2012).

6.3 Combining the Various Sources of Uncertainties

Combining uncertainties account for considering different sources of uncertainties within the active soft-sensing algorithm. Equation D- 1 was used to compute the uncertainty of the zonal properties calculated from uncertain measurements, such as pressure, temperature and well rate. Equation 6-1 is then used to evaluate the uncertainty of these parameters when different error sources (measurement & model) contribute to the uncertainty:

$$\delta_i = \sqrt{\delta_{i,model}^2 + \delta_{i,measurement}^2} \qquad 6\text{-}1$$

where it is assumed that the individual contributions are uncorrelated. δ_i represents the total uncertainty of each parameter (pressure, temperature and well rate) as a function of model and measurement uncertainties. This work considers the model uncertainty and induced random and drift errors in the measurements as the main sources of the uncertainties within the active soft-sensing workflow.

6.4 Estimation of Zonal Properties under Model Uncertainty

The necessary values required to implement the active soft-sensing algorithm were provided for a 3-zone horizontal I-well by the OLGA^{TM} simulator. This synthetic example is similar to the case presented in section 4.3.2. Figure 6-2 and Figure 6-3 illustrate the pressure and temperature profile along the wellbore. The ICV open flow areas are sufficiently large that a negligible pressure drop is observed between the annulus and tubing sections when they are fully open to flow. The slope of the temperature tubing profile changes in front of the second and third zone because the annular fluids are mixed with the tubing fluid coming from first (toe) zone. The tubing temperature slightly decreases in front of ICV_2 and ICV_3 as relatively cooler fluids enter the tubing section.

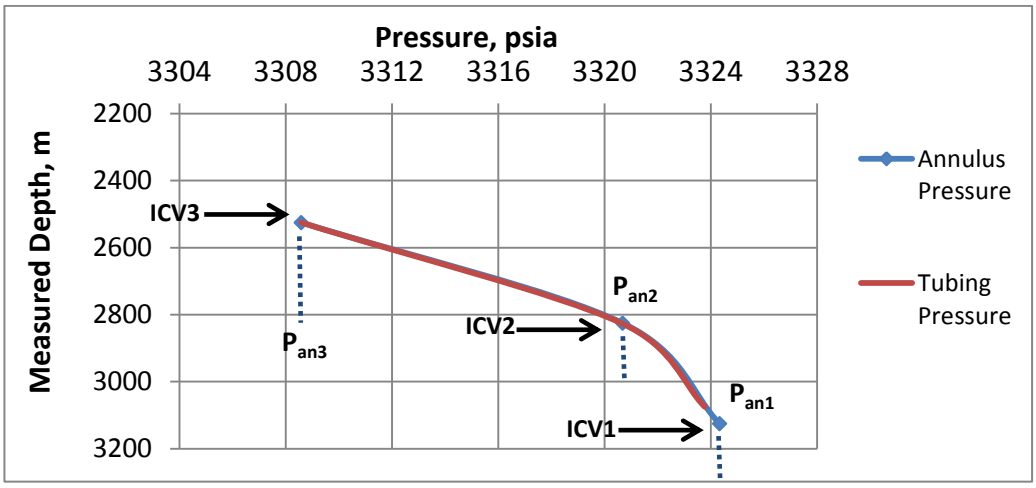

Figure 6-2 Profile of the annulus and tubing pressure along the wellbore

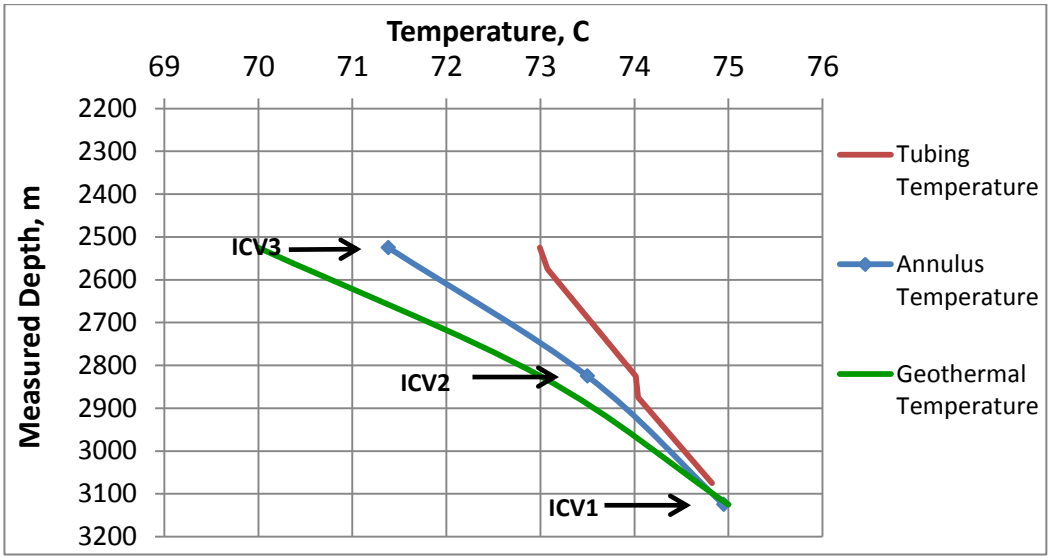

Figure 6-3 Geothermal, annulus and tubing temperature profile along the wellbore

We assumed that the measured values of the pressure, temperature and well rates are 100 percent accurate. However, uncertainties from the simplified analytical equations to simulate thermal and hydraulic interactions between reservoir, wellbore and IWC still be presented in the multi-phase flow model used to predict the measurements. The true values of zonal properties are input into our multi-phase model and OLGA and the outputs compared (see Table 6-1 to Table 6-3) for the maximum mismatch between the OLGA^{TM} simulated values and the same equivalent values predicted by our analytical multi-phase flow model. Table 6-4, the values used in the active soft-sensing algorithm to represent the model uncertainty, were based on the maximum mismatch between the outputs of the model and the OLGA^{TM} simulator. The multi-phase flow model is only able to predict pressure and temperature drops across ICVs that are fully or partially open. N/A indicates the cases where the corresponding ICV has been closed.

Table 6-1 Comparison between the predicted oil and water well rates by OLGA^{TM} and the multi-phase flow model

	Well Rates – OLGA^{TM}		**Well Rates – Multi-phase Flow Model**		**Relative Error (%)**	
Time (Day)	**Q_o (STB/D)**	**Q_w (STB/D)**	**Q_o (STB/D)**	**Q_w (STB/D)**	**Q_o**	**Q_w**
1	5397.63	5110.26	5366.61	5087.45	0.57	0.45
2	7576.51	2705.91	7532.97	2693.83	0.57	0.45
3	4611.86	5671.45	4585.36	5646.14	0.57	0.45
4	4872.18	5533.21	4844.18	5508.53	0.57	0.45
5	4268.24	5946.69	4243.71	5920.16	0.57	0.45
6	6627.92	3383.71	6589.83	3368.61	0.57	0.45
7	6758.89	2881.28	6720.05	2868.42	0.57	0.45
8	6858.98	1955.70	6819.56	1946.98	0.57	0.45
9	6935.29	2852.80	6895.43	2840.07	0.57	0.45
10	7245.73	2781.41	7204.09	2769.00	0.57	0.45
11	5384.51	4952.39	5353.56	4930.30	0.57	0.45

Table 6-2 Comparison between predicted pressure drop across the ICVs by OLGA^{TM} and the multi-phase flow model

	Pressure drop - OLGA, (psi)			**Pressure drop – Multiphase Flow Model, (psi)**			**Absolute Error (psi)**		
Time (Day)	ICV_1	ICV_2	ICV_3	ICV_1	ICV_2	ICV_3	ICV_1	ICV_2	ICV_3
1	0.56	0.05	0.01	0.15	0.05	0.01	0.41	0.00	0.00
2	N/A	0.26	0.05	N/A	0.26	0.05	N/A	0.01	0.00
3	1.00	N/A	0.02	0.26	N/A	0.02	0.74	N/A	0.00
4	0.73	0.07	N/A	0.19	0.07	N/A	0.54	0.00	N/A
5	1.12	76.12	56.02	0.29	76.66	57.46	0.83	0.54	1.44
6	153.30	0.33	105.36	156.21	0.32	105.84	2.90	0.01	0.47
7	N/A	0.55	N/A	N/A	0.57	N/A	N/A	0.02	N/A
8	N/A	400.20	213.76	N/A	396.49	216.59	N/A	3.71	2.83
9	N/A	0.50	159.18	N/A	0.50	162.36	N/A	0.00	3.18
10	N/A	0.38	83.35	N/A	0.37	85.04	N/A	0.01	1.69
11	41.60	67.50	0.52	42.19	69.13	0.52	0.60	1.63	0.00

Table 6-3 Comparison between the predicted temperature across ICV_1 and the temperature of the mixed annular and tubing fluids downstream of ICV_2 and ICV_3 by OLGA^{TM} and the multi-phase flow model

	Temperatures OLGA, ^{0}C			**Temperatures Multiphase Model, ^{0}C**			**Absolute Error (^{0}C)**		
Time (Day)	ΔT_1	T_{mix2}	T_{mix3}	ΔT_1	T_{mix2}	T_{mix3}	ΔT_1	T_{mix2}	T_{mix3}
1	0.12	74.01	72.99	0.00	73.88	72.88	0.12	0.13	0.11
2	N/A	72.97	71.63	N/A	72.97	71.39	N/A	0.00	0.24
3	0.07	74.57	73.10	0.00	74.51	72.90	0.07	0.06	0.20
4	0.11	74.02	73.37	0.00	73.88	73.27	0.11	0.14	0.10
5	0.08	74.48	73.54	0.00	74.44	73.53	0.08	0.03	0.02
6	0.45	73.17	72.43	0.03	73.12	72.39	0.42	0.04	0.03
7	N/A	72.96	72.43	N/A	72.95	72.35	N/A	0.00	0.08
8	N/A	72.77	70.43	N/A	72.63	70.07	N/A	0.14	0.37
9	N/A	72.96	72.35	N/A	72.96	72.33	N/A	0.00	0.02
10	N/A	72.97	72.02	N/A	72.97	71.92	N/A	0.00	0.10
11	0.10	74.22	72.72	0.01	74.13	72.49	0.09	0.08	0.23

Table 6-4 Model uncertainties used to predict the measurements

	Well Rates (STB/D)	**Pressure (psia)**	**Temperature (^{o}C)**
Model Uncertainty	$\pm 5\%$	$\pm 5 \sim \pm 0.15\%$	$\pm 0.5 \sim \pm 0.7\%$

Figure 6-4 shows that the active soft-sensing is terminated after the fifth simplex with a total misfit of 0, 0.03, 0.01 and 1.04 for the zonal reservoir pressures, zonal productivity indices, zonal water-cuts and the zonal annular gas mass fractions respectively (see Equation 4-3 for the definition of the total misfit). The ICVs position changes during the multi-rate flow test are summarised in

Table 6-5. Extra flow tests are required to, as accurately as possible, estimate the zonal annular gas mass fractions than are required for the other parameters. The resulting accuracy is still lower than that for the other zonal property estimates despite these extra flow tests since the flow models used and the measurement gauge response are intrinsically less sensitive to gas flow.

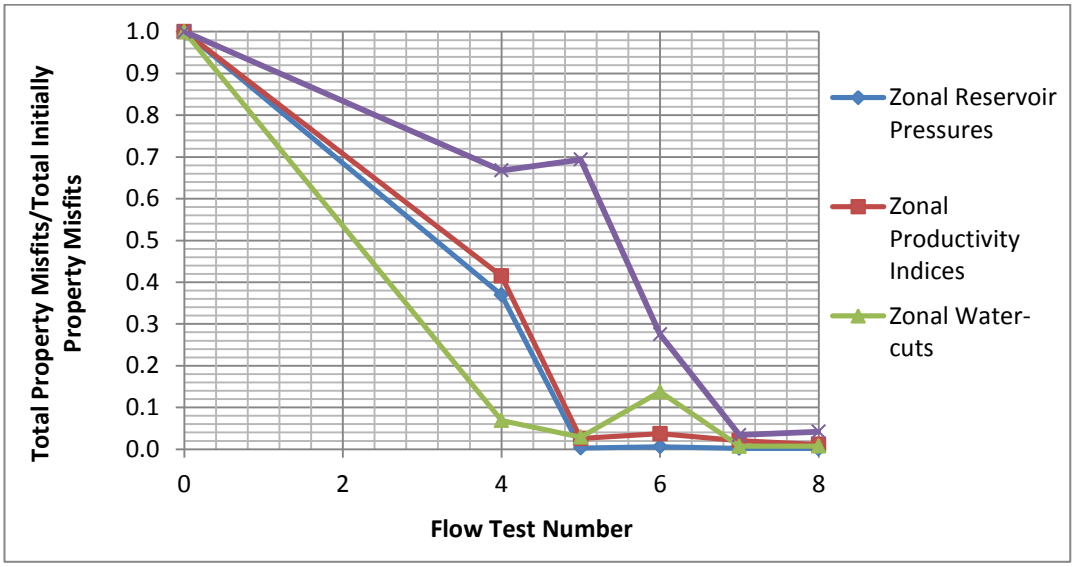

Figure 6-4 Zonal properties estimates under model uncertainty

Table 6-5 ICV configurations for flow tests designed under model uncertainty

ICVs Fraction Area Open to Flow				
Flow Test No.	**Simplex No.**	**ICV_1**	**ICV_2**	**ICV_3**
1	1	1	1	1
2		0	1	1
3		1	0	1
4		1	1	0
5	2	1	0.3	0.3
6	3	0.3	1	0.3
7	4	0	1	0
8	5	0	0.3	0.5

6.5 Estimation of Zonal Properties under Measurement Uncertainty

This section discusses the effect of uncertainties in the pressure, temperature and well rate measurements on the zonal properties estimated via the active soft-sensing algorithm. These results were then used to derive guidelines for designing a wellbore monitoring system. The investigation was split into three parts with each one being based on a different set of assumptions. The first part assumes that random errors are present in only one of the types of measurements. The second part evaluates the case where multiple noisy sensors are present. Gauge drift and its effect on the estimation of zonal properties is studied in the third part.

6.5.1 Random Errors - Single Measurement Uncertainty

Pressure, temperature and well rate are the main physical quantities measured by surface and downhole sensors in the active MPFR soft-sensing algorithm. The derived zonal properties estimates will be affected by any measurement that contains errors. Such errors result in the need for further measurements if one wishes to maximise the reliability of the zonal properties estimates.

Three different scenarios are considered in which only one type of noisy measurement exists while the other measurement sensors are highly accurate. Measurement uncertainty is defined as the standard deviation of measurement values around the true value of a measured quantity when active soft-sensing is implemented to calculate the most reliable zonal properties (

Table 6-6). These values chosen for his study are greater than typical accuracy of today's gauges. This was done in order to magnify the effect of the simulation of the noisy measurement conditions. An 0.3% to 2.8% measurement uncertainty in the estimated flow rate is equivalent to a much larger error in measured pressure and temperature. Note that this level of error in the flow rate measurements is less than the typical accuracy of a multi-phase flow meter. These values should be compared with Table 6-7's list of typical metrological data for downhole sensors (Silva et al. 2012).

Table 6-6 Measurement uncertainties of individual measurements

Scenario	**Physical Quantity**	**Measurement Uncertainty Values**				
1	Well Rate	±0.3%	±0.6%	±0.9%	±1.4%	±2.8%
2	Temperature	±0.22 °C (~±0.3%)	±0.43 °C (~±0.6%)	±0.65 °C (~±0.9%)	±1 °C (~±1.4%)	±2 °C (~±2.8%)
3	Pressure	±10 psi (~±0.3%)	±20 psi (~±0.6%)	±30 psi (~±0.9%)	±45 psi (~±1.4%)	±90 psi (~±2.8%)

Table 6-7 Typical metrological data for downhole sensors

Sensor	**Pressure Accuracy**	**Temperature Accuracy**	**Multi-phase Flow Rate Accuracy**
Single-point Pressure and Temperature Sensor (electronic)	±3 psi	±0.5 °C	***
Single-point Pressure and Temperature Sensor (fibre optic)	±2 psi	±0.1 °C	***
Quasi-distributed Temperature Sensor (electronic)	-	±0.1 °C	***
Quasi-distributed Temperature Sensor (fibre optic)	-	±0.5 °C	***
Single-phase and Two-phase Flowmeter (fibre optic)	-	-	±1 %*, ±5 %**

*: Single-phase accuracy (% of the measurement)

**: Volumetric flow rate, water-cut (WC) and gas void fraction (GVF) accuracy (% of the measurement

***: Variable, highly dependent on measurement device and multi-phase flow condition

Random errors are modelled within the specified interval of measurement uncertainty in

Table 6-6 and then added to the true measurements (the OLGA^{TM} output in our case). The active soft-sensing algorithm is stopped when the values of the zonal properties do not change after design of a new flow test or the DC optimisation method results in the same ICV positions for the next flow test. As expected, the number of flow tests required to find the most accurate estimation of zonal properties increases as the value of this random uncertainty within the measurement increases (Figure 6-5).

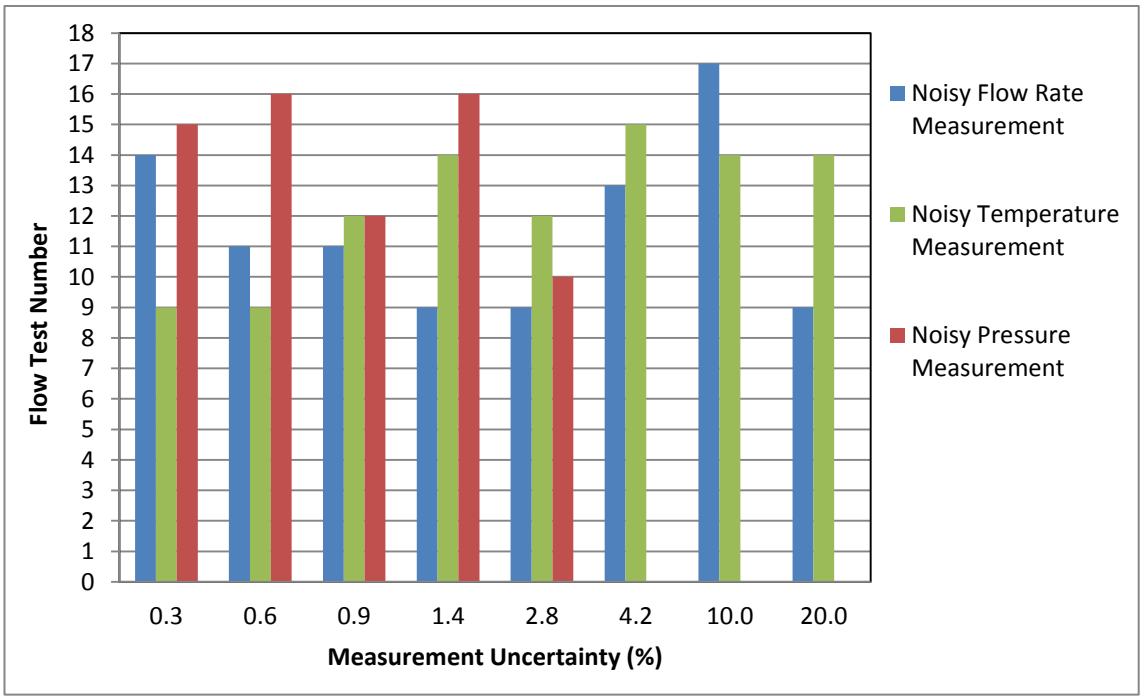

Figure 6-5 An increased number of flow tests are required as the single measurement uncertainty increases

Figure 6-6 to Figure 6-9 illustrate the soft-sensing algorithm's most accurate estimate of the zonal properties considering all the designed flow tests when there is uncertainty in one type of measurement. The linear trend lines indicate that the accuracy of the predicted zonal properties and zonal multi-phase flow rates decreases as the errors in the measurements increase. It also identifies that the accuracy of the pressure measurement uncertainty has the greatest effect on the estimated zonal properties.

The impact of measurement noise on the estimation of the zonal properties depends on the analytical equations used in the multi-phase flow model to predict the

measurements. This example uses the flow model in the active soft-sensing algorithm to account for the pressure changes in both the reservoir and ICV sections (Equations C-11 and C- 18); while the temperature equations simulate only some thermal changes within the well and the intelligent completions (Equations C- 28 and C- 28). The Equation C- 11 explicitly relates zonal reservoir pressures, productivity indices and water-cuts into noisy zonal annular pressures. This results in significant sensitivity of these parameters to zonal annulus pressure variations. It should be noted that the effect of pressure is carried over to the other parts, that is, the calculated deteriorated oil, water and gas inflow rates (using Equation C- 11) are then used to model the pressure and temperature changes along the wellbore and ICVs through equations C- 18, C- 28 and C- 28 (refer to Appendix C on more details about analytical equations used in the multi-phase flow model).

As a result, errors in measuring the temperature have the least effect on the estimated zonal property values and the accuracy of the estimated zonal properties while an increase in the pressure measurement uncertainty has a greater effect. Improved temperature sensors are required to detect the small changes of sandface temperature. Muradov and Davies (2011b) recommended the required test time, measurement accuracy and sensor resolution to perform a transient temperature analysis.

Well rate, being a summation of zonal inflow rates, implicitly appears in the equations used to predict the pressure and temperature measurements. Hence the measurement uncertainties greater only slightly influences the zonal property estimates in comparison to the trend observed for uncertainty in the pressure measurement.

The active soft-sensing algorithm thus provides a satisfactory estimate of the multi-phase zonal inflows when the measurements contain uncertainty. However, the calculation of the zonal gas inflow rate is the most error prone due to its high sensitivity to the accuracy of the downhole measurements. It should be noted that less weight was given to the outlier points when the results were analysed using linear trend lines in this study. For example, Figure 6-9 illustrates points (highlighted in the circle) with numerical problem where the Excel Solver is unable to find the optimum zonal gas inflow rate at low measurement uncertainties. It also shows that more accurate estimated zonal gas inflow rate is achieved at 20% flow rate measurement uncertainty compared to one obtained at 10 and 5% flow rate measurement uncertainty due to the better performance of optimisation algorithms in the active soft-sensing method.

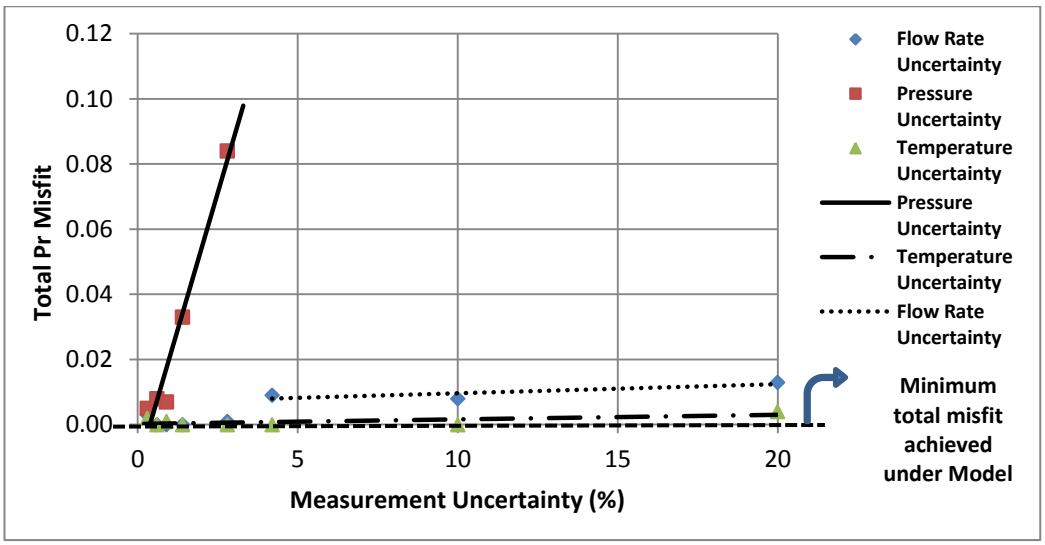

Figure 6-6 Estimation of the zonal reservoir pressures under model uncertainty and single measurement uncertainty

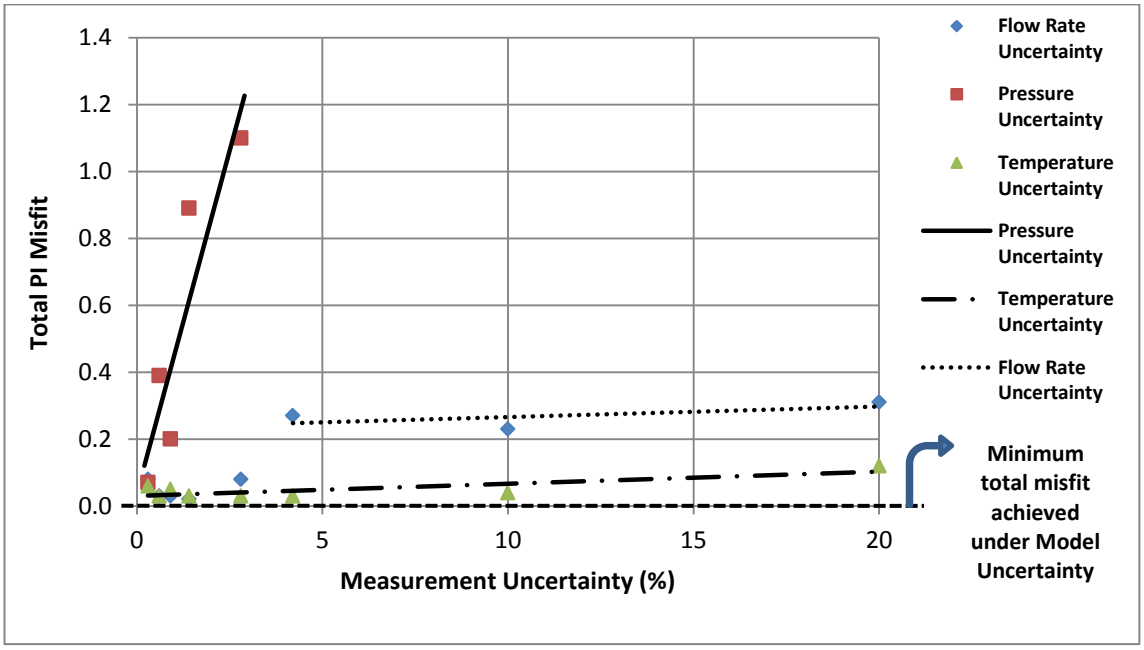

Figure 6-7 Estimation of the zonal productivity indices under model uncertainty and single measurement uncertainty

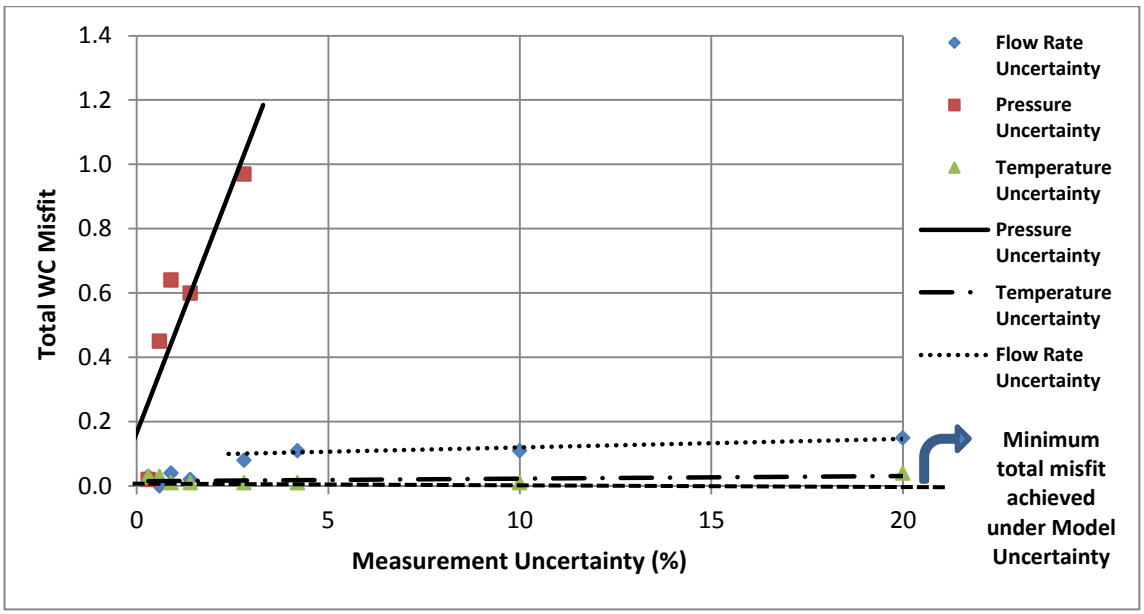

Figure 6-8 Estimation of the zonal water-cuts under model uncertainty and single measurement uncertainty

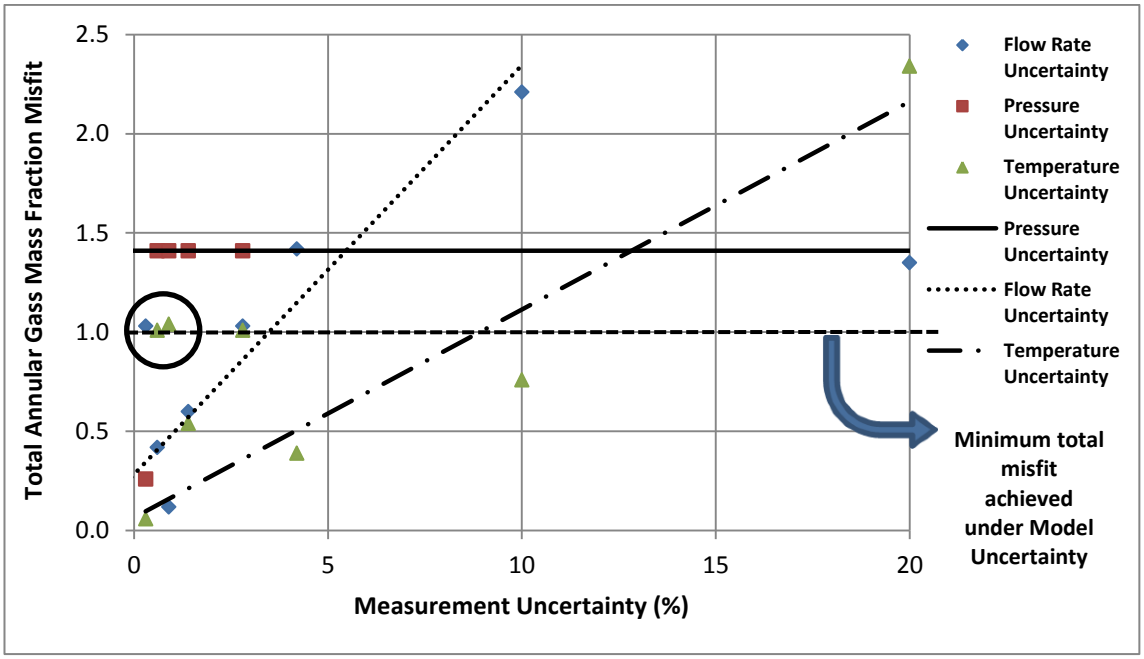

Figure 6-9 Estimation of the zonal annular gas mass fractions under model uncertainty and single measurement uncertainty

6.5.2 Random Errors - Multiple Measurement Uncertainty

This section assumes that multiple noisy measurements affect the implementation of the active soft-sensing algorithm. It was shown that the estimation of zonal properties is more sensitive to noise in the flow rate and pressure measurements than to the

temperature measurements. It was therefore decided to assume that only the measurement uncertainties in the pressure and flow rate readings will influence the active soft-sensing algorithm as it attempts to find the most accurate zonal properties. Scenarios have been defined in which the flow rate measurement uncertainty was varied while the pressure measurement uncertainty maintains a constant value (see Table 6-8). ±30 psi uncertainty is selected to generate moderately noisy pressure measurements. The flow rate measurement uncertainty is then changed to explore any cross correlation effects of the pressure and flow rate measurements.

Table 6-8 Multiple measurement uncertainty

Pressure Uncertainty: ±30 psi (~±0.9%)								
Measurement	**Flow Rate**							
Uncertainty	±0.3%	±0.6%	±0.9%	±1.4%	±2.8%	±4.2%	±10%	±20%

A similar approach to that described in the previous section was applied to generate Figure 6-10 to Figure 6-13 to compare the zonal properties estimate trend versus single and integrated pressure and flow rate measurements. Three linear trend lines have been added to indicate the trends in these single and multiple measurement uncertainty data. Outlier points have been indicated by the circles in these figures.

It can be seen that the estimation of the zonal properties is initially affected by noisy pressure rather than noisy flow rate data. As previously, increasingly noise pressure measurements rapidly increase the uncertainty values associated with the accuracy of the calculated zonal properties. The estimated zonal properties are much less affected by an increasing level of noise in the flow rate measurements. Figure 6-12 shows the zonal water-cuts estimates are less accurate under multiple measurement uncertainty than the single pressure measurement uncertainty (i.e. the predicted zonal properties will not be improved by using further flow tests). The Excel solver optimiser failed to find the optimum solution as its search space is limited to either upper or lower bounds of the interval defined for the water-cut constraint.

Once again, the estimated zonal annular gas mass fraction is very sensitive to the noisy measurements and do not show a consistent trend with increasing uncertainty (poor match obtained with straight lines, see Figure 6-13).

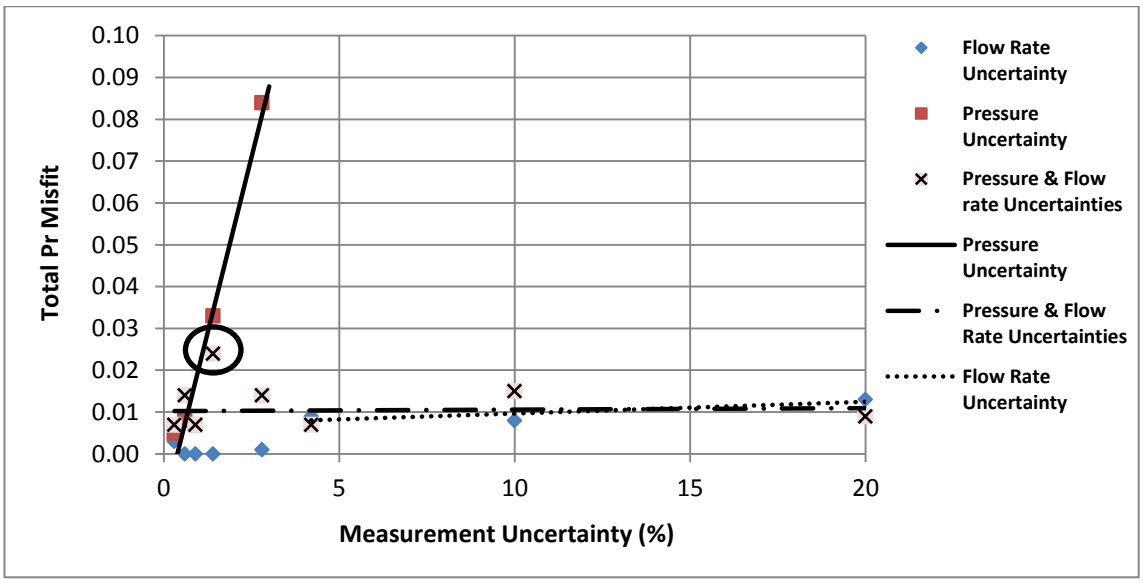

Figure 6-10 Estimated zonal reservoir pressures under single and integrated measurement uncertainties

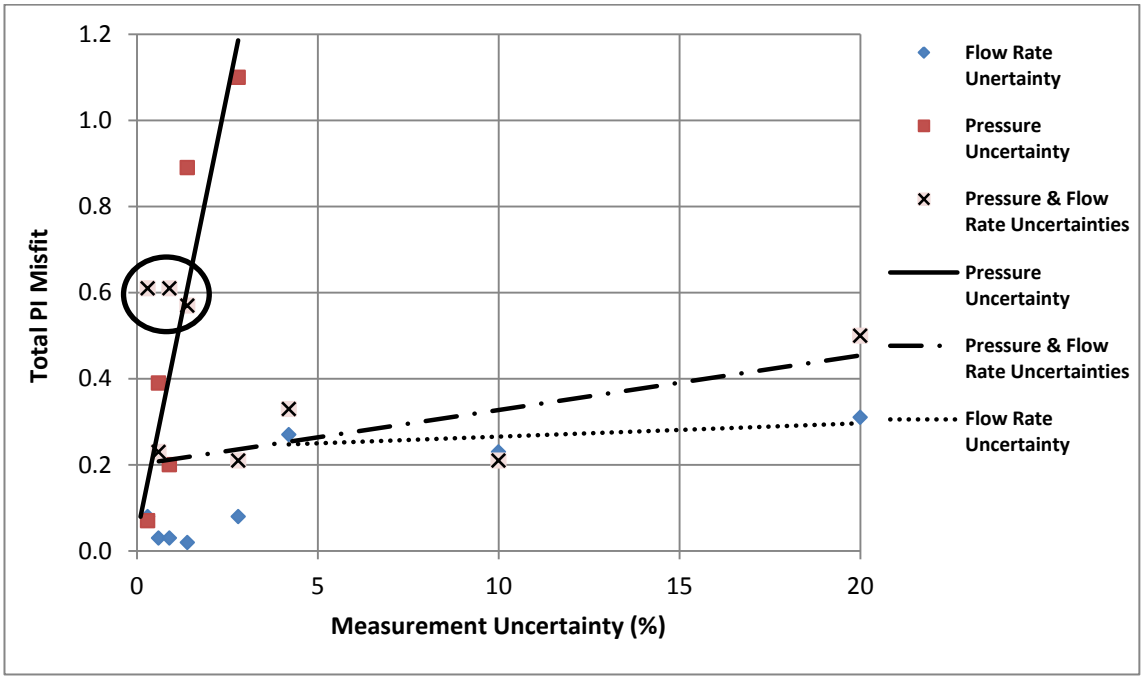

Figure 6-11 Estimated zonal productivity indices under single and integrated measurement uncertainties

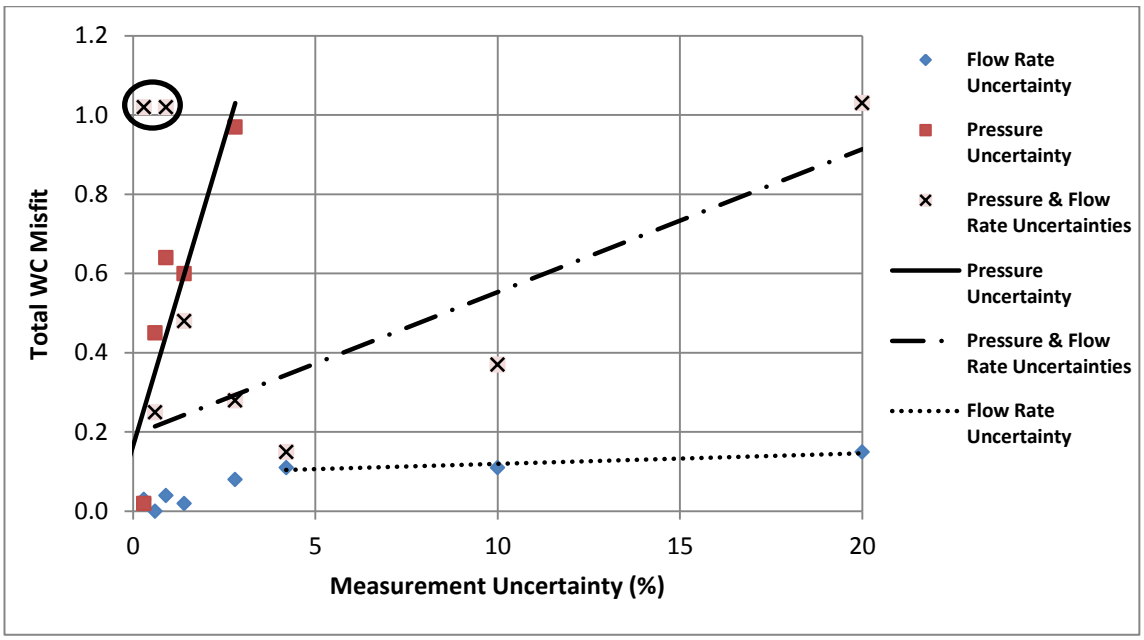

Figure 6-12 Estimated zonal water-cuts under single and integrated measurement uncertainties

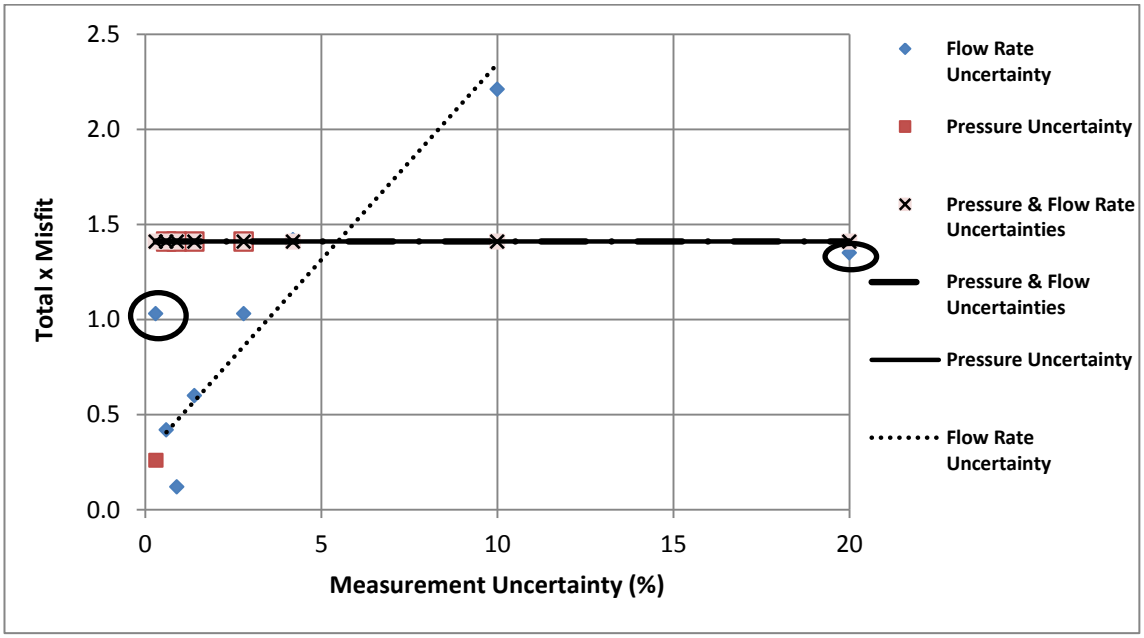

Figure 6-13 Estimated zonal annular gas mass fractions under single and integrated measurement uncertainties

6.5.3 Drift Errors in Gauge Pressure and Temperature Measurements

Pressure and temperature measurement instruments may have drift errors that affect the calculation of the zonal properties. Gauge drift is a deterministic error rather than being random. This study considered two cases: the first case considers a constant drift error

in zonal annular pressure measurements while the second case evaluates a constant measurement drift in zonal tubing temperatures.

The results (Figure 6-15 to Figure 6-16) show that an increase in the pressure drift error affects the accuracy of the estimated properties, though temperature drift errors do not significantly change the accuracy of the zonal properties. The estimation of zonal reservoir pressures is independent of pressure drift error. The accuracy of the other properties gradually decreases as the gauge error drift increases. The inconsistent trend of estimated zonal annular gas mass fractions is repeated when the drift errors are introduced in the measurements (e.g. the linear trend line was not plotted for estimated zonal annular gas mass fractions using drift errors in the temperature measurement). The total misfit of zonal annular gas mass fractions for a drift error between 0 and 15 psia is close to the value (1.04) obtained previously under model uncertainty. The high nonlinearity of the multi-phase flow model to the zonal annular gas mass fractions results in a higher total misfit being obtained under both model as well as measurement uncertainties.

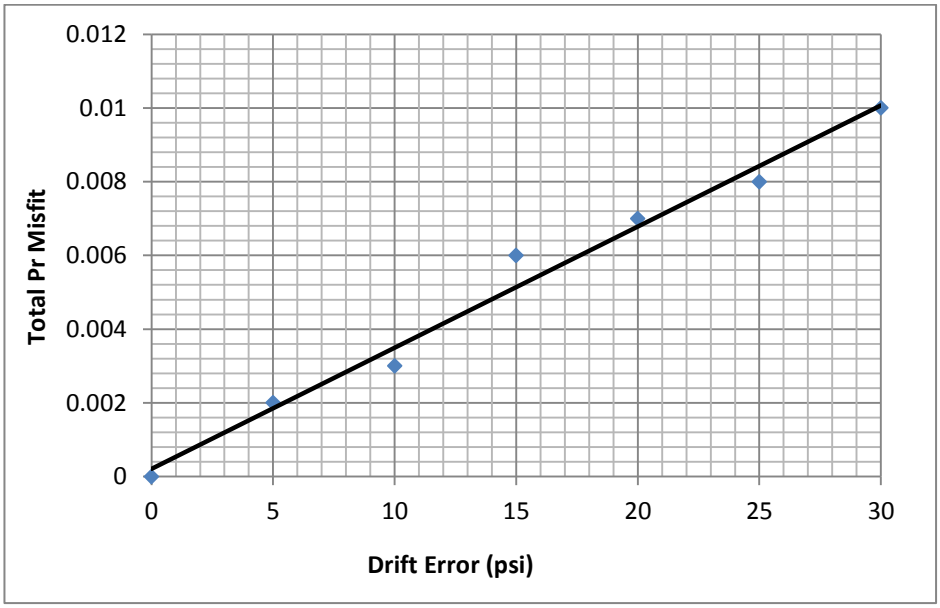

Figure 6-14 Effect of pressure gauge drift on the estimated zonal reservoir pressure

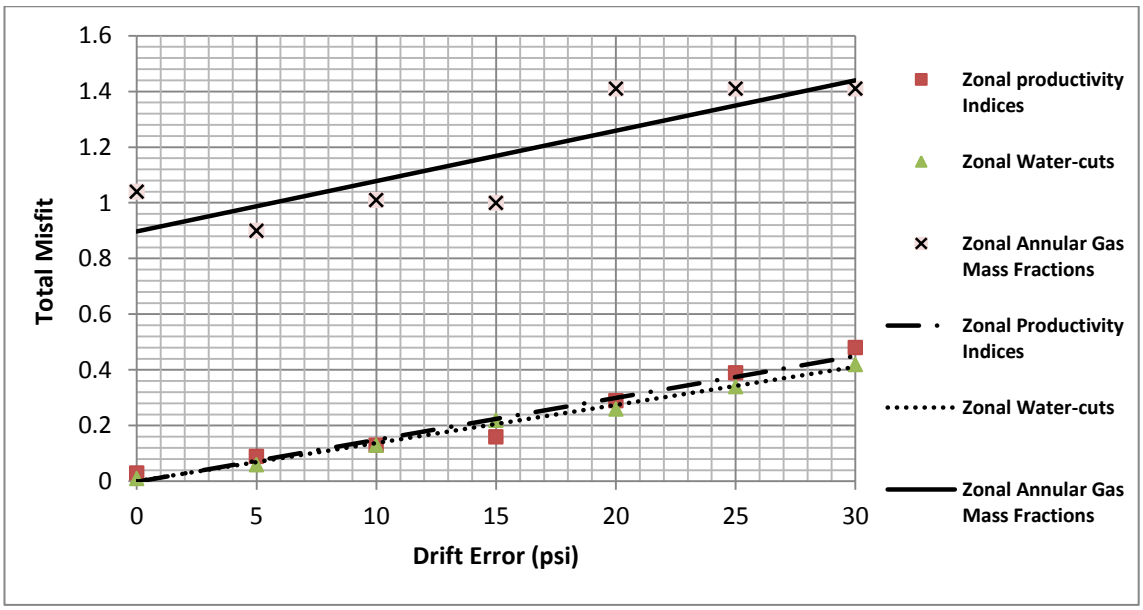

Figure 6-15 Effect of pressure gauge drift on the estimated zonal properties

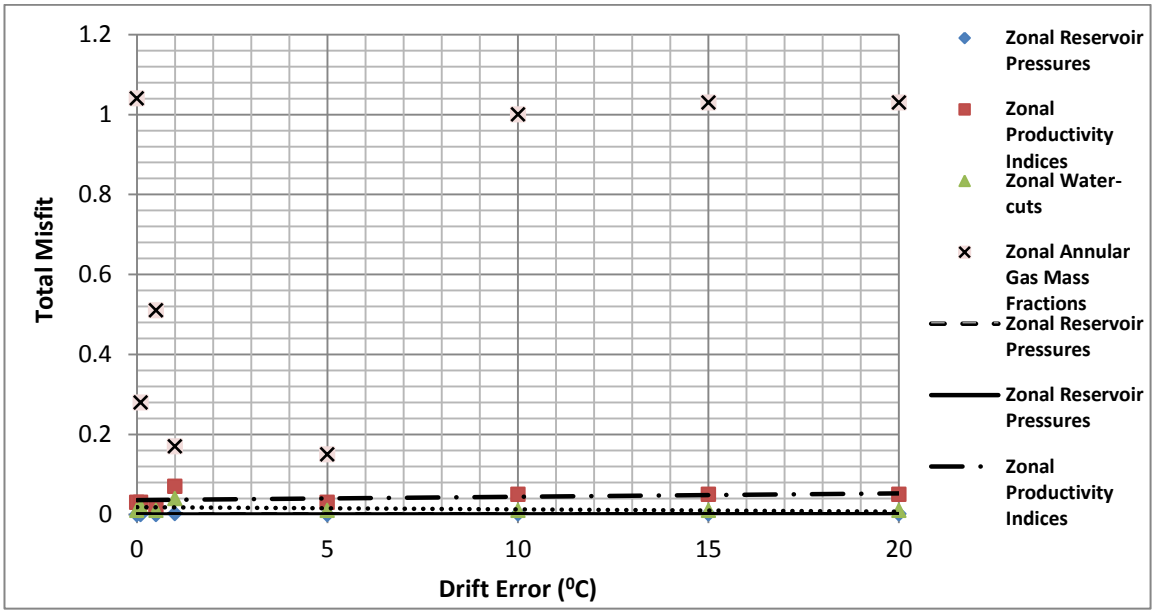

Figure 6-16 Effect of temperature gauge drift on the estimated zonal properties

6.6 Design of Wellbore Monitoring Systems

Downhole monitoring creates value through its ability to evaluate the reservoir potential, to optimise production and operations and to manage both cost and risk. Pressure and temperature sensors, together with multi-phase flow meters, are the tools required to monitor the zonal flow rates. Each measurement tool possesses its own metrological specifications in terms of accuracy, resolution, stability and etc. All these

measurement devices need to be sufficiently accurate to provide useful information for estimating the zonal multi-phase flow rate. An optimally designed well monitoring system should not only manages the budget spend; but should also has the potential to reduce the high cost of future well interventions. Well and reservoir surveillance data is required for managing both onshore and offshore wells. However, the incentive for downhole monitoring in deepwater and subsea well applications is higher because of the much greater intervention costs and risks (Forster and Dria, 2013).

6.6.1 Importance of Multi-phase Flow Meter Measurement Accuracy

Well rate measurements are used in the active soft-sensing algorithm. These measurements represent the total production of a well which can be measured by either surface or downhole multi-phase flow meters. Relative errors in the total liquid flow rate and gas flow rate measurements of less than ±5-10% and the water cut with an absolute error lower than ±2% are claimed (Falcone et al., 2001). However, these accuracy values do change with the different multi-phase flow regimes.

This study assumed the same measurement accuracy of the total oil and water flow rates during the implementation of active soft-sensing. However, the algorithm provides the option to define different measurement uncertainty for the separate phases. It should be noted that the algorithm assumes there is no free gas production from the reservoir. Figure 6-17 shows that the accuracy of the estimated zonal properties does not deteriorate when the measurement uncertainty of the multi-phase flow meter increases from 5% to 20% uncertainty. Unlike the noisy pressure measurements, the errors in the flow rate have less influence on the accuracy of zonal properties since the well rates are implicitly related to the zonal properties in the multi-phase flow model. Any reduction in the results from the errors associated with noise to the multi-phase flow meter require a flow rate measurement uncertainty of less than 5% in this particular example.

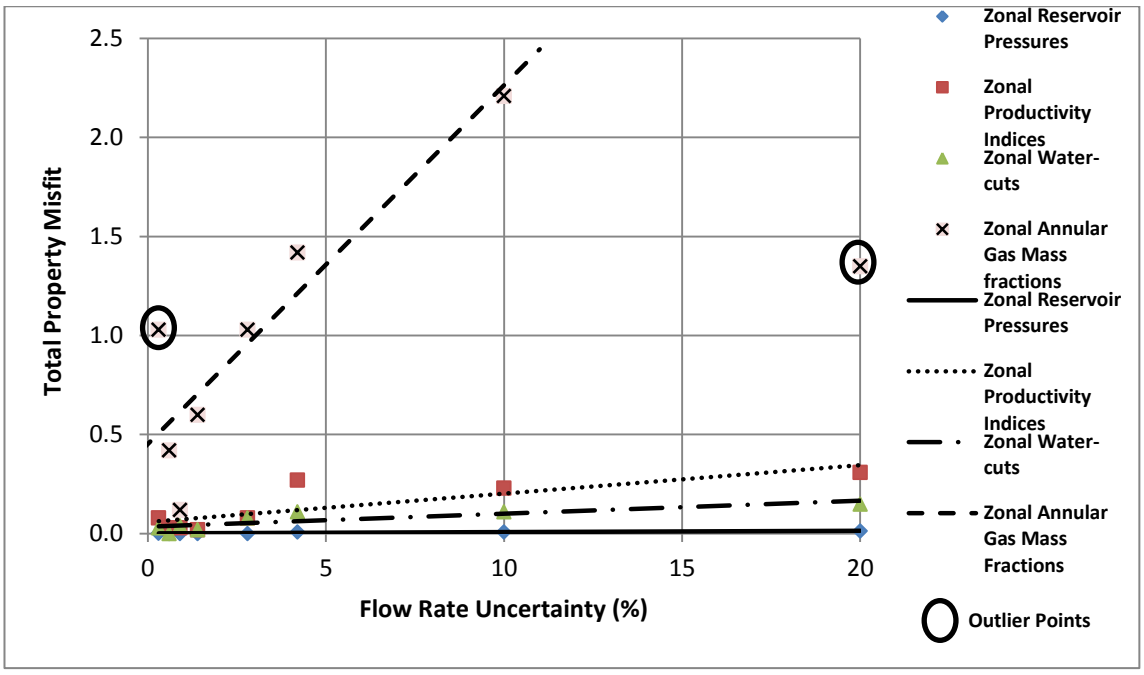

Figure 6-17 Effect of noisy multi-phase flow rate measurements on the estimated zonal properties

6.6.2 Importance of Pressure Measurement Accuracy

Both drift and random errors in pressure measurements result in a reduced of accuracy of the estimated zonal properties while it showed a considerable improvement in the downhole flow estimate if the measurement uncertainty due to random noise and drift errors are reduced to less than 1% and 5 psi respectively (Figure 6-15 and Figure 6-18). Zonal reservoir pressures are estimated more accurately under pressure measurement uncertainties while the other properties, especially zonal annular gas mass fractions, are poorly estimated at high measurement uncertainties. A similar trend is observed for the estimation of zonal properties under flow rate measurement uncertainties.

Figure 6-19 indicates that the accuracy of pressure measurements is the most important factor to improve the estimate of downhole flow rates even at low flow rate measurement uncertainties (below 5%).

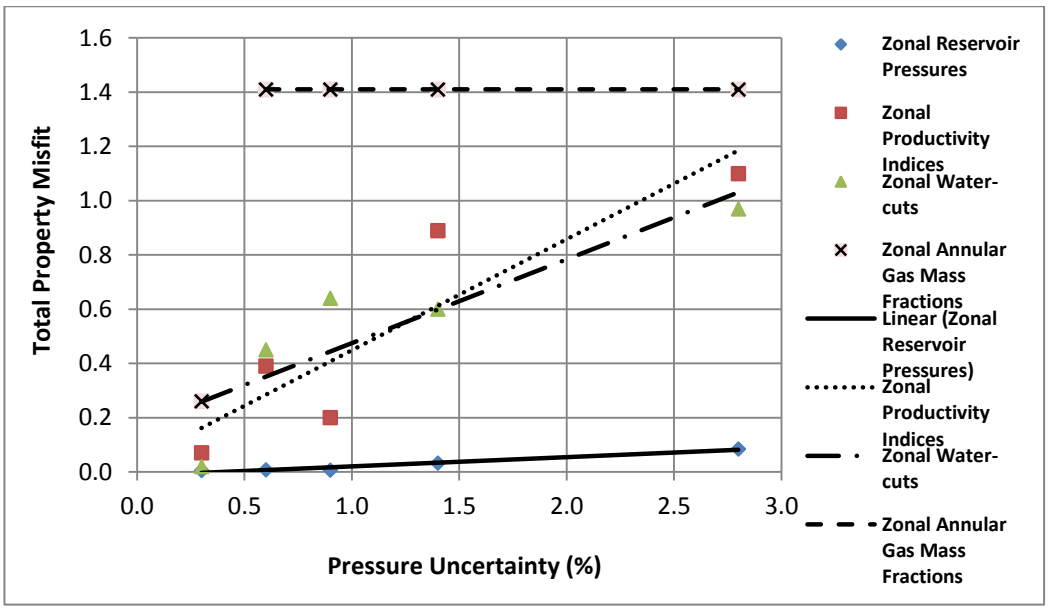

Figure 6-18 Estimation of the zonal properties under noisy pressure sensors

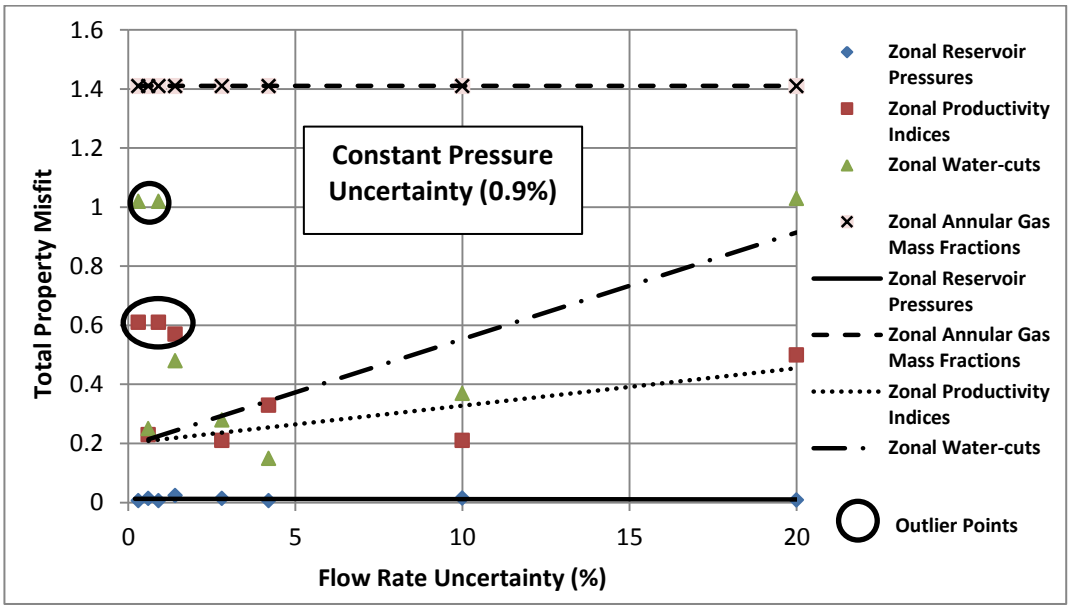

Figure 6-19 Estimated zonal properties from noisy multi-phase flow meter data at a constant level of pressure sensor uncertainty

6.6.3 Importance of Temperature Measurement Accuracy

Figure 6-20 illustrates that total misfit of zonal properties (reservoir pressures, productivity indices and water-cuts) achieved at different temperature uncertainty values (random noises) is less than that obtained in the case of noisy pressure and flow rate measurements. However, Figure 6-20 confirms that the accuracy of the predicted zonal properties may reduce if the temperature uncertainty is increased to a value greater than 10%; while Figure 6-16 shows that drift errors in the measured temperature have no influence on the accuracy of the estimated parameters. Similarly, zonal

reservoir pressures and annular gas mass fractions are the most and least accurate estimated parameters under temperature uncertainty.

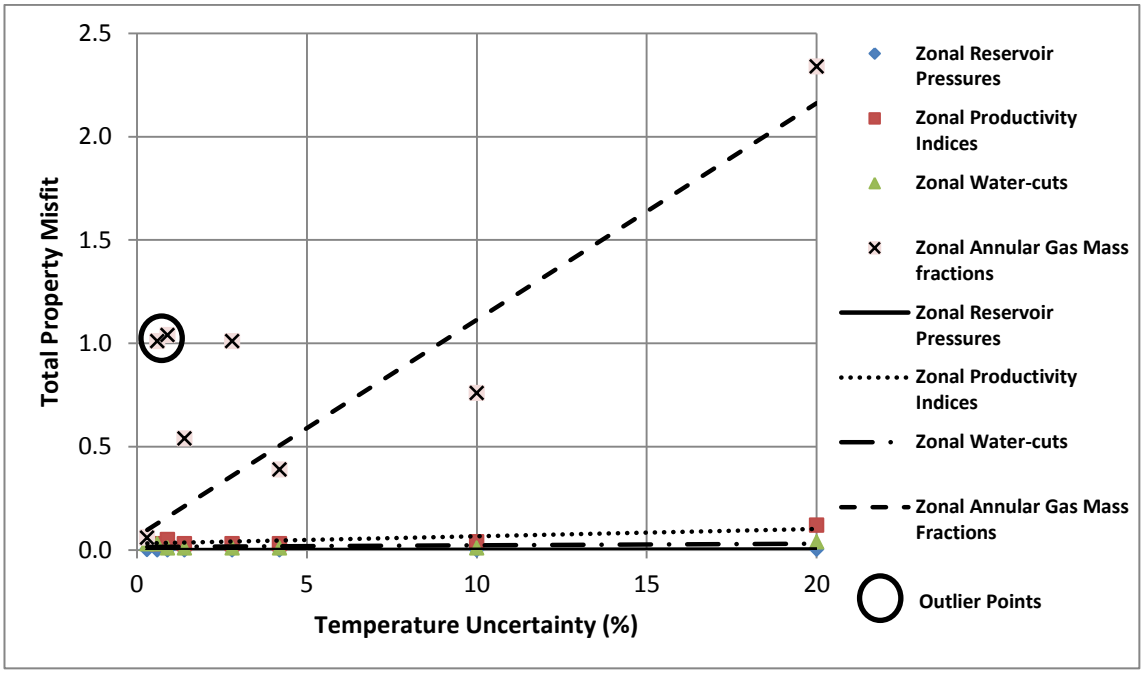

Figure 6-20 Estimated zonal properties using noisy temperature sensors

6.7 Summary

- The performance of proposed active MPFR soft-sensing was tested under model and measurement uncertainty. The accuracy of the estimated zonal properties deteriorates due to the presence of noisy sensors within the wellbore monitoring system. This also implies the number of flow tests required by the soft-sensing algorithm to estimate the reservoir properties in a noisy environment at a given probability level will increase as the severity of the measurement drift or random noise level in the data increases.
- An analysis of analytical reservoir/wellbore pressure and wellbore temperature models used in our algorithm concluded that errors in the temperature measurements have the least effect on the estimated zonal property values, when compared with errors in the measured well rates and pressures.
- Zonal reservoir pressure is the least sensitive parameter to noisy measurements (relatively) while zonal annular gas mass fractions are the most sensitive ones to measurements with errors.

- The active MPFR allocation workflow for active, MPFR allocation may also be used to design the wellbore monitoring system's measurement and downhole sensor metrology parameters to provide the best possible estimate of the downhole flow rates.
- Installation of accurate, stable pressure sensors has the greatest impact on the overall accuracy of the well monitoring system. An equivalent improvement in the accuracy of the multi-phase flow meters and temperature sensors provides a smaller benefit.

Chapter 7 Conclusions & Future Work

7.1 Conclusions

This thesis presents novel algorithms for reservoir monitoring and flow rate allocation of I-wells. The main results are summarised as:

1. An active multi-phase flow rate soft-sensing algorithm has been developed for production/injection allocation in commingled production systems including multi-zone I-wells.
2. This integrated control and monitoring workflow can design a series of optimum multi-rate flow tests to (1) maximise oil production or (2) maximise the reliability of the estimated multi-phase flow rates
3. The hypothesis test workflow was applied to compare the performance of two experiments corresponding to different optimisation objective functions
4. Guidelines to design the optimum well monitoring system in advanced wells have been provided.

The above achievements are summarised separately in detail in the following sections:

7.1.1 Active Multi-phase Flow Rate Soft-sensing Algorithm (Chapter 3)

Optimisation techniques and multi-phase flow model together with integrated measurements were combined to develop the active multi-phase flow rate soft-sensing in multi-zone I-wells:

1. The active soft-sensing technique consists of two sequential optimisation steps. First optimisation step calculates required zonal properties (reservoir pressure, productivity index, water-cut and annular gas mass fraction) to estimate multi-phase flow rates by minimising the mismatch between the measurements and predicted ones. The second optimisation step designs further multi-rate flow tests by regulating the ICVs.
2. GRG method is used to solve the constraint multi-variable optimisation problem in order to estimate the zonal properties. While DC simplex is selected as a direct search method to optimise the number of flow tests since it's difficult or sometimes impossible to relate ICVs position mathematically to the objective functions.

3. The multi-phase flow model used is a system of analytical equations to predict the well rates and pressure/temperature distribution in the wellbore and intelligent well completions. These equations account for pressure drop in the reservoir, across the ICV and temperature changes across the ICV and after commingle point of annular and tubing fluids.
4. Five versions, or levels, of the active soft-sensing algorithm are available depending on the complexity and of the measured downhole data. These levels provide different sets of measurements that are used to define the objective function of optimisation step one. They are also used in the optimisation step two if the objective function is the reliability of the estimated zonal properties.

7.1.2 Active Multi-phase Flow Rate Soft-sensing Algorithm Validation (Chapter 4)

Comparison of the results attained by active soft-sensing with those from dynamic well flow has demonstrated:

1. The algorithm efficiently provided estimates of the zonal properties and multi-phase flow rates regardless of the well deviation completed in either oil or gas field if the appropriate multi-phase flow equations are available to interpret the pressure, temperature and well rates measurements.
2. The algorithm has the potential to detect and quantify any cross-flow between zones in I-wells and evaluate the differential drift of downhole gauges.
3. The algorithm offers flexible selection of ICVs and wellhead choke to design multi-rate flow test. It was applied successfully for a case with a non-operational ICV installed in an I-well.
4. The algorithm's robustness was tested in noisy data environment. The confidence interval was applied to yield the interval estimations of zonal properties with a high confidence.

Additionally, performing the active soft-sensing algorithm in a real two-zone I-well showed that:

1. Production and well tests (build-up or drawdown) history data help defining appropriate initial points for constraining search variables used in the optimisation workflow.

2. The simplified analytical equations incorporated into the multi-phase flow model affect the estimation of properties and the decision to use the levels of active soft-sensing.
3. An improved estimate of zonal properties is achieved by adding more flow tests. However it also requires additional understanding of the reservoir rock and fluid properties.
4. The workflow described here offers a number of possible levels to apply the monitoring algorithm based on different types of measurements with acceptable resolution.
5. Use of active soft-sensing to predict the preferred ICV positions must be carried out reasonably quickly after the previous test since it is assumed that zonal properties are constant throughout the complete series of multi-rate flow tests.

7.1.3 Integrated Control and Monitoring in Multi-zone I-wells (Chapter 5)

The integrated, control and monitoring workflow was suggested for maximising I-well oil production via real-time zonal production control based on estimates of zonal reservoir properties and their updates. The following steps were carried out to implement the workflow:

1. The presented workflow employed an active soft-sensing algorithm which was initially developed and validated in Chapter 3 and Chapter 4 to design multi-rate, multi-zone flow tests in real time in order to maximise the test results' reliability.
2. The algorithm took a passive, soft-sensing approach where the zonal properties and/or flow rates are calculated indirectly from pressure, temperature and well rate measurements.
3. The algorithm then adds an optimisation level to identify the next flow-rate test design to maximise the reliability of the resulting zonal property and flow rate estimates.
4. A further advantage is that the initial (n+1) flow tests may be designed using reactive control to encourage production from the better zones, speed up the well start-up process, etc. while at the same time steering the choice of ICV positions to increase the downhole information's reliability. This approach identifies the "better producing zones" earlier.

The comparison between simultaneous and separate control/monitoring workflows indicated that higher accurate flow rates are obtained at a higher cost using separate control and monitoring approach while lower flow tests (reduced cost) is required to achieve maximum oil production through the simultaneous control and monitoring workflow.

The performance of integrated control and monitoring was discussed when different optimisation objective functions were considered. It was shown that:

- The ICM workflow for optimising the oil production is fast and identifies the best possible ICV positions. This implies that the ICM workflow has a small search space, leading to a less accurate estimation of the zonal properties. However, it demonstrates that very accurate zonal properties are not required to optimise the oil production.
- The ICM workflow used to maximise the reliability of the zonal property estimates is slower, uses a larger search space to design the multi-rate test, but results in a more accurate estimate of zonal properties from uncertain measurements.

The hypothesis test workflow was introduced for comparing the level of similarity of the results of one or two sets of experiments. It was applied to a synthetic case study where it was concluded that the ICM workflow based on the maximising the reliability of the estimated zonal properties provided a more accurate evaluation of zonal properties at the expense of requiring a greater number of flow tests.

7.1.4 Extension of Active Soft-sensing in Well Monitoring System Design (Chapter 6)

The proposed active multi-phase flow rate soft-sensing workflow can also be used to design a wellbore monitoring system capable of estimating better downhole flow information in terms of the required measurements and the downhole sensor metrology parameters. The algorithm was tested under single and integrated measurement uncertainties to derive guidelines on well monitoring system design:

1. The accuracy of the estimated zonal properties deteriorated due to the presence of drift and random errors in the wellbore monitoring system.

2. More measurements were required for the active soft-sensing algorithm can estimate the reservoir properties in a noisy environment.
3. Errors in the temperature measurements were shown to have the least effect on zonal property estimates compared to errors in the measured well rates and pressures.
4. Zonal reservoir pressures were the least sensitive parameters to noisy measurements (relatively), while zonal annular gas mass fractions were the most sensitive ones to measurements with errors.
5. This work suggested installation of accurate stable pressure sensors will have a greater impact on the overall accuracy of the well monitoring system compared to equivalent improvements in the accuracy of the multi-phase flow meters and temperature sensor for the models selected.

7.2 Recommendations for Future Study

1) The active soft-sensing algorithm provides better, and faster, estimates of the zonal flow rates by assuming that zonal properties are constant during multi-rate tests. The algorithm should be modified to account for changes of zonal properties during monitoring.

2) The effect of multi-phase flow regimes in the wellbore is not considered in this work. This is particularly important when active soft-sensing designs the optimum well start-up procedure in wells with slug flow regime problems.

3) A further study can be performed to compare the influence of using active soft-sensing levels on the accuracy of estimated zonal flow rates. This will investigate whether the addition of measurements would improve the accuracy of flow rates.

4) Only one example was used to test whether the accuracy of estimated flow rates varies when different optimisation objective functions are used. Further examples are required to generalise the conclusions on which optimisation strategy results in the more accurate zonal properties estimation.

5) Further works is required to investigate possible integration of active soft-sensing algorithm with the pressure and temperature transient analysis (PTTA) framework. For example, temperature transient analysis in the reservoir can be added to the current active soft-sensing algorithm to provide a more robust wellbore monitoring system.

Bibliography

Aakre, H., Halvorsen, B., Werswick, B. and Mathiesen, V. 2013. Smart Well With Autonomous Inflow Control Valve Technology. SPE-164348-MS, SPE Middle East Oil and Gas Show and Conference, Manama, Bahrain, Society of Petroleum Engineers.

Aakre, H., Halvorsen, B., Werswick, B. and Mathiesen, V. 2014. Autonomous Inflow Control Valve for Heavy and Extra-Heavy Oil. SPE 171141, SPE Heavy and Extra Heavy Oil Conference, Latin America, Colombia, Society of Petroleum Engineers.

Abadie, J. 1972. Application of the GRG Algorithm to Optimal Control Problems. Nonlinear and Integer Programming 191-211.

Abadie, J. and Carpentier, J. 1969. Generalisation of the Wolfe Reduced Gradient Method to the Case of the Nonlinear Constraints. Optimisation 37-47.

Agarwal, R. G. 1980. A New Method To Account For Producing Time Effects When Drawdown Type Curves Are Used To Analyze Pressure Buildup And Other Test Data. Society of Petroleum Engineers.

Aggrey, G. H., Davies, D. R. and Skarsholt, L. T. 2007. A Novel Approach of Detecting Water Influx Time in Multi-Zone and Multilateral Completions using Real-Time Downhole Pressure Data. SPE 105374, SPE Middle East Oil and Gas Show and Conference, Bahrain, Society of Petroleum Engineers.

Ahmed, A. and Lee, W. J. 1995. Development of a New Theoretical Model for Three-Layered Reservoirs With Unequal. Initial Pressures. SPE 29463, SPE Production Operations Symposium, Oklahoma City, Oklahoma, Society of Petroleum Engineers.

Ajayi, A., Fasasi, T. and Okuns, G. 2012. Real Time Flow Estimation Using Virtual Flow Measurement Techniques: A Field Application in Intelligent Well Completion. SPE 162948, Nigeria Annual International Conference and Exhibition, Lagos, Nigeria, Society of Petroleum Engineers.

Al-Kasim, F. T., Synøve, T., Jakobsen, K. A., Tang, Y. and Jalali, Y. 2002. Remotely Controlled In-Situ Gas Lift on the Norne Subsea Field. SPE 77660, SPE Annual Technical Conference and Exhibition, San Antonio, Texas, Society of Petroleum Engineers.

Al-Khelaiwi, F. 2013. A Comprehensive Approach to the Design of Advanced Well Completions. PhD, Heriot-Watt University.

Al-Khelaiwi, F. T., Birchenko, V. M., Konopczynski, M. R. and Davies, D. 2010. Advanced Wells: A Comprehensive Approach to the Selection Between Passive and Active Inflow-Control Completions. SPE Production & Operations **25**(03): 305-326.

Al-Khelaiwi, F. T. and Davies, D. R. 2007. Inflow Control Devices: Application and Value Quantification of a Developing Technology. SPE 108700, International Oil Conference and Exhibition in Mexico, Veracruz, Mexico, Society of Petroleum Engineers.

Al-Mutairi, F. H. and Davies, D. R. 2008. Detection of Scale Deposition Using Distributed Temperature Sensing. SPE 113595, SPE International Oilfield Scale Conference, Aberdeen, UK, Society of Petroleum Engineers.

Algeroy, J., Lovell, J., Tirado, G., Meyyappan, R., Brown, G., Greenaway, R., Carney, M., Meyer, J. H., Davies, J. E. and Pinzon, I. D. 2010. Permanent Monitoring: Taking It to the reservoir. Oilfield Review **22**(1): 34-41.

Aly, A. 1994. A New Technique for Analysis of Wellbore Pressure From Multi-Layered Reservoirs With Unequal Initial Pressures To Determine Individual Layer Properties. SPE 29176, SPE Eastern Regional Meeting, Charleston, West Virginia, Society of Petroleum Engineers.

Aly, A. and Lee, W. J. 1996. Characterizing Multi-Layered Reservoirs Using A New, Simple, Inexpensive and Environmentally Sensitive Pre-Production Well Test. SPE 36624, SPE Annual Technical Conference and Exhibition, Denver, Colorado, Society of Petroleum Engineers.

Arenas, E. and Dolle, N. 2003. Smart Waterflooding Tight Fractured Reservoirs Using Inflow Control Valves. SPE 84193, SPE Annual Technical Conference and Exhibition, Denver, Colorado, Society of Petroleum Engineers.

Beggs, D. H. and Brill, J. P. 1973. A Study of Two-Phase Flow in Inclined Pipes. Journal of Petroleum Technology **25**(05): 607-617.

Bellarby, J. E., Denholm, A., Grose, T., Norris, M. and Stewart, A. 2003. Design and Implementation of a High Rate Acid Stimulation through a Subsea Intelligent Completion. SPE 83950, Offshore Europe, Aberdeen, United Kingdom, Society of Petroleum Engineers.

Bendiksen, K. H., Maines, D., Moe, R. and Nuland, S. 1991. The Dynamic Two-Fluid Model OLGA: Theory and Application. SPE Production Engineering **6**(02): 171-180.

Betancourt, S., Dahlberg, K., Hovde, Ø. and Jalali, Y. 2002. Natural Gas-Lift: Theory and Practice. SPE 74391, SPE International Petroleum Conference and Exhibition, Villahermosa, Mexico, Society of Petroleum Engineers.

Bieker, H. P., Slupphaug, O. and Johansen, T. A. 2007. Real-Time Production Optimization of Oil and Gas Production Systems: A Technology Survey. SPE Production & Operations Journal **22**(04): 382-391.

Bloemen, H., Belfroid, S., Sturm, W. and Verhelst, F. 2006. Soft Sensing for Gas-Lift Wells. SPE Journal **11**(4): 454-463.

Bohannon, J. M. 1970. A Linear Programming Model for Optimum Development of Multi-Reservoir Pipeline Systems. Journal of Petroleum Technology **22**(11): 1429-1436.

Botto, G., Maggioni, B. and Schenato, A. 1994. Electronic, Fiber-Optic Technology: Future Options for Permanent Reservoir Monitoring. SPE 28484, SPE Annual Technical Conference and Exhibition, New Orleans, Louisiana, Society of Petroleum Engineers.

Box, M. J. 1965. A New Method of Constrained Optimization and a Comparison With Other Methods. The Computer Journal **8**(1): 42-52.

Brown, D. L., Wattenbarger, R. A. and Startzman, R. A. 1988. Linear Programming Optimization on Microcomputers. SPE 17777, Petroleum Computer Conference San Jose, California, Society of Petroleum Engineers.

Brown, G. A., Kennedy, B. and Meling, T. 2000. Using Fibre-Optic Distributed Temperature Measurements to Provide Real-Time Reservoir Surveillance Data on Wytch Farm Field Horizontal Extended-Reach Wells. SPE 62952, SPE Annual Technical Conference and Exhibition, Dallas, Texas, Society of Petroleum Engineers.

Brown, G. A., Sanchez, A., Carvalho, V. L. S., Wray, A. S. and Gutierrez Murillo, G. 2005. Slickline With Fiber-Optic Distributed Temperature Monitoring for Water-Injection and Gas Lift Systems Optimization in Mexico. SPE 94989, SPE Latin American and Caribbean Petroleum Engineering Conference, Rio de Janeiro, Brazil, Society of Petroleum Engineers.

Brown, K. E. and Lea, J. F. 1985. Nodal Systems Analysis of Oil and Gas Wells. Journal of Petroleum Technology **37**(10): 1751-1763.

Cannon, R. T. and Aminzadeh, F. 2013. Distributed Acoustic Sensing: State of the Art. SPE 163688, SPE Digital Energy Conference, The Woodlands, Texas, USA, Society of Petroleum Engineers.

Carnahan, Clanton, R. W., Koehler, K. D., Harkins, G. O. and Williams, G. R. 1999. Fiber Optic Temperature Monitoring Technology. SPE 54599, SPE Western Regional Meeting, Anchorage, Alaska, Society of Petroleum Engineers.

Chupin, G., Hu, B., Haugset, T., Sagen, J. and Claudel, M. 2007. Integrated Wellbore/Reservoir Model Predicts Flow Transients in Liquid-Loaded Gas Wells. SPE 110461, SPE Annual Technical Conference and Exhibition, Anaheim, California, USA, Society of Petroleum Engineers.

Clarke, A. A., Ayton, J., Lawton, D., Lean, J. C. and Burke, K. 2006. Case Study: Lennox - The Race to Produce Oil Prior to Gas Cap Blowdown. SPE 100126, SPE Europec/EAGE Annual Conference and Exhibition, Vienna, Austria, Society of Petroleum Engineers.

Conn, A. R., Scheinberg, K. and Vicente, L. N. 2009. Introduction to Derivative-Free Optimization, Society for Industrial and Applied Mathematics.

Cramer, R., Jakeman, S. V. J. and Berendschot, L. 2006. Well Test Optimization and Automation. SPE 99971, Intelligent Energy Conference and Exhibition, Amsterdam, The Netherlands, Society of Petroleum Engineers.

Crandall, K. C. and Seabloom, R. W. 1970. Engineering fundamentals in measurements, probability, statistics and dimensions, McGraw-Hill,

Da Silva, M. F., Muradov, K. M. and Davies, D. R. 2012. Review, Analysis and Comparison of Intelligent Well Monitoring Systems. Society of Petroleum Engineers.

Davidson, J. E. and Beckner, B. L. 2003. Integrated Optimization for Rate Allocation in Reservoir Simulation. SPE Reservoir Evaluation & Engineering Journal **6**(6): 426-432.

Drakeley, B. K., Johansen, E. S., Zisk, E. and Bostick, T., Iii. 2006. In-well Optical Sensing - State Of The Art Applications And Future Direction For Increasing Value in Production Optimization Systems. SPE 99696, Intelligent Energy Conference and Exhibition, Amsterdam, The Netherlands, Society of Petroleum Engineers.

Duns, H., Jr. and Ros, N. C. J. 1963. Vertical flow of gas and liquid mixtures in wells. WPC 10132, 6th World Petroleum Congress, Frankfurt am Main, Germany, World Petroleum Congress.

Earles, D. M., Stoesz, C. W., Amaral, A. D. S., Pearce, J. G., Dejongh, H. and Rambow, F. H. K. 2010. Real-Time Strain Monitoring of Sand-Control Completions. SPE 134555, SPE Annual Technical Conference and Exhibition, Florence, Italy, Society of Petroleum Engineers.

Ebadi, F. 2006. Screening of Reservoir Types for Decision-making on the application of Intelligent Wells. PhD, Heriot-Watt University.

Ebadi, F., Davies, D. R., Reynolds, M. A. and Corbett, P. W. M. 2005. Screening Of Reservoir Types For Optimisation Of Intelligent Well Design. SPE 94053, SPE Europec/EAGE Annual Conference, Madrid, Spain, Society of Petroleum Engineers.

Eck, J., Ewherido, U., Mohammed, J., Ogunlowo, R., Ford, J., Fry, L., Hiron, S., Osugo, L., Simonian, S. and Oyewole, T. 2000. Downhole Monitoring: The Story So Far. OilFeild Review **11**(4): 20-33.

Ehlig-Economides, C. A. and Joseph, J. 1987. A New Test for Determination of Individual Layer Properties in a Multilayered Reservoir. SPE Formation Evaluation **2**(03): 261-283.

Eisler, B. and Lanan, G. A. 2012. Fiber Optic Leak Detection Systems for Subsea Pipelines. OTC 23070, Offshore Technology Conference, Houston, Texas, USA, Offshore Technology Conference.

El-Sayed, M., Al Mutairi, A. M., Hassane, M. a. S., Kutty, S. M., Karrani, S. M. and Kurian, A. 2014. Three - Zone Commingled and Controlled Production Using Intelligent Well Completion. SPE 172166, Abu Dhabi International Petroleum Exhibition and Conference, Abu Dhabi, UAE, Society of Petroleum Engineers.

Ellis, T., Erkal, A., Goh, G., Jokela, T., Kvernstuen, S., Leung, E., Moen, T., Porturas, F., Skillingstad, T., Vorkinn, P. B. and Raffn, A. G. 2010. Inflow Control Devices-Raising Profiles. Oilfield Review **21**(4): 30-37.

Eltaher, E. K., Muradov, K., Davies, D. R. and Grebenkin, I. M. 2014. Autonomous Inflow Control Valves - their Modelling and Added Value. SPE 170780, SPE Annual Technical Conference and Exhibition, Amsterdam, The Netherlands, Society of Petroleum Engineers.

Ennaifer, A., Giordano, P., Vannuffelen, S., Nilssen, B. A., Nweagbogu, I., Sooklal, A. and Walden, C. 2014. Step Changes in Well Testing Operations. Oilfield Review **26**(3): 32-41.

Falcone, G., Hewitt, G. F., Alimonti, C. and Harrison, B. 2001. Multiphase Flow Metering: Current Trends and Future Developments. SPE 71474, SPE Annual Technical Conference and Exhibition, New Orleans, Louisiana, Society of Petroleum Engineers.

Fancher, G. H., Jr. and Brown, K. E. 1963. Prediction of Pressure Gradients for Multiphase Flow in Tubing. Society of Petroleum Engineers Journal **3**(01): 59-69.

Farshbaf Zinati, F., Jansen, M. D. and Luthi, S. M. 2010. Estimating Near-Wellbore Permeability by Distributed Pressure Sensing Using an Adjoint-Based Minimization Algorithm. SPE 135223, SPE Annual Technical Conference and Exhibition, Florence, Italy, Society of Petroleum Engineers.

Foo, D. B., Krislock, J., Meador, T. J. and Cheng, T. 2014. Horizontal Well Injection Profiling Using Distributed Temperature Sensing. SPE 171586, SPE/CSUR Unconventional Resources Conference, Calgary, Alberta, Canada, Society of Petroleum Engineers.

Forster, L. and Dria, D. E. 2013. Real-Time Subsea Fiber-Optic Monitoring. OTC 23930, Offshore Technology Conference, Texas, USA, Offshore Technology Conference.

Fripp, M., Zhao, L. and Least, B. 2013. The Theory of a Fluidic Diode Autonomous Inflow Control Device. SPE 167415, SPE Middle East Intelligent Energy Conference and Exhibition, Manama, Bahrain, Society of Petroleum Engineers.

Glandt, C. A. 2005. Reservoir Management Employing Smart Wells: A Review. SPE Drilling & Completion **20**(04): 281-288.

Glasbergen, G., Gualtieri, D., Domelen, M. S. V. and Sierra, J. 2009. Real-Time Fluid Distribution Determination in Matrix Treatments Using DTS. SPE Production & Operations **24**(1): 135-146.

Gonzalez, Y. J., Friese, A. M., Brown, G., Padilla, A., Sanchez, A. and Ward, L. A. 2012. Slickline DTS Measurements Provide Useful Information for Well Integrity Diagnostic, Stimulation Treatments, and Water Injector Wells Performance: North America Land Case Studies. SPE 154442, SPE/ICoTA

Coiled Tubing & Well Intervention Conference and Exhibition, The Woodlands, Texas, USA, Society of Petroleum Engineers.
Grebenkin, I. M. and Davies, D. R. 2012. A Novel Optimisation Algorithm for Inflow Control Valve Management. SPE 154472, SPE Europec/EAGE Annual Conference, Copenhagen, Denmark, Society of Petroleum Engineers.
Gryzlov, A., Mudde, R. F. and Schiferli, W. 2009. Inverse Modelling of the Inflow Distribution for the Liquid/Gas Flow in Horizontal Pipelines. BHR 2009, 14th International Conference on Multiphase Production Technology, Cannes, France, BHR Group.
Guyaguler, B. and Byer, T. J. 2008. A New Rate-Allocation-Optimization Framework. SPE Production & Operations Journal **23**(04): 448-457.
Guzman, M. 2012. Use of Distributed Temperature Sensing for Wax Detection and Treatment Optimization. SPE 156077, SPE International Production and Operations Conference & Exhibition, Doha, Qatar, Society of Petroleum Engineers.
Gysling, D. L. and Loose, D. H. 2003. Sonar-Based, Clamp-On Flow Meter for Gas and Liquid Applications. ISA EXPO, Houston, USA.
Hagedorn, A. R. and Brown, K. E. 1965. Experimental Study of Pressure Gradients Occurring During Continuous Two-Phase Flow in Small-Diameter Vertical Conduits. Journal of Petroleum Technology **17**(04): 475-484.
Haghighat Sefat, M., Muradov, K. M. and Davies, D. 2013. Field Management by Proactive Optimisation of Intelligent Wells - A Practical Approach. SPE 167453, SPE Middle East Intelligent Energy Conference and Exhibition, Dubai, UAE, Society of Petroleum Engineers.
Halvorsen, M., Elseth, G. and Naevdal, O. M. 2012. Increased oil production at Troll by autonomous inflow control with RCP valves. SPE 159634, SPE Annual Technical Conference and Exhibition, San Antonio, Texas, USA, Society of Petroleum Engineers.
Harris, D., Du Rieu, N. G. and Rollett, K. I. 2008. St. Joseph Field Waterflood Project: Fractured Water Injection Using Smart Well Technology. IPTC 12188, International Petroleum Technology Conference, Kuala Lumpur, Malaysia, International Petroleum Technology Conference.
Hu, B., Sagen, J., Chupin, G., Haugset, T., Ek, A. and Sommersel, T. 2007. Integrated Wellbore-Reservoir Dynamic Simulation. SPE 109162, Asia Pacific Oil and Gas Conference and Exhibition, Jakarta, Indonesia, Society of Petroleum Engineers.
Hu, B., Veeken, C. a. M., Yusuf, R. and Holmas, H. 2010. Use of Wellbore-Reservoir Coupled Dynamic Simulation to Evaluate the Cycling Capability of Liquid-Loaded Gas Wells. SPE 134948, SPE Annual Technical Conference and Exhibition, Florence, Italy, Society of Petroleum Engineers.
Huckabee, P. T. 2009. Optic Fiber Distributed Temperature for Fracture Stimulation Diagnostics and Well Performance Evaluation. SPE 11883, SPE Hydraulic Fracturing Technology Conference, The Woodlands, Texas, Society of Petroleum Engineers.
Hull, J. W., Gosselin, L. and Borzel, K. 2010. Well-Integrity Monitoring and Analysis Using Distributed Fiber-Optic Acoustic Sensors. SPE 128304, IADC/SPE Drilling Conference and Exhibition, New Orleans, Louisiana, USA, Society of Petroleum Engineers.
Hunter, B. 2014. Technology Overview of Permanent Downhole Distributed Pressure Sensing with Fiber Bragg Grating Sensing Technology. Available: http://smartfibres.com/docs/DPS_Overview.pdf.

In 'T Panhuis, P., Den Boer, H., Van Der Horst, J., Paleja, R., Randell, D., Joinson, D., Mcivor, P. B., Green, K. and Bartlett, R. 2014. Flow Monitoring and Production Profiling using DAS. SPE 170917, SPE Annual Technical Conference and Exhibition, Amsterdam, The Netherlands, Society of Petroleum Engineers.

Jackson, R. R. and Banerjee, R. 2000. Advances in Multilayer Reservoir Testing and Analysis using Numerical Well Testing and Reservoir Simulation. SPE 62917, SPE Annual Technical Conference and Exhibition, Dallas, Texas, Society of Petroleum Engineers.

Jackson, V. B. and Tips, T. R. 2001. Case Study: First Intelligent Completion System Installed in the Gulf of Mexico. SPE 71861, Offshore Europe, Aberdeen, United Kingdom, Society of Petroleum Engineers.

Jatmiko, W., Daltaban, T. S. and Archer, J. S. 1996. Multi-Phase Flow Well Test Analysis in Multi-Layer Reservoirs. SPE 36557, SPE Annual Technical Conference and Exhibition, Denver, Colorado, Society of Petroleum Engineers.

Johannessen, K., Drakeley, B. K. and Farhadiroushan, M. 2012. Distributed Acoustic Sensing - A New Way of Listening to Your Well/Reservoir. SPE 149602, SPE Intelligent Energy International, Utrecht, The Netherlands, Society of Petroleum Engineers.

Joshi, S. D. 1988. Augmentation of Well Productivity With Slant and Horizontal Wells (includes associated papers 24547 and 25308). Journal of Petroleum Technology **40**(6): 729-739.

Kabir, C. S., Izgec, B., Hasan, A. R., Wang, X. and Lee, J. 2008. Real-Time Estimation of Total Flow Rate and Flow Profiling in DTS-Instrumented Wells. IPTC 12343, International Petroleum Technology Conference, Kuala Lumpur, Malaysia, International Petroleum Technology Conference.

Kalman, R. E. 1960. A New Approach to Linear Filtering and Prediction Problems. Journal of Fluids Engineering **82**(1): 35-45.

Karaman, O. S., Kutlik, R. L. and Kluth, E. L. 1996. A Field Trial to Test Fiber Optic Sensors for Downhole Temperature and Pressure Measurements, West Coalinga Field, California. SPE 35685, SPE Western Regional Meeting, Anchorage, Alaska, Society of Petroleum Engineers.

Kent, A. W., Burkhead, D. W., Burton, R. C., Furui, K., Actis, S. C., Bjornen, K., Constantine, J. J., Gilbert, W. W., Hodge, R. M., Ledlow, L. B., Nozaki, M., Vasshus, A. and Zhang, T. 2014. Intelligent Completion Inside Uncemented Liner For Selective High-Rate Carbonate Matrix Acidizing. SPE Drilling & Completion **29**(02): 165-181.

Knabe, S. P., Carvajal, G. and Boisvert, I. 2014. A Smart Flow for SmartWells: Reactive and Proactive Modes. SPE 167821, SPE Intelligent Energy Conference & Exhibition, Utrecht, The Netherlands, Society of Petroleum Engineers.

Koelman, J. V. V., Lopez, J. L. and Potters, H. 2011. Fiber Optic Technology for Reservoir Surveillance. IPTC 14629, International Petroleum Technology Conference, Bangkok, Thailand, International Petroleum Technology Conference.

Koelman, J. V. V., Lopez, J. L. and Potters, H. 2012. Optical Fibers: The Neurons For Future Intelligent Wells. SPE 150203, SPE Intelligent Energy International, Utrecht, The Netherlands, Society of Petroleum Engineers.

Kruif, B. D., Leskens, M., Linden, R. V. D. and Alberts, G. 2008. Soft-sensing for multilateral wells with down hole pressure and temperature and surface flow measurements. SPE 1181, Abu Dhabi International Petroleum Exhibition and Conference, Abu Dhabi, UAE, Society of Petroleum Engineers.

Kuchuk, F. J., Ayestaran, L. and Karakas, M. 1986a. Well Testing and Analysis Techniques for Layered Reservoirs. SPE Formation Evaluation **1**(04): 342-354.

Kuchuk, F. J., Shah, P. C., Ayestaran, L. and Nicholson, B. 1986b. Application of Multilayer Testing and Analysis: A Field Case. SPE 15419, SPE Annual Technical Conference and Exhibition, New Orleans, Louisiana, Society of Petroleum Engineers.

Kuchuk, F. J. and Wilkinson, D. J. 1991. Transient Pressure Behavior of Commingled Reservoirs. SPE Formation Evaluation **6**(01): 111-120.

Kuznetsov, A. G. 1992. Non-linear Optimisation Toolbox, University of Oxford, OUEL 1936/92.

Lang, Z. X. and Horne, R. N. 1983. Optimum Production Scheduling Using Reservoir Simulators: A Comparison of Linear Programming and Dynamic Programming Techniques. SPE 12159, SPE Annual Technical Conference and Exhibition, San Francisco, California, Society of Petroleum Engineers.

Larsen, L. 1999. Determination of Pressure-Transient and Productivity Data for Deviated Wells in Layered Reservoirs. SPE Reservoir Evaluation & Engineering **2**(01): 95-103.

Lasdon, L. S., Fox, R. L. and Ratner, M. W. 1974. Nonlinear optimization using the generalized reduced gradient method. RAIRO - Operations Research - Recherche Opérationnelle **8**(V3): 73-103.

Lasdon, L. S., Waren, A. D., Jain, A. and Ratner, M. 1978. Design and Testing of a Generalized Reduced Gradient Code for Nonlinear Programming. ACM Trans. Math. Softw. **4**(1): 34-50.

Lau, H. C., Deutman, R., Al-Sikaiti, S. and Adimora, V. 2001. Intelligent Internal Gas Injection Wells Revitalise Mature S.W. Ampa Field. SPE 72108, SPE Asia Pacific Improved Oil Recovery Conference, Kuala Lumpur, Malaysia, Society of Petroleum Engineers.

Least, B., Greci, S., Konopczynski, M. and Thornton, K. 2013. Inflow Control Devices Improve Production in Heavy Oil Wells. SPE 167414, SPE Middle East Intelligent Energy Conference and Exhibition, Manama, Bahrain, Society of Petroleum Engineers.

Lee, J., Rollins, J. B. and Spivey, J. P. 2003. Pressure Transient Testing, Society of Petroleum Engineers.

Lefkovits, H. C., Hazebroek, P., Allen, E. E. and Matthews, C. S. 1961. A Study of the Behavior of Bounded Reservoirs Composed of Stratified Layers. Society of Petroleum Engineers Journal **1**(01): 43-58.

Leskens, M., Smeulers, J. P. M. and Gryzlov, A. 2008. Downhole Multiphase Metering In Wells By Means Of Soft-sensing. SPE 112046, Intelligent Energy Conference and Exhibition, Amsterdam, The Netherlands, Society of Petroleum Engineers.

Li, Z. and Zhu, D. 2009. Predicting Flow Profile of Horizontal Wells by Downhole Pressure and DTS Data for Infinite Waterdrive Reservoir. SPE 124873, SPE Annual Technical Conference and Exhibition, New Orleans, Louisiana, Society of Petroleum Engineers.

Lo, K. K., Starley, G. P. and Holden, C. W. 1995. Application of Linear Programming to Reservoir Development Evaluations. SPE Reservoir Engineering Journal **10**(1): 52-58.

Lorentzen, R. J., Fjelde, K. K., Frøyen, J., Lage, A. C. V. M., Nævdal, G. and Vefring, E. H. 2001. Underbalanced and Low-head Drilling Operations: Real Time Interpretation of Measured Data and Operational Support. SPE-71384-MS, SPE Annual Technical Conference and Exhibition, New Orleans, Louisiana, Society of Petroleum Engineers.

Lorentzen, R. J., Saevareid, O. and Naevdal, G. 2010a. Rate Allocation: Combining Transient Well Flow Modelling and Data Assimilation. SPE 135073, SPE Annual Technical Conference and Exhibition, Florence, Italy, Society of Petroleum Engineers.

Lorentzen, R. J., Saevareid, O. and Naevdal, G. 2010b. Soft Multiphase Flow Metering for Accurate Production Allocation. SPE 136026, SPE Russian Oil and Gas Conference and Exhibition, Moscow, Russia, Society of Petroleum Engineers.

Lorentzen, R. J., Stordal, A., Nævdal, G., Karlsen, H. A. and Skaug, H. J. 2014. Estimation of Production Rates With Transient Well-Flow Modeling and the Auxiliary Particle Filter. SPE Journal **19**(01): 172-180.

Luo, X., Lorentzen, R. J., Stordal, A. S. and Nævdal, G. 2014. Toward an Enhanced Bayesian Estimation Framework for Multiphase Flow Soft-sensing. 14th European Conference on the Mathematics of Oil Recovery, Catania, Sicily, Italy.

Macphail, W. F. P., Lisoway, B. and Banks, K. 2012. Fiber Optic Distributed Acoustic Sensing of Multiple Fractures in a Horizontal Well. SPE 152422, SPE Hydraulic Fracturing Technology Conference, The Woodlands, Texas, USA, Society of Petroleum Engineers.

Malakooti, R., Muradov, K., Davies, D. and Kuznetsov, A. 2015. Flow Control Optimisation to Maximise the Accuracy of Multi-phase Flow Rate Allocation. SPE 173873, SPE Bergen One Day Seminar, Bergen, Norway, Society of Petroleum Engineers.

Manrique, J. F. and Poe, B. D. 2007. A Unique Methodology for Evaluation of Multifractured Wells in Stacked-Pay Reservoirs Using Commingled Production and Rate Transient Analysis. SPE 110576, SPE Annual Technical Conference and Exhibition, Anaheim, California, U.S.A., Society of Petroleum Engineers.

Mateeva, A., Mestayer, J., Cox, B., Kiyashchenko, D., Wills, P., Lopez, J., Grandi, S., Hornman, K., Lumens, P., Franzen, A., Hill, D. and Roy, J. 2012. Advances in Distributed Acoustic Sensing (DAS) for VSP. SEG 2012-0739, SEG Annual Meeting, Las Vegas, Nevada, Society of Exploration Geophysicists.

Mathiesen, V., Werswick, B. and Aakre, H. 2014. The Next Generation Inflow Control, the Next Step to Increase Oil Recovery on the Norwegian Continental Shelf. SPE 169233, SPE Bergen One Day Seminar, Bergen, Norway, Society of Petroleum Engineers.

Mathiesen, V., Werswick, B., Aakre, H. and Elseth, G. 2011. Autonomous Valve, A Game Changer Of Inflow Control In Horizontal Wells. SPE 145737, Offshore Europe, Aberdeen, UK, Society of Petroleum Engineers.

Meshioye, O., Mackay, E., Ekeoma, E. and Martinez, C. 2010. Optimization of Waterflooding Using Smart Well Technology. SPE 136996, Nigeria Annual International Conference and Exhibition, Tinapa - Calabar, Nigeria, Society of Petroleum Engineers.

Mestayer, J., Cox, B., Wills, P., Kiyashchenko, D., Lopez, J., Costello, M., Bourne, S., Ugueto, G., Lupton, R., Solano, G., Hill, D. and Lewis, A. 2011. Field Trials of Distributed Acoustic Sensing For Geophysical Monitoring. SEG 2011-4253, SEG Annual Meeting, San Antonio, Texas, Society of Exploration Geophysicists.

Molenaar, M. M., Fidan, E. and Hill, D. 2012a. Real-Time Downhole Monitoring Of Hydraulic Fracturing Treatments Using Fibre Optic Distributed Temperature And Acoustic Sensing. SPE 152981, SPE/EAGE European Unconventional Resources Conference and Exhibition, Vienna, Austria, Society of Petroleum Engineers.

Molenaar, M. M., Hill, D., Webster, P., Fidan, E. and Birch, B. 2011. First Downhole Application of Distributed Acoustic Sensing (DAS) for Hydraulic Fracturing Monitoring and Diagnostics. SPE 140561, SPE Hydraulic Fracturing Technology Conference, The Woodlands, Texas, USA, Society of Petroleum Engineers.

Molenaar, M. M., Hill, D., Webster, P., Fidan, E. and Birch, B. 2012b. First Downhole Application of Distributed Acoustic Sensing for Hydraulic-Fracturing Monitoring and Diagnostics. SPE Drilling & Completion **27**(01): 32-38.

Montes, A., Nyhavn, F., Oftedal, G., Faevelen, E., Andresen, C. A., Leung, E. and Wikmark, V. 2013. Application of Inflow Well Tracers for Permanent Reservoir Monitoring in North Amethyst Subsea Tieback ICD wells in Canada. SPE 167463, SPE Middle East Intelligent Energy Conference and Exhibition, Manama, Bahrain, Society of Petroleum Engineers.

Montgomery, D. C. and Runger, G. C. 2011. Applied statistics and probability for engineers, Hoboken, NJ, Wiley.

Moradidowlatabad, M., Muradov, K. M. and Davies, D. 2014. Novel Workflow to Optimise Annular Flow Isolation in Advanced Wells. IPTC 17716, International Petroleum Technology Conference, Kuala Lumpur, Malaysia, International Petroleum Technology Conference.

Mullens, S., Lees, G. and Duvivier, G. 2010. Fiber-Optic Distributed Vibration Sensing Provides Technique for Detecting Sand Production. OTC 20429, Offshore Technology Conference, Houston, Texas, USA, Offshore Technology Conference.

Muradov, K. M. and Davies, D. R. 2008. Prediction of Temperature Distribution in Intelligent Wells. SPE 114772, SPE Russian Oil and Gas Technical Conference and Exhibition, Moscow, Russia, Society of Petroleum Engineers.

Muradov, K. M. and Davies, D. R. 2009a. Temperature Modelling and Analysis of Wells with Advanced Completion. SPE 121054, EUROPEC/EAGE Conference and Exhibition, Amsterdam, The Netherlands, Society of Petroleum Engineers.

Muradov, K. M. and Davies, D. R. 2009b. Zonal Rate Allocation in Intelligent Wells. SPE 121055, EUROPEC/EAGE Conference and Exhibition, Amsterdam, The Netherlands, Society of Petroleum Engineers.

Muradov, K. M. and Davies, D. R. 2011a. Application of Distributed Temperature Measurements to Estimate Zonal Flow Rate and Pressure. IPTC 15215, International Petroleum Technology Conference, Bangkok, Thailand, International Petroleum Technology Conference.

Muradov, K. M. and Davies, D. R. 2011b. Novel Analytical Methods of Temperature Interpretation in Horizontal Wells. SPE Journal **16**(03): 637-647.

Nævdal, G., Johnsen, L. M., Aanonsen, S. I. and Vefring, E. H. 2003. Reservoir Monitoring and Continuous Model Updating Using Ensemble Kalman Filter. SPE Journal **10**(01): 66-74.

Nævdal, G., Mannseth, T. and Vefring, E. H. 2002. Near-Well Reservoir Monitoring Through Ensemble Kalman Filter. SPE 75235, SPE/DOE Improved Oil Recovery Symposium, Tulsa, Oklahoma, Society of Petroleum Engineers.

Nath, D. K., Finley, D. B. and Kaura, J. D. 2006. Real-Time Fiber-Optic Distributed Temperature Sensing (DTS)-New Applications in the Oilfield. SPE 97912, SPE Annual Technical Conference and Exhibition, San Antonio, Texas, USA, Society of Petroleum Engineers.

Nelder, J. A. and Mead, R. 1965. A Simplex Method for Function Minimization. The Computer Journal **7**(4): 308-313.

Nutricato, G., Repetto, C., D'amico, A. S., Oftedal, G., Fævelen, E., Andresen, C., Leung, E. and Wikmark, V. 2013. Application of Chemical Tracers for Clean-Up and Production Inflow Monitoring With Onshore and Offshore Wells - eni Experiences and Lessons Learned. OMC 2013-128, Offshore Mediterranean Conference and Exhibition, Ravenna, Italy, Offshore Mediterranean Conference.

Oftedal, A., Davies, J., Kalia, N. and Van Dongen, H. 2013. Interwell Communication as a Means to Detect a Thief Zone Using DTS in a Danish Offshore Well. OTC 24152, Offshore Technology Conference, Houston, Texas, USA, Offshore Technology Conference.

Parker, T., Shatalin, S. and Farhadiroushan, M. 2014. Distributed Acoustic Sensing – a new tool for seismic applications. First Break **32**(1): 61-69.

Pearce, J., Rambow, F., De Jongh, H., Dria, D., Hall, T., Stoesz, C., Childers, B. and Dominique, T. 2010. Applications And Deployments Of The Real-Time Compaction Monitoring System. SPWLA 2010-69214, SPWLA 51st Annual Logging Symposium, Perth, Australia, Society of Petrophysicists and Well-Log Analysts.

Perrine, R. L. 1956. Analysis of Pressure-buildup Curves. API 56-482, Drilling and Production Practice, New York, USA, American Petroleum Institute.

Pike, R. W. 1986. Optimization for engineering systems, New York: Van Nostrand Reinhold.

Poe, B. D., Atwood, W. K., Kohring, J. J. and Brook, K. 2006. Evaluation of Commingled Reservoir Properties Using Production Logs. SPE 104013, International Oil Conference and Exhibition, Cancun, Mexico, Society of Petroleum Engineers.

Prats, M. and Vogiatzis, J. P. 1999. Calculation of Wellbore Pressures and Rate Distribution in Multilayered Reservoirs. SPE Journal **4**(04): 307-314.

Rahman, M., Zannitto, P. J., Reed, D. A. and Allan, M. E. 2011. Application of Fiber-Optic Distributed Temperature Sensing Technology for Monitoring Injection Profile in Belridge Field, Diatomite Reservoir. SPE 144116, SPE Digital Energy Conference and Exhibition, he Woodlands, Texas, USA, Society of Petroleum Engineers.

Rahmawati, S. D., Whitson, C. H., Foss, B. and Kuntadi, A. 2012. Integrated field operation and optimization. Journal of Petroleum Science and Engineering **81**(0): 161-170.

Ravet, F., Rochat, E., Borda, C. and Nikles, M. R. 2013. Qualification and Validation of DTS/DSS Technology for Umbilical Monitoring. OTC 24348, OTC Brasil, Rio de Janeiro, Brazil, Offshore Technology Conference.

Rawlins, E. L., Schellhardt, M. A. and Association, A. G. 1935. Back-pressure Data on Natural Gas Wells and Their Application to Production Practices, Lord Baltimore Press.

Rester, S., Thomas, J., Hilten, M. P.-V. and Vidrine, W. L. 1999. Application of Intelligent Completion Technology to Optimize the Reservoir Management of a Deepwater Gulf of Mexico Field Ã¢Â€Â" A Reservoir Simulation Case Study. SPE 56670, SPE Annual Technical Conference and Exhibition, Houston, Texas, Society of Petroleum Engineers.

Rykov, A. 1983. Simplex Algorithms for Unconstrained Minimisation. Problems of Control and Information Theory **12**(3): 195-208.

Rykov, A. 1995. Construction Principles of Deformed Configurations Methods. Identification & Optimisation Oriented for Use in Adaptive Control, Prague, Czech Republic.

Rykov, A. S. 1980. Simplex Direct Search Algorithms. Automation and Remote Control **41**(6): 784-793.

Sagen, J., Ostenstad, M., Hu, B., Irgens Henanger, K. E., Lien, S. K., Xu, Z.-G., Groland, S. and Sira, T. 2011. A Dynamic Model for Simulation of Integrated Reservoir, Well and Pipeline System. SPE 147053, SPE Annual Technical Conference and Exhibition, Denver, Colorado, USA, Society of Petroleum Engineers.

Sagen, J., Sira Terje, Ek Arild, Selberg Stig, Chaib Mohamed and Havard, E. 2007. A coupled dynamic reservoir and pipeline model - development and initial experience. 13th International Conference on Multiphase Production Technology, Edinburgh, UK.

Saputelli, L. A., Omole, O. A., Gonzalez, F. A., Chacon, A. J., Lissanon, S. J. and Sun, K. 2011. Inflow Performance Identification and Zonal Rate Allocation from Commingled Production Tests in Intelligent Wells-Offshore West Africa. SPE 146991, SPE Annual Technical Conference and Exhibition, Denver, Colorado, USA, Society of Petroleum Engineers.

Shah, P. C., Karakas, M., Kuchuk, F. and Ayestaran, L. C. 1988. Estimation of the Permeabilities and Skin Factors in Layered Reservoirs With Downhole Rate and Pressure Data. SPE Formation Evaluation **3**(03): 555-566.

Sharma, H. K., Al-Zain, A. K., Al-Salman, N. N. K., Al-Harbi, M. S. and Said, R. 2010. A Successful Application of Permanently Installed Distributed Temperature Sensing (DTS) for Optimization of Acid Treatment in Power Water Injector With Advanced Well Completion: Case Study. SPE 132746, SPE Annual Technical Conference and Exhibition, Florence, Italy, Society of Petroleum Engineers.

Shatalin, S. V., Treschikov, V. N. and Rogers, A. J. 1998. Interferometric optical time-domain reflectometry for distributed optical-fiber sensing. Applied Optics **37**(24): 5600-5604.

Shi, H., Holmes, J. A., Durlofsky, L. J., Aziz, K., Diaz, L., Alkaya, B. and Oddie, G. 2005. Drift-Flux Modeling of Two-Phase Flow in Wellbores. SPE Journal **10**(01): 24-33.

Sierra, J. R., Kaura, J. D., Gualtieri, D., Glasbergen, G., Sarkar, D. and Johnson, D. 2008. DTS Monitoring of Hydraulic Fracturing: Experiences and Lessons Learned. SPE 116182, SPE Annual Technical Conference and Exhibition, Denver, Colorado, USA, Society of Petroleum Engineers.

Skilbrei, O., Chia, R., Schrader, K. and Purkis, D. 2003. Case History Of A 5 Zone Multi-Drop Hydraulic Control Intelligent Offshore Completion In Brunei. Offshore Technology Conference.

Spath, J. B., Ozkan, E. and Raghavan, R. 1994. An Efficient Algorithm for Computation of Well Responses in Commingled Reservoirs. SPE Formation Evaluation **9**(02): 115-121.

Spendley, W., Hext, G. R. and Himsworth, F. R. 1962. Sequential Application of Simplex Designs in Optimisation and Evolutionary Operation. Technometrics **4**(4): 441-461.

Spivey, J. P. 2006. Estimating Layer Properties for Wells in Multilayer Low-Permeability Gas Reservoirs by Automatic History Matching Production and Production Log Data. SPE 100509, SPE Gas Technology Symposium, Calgary, Alberta, Canada, Society of Petroleum Engineers.

Stalford, H., Ahmed, R. and Soriano Arambulo, V. H. 2014. Intelligent Casing-Intelligent Formation (ICIF) Design. OTC 25161, Offshore Technology Conference, Houston, Texas, Offshore Technology Conference.

Sun, K., Omole, O. A., Saputelli, L. A. and Gonzalez, F. A. 2011. An Application Case of Transferring Intelligent Well System Triple-Gauge Data into Real-Time Flow Allocation Results. SPE 144259, SPE Digital Energy Conference and Exhibition, The Woodlands, Texas, USA, Society of Petroleum Engineers.

Tabatabaei, M. and Zhu, D. 2012. Fracture-Stimulation Diagnostics in Horizontal Wells Through Use of Distributed-Temperature-Sensing Technology. SPE Production & Operations **27**(04): 356-362.

Tabatabaei, M., Zhu, D. and Hill, D. 2011. Interpretation of Temperature Data during Acidizing Treatment of Horizontal Wells for Stimulation Optimization. IPTC 15214, International Petroleum Technology Conference, Bangkok, Thailand, International Petroleum Technology Conference.

Tolan, M., Boyle, M. and Williams, G. 2001. The Use of Fiber-Optic Distributed Temperature Sensing and Remote Hydraulically Operated Interval Control Valves for the Management of Water Production in the Douglas Field. SPE 71676, SPE Annual Technical Conference and Exhibition, New Orleans, Louisiana, Society of Petroleum Engineers.

Unalmis, O. H., Johansen, E. S. and Perry, L. 2010. Evolution in Optical Downhole Multiphase Flow Measurement: Experience Translates into Enhanced Design. SPE 126741, SPE Intelligent Energy Conference and Exhibition, Utrecht, The Netherlands, Society of Petroleum Engineers.

Van Nispen, D. J., Hunt, J. R., Trofimov, A. V. and Hartgill, D. 2006. Application of Smart, Fractured Water Injection Technology in the Piltun-Astokhskoye Field, Sakhalin Island, Offshore Russia. SPE 102310, SPE Russian Oil and Gas Technical Conference and Exhibition, Moscow, Russia, Society of Petroleum Engineers.

Vasper, A. C. 2008. Auto, Natural, or In-Situ Gas-Lift Systems Explained. SPE-104202-PA **23**(01): 75-80.

Veres, G. V., Tutty, O. R., Rogers, E. and Nelson, P. A. 2004. Global optimisation-based control algorithms applied to boundary layer transition problems. Control Engineering Practice **12**(4): 475-490.

Vogel, J. V. 1968. Inflow Performance Relationships for Solution-Gas Drive Wells. Journal of Petroleum Technology **20**(01): 83-92.

Wang, P., Aziz, K. and Litvak, M. L. 2002a. Optimization of Production From Mature Fields. WPC 32152, Rio de Janeiro, Brazil, World Petroleum Congress.

Wang, P., Litvak, M. and Aziz, K. 2002b. Optimization of Production Operations in Petroleum Fields. SPE 77658, SPE Annual Technical Conference and Exhibition, San Antonio, Texas, Society of Petroleum Engineers.

Wang, X. and Bussear, T. R. 2011. Real Time Horizontal Well Monitoring Using Distributed Temperature Sensing (DTS) Technology. OTC 22293, OTC Brasil, Rio de Janeiro, Brazil, Offshore Technology Conference.

Wen, X. H. and Chen, W. H. 2005. Real-Time Reservoir Model Updating Using Ensemble Kalman Filter. SPE 92991, PE Reservoir Simulation Symposium, The Woodlands, Texas, Society of Petroleum Engineers.

Williams, B. and Brough, R. B. 2012. Wireless Reservoir Surveillance In Deepwater Completions. SPE 155743, SPE Deepwater Drilling and Completions Conference, Galveston, Texas, USA, Society of Petroleum Engineers.

Williams, B. and Vilela, A. 2012. Wireless Reservoir Surveillance Using Intelligent Tracers. SPE 152660, SPE Latin America and Caribbean Petroleum Engineering Conference, Mexico City, Mexico, Society of Petroleum Engineers.

Woodrow, C. K. and Drummond, E. 2001. Heat Seeking Laser Sheds Light on Tern. SPE 67729, SPE/IADC Drilling Conference, Amsterdam, Netherlands, Society of Petroleum Engineers.

Xiao, J., Farhadiroushan, M., Clarke, A., Khalifa, Q., Mulhem, A., Forero Reyes, H., Parker, T. R., Shawash, J. and Milne, H. C. 2013a. Inflow Monitoring in Intelligent Wells using Distributed Acoustic Sensor. SPE 167447, SPE Middle East Intelligent Energy Conference and Exhibition, Manama, Bahrain, Society of Petroleum Engineers.

Xiao, J., Farhadiroushan, M., Clarke, A., Khalifa, Q., Mulhem, A., Forero Reyes, H., Parker, T. R., Shawash, J. and Milne, H. C. 2013b. Inflow Monitoring in Intelligent Wells using Distributed Acoustic Sensor. Society of Petroleum Engineers.

Xiao, J. J., Farhadiroushan, M., Clarke, A., Abdalmohsen, R. A., Alyan, E., Parker, T. R., Shawash, J. and Milne, H. C. 2014. Intelligent Distributed Acoustic Sensing for In-well Monitoring. SPE 172197, SPE Saudi Arabia Section Technical Symposium and Exhibition, Al-Khobar, Saudi Arabia, Society of Petroleum Engineers.

Yoshioka, K., Zhu, D., Hill, A. D. and Lake, L. W. 2009. A New Inversion Method to Interpret Flow Profiles From Distributed Temperature and Pressure Measurements in Horizontal Wells. SPE Production & Operations **24**(4): 510-521.

Yu, S., Davies, D. R. and Sherrard, D. W. 2000. The Modelling of Advanced Intelligent Well - An Application. SPE 62950, SPE Annual Technical Conference and Exhibition, Dallas, Texas, Copyright 2000, Society of Petroleum Engineers Inc.

Zuber, N. and Findlay, J. A. 1965. Average Volumetric Concentration in Two-Phase Flow Systems. Journal of Heat Transfer **87**(4): 453-468.

Appendix A

The Generalised Reduced Gradient Algorithm

Studies by (Abadie and Carpentier, 1969, Abadie, 1972) report the early efforts to formulate Generalised Reduced Gradient (GRG) Algorithm. (Lasdon et al., 1974, Lasdon et al., 1978) described the principles and logic behind a system of computer programs for solving a non-linear optimisation problem using the GRG algorithm. These papers concentrate on the software implementation of the algorithm rather than on its mathematical properties. The GRG algorithm solves the non-linear optimisation problem of the form:

Minimise $f(X)$

Subject to

$$g_i(X) = 0, \qquad i = \overline{1, neq} \tag{A- 1}$$

$$0 \le g_i(X) \le u_{n+i}, \qquad i = \overline{neq + 1, r} \tag{A- 2}$$

$$l_i \le X_i \le u_i, \qquad i = \overline{1, n} \tag{A- 3}$$

where X is a vector of n control (natural) variables and l_i, u_i are the lower and upper bounds respectively. neq represents the number of equality constraints which may be zero in some problems. It is assumed that objective function f and constraint functions g are differentiable and $r < n$ to present the feasible problem. The inequality constraint can be converted to the equality ones using slack variables $X_{n+1}, \ldots, X_{n+r}$ while $X_1, \ldots, X_n$ are the natural variables

Minimise $f(X)$

Subject to

$$g_i(X) - X_{n+i} = 0, \qquad i = \overline{1, r} \tag{A- 4}$$

$$l_i \le X_i \le u_i, \qquad i = \overline{1, n + r} \tag{A- 5}$$

$$l_i = u_i = 0, \qquad i = \overline{n + 1, n + neq} \tag{A- 6}$$

$$l_i = 0, \qquad i = \overline{n + neq + 1, n + r} \tag{A- 7}$$

Equations A- 6 and A- 7 indicate the bounds of the slack variables. In such conditions, the vector X contains both the natural variables of the problem and the slack variables.

The fundamental idea of the GRG algorithm is to partition the X vector into y vector of r "basic" variables and x vector of the remaining $n - r$ "non-basic" variables. Equality constraint can then be written as:

$$g(X) = g(y, x) = 0 \quad \text{A- 8}$$

where

$$g = (g_1, \dots, g_r) \quad \text{A- 9}$$

Based on the implicit function theorem, Equation A- 8 has a solution $y(x)$ for all x in neighbourhood of $\bar{x}$ (non-basic variables of feasible point $\bar{X}$) if the $r \times r$ basis matrix $B = \partial g/\partial y$ is non-singular at $\bar{X}$. The objective function f is expressed as a function of x only:

$$F(x) = f(y(x), x) \quad \text{A- 10}$$

The nonlinear problem is converted to a reduced problem with only upper and lower bounds at least for x close to $\bar{x}$:

Minimise $F(x)$ A- 11

Subject to $l \leq x \leq u$ A- 12

where l and u are the vectors of bounds for x. The function $F(x)$ and its gradient $\nabla F(x)$ are called the reduced objective and reduced gradient respectively. The GRG solves the original problem A- 1 to A- 3 by solving a sequence of reduced problems. A gradient method is applied to solve the reduced problem where the reduced gradient $\nabla F(\bar{x})$ is computed at a given iteration as follows:

$$\pi = (\partial f/\partial y)^T B^{-1} \quad \text{A- 13}$$

$$\partial F/\partial x_k = \partial f/\partial x_k - \pi\, \partial g/\partial x_k \quad \text{A- 14}$$

A search direction $\bar{d}$ is formed from $\nabla F(\bar{x})$ and a one-dimensional search is initiated to solve the problem:

Minimise $F(\bar{x} + \gamma \bar{d})$, $\gamma > 0$ A- 15

γ is chosen from a sequence of positive values $\{\gamma_1, \gamma_2, \dots\}$ which are generated through a subroutine research described by Lasdon et al. (1978). For each value γ_i $F(\bar{x} + \gamma \bar{d})$ or $f(y(\bar{x} + \gamma \bar{d}), \bar{x} + \gamma \bar{d})$ is computed where $\bar{x}$, $\bar{d}$ and γ_i are known and y is found from below equation. A variant of Newton's method is used to solve this equation.

$$g(y, \bar{x} + \gamma \bar{d}) = 0 \quad \text{A- 16}$$

The one-dimensional search can stop in one of three different ways (Lasdon et al., 1978):

1) Newton's method does not converge on the first step: γ is reduced to implement another trial. Otherwise, the search is stopped.
2) Newton's method converges but some g function constraints or basic variable bounds may be violated: a new γ value is obtained to meet at least one such new

constraint or variable at its bound while the others are satisfied. The new variable is added to the set of basic variables if the objective is less than at all previous points at this new point. When this occurs the one-dimensional search is stopped and a new reduced problem is solved.

3) If an objective value is found larger than the previous value: a quadratic function is now fitted to the three γ_i values. The minimum of the quadratic function is used to calculate F. The search is continued until the lowest F value is found while keeping the same reduced problem.

Appendix B

Deformed Configuration optimisation Method

The Deformed Configuration techniques may be based either on a configuration of simplex, as used in the active soft-sensing algorithm defined here, or on a configuration of complex (Rykov, 1995):

Definition 1. The points x^1, x^2, …, x^{n+1} in the space $\mathbb{R}^n$ are called **affine independent** if the vectors $x^1 - x^{n+1}$, $x^2 - x^{n+1}$, …, $x^n - x^{n+1}$ are linearly independent.

Definition 2. An ***n*-dimensional simplex** S in the space $\mathbb{R}^n$ is the convex hull of $(n+1)$ affine independent points $\{x^i\}_{i=1}^{n+1}$. These $(n+1)$ points are called **simplex vertices**. The simplex is **regular** if the distances between the simplex vertices are equal, otherwise it is **deformed**. For example, a 0-dimensional simplex is a point, a 1-dimensional simplex is a line, a 2-dimensional simplex is a triangle and a 3-dimensional simplex is a tetrahedron.

A complex configuration is a set of $c (c \geq n+1)$ vertices (points) in the space $\mathbb{R}^n$ not belonging simultaneously to a space with dimension less than n. The complex configuration becomes a simplex one when $c = n+1$.

Deformed simplex optimisation requires $(n+1)$ flow tests to initiate the active soft-sensing workflow in an n-zone intelligent well. Here, a vertex x^i, $i = \overline{1, n+1}$, represents a combination of n control variables, one for each zone. In this study, a vertex is one combination of fraction of ICVs area open to flow (a so-called flow test). As an example, a simplex forms a triangle whose 3 vertices are different combinations of fraction of ICVs area open to flow in a 2-zone, I-well case (**Error! Reference source not found.**).

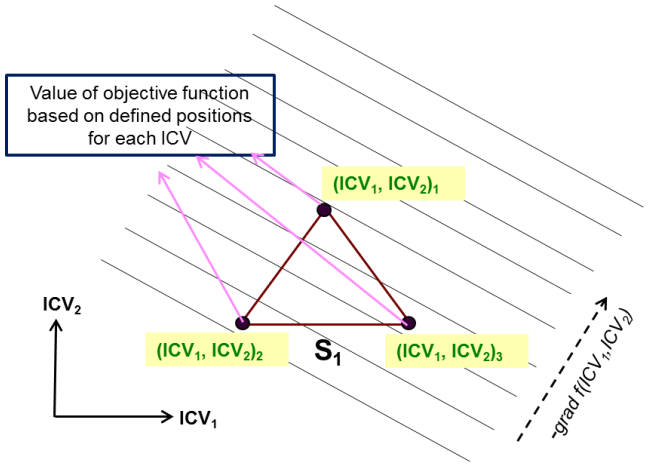

Figure B- 1 Construction of the triangle simplex with 3 different combinations of fraction of ICV_1 and ICV_2 areas open to flow

Each vertex corresponds to a combination of fraction of zonal ICVs area open to flow that are associated with a value of the objective function (the mismatch between this combination of modelled and observed measurements). We start with the first simplex S_1 and then form the new simplex S_2 by either reflection or displacement mapping of one or more vertices of S_1 to new locations (see Figure B- 2).

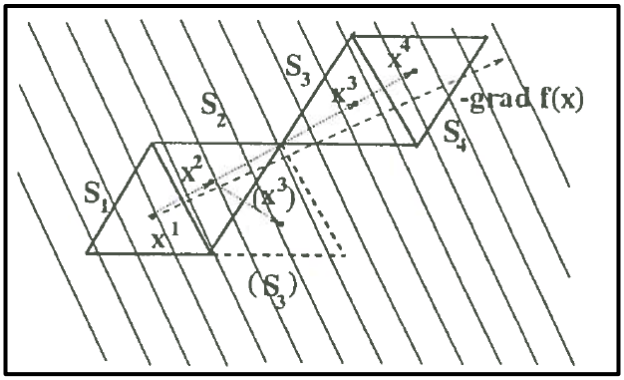

Figure B- 2 Example of mapping of one or several vertices at each step to create the next simplex (Rykov, 1995)

Rykov (1983) proposed ordering the vertices of every new simplex from worst to best in order to reduce the number of feasible mapping directions i.e.:

$$f(x^{N,1}) \leq f(x^{N,2}) \leq \cdots \leq f(x^{N,n+1}),$$

where $f(x^{N,i})$ is the objective function value at the vertex $x^{N,i}$ of the simplex S_N. Then the top vertex/vertices are discarded and new ones proposed. When applied to our case, where $f(x^{N,i})$ is calculated as mismatch, the above order implies that deformed simplex optimisation attempts to maximise the mismatch of the next flow test at each iteration step. Generating a new simplex requires dividing the vertices of the current simplex into 3 groups: m $(m = \overline{1,n})$ vertices to be reflected, k $(k = \overline{0,n-m})$ vertices to be displaced and the remaining $(n+1-m-k)$ vertices to remain at their original locations. The vector directed from the geometrical centre of m reflected vertices toward the centre of $(n+1-m-k)$ non-mapped vertices determines the direction of simplex centre displacement, and k displaced vertices are passed along the vector parallel to this direction.

Each maximisation step N generates a set Ω^N which includes $n(n+1)/2$ possible reflection and displacement combinations (directions) to construct the new simplex for a

given simplex of n vertices. The problem of selecting the optimal direction P^N out of Ω^N and the corresponding number of $m^N$and k^N vertices is solved using the following relation:

$$P^N = arg \max_{P^N \in \Omega^N} I^N \qquad \text{B- 1}$$

where I^N is the direction of optimal criteria whose computation is based on the objective function values in the simplex vertices and the number of $m^N$and k^N vertices. The direction of the optimal criteria can be selected from the following which each criterion corresponds to a certain type of maximisation algorithm:

- Maximum increase of the objective function at the simplex centroid: $I_1^N = \Delta f^N = f(x^{N+1}) - f(x^N)$
- Maximum increase of the objective function while considering the number of objective function evaluations: $I_2^N = \frac{1}{m+k}\Delta f^N$
- Proximity to the anti-gradient: $I_3^N = -(gradf(x^N), P)$
- Mapping of the vertices whose the objective function value is less than that at the simplex centre: $I_4^N = \sum_{i=1}^{m}[f(x^N) - f(x^{N,i})]$
- Mapping of the vertices whose the objective function value is less than $\emptyset_N = \frac{1}{2}[f(x^{N,1}) + f(x^{N,n+1})]$: $I_5^N = \sum_{i=1}^{m}[\emptyset_N - f(x^{N,i})]$
- $I_6^N = \frac{1}{m} I_5^N$

where $f(x^N)$ is the objective function value at the simplex centre which can be approximated by the arithmetic mean of the function values at the vertices.

$$f(x^N) = \frac{1}{n+1}\sum_{i=1}^{n+1} f(x^{N,i}) \qquad \text{B- 2}$$

The direction of the optimal criteria can be obtained from Equation B- 1. The new simplex is constructed according to several versions of the mapping formulations based on the number of m ($m = \overline{1,n}$) vertices to be reflected, k ($k = \overline{0,n-m}$) vertices to be displaced and the remaining $(n+1-m-k)$ vertices to remain at their original locations (Rykov, 1983). Following definitions of mappings are used to construct the new simplex:

Definition 1. The mapping of $m+k(m = \overline{1,n}; k = \overline{0,n-m})$ of simplex N is the transfer of $m+k$ of its vertices along the directed vector from geometrical centroid of m reflected vertices toward the centroid of $n+1-m-k$ non-mapped ones. The direction of the vector $x^{N+1} - x^N$ coincides with the prescribed direction.

Definition 2. The mapping of $m(m = \overline{1,n})$ of simplex N is the transfer of m of its vertices along the directed vector from geometrical centroid of m reflected vertices toward the centroid of $n+1-m$ non-mapped ones. The direction of the vector $x^{N+1} - x^N$ coincides with the prescribed direction.

- **Mapping 1**

$$x^{N+1,j} = x^{N,j} + \alpha\Delta_N(m,k), \qquad j = \overline{1,m} \qquad \text{B- 3}$$

$$x^{N+1,j} = x^{N,j} + \frac{\alpha m}{n+1-k}\Delta_N(m,k), \quad j = \overline{m+1,m+k} \qquad \text{B- 4}$$

$$x^{N+1,j} = x^{N,j}, \qquad j = \overline{m+k+1,n+1} \qquad \text{B- 5}$$

$$x^{N+1} = x^N + \frac{\alpha}{n+1-k}\Delta_N(m,k) \qquad \text{B- 6}$$

$$\Delta_N(m,k) = \frac{1}{n+1-m-k}\sum_{i=m+k+1}^{n+1} x^{N,i} - \frac{1}{m}\sum_{i=1}^{m} x^{N,i} \qquad \text{B- 7}$$

- **Mapping 2**

$$x^{N+1,j} = x^{N,j} + \alpha\Delta_N^j(m,k), \qquad j = \overline{1,m} \qquad \text{B- 8}$$

$$x^{N+1,j} = x^{N,j} + \frac{\alpha m}{n+1-k}\Delta_N^j(m,k), \quad j = \overline{m+1,m+k} \qquad \text{B- 9}$$

$$x^{N+1,j} = x^{N,j}, \qquad j = \overline{m+k+1,n+1} \qquad \text{B- 10}$$

$$x^{N+1} = x^N + \frac{\alpha}{n+1-k}\Delta_N^j(m,k) \qquad \text{B- 11}$$

$$\Delta_N^j(m,k) = \frac{1}{n+1-m-k}\sum_{i=m+k+1}^{n+1} x^{N,i} - x^{N,j} \qquad \text{B- 12}$$

- **Mapping 3**

$$x^{N+1,j} = x^{N,j} + \alpha\Delta_N(m), \qquad j = \overline{1,m} \qquad \text{B- 13}$$

$$x^{N+1,j} = x^{N,j}, \qquad j = \overline{m+1,n+1} \qquad \text{B- 14}$$

$$x^{N+1} = x^N - \frac{\alpha}{n+1-m}\sum_{i=1}^{m}(x^{N,i} - x^N) \qquad \text{B- 15}$$

$$\Delta_N(m) = \frac{1}{n+1-m}\sum_{i=m+1}^{n+1} x^{N,i} - \frac{1}{m}\sum_{i=1}^{m} x^{N,i} \qquad \text{B- 16}$$

- **Mapping 4**

$$x^{N+1,j} = x^{N,j} + \alpha\Delta_N^j(m), \qquad j = \overline{1,m} \qquad \text{B- 17}$$

$$x^{N+1,j} = x^{N,j}, \qquad j = \overline{m+1, n+1} \qquad \text{B- 18}$$

$$x^{N+1} = x^{N} - \frac{\alpha}{n+1-m}\sum_{i=1}^{m}(x^{N,i} - x^{N}) \qquad \text{B- 19}$$

$$\Delta_N^j(m) = \frac{1}{n+1-m}\sum_{i=m+1}^{n+1} x^{N,i} - x^{N,j} \qquad \text{B- 20}$$

- **Mapping 5**

$$x^{N+1,j} = x^{N,j} + \alpha\Delta_N^j(m), \qquad j = \overline{1, m} \qquad \text{B- 21}$$

$$x^{N+1,j} = x^{N,j}\alpha_1\Delta_N^j(m), \qquad j = \overline{m+1, n+1} \qquad \text{B- 22}$$

$$x^{N+1} = x^{N} - \frac{\alpha}{n+1-m}\sum_{i=1}^{m}(x^{N,i} - x^{N}) \qquad \text{B- 23}$$

$$\Delta_N^j(m) = \frac{1}{n+1-m}\sum_{i=m+1}^{n+1} x^{N,i} - x^{N,j} \qquad \text{B- 24}$$

$$\alpha_1 = \begin{cases} \alpha & at \quad \alpha \leq 1 \\ \alpha - 2 & at \quad \alpha > 1 \end{cases} \qquad \text{B- 25}$$

Mapping 1 and 2 correspond to the definition 1 while mapping 5 corresponds to the definition 2. Mapping 3 and 4 are special cases of mappings 1 and 2 with $k = 0$.

This study was limited to the directions $m = 1$ and $k = 0$ in order to minimise the number of changes in fraction of ICV area open to flow between each flow test to reduce the ICVs failure risk. Therefore, the $x^{N,1}$ vertex with the least mismatch is discarded and the coordinates of the new simplex vertex $x^{N+1,1}$ are calculated:

$$x^{N+1,1} = x^{N,1} + \alpha\Delta_N$$

$$\Delta_N = \frac{1}{n}\sum_{i=2}^{n+1} x^{N,i} - x^{N,1}$$

The constant $\alpha = 2$ preserves the simplex size and shape while achieving a satisfactory result (Spendley et al., 1962). However, deforming the simplex can also successfully optimise a non-linear function since diminishing the simplex size allows the function's optimum to be found more accurately. The parameter α maximises the objective function value at the simplex centre $f(x^N)$ at each iteration step. The initial step uses $\alpha = 2$. An increase in the value of α stretches the simplex by increasing $f(x^N)$. A step corresponding to a greater maximisation has thus been selected. Alternatively the simplex is contracted by selecting a step with $\alpha < 2$, e.g. with $\alpha = 1.5$ or, later, $\alpha = 0.5$.

Appendix C

C-1 Pressure Model in Multi-Zone Intelligent Well

The basis of pressure transient analysis technique is the line source (Ei-function) solution to the radial flow, diffusivity equation. Equation C- 1 expresses the relationship between flowing bottomhole pressure, p_{wf}, and the reservoir and well characteristics for a vertical well producing only oil at a constant flow rate from a single reservoir during the drawdown test assuming the following conditions (Lee et al., 2003):

- Constant flow rate
- Single oil phase
- Radial flow
- Darcy's law describes the relationship between flow velocity and pressure gradient
- It is assumed the porous medium is uniform and isotropic
- Gravity effects are negligible
- Conditions are isothermal

$$p_i - p_{wf} = \frac{162.6 q_o \mu_o B_o}{kh}\left[\log_{10}\left(\frac{kt}{\emptyset \mu_o c_t r_w^2}\right) - 3.23 + 0.869 s_d\right] \quad \text{C- 1}$$

In addition, the horizontal well testing analytical equation (Lee et al., 2003) can be incorporated into the active soft-sensing algorithm to predict the pressure during the build-up test. Three major flow regimes (early-radial flow, early-linear flow and late pseudo-radial flow) can be identified and important reservoir properties quantified during pressure transient analysis of a horizontal well in a homogeneous infinite-acting reservoir.

- Early-radial Flow:

$$p_i - p_{wf} = \frac{162.6 q_o \mu_o B_o}{\sqrt{k_x k_z} L_w}\left[\log_{10}\left(\frac{\sqrt{k_x k_z}\, t}{\emptyset \mu_o c_t r_w^2}\right) - 3.227 + 0.868 s_d\right] \quad \text{C- 2}$$

- Early-linear Flow:

$$p_i - p_{wf} = \frac{8.128 q_o B_o}{L_w h}\sqrt{\frac{\mu_o t}{k_x \emptyset c_t}} + \frac{141.2 q_o \mu_o B_o}{\sqrt{k_x k_z} L_w}(s_c + s_d) \quad \text{C- 3}$$

- Pseudo-radial Flow:

$$p_i - p_{wf} = \frac{162.6 q_o \mu_o B_o}{\sqrt{k_x k_z} L_w}\left[\log_{10}\left(\frac{k_y t}{\emptyset \mu_o c_t L_w^2}\right) - 2.303\right] + \frac{141.2 q_o \mu_o B_o}{\sqrt{k_x k_z} L_w}(s_c + s_d) \quad \text{C- 4}$$

Equations C- 2 to C- 4 describe the pressure changes during a drawdown test in which a horizontal well completed is producing only oil at a constant flow rate from a single reservoir. The total flow rate and total mobility were defined by (Perrine, 1956) for multi-phase flow conditions as:

$$\left(\frac{k}{\mu}\right)_t = \frac{k_o}{\mu_o} + \frac{k_w}{\mu_w} + \frac{k_g}{\mu_g} \quad \text{C- 5}$$

$$q_t = q_o B_o + q_w B_w + \frac{q_g B_g}{5.615} \quad \text{C- 6}$$

Agarwal (1980) generalised a superposition method using an equivalent time function for a build-up or drawdown test with a multi-rate history. Based on Agarwal's work, $(p_i - p_{wf})/q$ and elapsed time t in Equations C- 1 to C- 4 are replaced by rate-normalised pressure $\left(\frac{\Delta p}{\Delta q}\right)$ and equivalent time (Δt_e) respectively. If the analysed test period starts at $[T_j, p(T_j), q(T_j)]$:

$$\left(\frac{\Delta p}{\Delta q}\right) = \frac{p(T_j) - p(t)}{q(t) - q(T_j)} \quad \text{C- 7}$$

$$\log(\Delta t_e) = \frac{g_r(t) - g_r(T_j)}{q(t) - q(T_j)} \quad \text{C- 8}$$

$$g_r(t) = \sum_{i=1}^{M} q_i \log\left\{\frac{t - T_{i-1}}{t - T_i}\right\} + q(t)\log\{t - T_M\} \quad \text{C- 9}$$

$$g_r(T_j) = \sum_{i=1}^{j-1} q_i \log\left\{\frac{T_j - T_{i-1}}{T_j - T_i}\right\} + q(T_j)\log\{T_j - T_{j-1}\} \quad \text{C- 10}$$

where $T_i (i = 1,2, \ldots M)$ are rate changes times prior to the data point at t. (T_M, q_M) is the last rate change before the data point at t. Figure C- 1 represents a typical multiple rate testing consists of flowing a well at a constant rate q_1 for time, T_1, at rate q_2 for time T_1 to T_2 and so on. The final rate is q_t for time T_M to any incremental time, Δt.

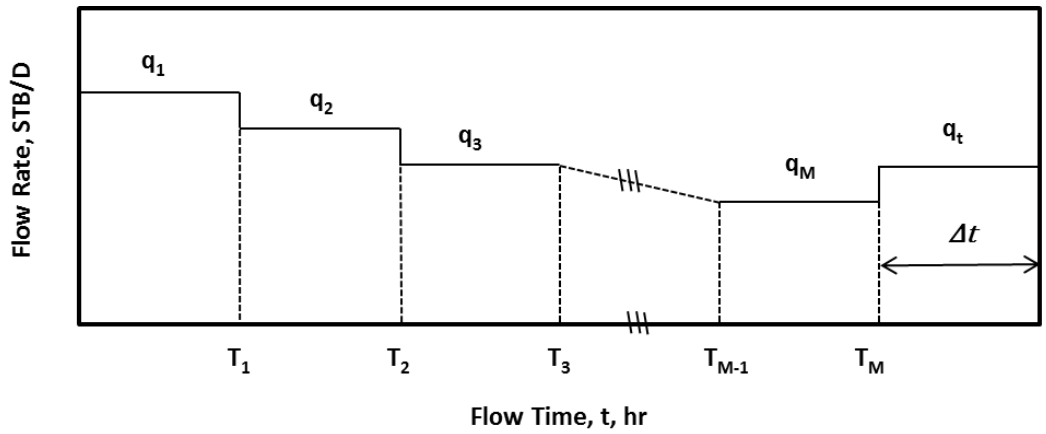

Figure C- 1 Schematic of multiple rate testing (Agarwal, 1980)

The Inflow performance relationship (IPR) relates the zonal oil flow rate to the drawdown (difference between average reservoir pressure and stabilised annulus pressure). A Linear IPR or Vogel's correlation (Vogel, 1968) is applied in the active soft-sensing depending on the following two types of reservoirs:

- Linear IPR for an Undersaturated oil reservoir ($P_{ave} > P_{bp}$):

$$\mathrm{q_{o_i}} = \mathrm{PI}_{o_i}(\mathrm{p_{ave_i}} - \mathrm{p_{an_i}}) \quad \text{C- 11}$$

- Vogel's correlation for Saturated oil reservoirs ($P_{ave} < P_{bp}$)::

$$\frac{q_{o_i}}{(q_{o_i})_{max}} = 1 - 0.2\left(\frac{p_{an_i}}{p_{ave_i}}\right) - 0.8\left(\frac{p_{an_i}}{p_{ave_i}}\right)^2 \quad \text{C- 12}$$

where i represents the number of completion zones and $q_{o_{max}}$ is the maximum oil rate or absolute open flow (AOF) when the annulus pressure equals zero.

"Zonal water-cut" *(wc)* and "zonal gas-oil ratio" *(GOR)* are introduced to calculate the downhole phase flow rates from individual zone:

$$wc_i = \frac{\mathrm{q_{w_i}}}{\mathrm{q_{o_i}} + \mathrm{q_{w_i}}} \quad \text{C- 13}$$

$$GOR_i = \frac{\mathrm{q_{g_i}}}{\mathrm{q_{o_i}}} \quad \text{C- 14}$$

The total well production measured at the surface is the summation of the phase flow rates of n zones:

$$\mathrm{Q}_o = \sum_{i=1}^{n} q_{o\,i} \quad \text{C- 15}$$

$$\mathrm{Q}_w = \sum_{i=1}^{n} q_{w\,i} \quad \text{C- 16}$$

$$Q_g = \sum_{i=1}^{n} q_{g_i}$$ C- 17

The ICV's performance is modelled with the Bernoulli equation. It describes the relationship between pressure drop, in-situ volumetric flow rate and in-situ fluid momentum density:

$$p_{an} - p_{tub} = 0.5 C_u \rho_m \left[\left(\frac{A}{C_d A_o}\right)^2 - 1\right]\left(\frac{q_V}{A}\right)^2$$ C- 18

The equations:

$$\frac{1}{\rho_m} = \frac{x}{\rho_g} + \frac{1-x}{\rho_l}$$ C- 19

$$x = \frac{M_g}{M}$$ C- 20

are used to calculate the momentum density of fluid in the presence of gas and liquid flow in the annulus section.

The total in-situ flow rate, q_V, across each production interval accounts for the presence of all three phases and is calculated by C- 21 where the definition of gas mass fraction, x, is used to express the in-situ gas flow rate as a function of in-situ liquid flow rate:

$$q_V = (1 + \frac{x\rho_l}{(1-x)\rho_g})(q_o B_o + q_g B_g)$$ C- 21

The pressure loss in the tubing needs to be calculated if the bottom-hole pressure at the top of the zones is measured instead of the zonal annulus pressure and tubing pressure. The pressure drop between any two points in the pipe is the sum of three components:

- The hydrostatic term due to changes in the fluid level
- The frictional term due to the drag of the fluids on the walls of the pipe
- The acceleration term due to the increase in fluid kinetic energy as they expand and accelerate with decreasing pressure

The Equation C- 22 states the principle of energy conservation over the length of an element of tubing that can be used to predict the pressure drop in the tubing due to the effects of gravity, friction and acceleration. The fluid density ρ_f is obtained based on volumetric fraction (hold-up) of liquid and gas phases in the tubing section.

$$\frac{dP}{dZ_{total}} = \frac{g}{g_c}\rho_f cos\theta + \frac{f\rho_f v^2}{2g_c d} + \frac{\rho_f v dv}{g_c dZ}$$ C- 22

$$\rho_f = H_l\rho_l + (1 - H_l)\rho_g$$ C- 23

Someone may use the above equation to calculate the pressure drop in the annulus. Several models are available to calculate the liquid hold-up (H_l) and friction factor f for

different multi-phase flow regimes as they are the key parameters in the pressure drop calculation. These models include 1) homogeneous flow model, 2) drift flux slip model (Zuber and Findlay, 1965) and 3) multi-phase flow correlations (Hagedorn and Brown, 1965, Beggs and Brill, 1973, Duns and Ros, 1963, Fancher and Brown, 1963).

The homogeneous model is relatively simple, continuous and differentiable and assumes no slip between the phases. These models may also consider slip between the phases, and this requires a number of empirical parameters. Homogenous models with slip effect are called drift flux model. The drift flux model is continuous across the range of flowing conditions. It describes slip between liquid and gas phases as a combination of two mechanisms. One mechanism is related to the non-uniform profile velocity and phase distribution over the pipe cross section. The other one results from the tendency of gas to rise vertically through liquid due to buoyancy effect (Shi et al., 2005). Multi-phase flow correlations are based on curve fitting of experimental data. This limits their application to the range of variables explored in the experiments. Such correlations may be suitable only for a specific flow pattern, but can also be flow pattern independent. The drift flux model is less accurate than using multi-phase flow correlations, but is often used because of the need for simplicity and continuity in the model.

Many soft-sensor techniques have used the above models to address the pressure drop in the wellbore flow model. Aggrey et al. (2007) used a drift flux model together with multi-phase slip correlations to identify the time and location of water influx into a multi-zone I-well by use of a multi pressure drop trending algorithm (dP trending). A homogeneous flow model was assumed by Gryzlov et al. (2009) to estimate the liquid and gas inflow rates along the horizontal wellbore. Leskens et al. (2008) showed that downhole pressure and temperatures measurements can be used to estimate in real-time the water, oil and gas flow rates in a well where the well flow model was described using the drift flux approach. They also allocated the inflow of gas and oil in specific location along the wellbore by assuming that a dispersed bubble flow regime is well mixed and, therefore, any slip between gas and liquid phases is negligible.

It is important to consider complex models that describe all ranges of flow regimes accurately by incorporating rigorous transition mechanisms. The flow regime is a source of uncertainty during wellbore modelling. Multiple flow obstructions and rapid changes of well geometry can greatly affect the well flow pattern which, in turn, causes inaccurate estimation of downhole inflow rates.

The pressure model of the active soft-sensing algorithm is mainly relied on using annular and tubing pressure to describe inflow performance relationship and the pressure drop across the flow control devices as downhole gauges has increased the data set richness by measuring pressure at different downhole locations. However, more complex well flow models can also be added to the algorithm to provide accurate pressure drop along the tubing and annulus sections.

C-2 Temperature Model of a Multi-Zone Intelligent Well

The temperature model used to predict the temperature distribution in multi-zone I-well requires a system of equations describing the:

- Temperature distribution in the well due to simultaneous axial flow in the tubing and annulus
- Temperature changes across the ICVs
- Tubing and annular fluid mixing temperature

Figure C- 2 shows a multi-zone I-well with possible locations of temperature and pressure measurements using downhole P/T gauges. The in-and out-flow temperature and pressure of the toe zone ICV are directly measured by P/T downhole gauges installed either side of the valve. The equivalent values from the middle zone and heel zones are measured at locations “a” and “d”. The measured mixture temperatures (locations b and d) are calculated using the Muradov and Davies (2008) semi-analytical model.

The Muradov and Davies (2008) model assumes that all the phases in a particular segment are at the same pressure and temperature while steady-state fluid and heat flows exist within the well. They developed the following equations in which the summation of phase properties f in volume v is represented as:

$$\sum_{j} f_{vj} \equiv (f)_v \qquad \text{C- 24}$$

(a) Temperature distribution in the annulus:

$$\frac{dT_{an}}{dx} = (2\pi R_{ci}(1-y)U_{af}\left(T_f - T_{an}\right) - 2\pi R_{ti}U_{at}(T_{an} - T_{tub}) \quad \text{C- 25}$$
$$+ \left(w'C_p(T_I - T_{an})\right)_I + (w)_{an}gsin\theta$$
$$+ \left[\left(wC_pK_{JT}\right)_{an} + h_{lat,jj,}w_{anj,}\left(\frac{\rho_{anj}}{\rho_{anj,}}\frac{dR_s}{dP}\Big|_T\right)\right]\frac{dP_{an}}{dx})$$
$$\times (wC_p)_{an}^{-1}$$

(b) Temperature distribution in the tubing:

$$\frac{dT_{tub}}{dx} = (2\pi R_{ti}U_{at}(T_{an} - T_{tub}) + (w)_{tub}gsin\theta \quad \text{C- 26}$$
$$+ \left[\left(wC_pK_{JT}\right)_{tub} + h_{lat,jj,}w_{tubj,}\left(\frac{\rho_{tubj}}{\rho_{tubj,}}\frac{dR_s}{dP}\Big|_T\right)\right]\frac{dP_{tub}}{dx})$$
$$\times (wC_p)_{tub}^{-1}$$

(c) Temperature changes across the ICV:

$$T_{d,ICV} = T_{an} - \Delta T_{ICV} = T_{an} - (P_{an} - P_{tub})\frac{(wC_pK_{JT})_{an}}{(wC_p)_{an}} \quad \text{C- 27}$$

(d) Tubing and annular fluids mixing temperature:

$$T_{mix} = \frac{(wC_p)_{tub}T_{tub} + (wC_p)_{an}T_{d,ICV}}{(wC_p)_{tub} + (wC_p)_{an}} \quad \text{C- 28}$$

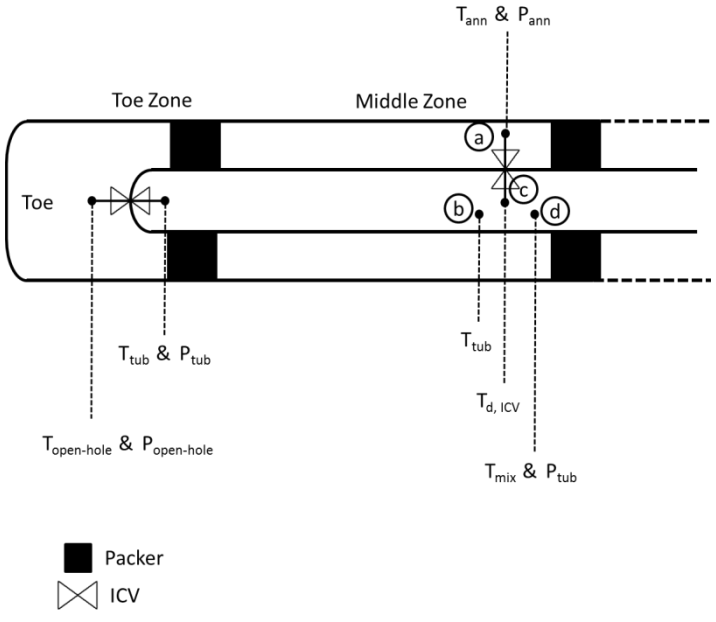

Figure C- 2 Locations of temperature and pressure measurements using downhole gauges

Appendix D

Calculation of uncertainty of estimated zonal properties

The estimated values and the associated errors of the reservoir and well properties depend on the number of measurements and the limitation of the estimation model. The combined uncertainty is derived from the function describing the propagation of uncertainty (or error):

if f is a function of several variables such as *A, B,…, M*, where each term has its individual, independent total uncertainty δ_m, then the general equation for error propagation describes the uncertainty of f as:

$$\delta_m{}^2(f) = (\frac{\partial f}{\partial A}\delta_{mA})^2 + (\frac{\partial f}{\partial B}\delta_{mB})^2 + \cdots + (\frac{\partial f}{\partial N}\delta_{mM})^2 \quad \text{D- 1}$$

The following two equations are used to relate the measurements to zonal reservoir pressure, productivity index and water-cut:

$$q_o = PI_o(P_{res} - P_{an}) \quad \text{D- 2}$$

$$q_w = \frac{wcq_o}{1-wc} \quad \text{D- 3}$$

Equation D- 1 is used to compute the zonal properties uncertainty:

$$\delta_{PI}^2 = \left(\frac{\delta q_o}{P_{res} - P_{an}}\right)^2 + \left(\frac{q_o}{(P_{res} - P_{an})^2}\delta P_{an}\right)^2 + \left(\frac{q_o}{(P_{res} - P_{an})^2}\delta P_{res}\right)^2 \quad \text{D- 4}$$

$$\delta_{P_{res}}^2 = \left(\frac{\delta q_o}{PI}\right)^2 + \left(\frac{\delta PI}{PI^2}\right)^2 + \delta_{P_{an}}^2 \quad \text{D- 5}$$

$$\delta_{wc}^2 = \left(\frac{q_o}{(q_o + q_w)^2}\delta q_w\right)^2 + \left(\frac{q_w}{(q_o + q_w)^2}\delta q_o\right)^2 \quad \text{D- 6}$$

It is assumed that zonal multi-phase flow rates have the same uncertainty as measured well rates and errors in the measurements and estimated properties are statically independent. Equations D- 4 and D- 5 are solved simultaneously to calculate the uncertainty of productivity index and reservoir pressure. Equation C- 18 is used when three phase flow is present downhole so that the uncertainty in the estimated annular in-situ gas mass fraction is included.

Appendix E

Confidence Interval

If X_E is the estimated value of the parameter with known, normally distributed uncertainty δ_m a $100(1-\alpha)$ percent confidence interval on true value of the parameter X_T is given by:

$$X_E - Z_{\alpha/2}\delta_m \leq X_T \leq X_E + Z_{\alpha/2}\delta_m \qquad \text{E- 1}$$

where $Z_{\alpha/2}$ is the upper $\alpha/2$ percentage point of the standard normal distribution of Z as shown in Figure E- 1. Table E- 1 lists values of Z that reflect a number of different confidence intervals (Crandall and Seabloom, 1970).

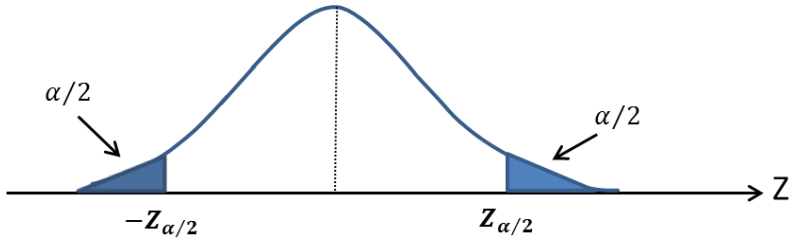

Figure E- 1 The standard normal distribution of Z

Table E- 1 Values of Z used with the confidence intervals (Crandall and Seabloom, 1970)

Z	One-sided confidence, %	Two-sided confidence, %
0.842	80	60
1.00	84.2	68.3
1.282	90	80
1.645	95	90
1.960 (2.0)	97.5	95
2.326	99	98
2.576	99.5	99

Appendix F

Hypothesis Test

The hypothesis test on the mean of a single population with known or unknown variance is discussed to understand better the hypothesis test procedure. Then the hypothesis test on the means of two normal distributions with unknown variances is presented.

Hypothesis Test on the Mean, Variances Known

The population of interest has mean μ and known variance σ^2. The test statistic is based on the sample mean $\bar{X}$ and assumes the population is normally distributed. That means that the distribution of $\bar{X}$ is approximately normal with mean μ and variance σ^2.

The hypothesis test on the mean is defined as:

$$H_0: \mu = \mu_0 \qquad \text{F- 1}$$
$$H_1: \mu \neq \mu_0$$

where μ_0 is a constant value. The test procedure for $H_0: \mu = \mu_0$ uses the below test statistic (Montgomery and Runger, 2011):

$$z_0 = \frac{\bar{X} - \mu_0}{\sigma/\sqrt{n}} \qquad \text{F- 2}$$

If $H_0: \mu = \mu_0$ is true, then $E(\bar{X}) = \mu_0$, and it follows that z_0 has the standard normal distribution. According to Figure F- 1, the probability is $1 - \alpha$ that the test statistic z_0 falls between $-z_{\alpha/2}$ and $z_{\alpha/2}$ if the null hypothesis is true. Thus, the null hypothesis is rejected for a given significance level α if z_0 is placed in the critical region:

$$\text{either } z_0 < -z_{\alpha/2} \text{ or } z_0 > z_{\alpha/2} \qquad \text{F- 3}$$

and it is failed to reject the null hypothesis if z_0 falls in the acceptance region:

$$-z_{\alpha/2} < z_0 < z_{\alpha/2} \qquad \text{F- 4}$$

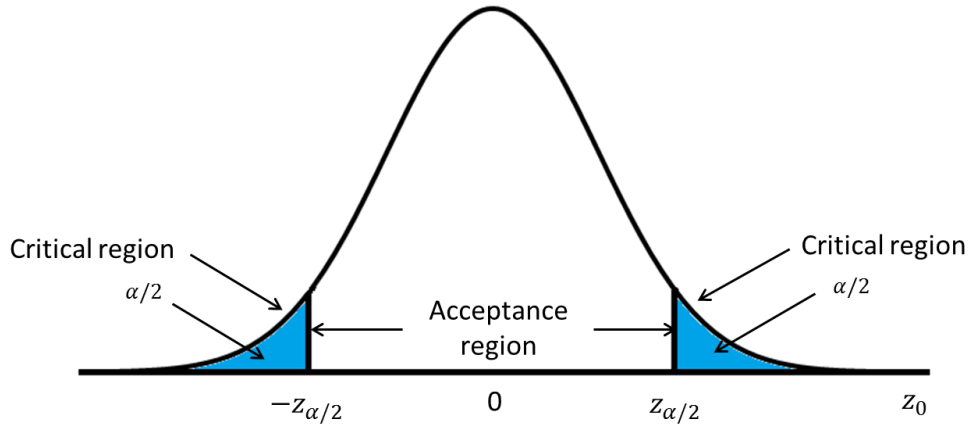

Figure F- 1 The distribution of z_0 when $H_0: \mu = \mu_0$ is true, with critical region for $H_1: \mu \neq \mu_0$

If the alternative hypothesis is one-sided:

$H_0: \mu = \mu_0$ F- 5

$H_1: \mu > \mu_0$

the negative value of z_0 will never result in the conclusion that $H_0: \mu = \mu_0$ is false. Thus, the critical region is placed in the upper tail of the normal distribution and H_0 is rejected if $z_0 > z_\alpha$.

Similarly, to test

$H_0: \mu = \mu_0$

$H_1: \mu < \mu_0$ F- 6

We would reject H_0 if $z_0 < -z_\alpha$.

It is recommended to follow the sequential steps to apply the hypothesis-testing methodology (Montgomery and Runger, 2011):

1. Identify the parameter of the interest from the problem
2. Sate the null hypothesis, H_0.
3. State the alternative hypothesis, H_1.
4. Choose a significance level α.
5. State an appropriate test statistic.
6. State the rejection region for the statistic.
7. Compute any necessary sample quantities, substitute these into the equation of test statistic and calculate that value.
8. Decide if H_0 should be rejected.

Hypothesis Test on the Mean, Variances Unknown

The procedure discussed in the previous section can be used to test the hypothesis about the mean of a population with unknown variance if the sample size is large (n ≥ 30). It is valid based on the central limit theorem regardless whether the underlying population is normal or not. Central limit theorem states that "the distribution of the sum (or average) of a large number of independent, identically distributed variables will be approximately normal, regardless of the underlying distribution". However, when the sample is small and the variance is unknown, stronger assumption is required which is the underlying distribution is normal.

Suppose that a random sample of size n is available and $\bar{X}$ and S^2 are the sample mean and variance respectively. To test the two-sided alternative hypothesis

$$H_0: \mu = \mu_0$$
$$H_1: \mu \neq \mu_0 \qquad \text{F- 7}$$

the test procedure is based on the statistic (Montgomery and Runger, 2011)

$$t_0 = \frac{\bar{X} - \mu_0}{S/\sqrt{n}} \qquad \text{F- 8}$$

which follows the t distribution with $n - 1$ degrees of freedom. Therefore, the value of the test statistic t_0 must be calculated to test the null hypothesis, and H_0 is rejected if either $t_0 > t_{\alpha/2,n-1}$ or $t_0 < -t_{\alpha/2,n-1}$. $t_{\alpha/2,n-1}$ and $-t_{\alpha/2,n-1}$ are the upper and lower $100\,\alpha/2$ percentage points of the t distribution with $n - 1$ degrees of freedom (Figure F- 2).

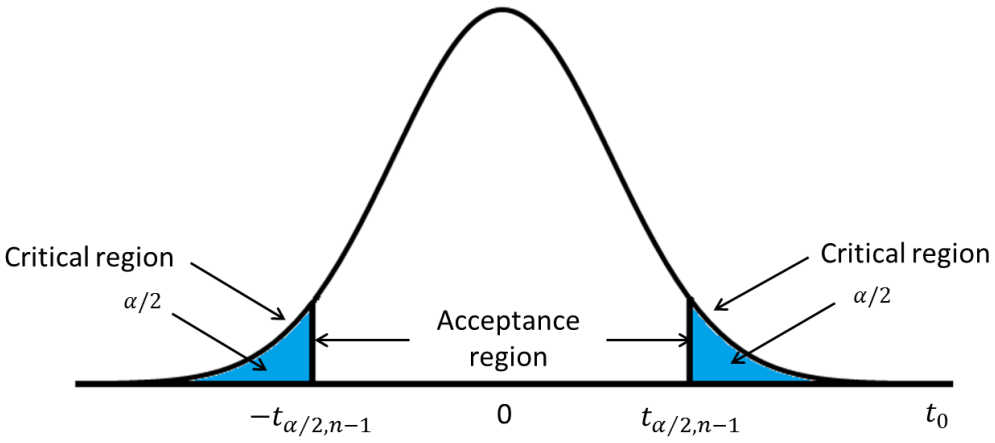

Figure F- 2 The t distribution with $n - 1$ degrees of freedom

For the one-sided alternative hypothesis

$H_0: \mu = \mu_0$ F- 9

$H_1: \mu > \mu_0$

the null hypothesis is rejected if $t_0 > t_{\alpha,n-1}$ and similarly the rejection criteria $t_0 < -t_{\alpha,n-1}$ is used to reject the null hypothesis in the other one-sided alternative test

$H_0: \mu = \mu_0$ F- 10

$H_1: \mu < \mu_0$.

Hypothesis Test on the Means of Two Normal Distributions, Variances Unknown

This part considers the hypothesis test on the equality of the means μ_1 and μ_2 of two normal distributions with unknown variances σ_1^2 and σ_1^2. Although the normality assumption is required to apply the test procedure, moderate deviations from the normal distribution do not significantly affect the procedure.

Suppose two independent normal populations with unknown means and variances (the variances are equal, i.e. $\sigma_1^2 = \sigma_2^2 = \sigma^2$), the null and alternative hypothesise are:

$H_0: \mu_1 = \mu_2$ F- 11

$H_1: \mu_1 \neq \mu_2$

If $\overline{X_1}$, $\overline{X_2}$, S_1^2 and S_2^2 are the means and variances of the random samples of sizes n_1 and n_2 respectively, the individual sample variances may be combined to form a single estimate (Montgomery and Runger, 2011):

$S_p^2 = \frac{(n_1-1)S_1^2+(n_2-1)S_2^2}{n_1+n_2-2}$ F- 12

S_p^2 is a combined (or "pooled") estimator of σ^2 that is better than either S_1^2 and S_2^2 individually. The following test statistic t_0 is introduced to test $H_0: \mu_1 = \mu_2$ (Montgomery and Runger, 2011):

$$t_0 = \frac{\overline{X_1} - \overline{X_2}}{S_p/\sqrt{\frac{1}{n_1} + \frac{1}{n_2}}} \quad \text{F- 13}$$

The null hypothesis is rejected if either $t_0 > t_{\alpha/2,n_1+n_2-2}$ or $t_0 < -t_{\alpha/2,n_1+n_2-2}$. Similarly, the rejection criterions $t_0 > t_{\alpha,n_1+n_2-2}$ and $t_0 < -t_{\alpha,n_1+n_2-2}$ are used to reject the $H_0: \mu_1 = \mu_2$ if the one-sided alternatives are $\mu_1 > \mu_2$ and $\mu_1 < \mu_2$ respectively.

Sometimes the unknown variances of the two independent populations are not equal ($\sigma_1^2 \neq \sigma_2^2$). Here, it is assumed that the statistic t_0^* (Montgomery and Runger, 2011)

$$t_0^* = \frac{\overline{X_1} - \overline{X_2}}{\sqrt{\frac{S_1^2}{n_1} + \frac{S_2^2}{n_2}}} \qquad \text{F- 14}$$

is distributed approximately as t_0 with degrees of freedom ϑ (Montgomery and Runger, 2011):

$$\vartheta = \frac{(\frac{S_1^2}{n_1} + \frac{S_2^2}{n_2})^2}{\frac{(S_1^2/n_1)^2}{n_1 + 1} + \frac{(S_2^2/n_2)^2}{n_2 + 1}} - 2 \qquad \text{F- 15}$$

if the null hypothesis H_0: $\mu_1 = \mu_2$ is true. Consequently, the hypothesis of Equation F-11 is tested with t_0^* as the test statistic and $n_1 + n_2 - 2$ is replaced by ϑ in determining the degrees of freedom for the test.